Politecnico di Torino

SYSTRA

POLITECNICO DI TORINO

Department of Environmental, Land and Infrastructure Engineering

Master of Science in Georesources and Geoenergy Engineering

Sustainable Mining Path

Advanced Numerical Investigation of Excavation Geometry and Tunnel Support System Behavior in Deep Large-Span Caverns Subjected to Variable In-Situ Stress Regimes

Supervisor:
Prof. Daniele Peila

Candidate:
Yazdan Khalili

Co-Supervisor(s):
Michele Palomba
Tolga Yerlikaya

Academic Year 2025-2026

Abstract

The design and construction of deep, large span caverns in rock mass require careful assessment of excavation sequencing, in situ stress conditions, and the interaction between the ground and support system. This thesis evaluates excavation strategies for cavern type openings through a two-dimensional finite element analysis. Three different excavation sequences (Radial Progressive Enlargement, Side Drifts, and Top Heading & Bench) are compared across different horizontal to vertical stress ratios. Each sequence is analyzed to evaluate ground response, support demand, and tunnel lining performance. The results offer practical guidance for selecting excavation methods that improve stability, safety, and cost efficiency under high overburden. They also outline key design considerations for engineers and highlight priorities for advancing support practices. In addition, the study identifies where further research can strengthen support design in deep underground excavations.

Keywords: numerical analysis, tunnels, caverns, in situ stress, sequential excavation method (SEM), tunnel support systems, tunnel lining, q system classification, reinforced ribs of sprayed concrete (RRS).

Acknowledgements

First and foremost, I would like to express my sincere gratitude to my supervisor, Professor Daniele Peila, for his constant support and for believing in my potential by offering me this research opportunity and recommending me to SYSTRA. His charisma, passion, and profound expertise have been a continuous source of inspiration, further strengthening my interest in tunneling and geotechnical engineering.

I would also like to extend my appreciation to Eng. Michele Palomba, under whose supervision this research was carried out. His trust in my abilities and confidence in granting me this opportunity played a crucial role in shaping the direction of this work. His dedication to maintaining high research standards was fundamental to the successful completion of this thesis. I am equally grateful to SYSTRA S.p.A team, particularly the Tunneling and Geotechnical Engineering Department, for providing a professional and supportive environment that greatly enriched the development of this study.

My heartfelt thanks also go to Eng. Tolga Yerlikaya for his continuous guidance and constant availability whenever clarification was needed. His encouragement, patience, and willingness to engage in detailed technical discussions were invaluable in overcoming the challenges encountered throughout this research. His mentorship not only enhanced the technical quality of this thesis but also contributed significantly to my development as a young engineer.

Finally, I would like to express my deepest gratitude to my family, to whom I dedicate this academic milestone. Their unwavering support, encouragement, and belief in me have been the foundation of every achievement in my life. I am especially grateful to my father for his bravery and strength in standing for honor and liberty. I also wish to express my profound respect and heartfelt remembrance for my compatriots in Iran, whose resilience and courage in their pursuit of freedom continue to inspire me and strengthen my pride in my homeland.

Table of Contents

Table of Figures

Chapter 1. Introduction

1.1. Research Framework

This research provides investigations into the design and construction of large caverns situated within rock masses under significant overburden. The main objective is to provide the constructability and structural integrity of these underground spaces by comparing various **Sequential Excavation Methods (SEM)** with advanced numerical modeling. The study rigorously analyzes the interaction between rock mass behavior and support system performance, specifically focusing on how these dynamics shift under variable **horizontal-to-vertical stress ratio (k)** regimes.

The scope of this work is shaped by the geotechnical challenges frequently encountered in large Norwegian tunnelling projects. Many different tunnels in Norway had to be constructed under demanding conditions, including high overburden, weak rock mass, and variable horizontal-to-vertical stress ratios. These factors make stability assessment and support design particularly complex, and the Q-system is a widely used empirical tool in Norwegian tunneling practices for that reason. Considering these conditions as fundamentals of this central case study, the research not only examines the challenges in detail but also aims to provide a reliable technical reference for engineers and researchers. The intention is that the insights gained here can support the design and evaluation of deep tunneling projects in different geological settings around the world, where similar conditions and uncertainties may arise.

The findings are intended to address the complexities of managing different stress environments and poor rock conditions that are common in mountainous or deep-crustal excavations. To establish a reliable research foundation for future engineering works, this study adopts a dual-methodological approach utilizing industry-standard empirical classification systems alongside advanced numerical modeling. These simulations are used to predict stress redistribution, deformation patterns, formation of plastic zones around the cavern and support system performance.

By synthesizing these approaches, the research provides a framework for optimizing excavation sequences and support designs, ensuring both safety and efficiency in the construction of large-span underground structures.

While empirical classification systems such as the **Q-system**, **Rock Mass Rating (RMR)**, and **Geological Strength Index (GSI)** serve as foundational tools in global tunneling projects, their inherent reliance on generalized assumptions necessitates a more rigorous, project-specific approach to ensure engineering conservatism. These empirical methods are inherently limited by their approximation of rock mass conditions, often failing to account for the unique anomalies and specific stress environments characteristic of complex excavations. Q-system is the primary reference used in this study, but it is built around favorable and relatively standard tunnel shapes. In our case, the span reaches 30 m, which is beyond the range where the Q-system performs reliably. The method generally works best for spans up to about 20 m and

for more circular tunnel geometries. Because of this, it cannot suggest a precise or well-fitted support recommendation for the unusually large and irregular cavern shape in this project. Consequently, integrating **Numerical Modeling** is essential to validate empirical outputs and provide a conservative simulation of localized mechanical behaviors.

This study adopts 2D Finite Element Method software named **RS2** powered by **Rocscience Co** which is popular in terms of advanced numerical modeling; Also, structural verifications have been done using the software.

1.2. Thesis Overview

Chapter 2. Literature review - Presents the scientific principles and fundamental concepts related to the topic. It offers a broad discussion of the problem, along with the existing knowledge surrounding the subject and its sub-topics. The chapter introduces key background information such as the basics of tunneling, the behavior of rock masses, stress conditions within rock formations, comparable case studies, and other relevant themes that help build a solid foundation for the research.

Chapter 3. Description of the Case Study - Describes the case study used in the thesis and explains the methods applied to collect the data required as input for the analysis.

Chapter 4. Methodology - Describes input data of the study, the conditions involved, and the modeling procedures followed to obtain reliable information as results. Each model is discussed in detail so the reader can understand how the results were produced step by step and why these approaches were chosen.

Chapter 5. Results - Describes final outputs of the analysis and presents the data achieved.

Chapter 6. Conclusion - Presents the final viewpoints based on comparing and analyzing the results shown in the fifth chapter. It brings together the knowledge discussed throughout the thesis, linking the background concepts, case study information, and analytical findings. By combining these elements, the chapter delivers the overall conclusion of the work and offers suggestions for future research. It also explains how this thesis can serve as a foundation for further studies on the topic.

Chapter 2. Literature review

2.1. Excavation of Caverns

Underground excavation plays a central role in modern engineering, supporting mining, transportation, hydroelectric development, and civil construction by enabling the creation of tunnels, caverns, and shafts that access subsurface resources, improve urban mobility, and house essential utilities, all while requiring careful evaluation of rock-mass conditions, in-situ stresses, and excavation methods because the surrounding rock interacts directly with the newly created void and undergoes complex stress redistribution (Barton & Choubey, The shear strength of rockfill materials, 1977). Within this broader context, a cavern represents a large underground chamber designed to provide substantial enclosed space for facilities such as hydropower stations, storage reservoirs, transport hubs, or military installations, differing from tunnels by offering a wide, volumetric space rather than a long, linear passage (Brown & Hoek, 1980).

Caverns are chosen when surface construction is impractical due to terrain, environmental constraints, or the need for protection and stability, and their geometry—ranging from rectangular and circular to horseshoe, elliptical, or multi-arch forms—is selected based on rock-mass quality, stress conditions, and functional requirements. Their design necessitate a step-by-step excavation by dividing the face into smaller portions according to their large section it is not possible to be excavated in full face scenario also it demands understanding of stress redistribution and often more robust support systems than those used for tunnels, especially for large spans, as demonstrated in engineering practice and in case studies such as Norwegian hydropower caverns (Palmstrom & Broch, 2006).

Figure 2-1. A Road Tunnel (Cavern) in Norway (Islands, n.d.)

Figure 2-2. Laerdal Tunnel: The World's Longest Road Tunnel (Amusing Planet, 2015)

2.1.1. Sequential Excavation Method (SEM)

The Sequential Excavation Method (SEM) is widely used for tunnel and cavern construction. Its core principle is to mobilize the ground's natural self-supporting capacity by allowing controlled deformation and applying support in carefully planned stages. Originating from alpine tunneling practices in the 1960s, SEM has become a flexible method for both rock and soft-ground conditions, especially in urban settings where precise deformation control is essential (FHWA, 2009). Unlike rigid support philosophies, SEM treats the surrounding ground as an active load-bearing component, using thin shotcrete linings and reinforcement to mobilize ground strength and redistribute stress.

SEM relies on the interaction between the support system and the rock mass, using the inherent strength of the ground to contribute to stability. Carefully sequenced excavation, timely support installation, and continuous monitoring allow the rock to deform slightly and develop its own load-carrying capacity. This approach has shown strong performance in weak or highly stressed rock masses, often outperforming classical full-face excavation (Sharifzadeh & Kiani, 2013) (Gall, 2013).

The tunnel cross-sections are typically curved to minimize stress concentrations. SEM typically employs a two-lining system:

- **Initial lining:** fiber-reinforced shotcrete.
- **Final lining:** cast-in-place concrete or reinforced shotcrete.

Ground is assessed using classification systems (RMR, Q-system or GSI). These are translated into Ground Response Classes (GRCs) and then into Excavation and Support Classes (ESCs), which specify subdivision, round lengths, and required support.

2.1.1.1. Excavation Sequences and Styles

SEM excavation is tailored to ground conditions. Drill-and-blast in hard rock, roadheaders in medium rock, and backhoes in soft ground are typical. Excavation may be full-face, top heading and bench, or subdivided into multiple drifts. Pre-support such as spilling, pipe umbrellas, or ground treatment is included in weak ground (FHWA, 2009).

Several typical layouts are utilized depending on cavern size, rock quality, and stress conditions:

- **Top Heading and Bench Method:** The top heading is driven and supported first, followed by the lower bench.
- **Side-Drift Method:** It begins with one or two sidewall drifts, which are then opened up to the full cross-section.
- **Central Drift Method:** A pilot drift is mined through the center of the profile to relieve stress before enlarging to full section.
- **Multiple Drift (Staggered) Excavation:** The face is divided into a number of headings and benches (3–6 drifts), which are mined in sequence with temporary support walls or inverts.
- **Full-Face SEM:** The entire cross-section may be excavated in extremely competent rock with immediate support installation, which is the fastest sequence.

These variations demonstrate the versatility of SEM and the potential to tailor the excavation sequence to ground response, deformation control required, and surface settlement limitations.

Figure 2-3 describes examples of the SEM in tunneling (Hoek, Big Tunnels in Bad Rock, 2000).

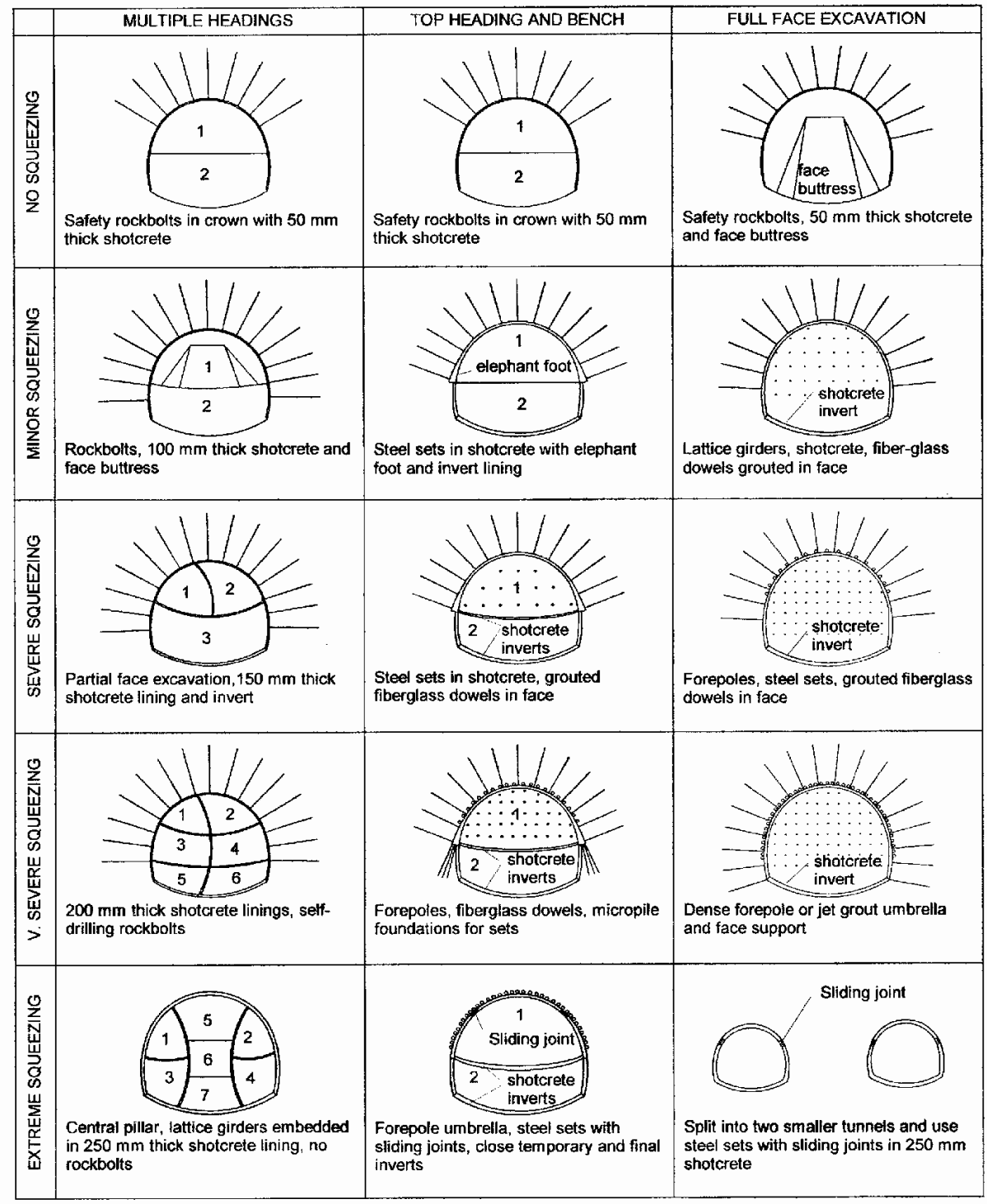

Figure 2-3. Examples of different ways in face excavation with SEM (Hoek, Big Tunnels in Bad Rock, 2000).

2.1.1.2. Ground Support Elements

Support typically includes shotcrete linings, patterned rock bolting, lattice girders, and pre-support systems such as spiles, pipe arches, or grouting. Their stiffness and timing determine how loads are transferred between ground and lining.

SEM design is based on the principle of ground–support interaction. Numerical modeling, ground reaction curves, and convergence–confinement analysis are utilized to estimate support demands, stresses, and deformations. Final linings are engineered with long-term durability and groundwater impacts in consideration (FHWA, 2009).

2.1.1.3. Monitoring

Instrumentation is the essence of SEM. Convergence pins, extensometers, piezometers, and surface settlement markers provide real-time feedback. Monitoring observations are compared with predictions and support measures are adjusted as required, using the observational method. SEM requires flexibility in contracts and experienced personnel, as the method depends upon progressive interpretation of monitoring data.

2.1.1.4. Criteria for Optimal Construction

The excavation sequence is designed according to geological variability, in-situ stress orientation, and rock mechanical properties. By allowing limited deformation, SEM mobilizes the rock's self-supporting capacity while preventing failure. Large caverns are typically excavated in parts such as top heading, bench, invert, side drift and central drift following a sequence optimized through numerical modeling and field observations to ensure overall stability.

Several engineering and geomechanically criteria govern the selection of optimum excavation sequences for large caverns. These include:

- Stress control – maintaining induced stresses within critical failure limits.
- Deformation control – maintaining displacements within tolerance for support and lining systems.
- Support effectiveness – synchronizing support installation with stress development and deformation.
- Construction efficiency – balancing safety with progress rate and resource utilization.

2.2. Rock Mass in Tunneling

Rock refers to a naturally occurring solid aggregate of minerals, while a rock mass represents the in-situ assemblage of rock blocks, discontinuities, joints, fractures, and weathered zones that collectively govern the mechanical behavior of the ground in engineering works (Brown & Hoek, 1980). In tunneling projects, the distinction becomes critical because excavation stability is controlled far more by the structure and condition of the rock mass than by the intact strength of the rock itself; factors such as joint orientation, spacing, roughness, infilling, and groundwater conditions dominate deformation and failure mechanisms, making rock-mass characterization essential for support design, excavation method selection, and predicting stress redistribution around the opening (Barton & Choubey, The shear strength of rockfill materials, 1977).

2.2.1. Characterization of Rock Mass

Strength, discontinuities, and geological heterogeneity of the rock mass play a critical role in underground excavation design. Rock mass classification schemes, i.e., Rock Mass Rating (RMR) system, Q-system, and Geological Strength Index (GSI), are widely used to measure rock quality and predict its behavior to stress. These systems provide engineers guidelines for the selection of excavation systems, support systems, and excavation sequences. Controlled excavation, instantaneous support installation, or staged excavation may be required in low-quality rock masses to prevent collapse and ensure safety (Hoek, Practical Rock Engineering, 2006).

2.2.1.1. Rock Mass Rating (RMR) system

Bieniawski published the details of a rock mass classification called the Geomechanics Classification or the Rock Mass Rating (*RMR*) system. Over the years, this system has been successively refined as more case records have been examined, and the reader should be aware that Bieniawski has made significant changes in the ratings assigned to different parameters. The discussion which follows is based upon the 1989 version of the classification. Both this version and the 1976 version deal with estimating the strength of rock masses. The following six parameters are used to classify a rock mass using the *RMR* system:

- Uniaxial compressive strength of rock material.
- Rock Quality Designation (*RQD*).

$$RQD = \frac{\Sigma\ Length\ of\ pieces\ longer\ than\ 10\ cm}{total\ length\ of\ Core\ run}$$

- Spacing of discontinuities.
- Condition of discontinuities.
- Groundwater conditions.
- Orientation of discontinuities.

In applying this classification system, the rock mass is divided into several structural regions, and each region is classified separately. The boundaries of the structural regions usually coincide with a major structural feature such as a fault or with a change in rock type. In some cases, significant changes in discontinuity spacing or characteristics, within the same rock type,

may necessitate the division of the rock mass into a few structural regions (Hoek, Practical Rock Engineering, 2006).

The Rock Mass Rating system is giving the ratings for each of the six parameters listed above. These ratings are summed up to give a value of *RMR*. Figure 2-4 shows the RMR system table.

A. CLASSIFICATION PARAMETERS AND THEIR RATINGS									
Parameter			Range of values						
1	Strength of intact rock material	Point-load strength index	>10 MPa	4 - 10 MPa	2 - 4 MPa	1 - 2 MPa	For this low range - uniaxial compressive test is preferred		
		Uniaxial comp. strength	>250 MPa	100 - 250 MPa	50 - 100 MPa	25 - 50 MPa	5 - 25 MPa	1 - 5 MPa	< 1 MPa
	Rating		15	12	7	4	2	1	0
2	Drill core Quality *RQD*		90% - 100%	75% - 90%	50% - 75%	25% - 50%	< 25%		
	Rating		20	17	13	8	3		
3	Spacing of discontinuities		> 2 m	0.6 - 2 . m	200 - 600 mm	60 - 200 mm	< 60 mm		
	Rating		20	15	10	8	5		
4	Condition of discontinuities (See E)		Very rough surfaces Not continuous No separation Unweathered wall rock	Slightly rough surfaces Separation < 1 mm Slightly weathered walls	Slightly rough surfaces Separation < 1 mm Highly weathered walls	Slickensided surfaces or Gouge < 5 mm thick or Separation 1-5 mm Continuous	Soft gouge >5 mm thick or Separation > 5 mm Continuous		
	Rating		30	25	20	10	0		
5	Groundwater	Inflow per 10 m tunnel length (l/m)	None	< 10	10 - 25	25 - 125	> 125		
		(Joint water press)/ (Major principal σ)	0	< 0.1	0.1, - 0.2	0.2 - 0.5	> 0.5		
		General conditions	Completely dry	Damp	Wet	Dripping	Flowing		
	Rating		15	10	7	4	0		

B. RATING ADJUSTMENT FOR DISCONTINUITY ORIENTATIONS (See F)						
Strike and dip orientations		Very favourable	Favourable	Fair	Unfavourable	Very Unfavourable
Ratings	Tunnels & mines	0	-2	-5	-10	-12
	Foundations	0	-2	-7	-15	-25
	Slopes	0	-5	-25	-50	

C. ROCK MASS CLASSES DETERMINED FROM TOTAL RATINGS					
Rating	100 ← 81	80 ← 61	60 ← 41	40 ← 21	< 21
Class number	I	II	III	IV	V
Description	Very good rock	Good rock	Fair rock	Poor rock	Very poor rock

D. MEANING OF ROCK CLASSES					
Class number	I	II	III	IV	V
Average stand-up time	20 yrs for 15 m span	1 year for 10 m span	1 week for 5 m span	10 hrs for 2.5 m span	30 min for 1 m span
Cohesion of rock mass (kPa)	> 400	300 - 400	200 - 300	100 - 200	< 100
Friction angle of rock mass (deg)	> 45	35 - 45	25 - 35	15 - 25	< 15

E. GUIDELINES FOR CLASSIFICATION OF DISCONTINUITY conditions					
Discontinuity length (persistence)	< 1 m	1 - 3 m	3 - 10 m	10 - 20 m	> 20 m
Rating	6	4	2	1	0
Separation (aperture)	None	< 0.1 mm	0.1 - 1.0 mm	1 - 5 mm	> 5 mm
Rating	6	5	4	1	0
Roughness	Very rough	Rough	Slightly rough	Smooth	Slickensided
Rating	6	5	3	1	0
Infilling (gouge)	None	Hard filling < 5 mm	Hard filling > 5 mm	Soft filling < 5 mm	Soft filling > 5 mm
Rating	6	4	2	2	0
Weathering	Unweathered	Slightly weathered	Moderately weathered	Highly weathered	Decomposed
Ratings	6	5	3	1	0

F. EFFECT OF DISCONTINUITY STRIKE AND DIP ORIENTATION IN TUNNELLING**			
Strike perpendicular to tunnel axis		Strike parallel to tunnel axis	
Drive with dip - Dip 45 - 90°	Drive with dip - Dip 20 - 45°	Dip 45 - 90°	Dip 20 - 45°
Very favourable	Favourable	Very unfavourable	Fair
Drive against dip - Dip 45-90°	Drive against dip - Dip 20-45°	Dip 0-20 - Irrespective of strike°	
Fair	Unfavourable	Fair	

* Some conditions are mutually exclusive . For example, if infilling is present, the roughness of the surface will be overshadowed by the influence of the gouge. In such cases use A.4 directly.
** Modified after Wickham et al (1972).

Figure 2-4. RMR system (Hoek, Practical Rock Engineering, 2006)

After defining the class number of the rock, it can be referred to Figure 2-5, in order to have a suggestion of general support system (Hoek, Practical Rock Engineering, 2006).

Rock mass class	Excavation	Rock bolts (20 mm diameter, fully grouted)	Shotcrete	Steel sets
I - Very good rock *RMR*: 81-100	Full face, 3 m advance.	Generally no support required except spot bolting.		
II - Good rock *RMR*: 61-80	Full face , 1-1.5 m advance. Complete support 20 m from face.	Locally, bolts in crown 3 m long, spaced 2.5 m with occasional wire mesh.	50 mm in crown where required.	None.
III - Fair rock *RMR*: 41-60	Top heading and bench 1.5-3 m advance in top heading. Commence support after each blast. Complete support 10 m from face.	Systematic bolts 4 m long, spaced 1.5 - 2 m in crown and walls with wire mesh in crown.	50-100 mm in crown and 30 mm in sides.	None.
IV - Poor rock *RMR*: 21-40	Top heading and bench 1.0-1.5 m advance in top heading. Install support concurrently with excavation, 10 m from face.	Systematic bolts 4-5 m long, spaced 1-1.5 m in crown and walls with wire mesh.	100-150 mm in crown and 100 mm in sides.	Light to medium ribs spaced 1.5 m where required.
V – Very poor rock *RMR*: < 20	Multiple drifts 0.5-1.5 m advance in top heading. Install support concurrently with excavation. Shotcrete as soon as possible after blasting.	Systematic bolts 5-6 m long, spaced 1-1.5 m in crown and walls with wire mesh. Bolt invert.	150-200 mm in crown, 150 mm in sides, and 50 mm on face.	Medium to heavy ribs spaced 0.75 m with steel lagging and forepoling if required. Close invert.

Figure 2-5. Support type suggestion in RMR system (Hoek, Practical Rock Engineering, 2006).

2.2.1.2. Geological Strength Index, GSI

The strength of a jointed rock mass depends on the properties of the intact rock pieces and upon the freedom of these pieces to slide and rotate under different stress conditions. This freedom is controlled by the geometrical shape of the intact rock pieces as well as the condition of the surfaces separating the pieces. Angular rock pieces with clean, rough discontinuity surfaces will result in a much stronger rock mass than one which contains rounded particles surrounded by weathered and altered material (Hoek, Practical Rock Engineering, 2006).

The Geological Strength Index (GSI), introduced by Hoek, Kaiser and Bawden provides a number which, when combined with the intact rock properties, can be used for estimating the reduction in rock mass strength for different geological conditions. This system is presented for blocky rock masses, and for heterogeneous rock masses such as flysch. It has also been extended to deal with molassic rocks and ophiolites. Before the introduction of the GSI system in 1994, the application of the Hoek-Brown criterion in the field was based on a correlation with the 1976 version of Bieniawski Rock Mass Rating, with the Groundwater rating set to 10 (dry) and the Adjustment for Joint Orientation set to 0 (very favorable). If the 1989 version of Bieniawski RMR classification is used, then the Groundwater rating is set to 15 and the Adjustment for Joint Orientation is set to zero. During the early years of the application of the GSI system the value of GSI was estimated directly from RMR.

However, this correlation has proved to be unreliable, particularly for poor quality rock masses and for rocks with lithological peculiarities that cannot be accommodated in the RMR classification. Consequently, it is recommended that GSI should be estimated directly by means of the charts and not from the RMR classification (Hoek, Practical Rock Engineering, 2006).

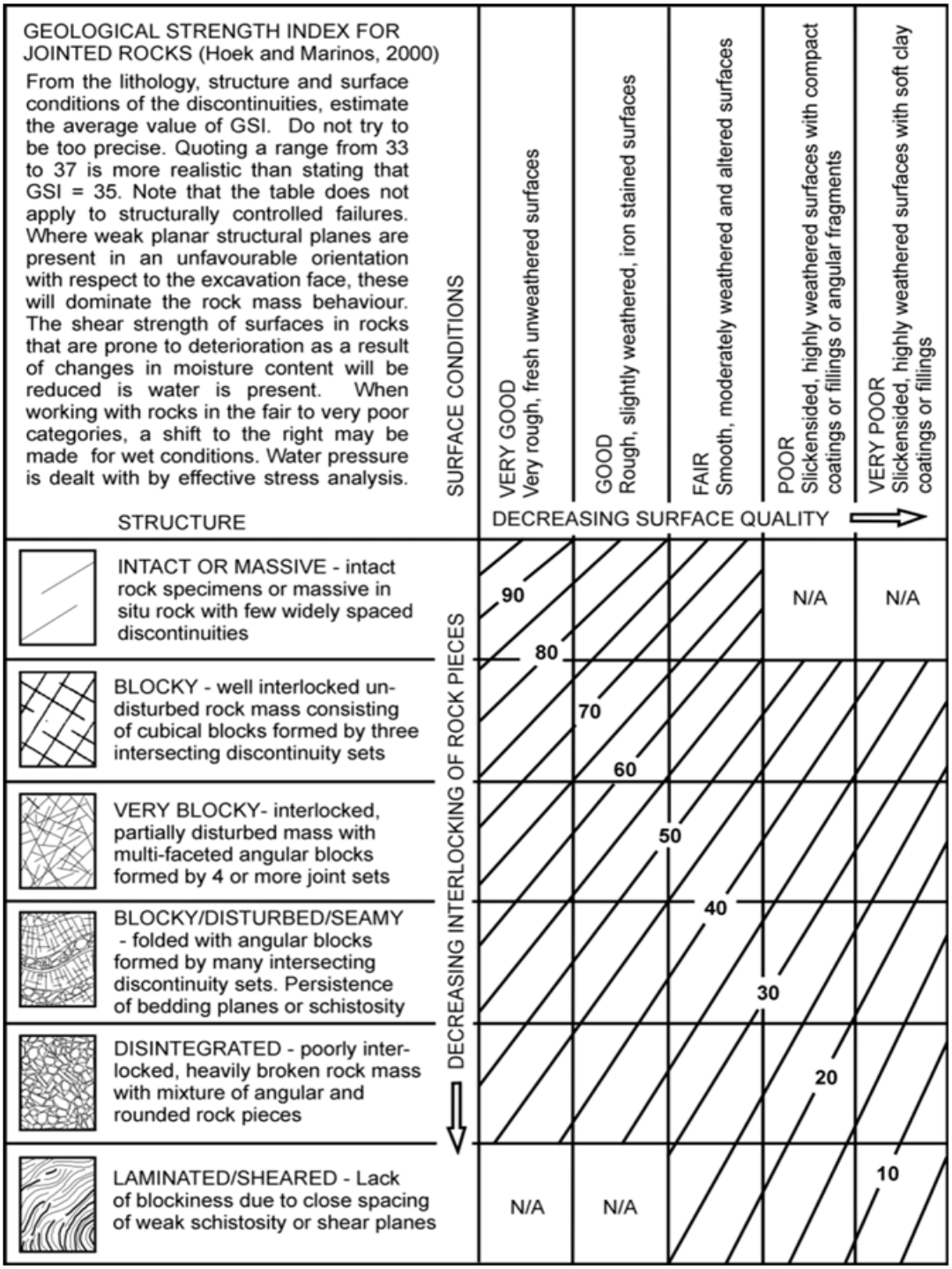

Figure 2-6. GSI system for blocky rock mass (Hoek, Practical Rock Engineering, 2006).

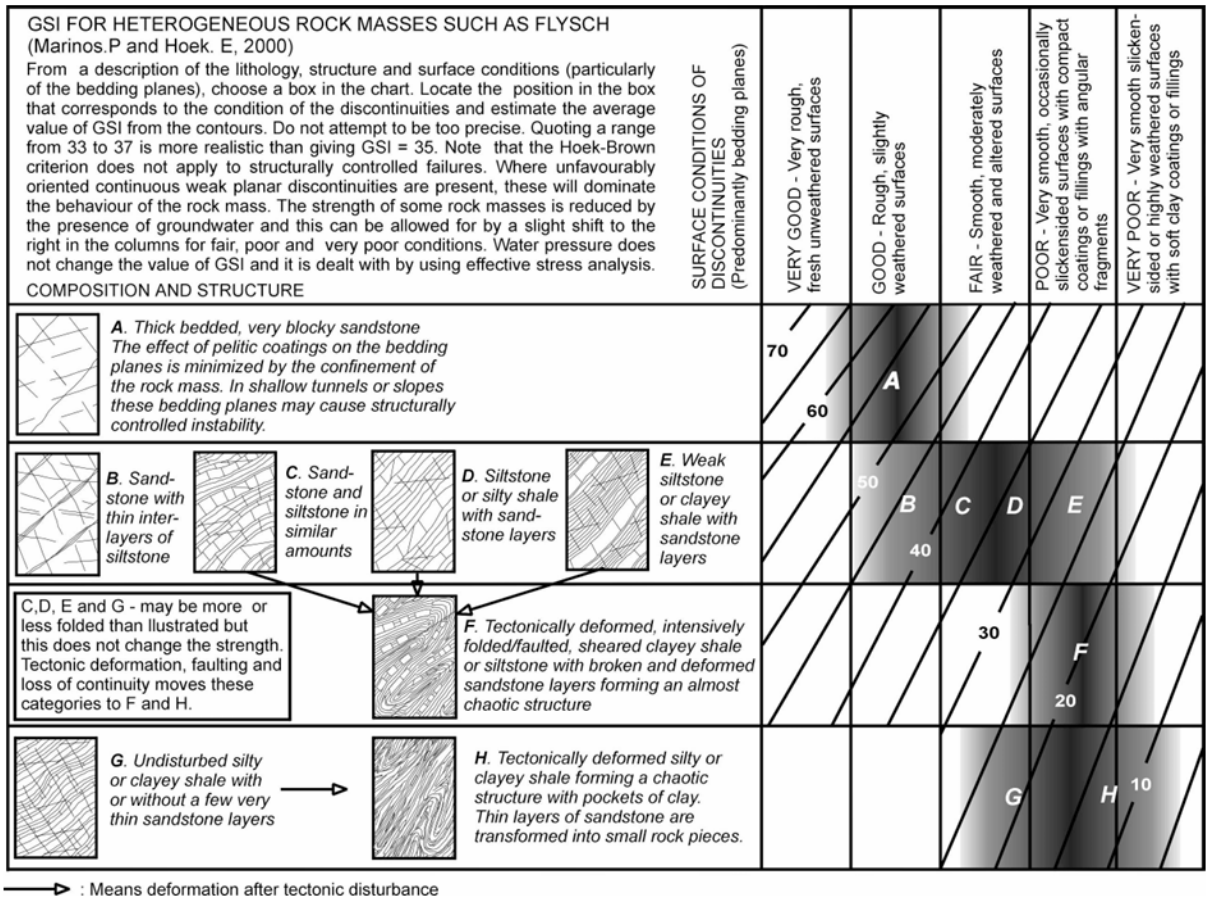

Figure 2-7. GSI for heterogenous rock mass (Hoek, Practical Rock Engineering, 2006).

2.2.1.3. Rock Tunnelling Quality Index, Q

Based on an evaluation of many case histories of underground excavations, Barton et al (1974) of the Norwegian Geotechnical Institute proposed Tunnelling Quality Index (Q) for the determination of rock mass characteristics and tunnel support requirements (Bieniawski, 1989). The numerical value of the index Q varies on a logarithmic scale from 0.001 to a maximum of 1,000 and is defined by:

$$Q = \frac{RQD}{Jn} \times \frac{Ja}{Jn} \times \frac{Jw}{SRF}$$

Where:

- RQD is the Rock Quality Designation
- Jn is the joint set number
- Jr is the joint roughness number
- Ja is the joint alteration number
- Jw is the joint water reduction factor
- SRF is the stress reduction factor

It appears that the rock tunnelling quality Q can now be a function of only three parameters which are crude measures of:

- 1. Block size (RQD/Jn)
- 2. Inter-block shear strength (Jr/ Ja)
- 3. Active stress (Jw/SRF)

Undoubtedly, there are several other parameters which could be added to improve the accuracy of the classification system. One of these would be joint orientation. Although many case records include the necessary information on structural orientation in relation to excavation axis, it was not found to be the important general parameter that might be expected. Part of the reason for this may be that the orientations of many types of excavations can be, and normally are, adjusted to avoid the maximum effect of unfavorably oriented major joints. However, this choice is not available in the case of tunnels, and more than half the case records were in this category. The parameters Jn, Jr and Ja appear to play a more important role than orientation, because the number of joint sets determines the degree of freedom for block movement (if any), and the frictional and dilutional characteristics vary more than the down-dip gravitational component of unfavorably oriented joints. If joint orientations had been included the classification would have been less general, and its essential simplicity lost. The following figures will show the coefficients of each parameter in the formula by considering the descriptive characteristics pf the rock mass (Hoek, Practical Rock Engineering, 2006).

DESCRIPTION	VALUE	NOTES
1. ROCK QUALITY DESIGNATION	***RQD***	
A. Very poor	0 - 25	1. Where *RQD* is reported or measured as ≤ 10 (including 0),
B. Poor	25 - 50	a nominal value of 10 is used to evaluate *Q*.
C. Fair	50 - 75	
D. Good	75 - 90	2. *RQD* intervals of 5, i.e. 100, 95, 90 etc. are sufficiently
E. Excellent	90 - 100	accurate.
2. JOINT SET NUMBER	J_n	
A. Massive, no or few joints	0.5 - 1.0	
B. One joint set	2	
C. One joint set plus random	3	
D. Two joint sets	4	
E. Two joint sets plus random	6	
F. Three joint sets	9	1. For intersections use ($3.0 \times J_n$)
G. Three joint sets plus random	12	
H. Four or more joint sets, random,	15	2. For portals use ($2.0 \times J_n$)
heavily jointed, 'sugar cube', etc.		
J. Crushed rock, earthlike	20	
3. JOINT ROUGHNESS NUMBER	J_r	
a. Rock wall contact		
b. Rock wall contact before 10 cm shear		
A. Discontinuous joints	4	
B. Rough and irregular, undulating	3	
C. Smooth undulating	2	
D. Slickensided undulating	1.5	1. Add 1.0 if the mean spacing of the relevant joint set is
E. Rough or irregular, planar	1.5	greater than 3 m.
F. Smooth, planar	1.0	
G. Slickensided, planar	0.5	2. J_r = 0.5 can be used for planar, slickensided joints having
c. No rock wall contact when sheared		lineations, provided that the lineations are oriented for
H. Zones containing clay minerals thick	1.0	minimum strength.
enough to prevent rock wall contact	(nominal)	
J. Sandy, gravely or crushed zone thick	1.0	
enough to prevent rock wall contact	(nominal)	
4. JOINT ALTERATION NUMBER	J_a	ϕr degrees (approx.)
a. Rock wall contact		
A. Tightly healed, hard, non-softening,	0.75	1. Values of ϕr, the residual friction angle,
impermeable filling		are intended as an approximate guide
B. Unaltered joint walls, surface staining only	1.0	25 - 35 to the mineralogical properties of the
C. Slightly altered joint walls, non-softening	2.0	25 - 30 alteration products, if present.
mineral coatings, sandy particles, clay-free		
disintegrated rock, etc.		
D. Silty-, or sandy-clay coatings, small clay-	3.0	20 - 25
fraction (non-softening)		
E. Softening or low-friction clay mineral coatings,	4.0	8 - 16
i.e. kaolinite, mica. Also chlorite, talc, gypsum		
and graphite etc., and small quantities of swelling		
clays. (Discontinuous coatings, 1 - 2 mm or less)		

Figure 2-8. Q- system tables (Hoek, Practical Rock Engineering, 2006).

4, JOINT ALTERATION NUMBER	J_a	ϕr degrees (approx.)	
b. Rock wall contact before 10 cm shear			
F. Sandy particles, clay-free, disintegrating rock etc.	4.0	25 - 30	
G. Strongly over-consolidated, non-softening clay mineral fillings (continuous < 5 mm thick)	6.0	16 - 24	
H. Medium or low over-consolidation, softening clay mineral fillings (continuous < 5 mm thick)	8.0	12 - 16	
J. Swelling clay fillings, i.e. montmorillonite, (continuous < 5 mm thick). Values of J_a depend on percent of swelling clay-size particles, and access to water.	8.0 - 12.0	6 - 12	
c. No rock wall contact when sheared			
K. Zones or bands of disintegrated or crushed	6.0		
L. rock and clay (see G, H and J for clay	8.0		
M. conditions)	8.0 - 12.0	6 - 24	
N. Zones or bands of silty- or sandy-clay, small clay fraction, non-softening	5.0		
O. Thick continuous zones or bands of clay	10.0 - 13.0		
P. & R. (see G.H and J for clay conditions)	6.0 - 24.0		
5. JOINT WATER REDUCTION	J_w	approx. water pressure (kgf/cm^2)	
A. Dry excavation or minor inflow i.e. < 5 l/m locally	1.0	< 1.0	
B. Medium inflow or pressure, occasional outwash of joint fillings	0.66	1.0 - 2.5	
C. Large inflow or high pressure in competent rock with unfilled joints	0.5	2.5 - 10.0	1. Factors C to F are crude estimates; increase J_w if drainage installed.
D. Large inflow or high pressure	0.33	2.5 - 10.0	
E. Exceptionally high inflow or pressure at blasting, decaying with time	0.2 - 0.1	> 10	2. Special problems caused by ice formation are not considered.
F. Exceptionally high inflow or pressure	0.1 - 0.05	> 10	
6. STRESS REDUCTION FACTOR ***a. Weakness zones intersecting excavation, which may cause loosening of rock mass when tunnel is excavated***		***SRF***	
A. Multiple occurrences of weakness zones containing clay or chemically disintegrated rock, very loose surrounding rock any depth)		10.0	1. Reduce these values of *SRF* by 25 - 50% but only if the relevant shear zones influence do not intersect the excavation
B. Single weakness zones containing clay, or chemically disintegrated rock (excavation depth < 50 m)		5.0	
C. Single weakness zones containing clay, or chemically disintegrated rock (excavation depth > 50 m)		2.5	
D. Multiple shear zones in competent rock (clay free), loose surrounding rock (any depth)		7.5	
E. Single shear zone in competent rock (clay free). (depth of excavation < 50 m)		5.0	
F. Single shear zone in competent rock (clay free). (depth of excavation > 50 m)		2.5	
G. Loose open joints, heavily jointed or 'sugar cube', (any depth)		5.0	

Figure 2-9. Q-system tables (Hoek, Practical Rock Engineering, 2006).

DESCRIPTION		VALUE		NOTES
6. STRESS REDUCTION FACTOR			***SRF***	
b. Competent rock, rock stress problems				
	σ_c/σ_1	$\sigma_t\sigma_1$		2. For strongly anisotropic virgin stress field
H. Low stress, near surface	> 200	> 13	2.5	(if measured): when $5 \le \sigma_1/\sigma_3 \le 10$, reduce σ_c
J. Medium stress	200 - 10	13 - 0.66	1.0	to $0.8\sigma_c$ and σ_t to $0.8\sigma_t$. When σ_1/σ_3 > 10,
K. High stress, very tight structure	10 - 5	0.66 - 0.33	0.5 - 2	reduce σ_c and σ_t to $0.6\sigma_c$ and $0.6\sigma_t$, where
(usually favourable to stability, may				σ_c = unconfined compressive strength, and
be unfavourable to wall stability)				σ_t = tensile strength (point load) and σ_1 and
L. Mild rockburst (massive rock)	5 - 2.5	0.33 - 0.16	5 - 10	σ_3 are the major and minor principal stresses.
M. Heavy rockburst (massive rock)	< 2.5	< 0.16	10 - 20	3. Few case records available where depth of
c. Squeezing rock, plastic flow of incompetent rock				crown below surface is less than span width.
under influence of high rock pressure				Suggest *SRF* increase from 2.5 to 5 for such
N. Mild squeezing rock pressure			5 - 10	cases (see H).
O. Heavy squeezing rock pressure			10 - 20	
d. Swelling rock, chemical swelling activity depending on presence of water				
P. Mild swelling rock pressure			5 - 10	
R. Heavy swelling rock pressure			10 - 15	

ADDITIONAL NOTES ON THE USE OF THESE TABLES

When making estimates of the rock mass Quality (Q), the following guidelines should be followed in addition to the notes listed in the tables:

1. When borehole core is unavailable, *RQD* can be estimated from the number of joints per unit volume, in which the number of joints per metre for each joint set are added. A simple relationship can be used to convert this number to *RQD* for the case of clay free rock masses: $RQD = 115 - 3.3\ J_v$ (approx.), where J_v = total number of joints per m^3 ($0 < RQD < 100$ for $35 > J_v > 4.5$).
2. The parameter J_n representing the number of joint sets will often be affected by foliation, schistosity, slaty cleavage or bedding etc. If strongly developed, these parallel 'joints' should obviously be counted as a complete joint set. However, if there are few 'joints' visible, or if only occasional breaks in the core are due to these features, then it will be more appropriate to count them as 'random' joints when evaluating J_n.
3. The parameters J_r and J_a (representing shear strength) should be relevant to the weakest significant joint set or clay filled discontinuity in the given zone. However, if the joint set or discontinuity with the minimum value of J_r/J_a is favourably oriented for stability, then a second, less favourably oriented joint set or discontinuity may sometimes be more significant, and its higher value of J_r/J_a should be used when evaluating Q. The value of J_r/J_a should in fact relate to the surface most likely to allow failure to initiate.
4. When a rock mass contains clay, the factor *SRF* appropriate to loosening loads should be evaluated. In such cases the strength of the intact rock is of little interest. However, when jointing is minimal and clay is completely absent, the strength of the intact rock may become the weakest link, and the stability will then depend on the ratio rock-stress/rock-strength. A strongly anisotropic stress field is unfavourable for stability and is roughly accounted for as in note 2 in the table for stress reduction factor evaluation.
5. The compressive and tensile strengths (σ_c and σ_t) of the intact rock should be evaluated in the saturated condition if this is appropriate to the present and future in situ conditions. A very conservative estimate of the strength should be made for those rocks that deteriorate when exposed to moist or saturated conditions.

Figure 2-10. Q-system tables (Hoek, Practical Rock Engineering, 2006).

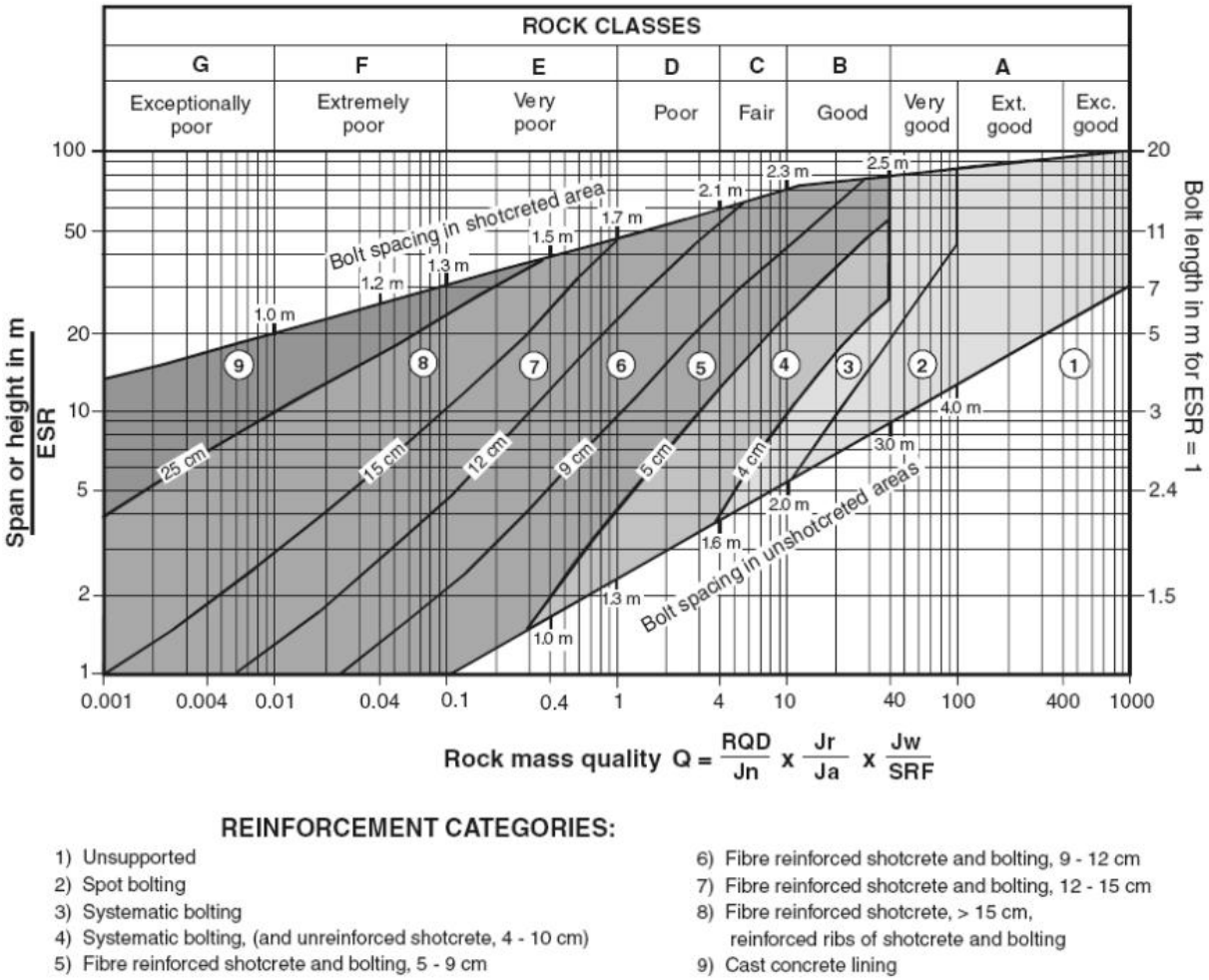

Figure 2-11. Q-system support suggestion (Hoek, Practical Rock Engineering, 2006)

The value of ESR is related to the intended use of the excavation and to the degree of security which is demanded of the support system installed to maintain the stability of the excavation. Barton suggests the following values:

Table 2-1. ESR values in Q system (Hoek, Practical Rock Engineering, 2006)

Excavation category	*ESR*
A. Temporary mine openings.	3-5
B. Permanent mine openings, water tunnels for hydro power (excluding high pressure penstocks), pilot tunnels, drifts and headings for large excavations.	1.6
C. Storage rooms, water treatment plants, minor road and railway tunnels, surge chambers, access tunnels.	1.3
D. Power stations, major road and railway tunnels, civil defense chambers, portal intersections.	1
E. Underground nuclear power stations, railway stations, sports and public facilities, factories.	0.8

Barton provides additional information on rock bolt length, maximum unsupported spans and roof support pressures to supplement the support recommendations published in the original 1974 paper.

The length L of rock bolts can be estimated from the excavation width B and the Excavation Support Ratio ESR:

$$L = 2 + \frac{0.15\ B}{ESR}$$

The maximum unsupported span is:

$$Maximum\ unsupported\ span = 2\ ESR\ Q^{0.4}$$

Based upon analyses of case records, Grimstad and Barton suggest that the relationship between the value of Q and the permanent roof support pressure P_{roof} is estimated from:

$$P_{roof} = \frac{2Q^{(\frac{-1}{3})}\sqrt{Jn}}{3\ Jr}$$

It can be noted that the value of RMR can be approximately found by Q value using the following empirical equation (Bieniawski, 1989):

$$RMR = 9 \ln Q + 44$$

Q-system has been revised and updated many times by different researchers to make it more adaptable to modern tunneling practices.

One research that was conducted by Palmstrom & Broch indicates that maximum reliability of this empirical method happens for tunnels up to 20m of span and for larger dimensions the system should be revised or modified based on the site-specific conditions. Figure 2-12 shows the white zone in the middle of the chart where the chart works with highest accuracy and reliability (Palmstrom & Broch, 2006).

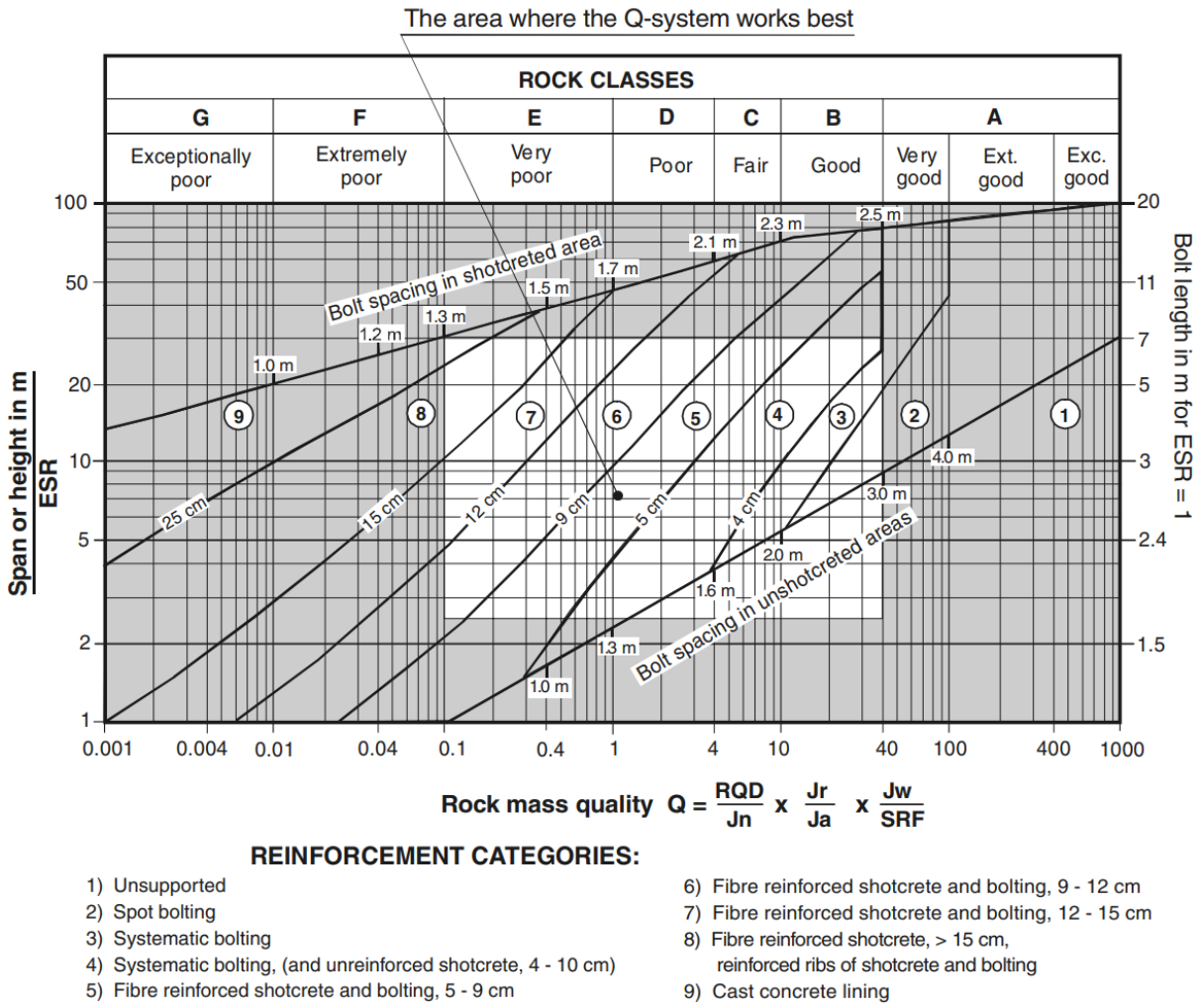

Figure 2-12. Limitations in the Q rock support diagram. Outside the unshaded area supplementary methods/evaluations/calculations should be applied (Palmstrom & Broch, 2006)

By advancing technology and science, as new support materials have been introduced, analytical approaches have improved, and scientific understanding has advanced, the empirical chart has been refined to remain practical and relevant. The most recent update was carried out by the **Norwegian Tunneling Society** (Figure 2-13), incorporating new empirical experience and modern support technologies. One important addition is the inclusion of Reinforced Ribs of Sprayed Concrete (RRS), which can now be selected directly from the updated chart without the need for extra calculations to determine the final support properties of a proposed system (NGI, 2025).

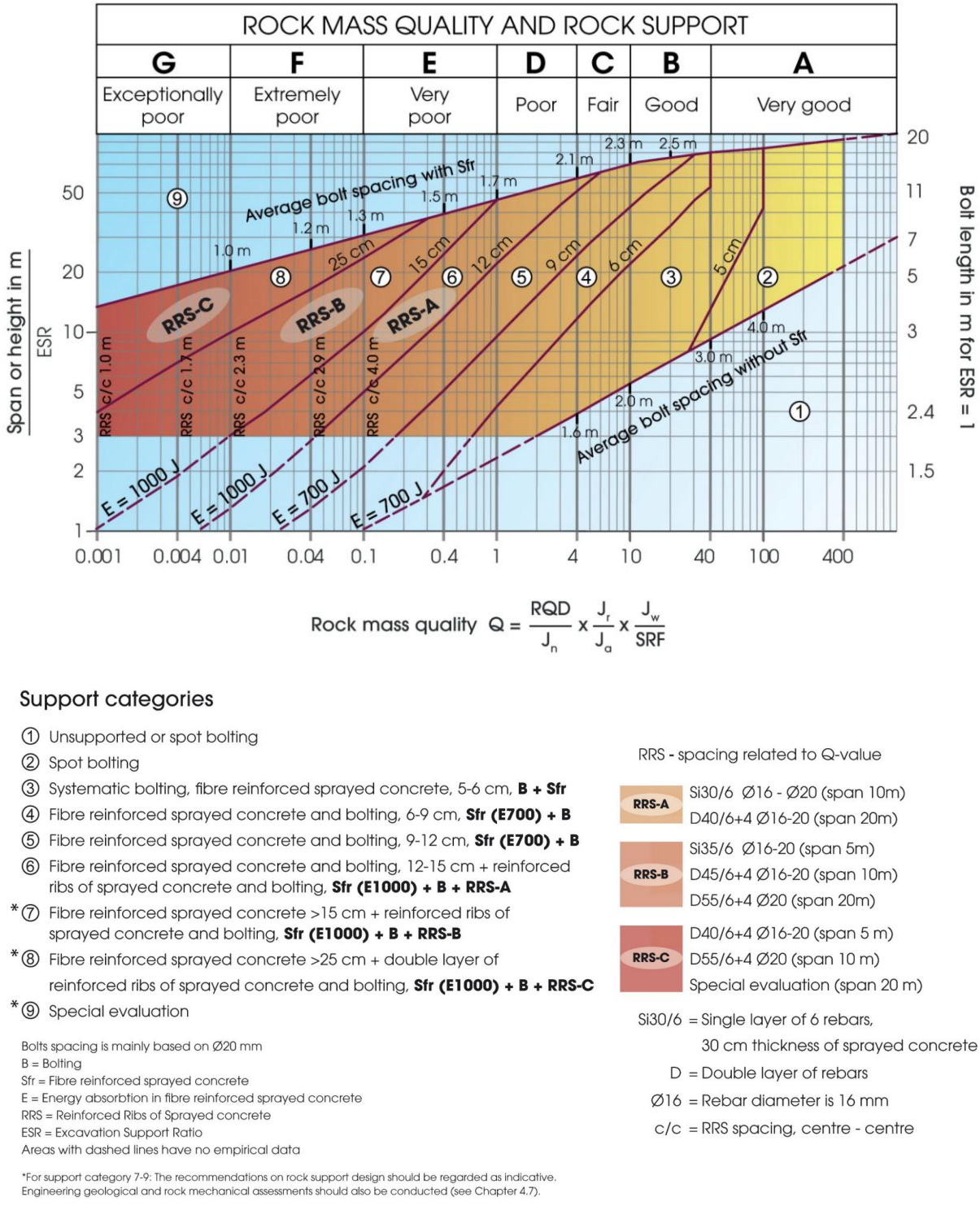

Support categories

① Unsupported or spot bolting
② Spot bolting
③ Systematic bolting, fibre reinforced sprayed concrete, 5-6 cm, **B + Sfr**
④ Fibre reinforced sprayed concrete and bolting, 6-9 cm, **Sfr (E700) + B**
⑤ Fibre reinforced sprayed concrete and bolting, 9-12 cm, **Sfr (E700) + B**
⑥ Fibre reinforced sprayed concrete and bolting, 12-15 cm + reinforced ribs of sprayed concrete and bolting, **Sfr (E1000) + B + RRS-A**
*⑦ Fibre reinforced sprayed concrete >15 cm + reinforced ribs of sprayed concrete and bolting, **Sfr (E1000) + B + RRS-B**
*⑧ Fibre reinforced sprayed concrete >25 cm + double layer of reinforced ribs of sprayed concrete and bolting, **Sfr (E1000) + B + RRS-C**
*⑨ Special evaluation

Bolts spacing is mainly based on Ø20 mm
B = Bolting
Sfr = Fibre reinforced sprayed concrete
E = Energy absorbtion in fibre reinforced sprayed concrete
RRS = Reinforced Ribs of Sprayed concrete
ESR = Excavation Support Ratio
Areas with dashed lines have no empirical data

*For support category 7-9: The recommendations on rock support design should be regarded as indicative. Engineering geological and rock mechanical assessments should also be conducted (see Chapter 4.7).

RRS - spacing related to Q-value

RRS-A
Si30/6 Ø16 - Ø20 (span 10m)
D40/6+4 Ø16-20 (span 20m)

RRS-B
Si35/6 Ø16-20 (span 5m)
D45/6+4 Ø16-20 (span 10m)
D55/6+4 Ø20 (span 20m)

RRS-C
D40/6+4 Ø16-20 (span 5 m)
D55/6+4 Ø20 (span 10 m)
Special evaluation (span 20 m)

Si30/6 = Single layer of 6 rebars, 30 cm thickness of sprayed concrete
D = Double layer of rebars
Ø16 = Rebar diameter is 16 mm
c/c = RRS spacing, centre - centre

Figure 2-13. Q-System support suggestion ((NGI, 2025)

Reinforced Ribs of Sprayed Concrete (RRS): This support material is commonly used in Norway tunneling projects. In areas with very poor to exceptionally poor rock quality (Q < 1, support categories 6- 8), reinforced ribs of sprayed concrete (RRS) are often a preferred alternative to cast concrete lining. The ribs are constructed with a combination of steel bars (usually with a diameter of 16 mm or 20 mm), sprayed concrete, and rock bolts. When using

steel bars of 20 mm, the bars must be pre-bent to achieve a smooth profile. The thickness of the ribs, the spacing between them, and the number and diameter of the reinforcing bars are adapted to the dimensions of the underground opening and the quality of the rock mass in accordance with the support chart (NGI, 2025).

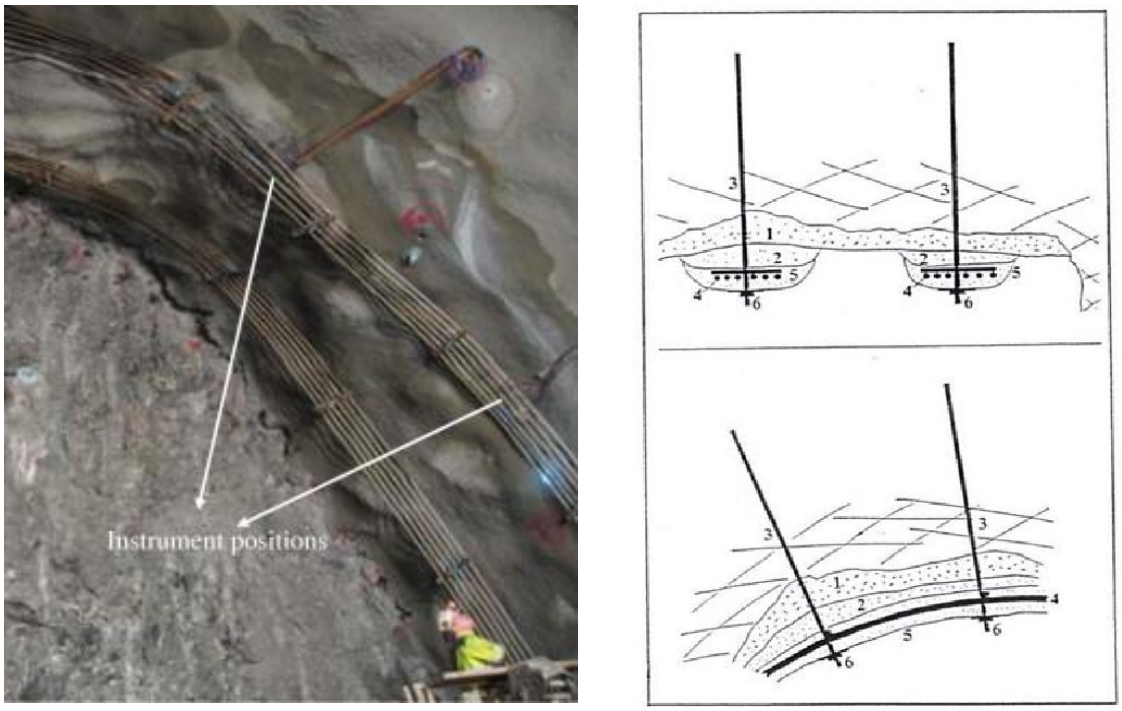

Figure 2-14. Installed RRS ((Mao & Nilsen, 2011))

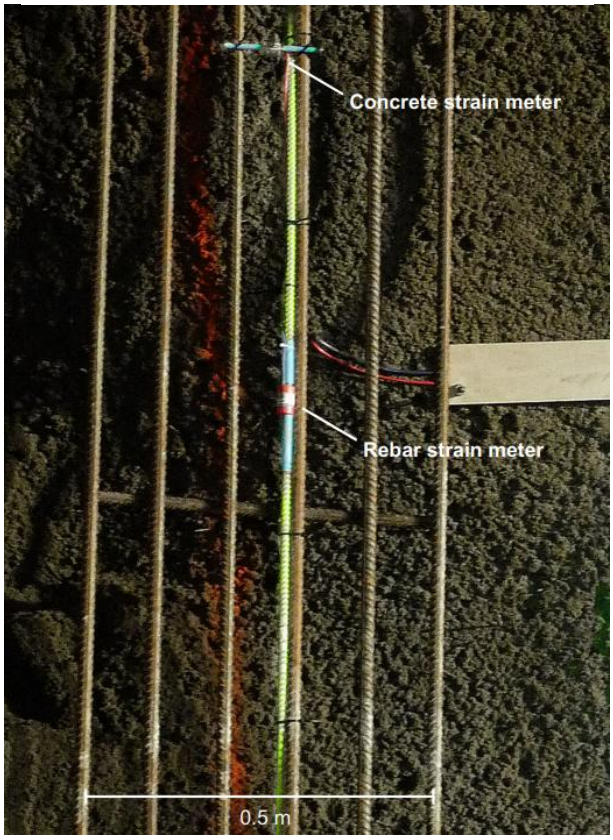

Figure 2-15. RRS figure (Havard & Nilsen, 2018)

Support diagram includes three RRS categories: RRS-A, RRS-B, and RRS-C. Guidelines for the use of RRS in relation to Q-values, equivalent dimensions (De), and spans for underground chambers are provided in the support chart and the accompanying explanatory text.

In the description of the support diagram, the following abbreviations are used:

- “Sfr”: Fiber-reinforced sprayed concrete
- "Si": Single layer of steel bars
- "D": Double layer of steel bars
- "45": Total rib thickness of 45 cm
- "6": Six steel bars
- "c/c = 2-3": Centre-to-Centre spacing, 2 to 3 meters between the ribs
- "16" or "20": Diameter of the steel bars, in mm

Note that in the support chart, the recommendations for RRS follow the support classes, meaning that the same rib dimensions are maintained diagonally across the chart. Within each area, there will be a range where the suggested spacing between the ribs will vary. An engineering geological assessment must be conducted in each case to determine the appropriate spacing between the ribs (NGI, 2025).

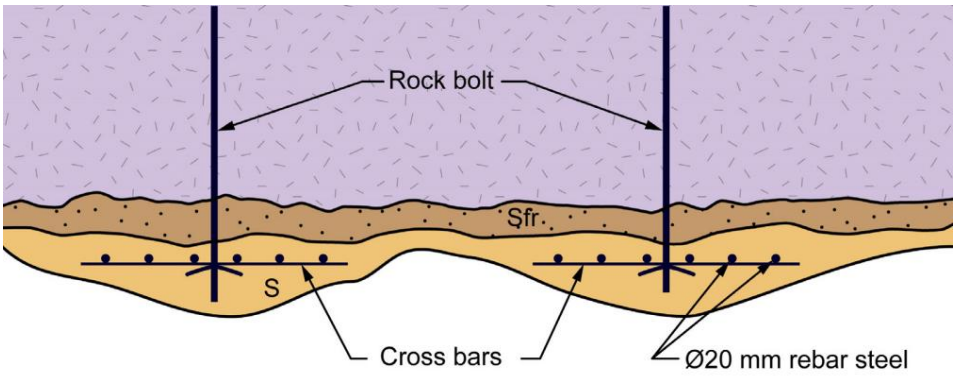

Figure 2-16. Construction principle for reinforced ribs of sprayed concrete (RRS).

**Note that the initial layer (smoothening layer) closest to the rock surface is fiber-reinforced sprayed concrete (Sfr), while the outermost layer of sprayed concrete is without fiber (S) (NGI, 2025)*

In cases where the Q-value indicates the need for RRS, a 12-15 cm thick layer of fiber-reinforced sprayed concrete is typically applied before the ribs can be installed. This layer serves as temporary support and helps to smoothen the rock surface, ensuring optimal arching effect (applicable for pre-bent reinforcement bars, Ø20 mm). The thickness of this layer is included in the total thickness of the RRS. The sprayed concrete layer applied on top of the installed reinforcement ribs should preferably be without fiber (Figure 2-16). As shown in the explanation of the support chart in, it is recommended for support categories 6–9 to conduct further assessments for a more comprehensive rock mass characterization before determining the final rock support. This is particularly relevant for rock mass conditions that are not fully accounted for in the reference cases on which the support chart is based. See Chapter 4.7 for

more details. In support categories 7-9 additional anchoring of the RRS at the base or the need for a cast concrete invert cast concrete should be considered (NGI, 2025).

2.2.1.4. Relationship between RMR, GSI and Q-system

All three main classification methods can be connected, and their index can be assumed having value of other systems by using empirical equations. For example, by having Q-system value of a rock mass, it is possible to estimate its RMR value using the relation indicated below (Bieniawski, 1989).

$$RMR = 9lnQ + 44.$$

GSI can also be found from RMR value, by using following empirical equations (Brown & Hoek, 1980):

$$RMR_{Corrected} = RMR + (15 - A5)$$

$$GSI = RMR_{Corrected} - 5$$

Where:

$RMR_{corrected}$ is the value of RMR neglecting the groundwater condition factor (Bieniawski, 1989).

2.3. In-Situ Stress

In-situ stress represents the natural state of stress existing in a rock mass before any engineering disturbance. It results from lithostatic weight, tectonic activity, and residual geological processes accumulated over millions of years. These stresses form the background field that governs how the rock responds when excavations such as tunnels or caverns are created. The redistribution of in-situ stress around an opening dictate whether the rock remains stable or fails. Proper knowledge of this stress field is a fundamental prerequisite for the design, stability evaluation, and safety of underground excavations, particularly large caverns where stress concentrations are magnified due to their size and shape.

The in-situ stress tensor generally comprises three principal components: vertical, maximum horizontal, and minimum horizontal stress. The vertical component σ_v is primarily controlled by the weight of the overburden, calculated with following equation.

$$\sigma_v = \gamma H$$

where H is the depth and γ the intact rock unit weight. The horizontal stresses are more complex and can be found by multiplying a coefficient k to vertical stress; the amount of k depends on Poisson's ratio, tectonic compression, geological anisotropy and depth of the cavern.

$$\sigma_h = k.\sigma_v$$

In tectonically active areas, horizontal stresses often exceed vertical stress, producing anisotropic stress fields that significantly affect excavation performance. The magnitude and orientation of these principal stresses strongly influence the mechanical response of the rock mass, making their determination crucial for design optimization (Brown & Hoek, 1980).

2.3.1. Measurement and Estimation techniques

Reliable determination of in-situ stress is achieved through both direct and indirect methods. Common direct methods include over-coring, hydraulic fracturing, and borehole slotting, which provide quantitative values of stress magnitudes and orientations. **Over-coring** measures relieve strains in a cored sample, while **Hydraulic Fracturing** identifies stress directions by analyzing crack initiation pressure. Indirect methods, such as **Borehole Breakout Analysis**, **Acoustic Emissions**, and **Numerical Back-Analysis**, are applied when direct testing is impractical (Barton & Choubey, The shear strength of rockfill materials, 1977) (Sharifzadeh & Kiani, 2013). Combining multiple approaches increases confidence in results, particularly for heterogeneous or jointed rock masses. These measurements are later used to calibrate numerical models, enabling a realistic representation of stress redistribution during excavation.

The achieved in situ stress cannot be reliable for the real case studies in rock mass; the mentioned methods can only show the lateral and vertical stresses in the region and as was explained previously that knowing these two forces is not enough to do the design. Every rock mass has its own properties that should be considered in the calculations therefore

we need to use models which can represent the properties of rock mass and also the presented loads in the construction point (Hoek, Practical Rock Engineering, 2006).

Rock stresses in Scandinavian regions are often influenced by plate tectonics and can variable horizontal to vertical stress ratios; This can result in stress-related problems.

2.3.1.1. World Stress Map

World Stress Map is an accessible map from [WSM website] has been prepared by many geologists and geophysicists from all over the world. The **World Stress Map (WSM)** is a public domain database and visualization tool that represents the contemporary tectonic stress field in the Earth's lithosphere. The map titled "World Stress Map 2025", is a key global resource for understanding crustal mechanics. The map displays the **orientation of the maximum horizontal stress** using color-coded symbols, which are vital for research into plate driving forces, fault mechanics, and the stability of engineered structures (WSM, 2025).

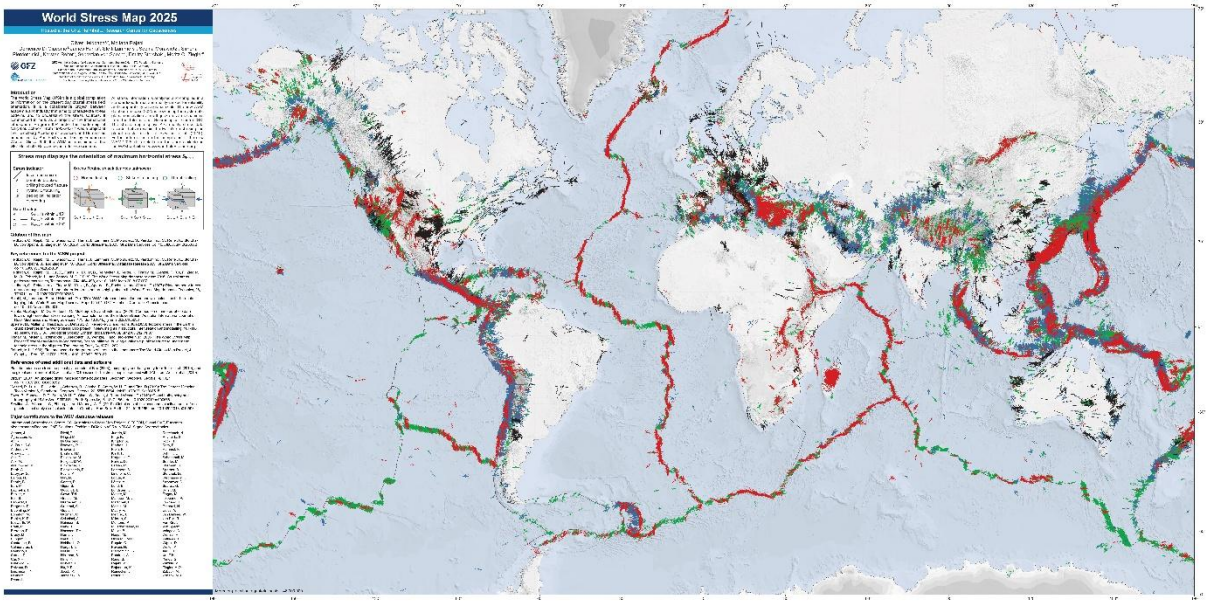

Figure 2-17. World Stress Map (WSM, 2025)

As it was explained before k value is a variable value based on conditions of the project area According to a research on the horizontal-to-vertical stress ratio in Norway, range of stress values based on the amount of overburden, can be observed in the graphs provided (Sanyam & Kirishna, 2025).

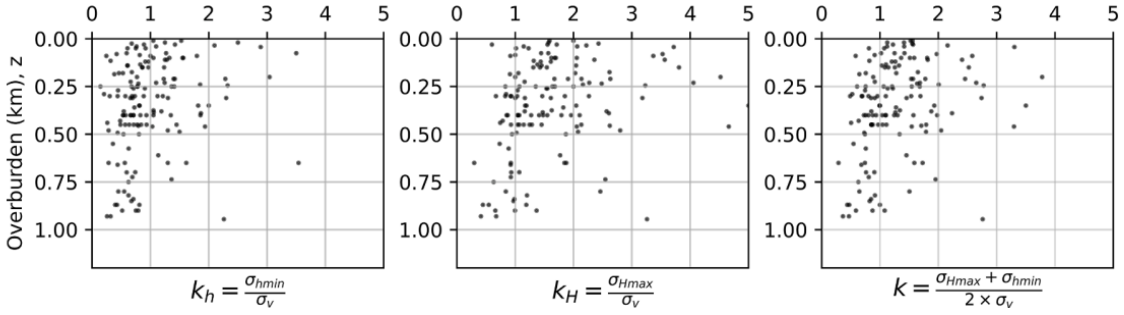

Figure 2-18. Analysis Stress ratio vs Depth in Norway (Sanyam & Kirishna, 2025).

According to Figure 2-18, it can be declared that for overburden higher than 500 m, the range of k value is between 0.5 to 2 (Sanyam & Kirishna, 2025).

2.3.2. Stress in Rock Mass

The behavior of a rock mass is fundamentally different from that of intact rock because once joints, fractures, and other discontinuities are present, the material no longer responds as a single, uniform body. To understand how principal stresses act on such a fractured medium, engineers need to adjust the mechanical properties of the rock mass and use a failure criterion that reflects both the intact rock strength and the influence of discontinuities. This is why rock-mass–based strength models are essential in tunneling and other underground works. The Generalized Hoek–Brown criterion provides a nonlinear way to capture how geological conditions reduce rock-mass strength, while the Mohr–Coulomb criterion offers a simpler linear approximation that is widely used in design analyses to estimate shear failure under stress.

2.3.2.1. Generalized Hoek-Brown Criterion

the Generalized Hoek-Brown failure criterion for jointed rock masses is defined by:

$$\sigma_1 = \sigma_3 + \sigma_{ci}(m_b \frac{\sigma_3}{\sigma_{ci}} + s)^a$$

Where σ_3 and σ_1 are the maximum and minimum effective principal stresses at failure, m_b the value of the Hoek-Brown constant for the rock mass, s and a are constants which depend upon the rock mass characteristics, and σ_{ci} is the uniaxial compressive strength of the intact rock.

For intact rock the value of s is 1 and a is 0.5 and m_b is equal to m_i which is a range of numbers for different rocks (Hoek, Practical Rock Engineering, 2006) (Figure 2-19).

Generally, the constants can be found using GSI and D (blasting disturbance factor, Figure 2-20).

$$m_b = m_i e^{\frac{GSI-100}{28-14D}}$$

$$s = e^{\frac{GSI-100}{9-3D}}$$

$$a = \frac{1}{2} + \frac{1}{6}(e^{\frac{-GSI}{15}} - e^{\frac{-20}{3}})$$

Uniaxial compressive σ_{cm} and tensile strength σ_t of the rock mass are calculated by following equations (Hoek, Practical Rock Engineering, 2006):

$$\sigma_{cm} = \sigma_{ci} \times s^a$$

$$\sigma_t = -\frac{s\sigma_{ci}}{m_b}$$

Rock type	Class	Group	Texture			
			Coarse	Medium	Fine	Very fine
SEDIMENTARY	Clastic		Conglomerates* (21 ± 3) Breccias (19 ± 5)	Sandstones 17 ± 4	Siltstones 7 ± 2 Greywackes (18 ± 3)	Claystones 4 ± 2 Shales (6 ± 2) Marls (7 ± 2)
	Non-Clastic	Carbonates	Crystalline Limestone (12 ± 3)	Sparitic Limestones (10 ± 2)	Micritic Limestones (9 ± 2)	Dolomites (9 ± 3)
		Evaporites		Gypsum 8 ± 2	Anhydrite 12 ± 2	
		Organic				Chalk 7 ± 2
METAMORPHIC	Non Foliated		Marble 9 ± 3	Hornfels (19 ± 4) Metasandstone (19 ± 3)	Quartzites 20 ± 3	
	Slightly foliated		Migmatite (29 ± 3)	Amphibolites 26 ± 6		
	Foliated**		Gneiss 28 ± 5	Schists 12 ± 3	Phyllites (7 ± 3)	Slates 7 ± 4
IGNEOUS	Plutonic	Light	Granite 32 ± 3 Granodiorite (29 ± 3)	Diorite 25 ± 5		
		Dark	Gabbro 27 ± 3 Norite 20 ± 5	Dolerite (16 ± 5)		
	Hypabyssal		Porphyries (20 ± 5)		Diabase (15 ± 5)	Peridotite (25 ± 5)
	Volcanic	Lava		Rhyolite (25 ± 5) Andesite 25 ± 5	Dacite (25 ± 3) Basalt (25 ± 5)	Obsidian (19 ± 3)
		Pyroclastic	Agglomerate (19 ± 3)	Breccia (19 ± 5)	Tuff (13 ± 5)	

* Conglomerates and breccias may present a wide range of m_i values depending on the nature of the cementing material and the degree of cementation, so they may range from values similar to sandstone to values used for fine grained sediments.

* *These values are for intact rock specimens tested normal to bedding or foliation. The value of m_i will be significantly different if failure occurs along a weakness plane.

Figure 2-19. factor of m_i for different rocks (Hoek, Practical Rock Engineering, 2006).

Appearance of rock mass	Description of rock mass	Suggested value of D
	Excellent quality controlled blasting or excavation by Tunnel Boring Machine results in minimal disturbance to the confined rock mass surrounding a tunnel.	D = 0
	Mechanical or hand excavation in poor quality rock masses (no blasting) results in minimal disturbance to the surrounding rock mass. Where squeezing problems result in significant floor heave, disturbance can be severe unless a temporary invert, as shown in the photograph, is placed.	D = 0 D = 0.5 No invert
	Very poor quality blasting in a hard rock tunnel results in severe local damage, extending 2 or 3 m, in the surrounding rock mass.	D = 0.8
	Small scale blasting in civil engineering slopes results in modest rock mass damage, particularly if controlled blasting is used as shown on the left hand side of the photograph. However, stress relief results in some disturbance.	D = 0.7 Good blasting D = 1.0 Poor blasting
	Very large open pit mine slopes suffer significant disturbance due to heavy production blasting and also due to stress relief from overburden removal. In some softer rocks excavation can be carried out by ripping and dozing and the degree of damage to the slopes is less.	D = 1.0 Production blasting D = 0.7 Mechanical excavation

Figure 2-20. disturbance factor D (Hoek, Practical Rock Engineering, 2006).

2.3.2.2. Mohr-Coulomb criterion

If we want to linearize the criterion of the Hoek-Brown, we can set an average of the curves for the values of σ_3 between the tensile stress and the maximum σ_3 by considering two other values of friction angle and cohesion (Hoek, Practical Rock Engineering, 2006).

$$\phi = sin^{-1}[\frac{6am_b(s + m_b\sigma_{3n})^{a-1}}{2(a+1)(2+a) + 6am_b(s + m_b\sigma_{3n})^{a-1}}]$$

$$c = \frac{\sigma_{ci}[(1+2a)s + (1-a)m_b\sigma_{3n}](s + m_b\sigma_{3n})^{a-1}}{(1+a)(2+a)\sqrt{1 + (6am_b(s + m_b\sigma_{3n})^{a-1})/((1+a)(2+a))}}$$

Where $\sigma_{3n} = \sigma_{3max}/\sigma_{ci}$

The Mohr-Coulomb shear strength τ for a given normal stress σ is found by substitution of these values of c and ϕ into the equation:

$$\tau = c + \sigma\, tan\phi$$

The rock mass strength is:

$$\sigma_{cm} = \frac{2c\, cos\phi}{1 - sin\phi}$$

And the relationship between σ_3 and σ_1 is defined by:

$$\sigma_1 = \sigma_{cm} + \frac{1 + sin\phi}{1 - sin\phi}\sigma_3$$

Figure 2-21 shows the graphs of relationship between Major and minor principal stress based on both Hoek-Brown and Mohr-Coulomb criteria. Also Figure 2-22 shows the graph of relationships between normal and shear stress both for the Hoek-Brown and Mohr-Coulomb criterion

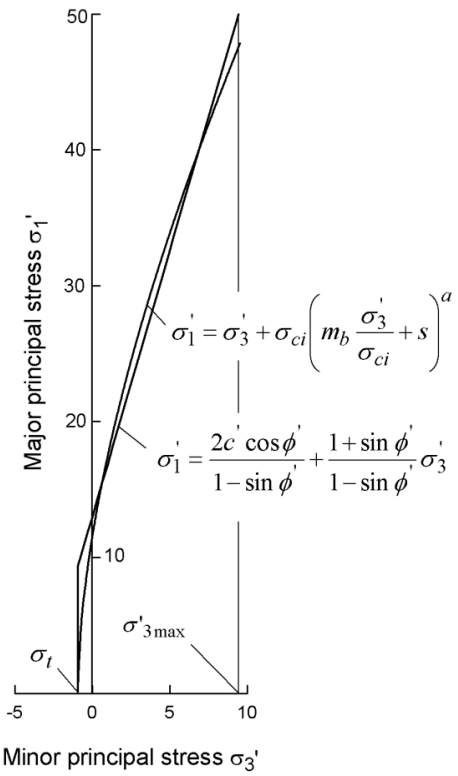

Figure 2-21. Relationships between major and minor principal stresses Hoek-Brown and equivalent Mohr-Coulomb criteria (Hoek, Practical Rock Engineering, 2006).

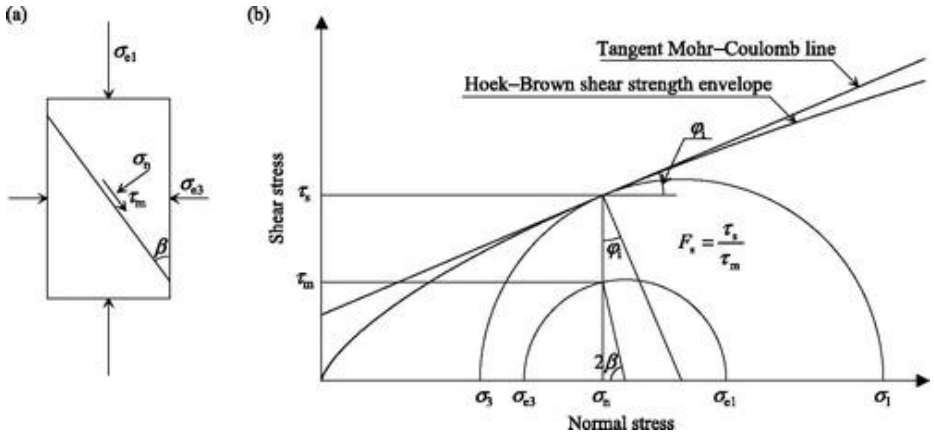

Figure 2-22. Relationships between shear and normal stress based on Hoek-Brown and Mohr-Coulomb criteria (Wei & Fu, 2019).

We can also know the deformability modulus of rock mass by having Young's modulus of the intact rock E_i, using following equation provided by Hoek and Diederichs (Diedrichs & Hoek, 2006).

$$E_{rockmass} = E_i \left(0.02 + \frac{1 - \frac{D}{2}}{1 + e^{\frac{60 + 15D - GSI}{11}}} \right)$$

2.3.3. Stress Redistribution Due to Excavation

Excavation of underground openings alters the equilibrium of the in-situ stress field, producing zones of stress concentration and stress relief around the cavity. The magnitude and pattern of stress redistribution are influenced by multiple factors, including the geometry of the opening, the in-situ stress ratio, excavation sequence, and the mechanical properties of the rock mass.

2.3.3.1. Influence of shape and in situ stress ratio

Graphs in Figure 2-23 illustrate how both the **shape of an underground opening** and the **horizontal-to-vertical in situ stress ratio** influence stress concentrations around a cavern. Each curve corresponds to a different geometry, showing how roof and sidewall stresses increase or decrease as the stress ratio changes (Brown & Hoek, 1980).

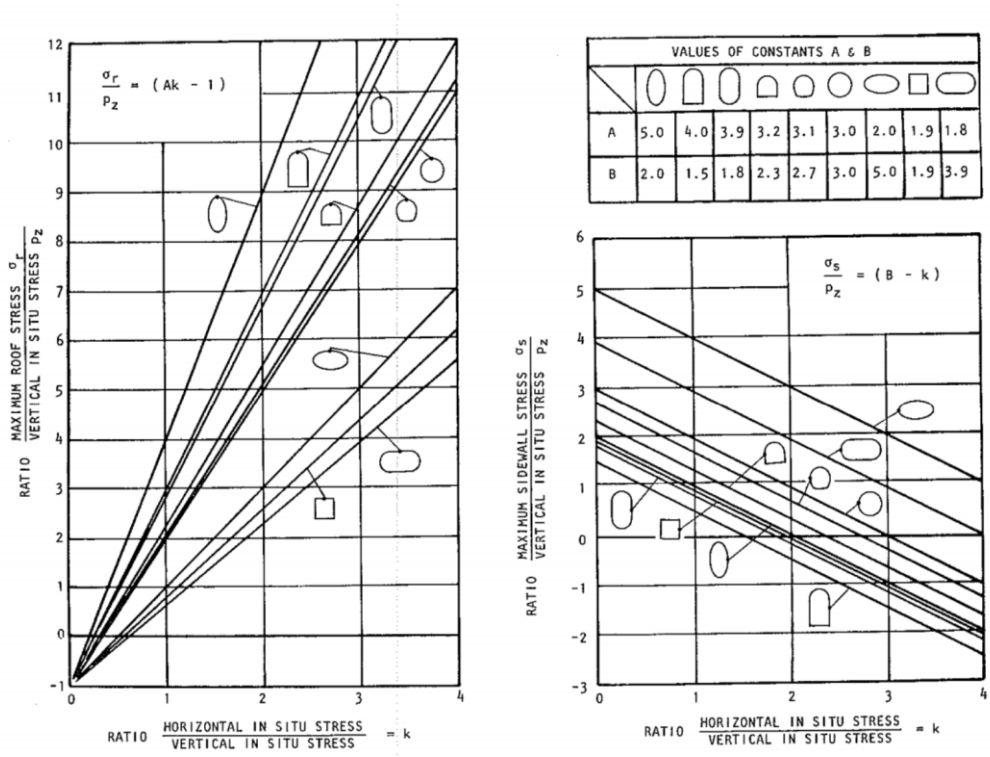

Figure 2-23. Influence of excavation shape and stress ration upon the excavation boundary (Brown & Hoek, 1980).

Understanding these redistribution mechanisms is critical for the safe design and staged excavation of large caverns. For instance, wide caverns tend to experience tensile stresses in the roof when the horizontal stress is low, because the large span reduces the natural arching effect and makes the roof more vulnerable to cracking. As the horizontal stress increases, the roof shifts into compression, which generally improves stability until the compression becomes excessive, at which point spalling may occur in brittle rock. The sidewalls show the opposite trend: at low horizontal stress they carry most of the load and are highly compressed, making them prone to shear failure, while at high horizontal stress they may enter tension and develop cracking or bulging. Overall, wide openings are most stable when the horizontal and vertical stresses are roughly balanced, while very low or very high stress ratios tend to create critical zones either in the roof or in the sidewalls.

2.4. Failure Mechanisms in Rock Caverns

Rock-mass failure can occur through several mechanisms depending on geological conditions, discontinuity patterns, and how the rock mass responds to the stresses redistributed around an underground opening. When a tunnel or cavern is excavated, the removal of material disturbs the in-situ stress field, and the rock mass may fail through shear along joints, tensile fracturing, block or wedge detachment, spalling, or more complex combinations of these processes. Understanding these mechanisms is essential for predicting deformation, designing support, and ensuring excavation stability.

2.4.1. Elasto-Plastic Behavior

Around a tunnel excavation, a **plastic zone** typically forms adjacent to the boundary, surrounded by an **outer elastic zone**, and beyond this the stresses return to their undisturbed in-situ state. The radius of the plastic zone depends on in-situ stress, tunnel size, shape and rock mass strength, and it grows with excavation until support or confinement stabilizes the ground.

2.4.1.1. Elastic Stress Redistribution

In an idealized, homogeneous, isotropic elastic medium, the stress distribution around a circular tunnel can be described using **Kirsch's solution (1898)**. The following figures show the equation of Kirsh for stress in each point around a circular excavated tunnel which expects the present vertical pressure of p (Kirsch, 1898).

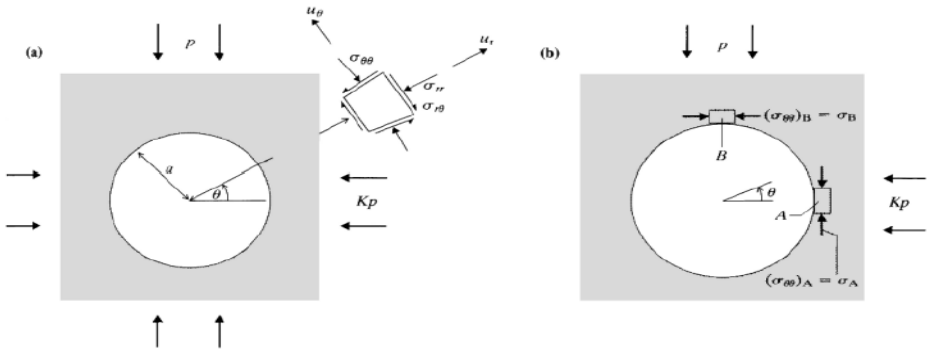

$$\sigma_{rr} = \frac{p}{2}\left[(1+K)\left(1-\frac{a^2}{r^2}\right)-(1-K)\left(1-4\frac{a^2}{r^2}+\frac{3a^4}{r^4}\right)\cos 2\theta\right]$$

$$\sigma_{\theta\theta} = \frac{p}{2}\left[(1+K)\left(1+\frac{a^2}{r^2}\right)+(1-K)\left(1+\frac{3a^4}{r^4}\right)\cos 2\theta\right]$$

$$\sigma_{r\theta} = \frac{p}{2}\left[(1-K)\left(1+\frac{2a^2}{r^2}-\frac{3a^4}{r^4}\right)\sin 2\theta\right]$$

$$u_r = -\frac{pa^2}{4Gr}\left[(1+K)-(1-K)\left\{4(1-\nu)-\frac{a^2}{r^2}\right\}\cos 2\theta\right]$$

$$u_\theta = -\frac{pa^2}{4Gr}\left[(1-K)\left\{2(1-2\nu)+\frac{a^2}{r^2}\right\}\sin 2\theta\right]$$

In these expressions u_r, u_θ are displacements induced by excavation, while $\sigma_{rr}, \sigma_{\theta\theta}, \sigma_{r\theta}$ are total stresses after generation of the opening.

Figure 2-24. Kirsch equations (Kirsch, 1898)

2.4.1.2. Plastic Zone Formation

Plastic zone formation around an underground excavation occurs when the redistribution of stresses caused by excavation exceeds the strength of the surrounding rock. As the opening is created, the radial stress at the boundary decreases while tangential stresses rise, leading the rock near the excavation wall to yield and enter a strain-softening state. This yielded region forms an annular plastic zone whose size and shape depend on the in-situ stress conditions, rock-mass properties, and excavation geometry. Within this zone, the rock undergoes irreversible deformation and a gradual reduction in strength, while still contributing to the overall load-bearing mechanism of the ground. As the stress increase, the plastic zone may expand outward until the rock reaches a residual-strength state, beyond which a broken or loosened zone can develop. Understanding how and when this plastic zone forms is essential for predicting ground response, assessing stability, and designing appropriate support systems for tunnels and pressure conduits (Zhang & Wang, 2009).

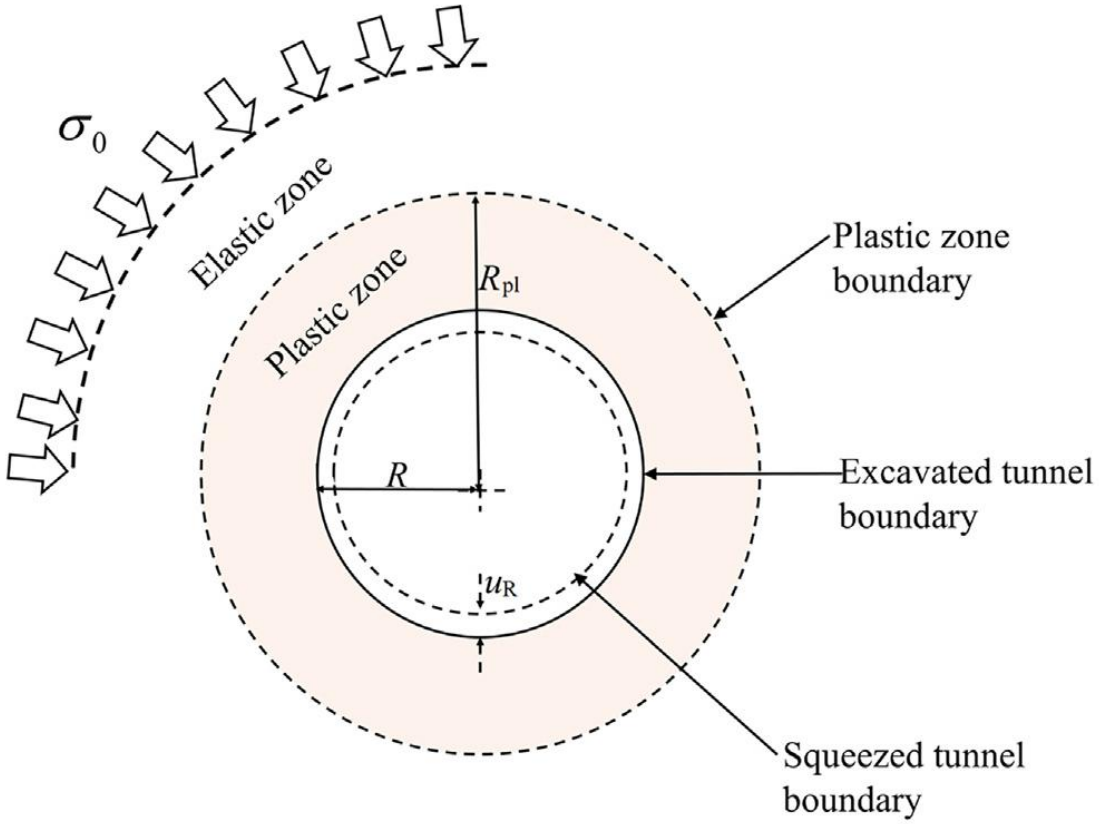

Figure 2-25. Cross-section of a circular tunnel in isotropic in situ stress field and squeezing ground condition. R is the radius of tunnel, R_{pl} is radius of plastic zone, and u_R is the tunnel convergence (Ketan, Gutierrez, & Hedayat, 2020).

2.4.1.3. Convergence-Confinement-Method

The Convergence–Confinement Method (CCM) is a widely used analytical approach for assessing the interaction between ground deformation and tunnel support systems. Tunnel excavation disturbs the initial stress field, producing stress redistribution and inward displacements (convergence) of the tunnel boundary. The CCM addresses this process through

the combination of two fundamental curves: the **ground response curve** and the **support response curve**. The ground response curve (also called the convergence–confinement curve) represents the relationship between the decreasing internal pressure acting on the tunnel boundary and the corresponding radial displacements. Initially, the ground behaves elastically, but as confinement decreases, yielding occurs and a plastic zone develops around the tunnel. The support response curve, on the other hand, expresses the mechanical behavior of the lining system, which may be stiff (resisting convergence strongly) or yielding (allowing larger deformations before taking load) (Panet, Recomendations of Convergence Confinement Method, 2001).

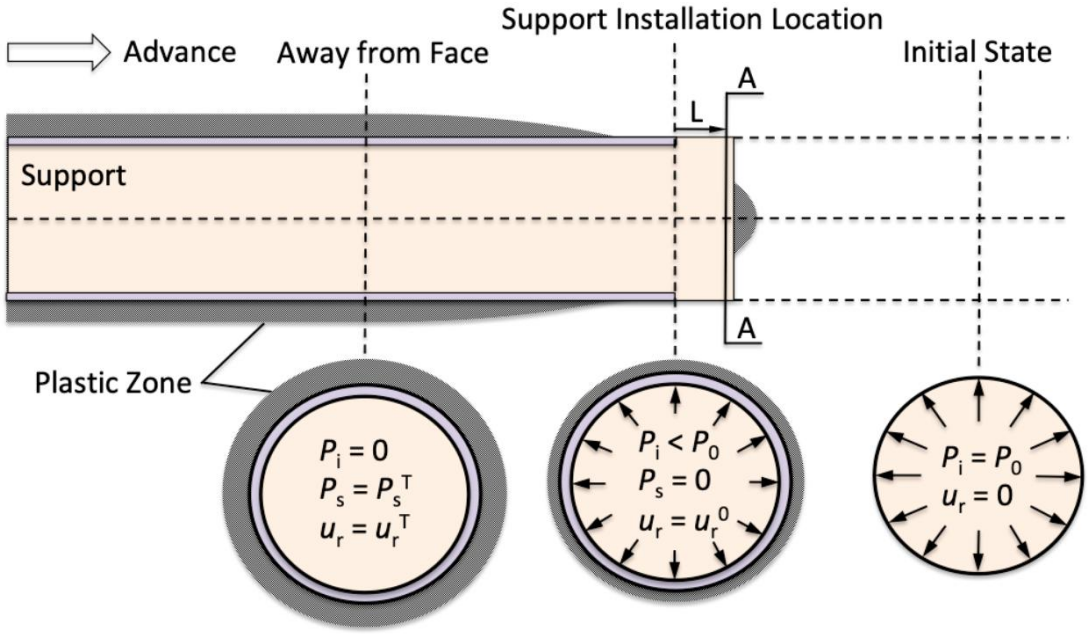

Figure 2-26. plastic Zone formation around the excavation boundary (Vlachopoulos & Su, 2019)

The **main CCM graph** is obtained by plotting both curves on the same axes. The point of intersection defines the **equilibrium state**, corresponding to the final tunnel wall displacement and the pressure carried by the support. If no intersection exists, the system is unstable, while an early intersection in the elastic range indicates an overly rigid and potentially uneconomical design. By interpreting this equilibrium, CCM provides a practical tool for selecting and optimizing tunnel support, ensuring stability while preventing unnecessary overdesign (Panet, Recomendations of Convergence Confinement Method, 2001).

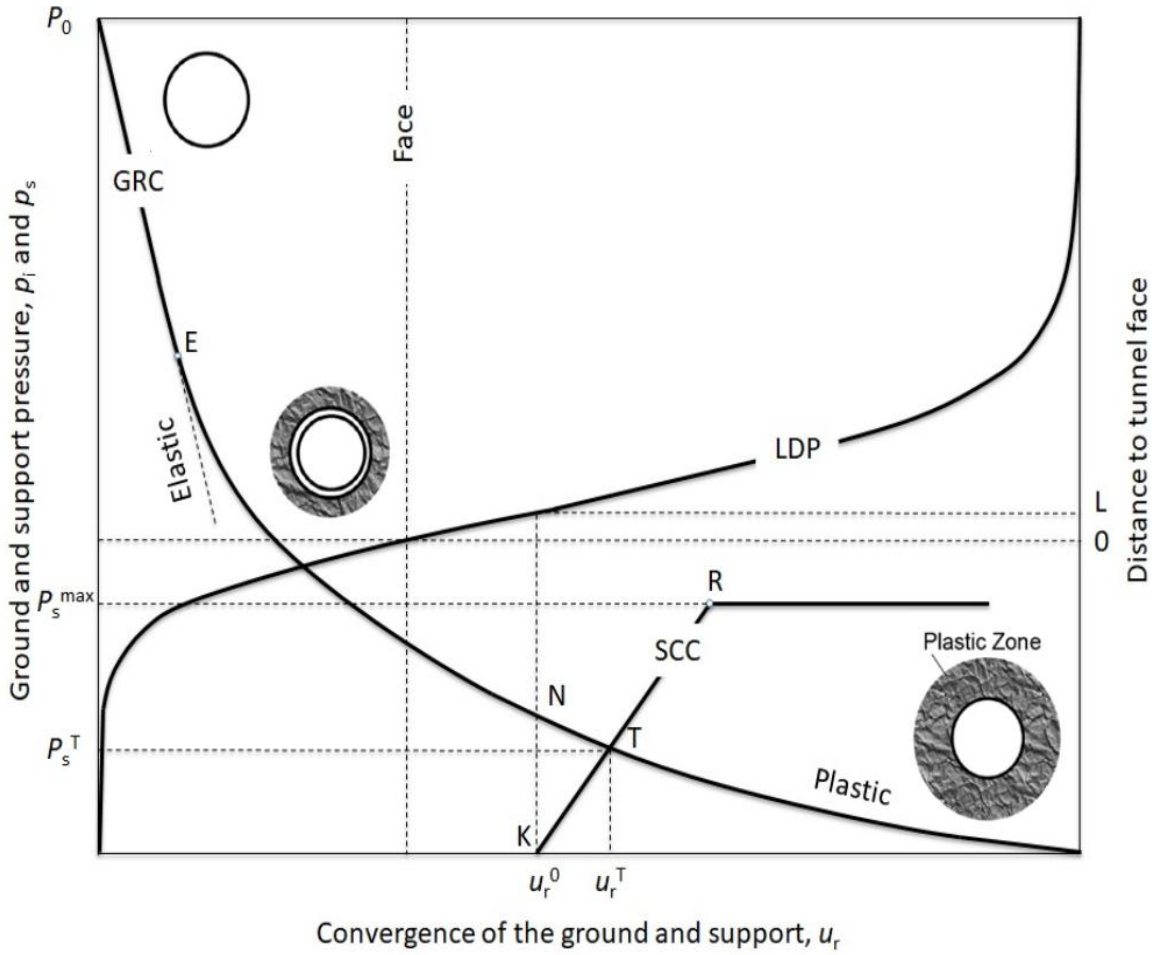

Figure 2-27. Convergence Confinement Method plot (Vlachopoulos & Su, 2019)

The CCM is a widely used method and has been notably reintroduced by many researchers. The **Panet and Guénot method**, **1982** is one of the most significant contributions to this framework, specifically providing the mathematical tools to account for the "three-dimensional effect" of the tunnel face in a 2D model (Panet & Guénot, Analysis of Convergence Behind The Face of A Tunnel, 1982).

Before Panet and Guénot, it was difficult to determine exactly when to "trigger" the support in a 2D simulation. Since the tunnel face provides temporary "fictitious" support, the ground does not collapse immediately upon excavation.

As a tunnel is excavated, the ground ahead of the face and just behind it undergoes deformation. By the time you install support at a distance (x) from the face, the ground has already converged by an amount (u_0). They proposed a widely used empirical equation to calculate the convergence at a distance from the tunnel face (Panet & Guénot, Analysis of Convergence Behind The Face of A Tunnel, 1982).

$$u(x) = u_\infty[1 - \left(\frac{0.75R}{0.75R + x}\right)^2]$$

Where:

- u_∞: The final convergence of the unsupported tunnel at an infinite distance from the face.
- R: The radius of the tunnel.
- x: The distance from the face.

Panet and Guénot also popularized the use of the **de-confinement ratio** or **stress reduction factor** (λ).

$$\lambda(x) = \lambda_0 + (1 - \lambda_0)[1 - \left(\frac{0.75R}{0.75R + x}\right)^2]$$

The Stress reduction factor (λ) will be applied to **Internal Pressure (P_0)**.

$$P_i = \sigma_0\big(1 - \lambda(x)\big)$$

Where σ_0 is the **initial in-situ stress**.

In a 2D Finite Element model:

- $\lambda = 0$: No excavation (full in-situ stress).
- $\lambda = 1$: Full excavation (zero internal pressure).

The method allows engineers to stop the stress reduction at a specific (the "fictitious" pressure) distance from the face to simulate the exact moment the support is installed.

2.4.2. Types of Failure types Induced by Stress

During excavation of a cavern, the local stress distribution is significantly altered, generally exceeding rock mass strength and causing various forms of failure. These failures, which are induced by stress, vary from spalling, rockbursting, squeezing, and shear-induced failure, depending on stress magnitude, rock type, and structural discontinuities. In large caverns, the redistribution of in-situ stress is more pronounced compared to small tunnels because of the greater span and greater volume of excavation, which increase the concentration of stress along the boundary.

Spalling, or slabbing, is a brittle failure that occurs when tangential compressive stresses near the edge of the excavation exceed the rock's tensile strength. It typically manifests as parallel, thin fractures that spall rock layers progressively in the form of slabs. It is most seen in hard, brittle rocks such as quartzite or granite, where low confinement allows the possibility of sudden stress release. Spalling can evolve into severe damage if not identified early, particularly in deep cavities where the tangential stress ratio is high. Its identification through microseismical monitoring or borehole camera permits early remedial measures through the reduction of the excavation rate or the enhancement of support (Pei, 2023).

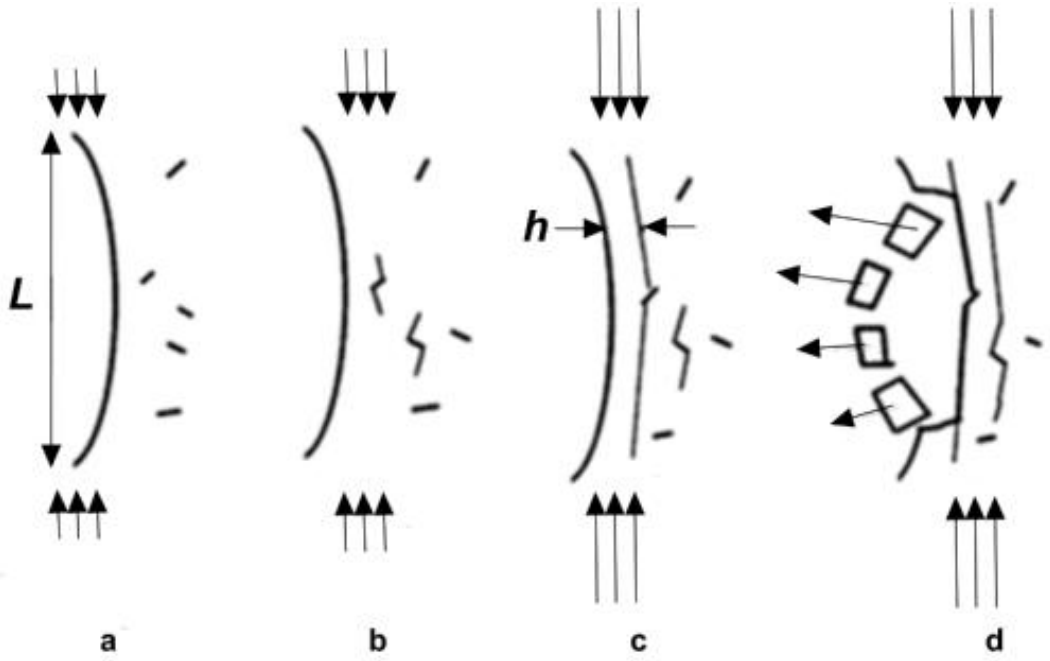

a. Existing microcracks in the rock adjacent to the excavation boundary
b. Propagation of wing cracks from isolated microcracks as stress increases
c. Propagation of wing cracks from microcrack close to excavation boundary due to lack of confinement
d. Buckling failure of spall adjacent to excavation boundary and creation of a new spall due to lateral stress relief

Figure 2-28. Spal formation (Dyskin & Germanovich, 1993).

Squeezing occurs in weak or ductile rocks when the tangential stress exceeds the yield strength of the rock and there is plastic flow towards the excavation cavity. It is common in rocks such as shale, phyllite, or claystone, especially at high depth or high-water content. The deformation develops slowly, and it will continue long after excavation due to time-dependent creep effects. Squeezing will result in excessive convergence and overstress of the support system unless managed by flexible supports and staged excavation. Numerical simulations are required to predict the extent of squeezing and to design suitable countermeasures (Hoek, Big Tunnels in Bad Rock, 2000).

Figure 2-29. Rock squeezing in tunnel boundary (Sulem & manh, 2014).

Rock bursts are sudden, violent failures caused by dynamic energy release from overstressed rock masses. They occur most commonly in deep, high-stress environments and in high compressive strength rocks such as basalt or gneiss. The phenomenon is accompanied by loud noises, dynamic rock ejection, and localized structural damage. Rock burst hazard increases with depth, high tangential stress ratios, and rapid excavation. Its control measures include stress relief drilling, pre-conditioning, and energy-absorbing support systems. Empirical indices and numerical modeling are frequently used to assess the likelihood and intensity of rock bursts in large caverns (Hoek, Big Tunnels in Bad Rock, 2000).

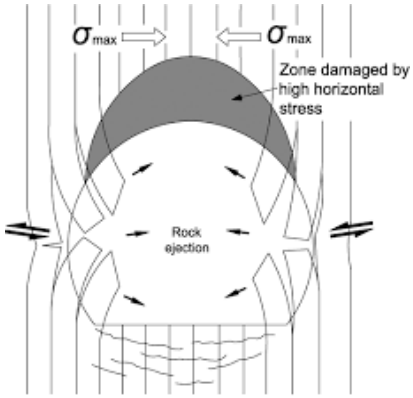

Figure 2-30. Rock burst (Mazaira & Konicek, 2015).

In jointed or fractured rock masses, **wedge and shear failures** are caused by the induced shear stress reaching the shear strength along discontinuities. The geometry and orientation of joints, bedding planes, or faults control the possibility of such failures. Wedge failures are particularly problematic in large caverns with multiple joint sets that intersect and form unstable rock blocks. In contrast to spalling or rock bursting, these failures are structural as opposed to stress-controlled, even though high in-situ stresses can accelerate their development. Analytical and blocky numerical codes such as UDEC and 3DEC are widely used to analyze their stability and design suitable reinforcement.

Large caverns experience combined failure mechanisms rather than a single instability failure mode. For example, spalling may occur in the roof area while squeezing deformation occurs at the sidewalls or floor. Rock lithology change, anisotropy, and stress direction creates such compound interactions more likely. Field observation from hydropower and transport caverns indicates that those composite failures evolve step-by-step with the advancement of excavation. Sequential support and flexible excavation methods are therefore required to manage these evolving stress conditions (Li, 2022).

2.5. Numerical Modeling Approach

Underground excavations rarely exhibit simple geometries. Their shapes are often irregular, and they commonly occur in clusters that form complex three-dimensional configurations. Added to this geometric complexity is the inherent variability of geological conditions: faults, dykes, and other structural features create significant spatial variations in rock mass properties. Because of these factors, closed-form analytical solutions have limited applicability when attempting to predict stresses, displacements, or potential failure mechanisms around underground openings. To address these challenges, a range of computer-based numerical methods has been developed over recent decades, providing practical means for obtaining approximate solutions to such problems.

Domain methods operate by subdividing the rock mass into a collection of geometrically simple elements, each assigned specific material properties. The collective interaction of these elements is used to approximate the overall mechanical response of the rock mass. This approach allows the incorporation of complex, heterogeneous, and non-linear material models.

Finite element (FEM) and finite difference (FDM) methods treat the rock mass as a continuum, whereas the distinct element method (DEM) represents the rock mass as an assembly of discrete blocks. Despite their conceptual differences, FEM and FDM are often similar in practical applications and are therefore commonly discussed together (Hoek, Practical Rock Engineering, 2006).

2.5.1. Finite Element Modeling

In FEM, the problem domain is discretized into elements connected at nodal points. The state of stress and deformation within each element is determined from the conditions at these nodes. This makes FEM particularly effective for modelling heterogeneous or non-linear materials, since each element can explicitly represent the behavior of the material it contains.

The finite element method (FEM) is widely used in rock engineering to analyze the mechanical response of underground excavations. However, FEM faces inherent challenges when modelling infinite or semi-infinite domains, which are typical in underground settings. Because the method requires discretization of a finite region, the analyst must approximate the far-field boundaries of what is an unbounded rock mass.

A common strategy is to extend the model boundaries sufficiently far beyond the excavation so that the imposed boundary conditions do not influence the results within the zone of interest. Alternatively, specialized “infinite” or “far-field” elements can be used, which mathematically extend to infinity and reduce artificial boundary effects. Modern pre- and post-processing tools make it feasible to perform parametric studies to evaluate the sensitivity of results to these boundary approximations.

Discontinuities such as joints can be incorporated explicitly using dedicated joint elements. Although several formulations exist, no single joint-element approach has achieved universal acceptance. Joint interfaces may be assigned general constitutive laws, but this often increases

computational cost depending on the numerical solution technique employed (Hoek, Practical Rock Engineering, 2006).

2.5.1.1. Solution Techniques: Implicit vs. Explicit

Once the model geometry, material properties, and loading conditions are defined, FEM requires redistribution of unbalanced forces to reach a new equilibrium state. Numerical solution algorithms used in FEM fall broadly into two categories: implicit and explicit methods.

2.5.1.2. Implicit (Matrix-Based) Methods

Implicit FEM solvers assemble and solve systems of linear equations using matrix reduction techniques. Non-linear behavior is handled iteratively by updating stiffness matrices (secant methods) or adjusting internal variables (initial stress or initial strain approaches). Because the response of non-linear systems depends on the loading sequence, the total load must be applied incrementally. Each load increment must be sufficiently small to ensure convergence within a reasonable number of iterations. As the degree of non-linearity increases, the required load increments become smaller, leading to more frequent matrix reformations and higher computational cost. For this reason, implicit methods are efficient for linear or moderate non-linear problems but become increasingly expensive for strongly non-linear analyses (Hoek, Practical Rock Engineering, 2006).

2.5.1.3. Explicit (Dynamic Relaxation) Methods

To address the limitations of implicit solvers in highly non-linear problems, explicit solution techniques—particularly the dynamic relaxation method—have been developed. This approach avoids matrix assembly entirely. Instead, unbalanced forces at each integration point generate accelerations according to Newton's second law, expressed in finite-difference form. Incremental displacements are computed, constitutive laws are applied, and the solution advances step by step in time.

Explicit methods naturally accommodate both geometric and material non-linearities with relatively modest additional computational effort. Their computational cost increases only linearly with the number of elements, making them well suited for large-scale, highly non-linear simulations. A practical advantage is that numerical divergence typically manifests as clearly unrealistic physical behavior, making it easier for users, especially less experienced ones to identify modelling issues (Hoek, Practical Rock Engineering, 2006). Following figure depicts an example of 2D FEM modeling.

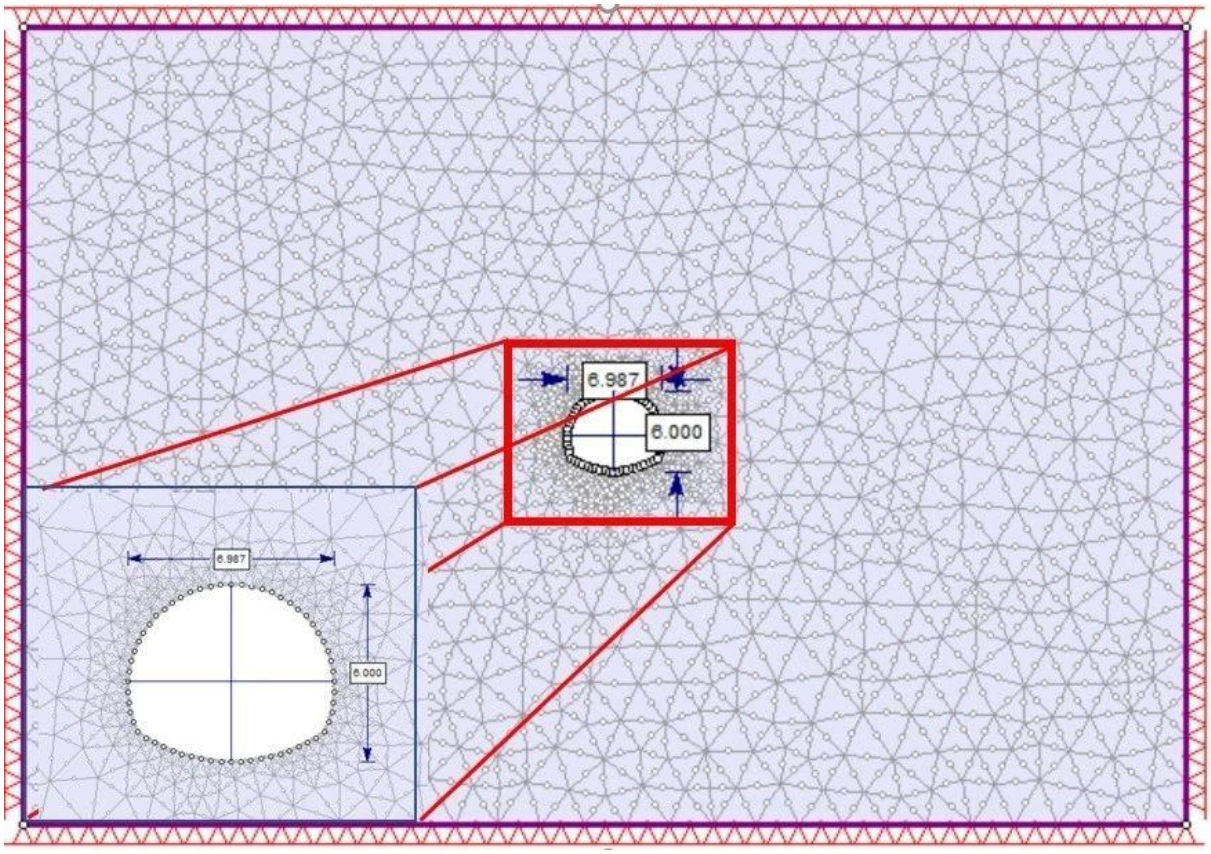

Figure 2-31. Finite Element Method, triangular mesh modeling of the material and excavation boundaries

2.5.2. Practical Considerations

Most commercial finite element packages rely on implicit solvers, which are efficient for linear or moderate non-linear problems. However, as non-linearity intensifies, the need for smaller load increments and repeated matrix reformations makes implicit methods increasingly expensive. In contrast, explicit solvers become more advantageous for strongly non-linear problems, where their robustness and scalability offer significant benefits (Hoek, Practical Rock Engineering, 2006); following picture that has been clipped from Hoek, practical rock engineering handbook , indicates an example of numerical modeling responses for a rock mass with different shapes excavation.

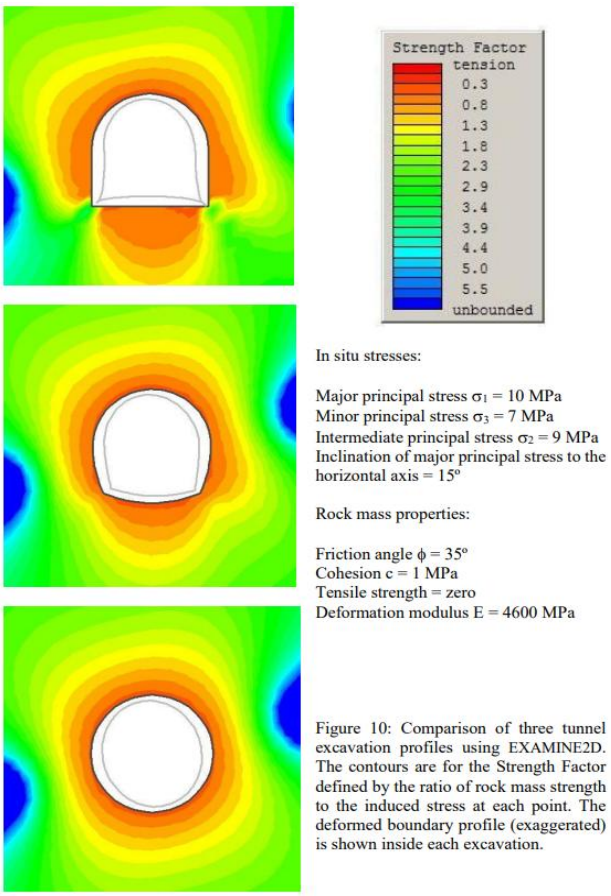

Figure 2-32. Strength factor values around different tunnel shapes (Hoek, Practical Rock Engineering, 2006),

In SEM applications, **Numerical Modeling** is particularly valuable, as it can evaluate how different excavation sequences and shapes affect the evolution of stresses and displacements (Li, 2022) (Wang, 2024).

2.5.3. Support System Interaction

Interaction between the support systems and the rock mass is a key component of numerical modeling. Numerical models simulate how shotcrete, rock bolts, lattice girders or lining systems influence stress redistribution and deformation. Parametric analyses may be able to assess the effects of different support systems and excavation phases on overall stability so that construction techniques can be optimized for economy and safety (Li, 2022).

2.5.4. Applications and Software

In practice, numerical modeling is used both in the **design phase**—to compare excavation methods and optimize supports—and in the **construction phase**, where monitoring results are fed back into the model for back-analysis.

Common tools include **RS2/RS3 (Rocscience)** for 2D and 3D FEM, **PLAXIS** for soil–structure interaction n, **FLAC3D (Itasca)** for large-deformation rock mechanics, and **UDEC/3DEC (Itasca)** for jointed rock masses. These are now standard tools in major tunneling projects worldwide.

2.6. Support Capacity

The concept of support capacity refers to the ability of a tunnel lining or support system to safely resist the loads imposed by the surrounding rock mass after excavation. When a tunnel is created, the in-situ stress field becomes redistributed, and the rock mass tends to deform toward the opening. The role of the support system, whether shotcrete, rock bolts, steel ribs, or reinforced-concrete linings, provide sufficient resistance to these deformations, preventing instability, excessive convergence, or structural failure. Support capacity therefore represents the combined structural strength and deformation tolerance of the support elements, expressed in terms of axial force, bending moment, shear capacity, and allowable strain or displacement (Brown & Hoek, 1980) (Brady & Brown, 2006). Because rock masses behave nonlinearly and are influenced by discontinuities, groundwater, and stress anisotropy, support capacity must be evaluated using analytical, empirical, or numerical methods that reflect the interaction between the rock and the support system (Hoek, Support of underground excavations in hard rock. A.A. Balkema, 1995) (Barton, Engineering classification of rock masses for the design of tunnel support, 1974).

2.6.1. Design Domain and Frameworks

To evaluate whether a lining or support system can withstand the loads imposed by the rock mass, engineers often use interaction diagrams or capacity domains. These diagrams graphically represent the combinations of axial force, bending moment, and sometimes shear force that a support element can safely resist. Several widely used frameworks exist:

2.6.1.1. Carranza-Torres & Diederichs Support Capacity Domain

This method provides a unified, tunnel-specific N–M–T capacity domain for linings subjected to ground pressure, derived from elastic–plastic analysis of circular tunnels It is particularly suited for numerical-model outputs, where axial force, bending moment, and shear force are obtained directly from the lining elements.

2.6.1.2. Eurocode 2 / Eurocode 7 Interaction Domains

Eurocode-based design uses axial force–bending moment (N–M) interaction curves derived from reinforced-concrete theory. These curves define the ultimate capacity of concrete sections under combined loading, accounting for reinforcement ratio, concrete strength, and ductility. (In tunneling, Eurocode 7 complements this by requiring geotechnical verification of ground structure interaction.

2.6.1.3. ACI and Classical Reinforced-Concrete Interaction Diagrams

The American Concrete Institute (ACI) provides similar N–M interaction diagrams for reinforced-concrete sections, widely used in underground structures in North America These diagrams are based on strain compatibility and nonlinear stress–strain relationships.

2.6.2. Carranza-Torres & Diederichs Domain

The Carranza-Torres domain is a graphical representation of the structural capacity of tunnel linings under combined axial force, bending moment, and shear. It was developed to bridge the

gap between classical reinforced-concrete design and the specific loading conditions encountered in underground excavations (Carranza-Torres & Diederichs, 2009).

The concept proposed a method to evaluate the **interaction between the rock mass and the lining**, using a capacity domain that defines the safe combinations of:

- Axial Force (N)
- Bending Moment (M)
- Shear Force (T)

The domain is constructed using reinforced-concrete theory (strain compatibility and nonlinear material behavior) but adapted to the **curved geometry and loading conditions** typical of tunnel linings.

The domain is generated by:

- Defining the reinforced-concrete section geometry and material properties.
- Applying strain-compatibility and nonlinear constitutive laws.
- Computing ultimate capacity for multiple combinations of N, M, and T.
- Plotting the resulting envelope in 2D space.

Applications

- Design of reinforced-concrete tunnel linings.
- Verification of numerical-model outputs.
- Assessment of lining performance under asymmetric loading.
- Comparison of different reinforcement layouts.

2.6.2.1. Capacity Diagrams

The graphical representation of the axial thrust and bending moment induced in a tunnel liner, plotted together with the corresponding failure envelope that defines the maximum allowable combinations of these forces, is known as a thrust–bending moment interaction diagram. In a similar way, plotting axial thrust against shear force, along with its associated failure boundary, produces a thrust–shear force interaction diagram. In structural and concrete engineering, these diagrams are collectively referred to as support capacity diagrams. They serve as practical tools for tunnel-liner design because they allow engineers to quickly assess whether the forces acting on the lining remain within safe limits or exceed the structural capacity of the support system. Over the years, several researchers and practitioners have adapted these diagrams specifically for tunnel applications, demonstrating their usefulness in evaluating liner performance under complex loading conditions (Carranza-Torres & Diederichs, 2009). Figure 2-33 shows example of an excavated tunnel in a rock mass; further figures show graphs to represent the axial force, bending moment and other data of the lining in support capacity based on Carranza-Torres & Diedrichs approach.

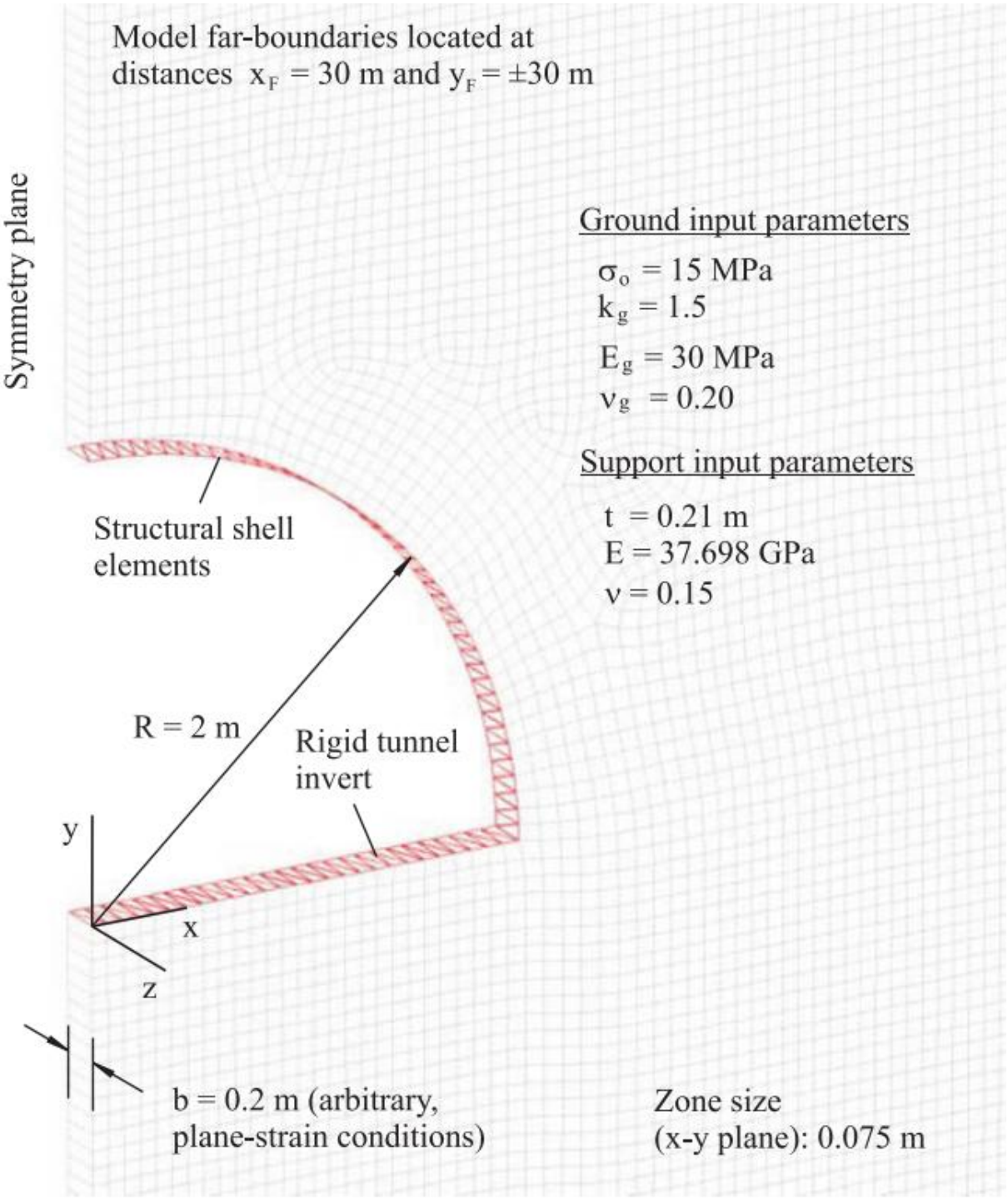

Figure 2-33. Example of a numerical modeling of rock mass under a tunnel excavation (Carranza-Torres & Diederichs, 2009)

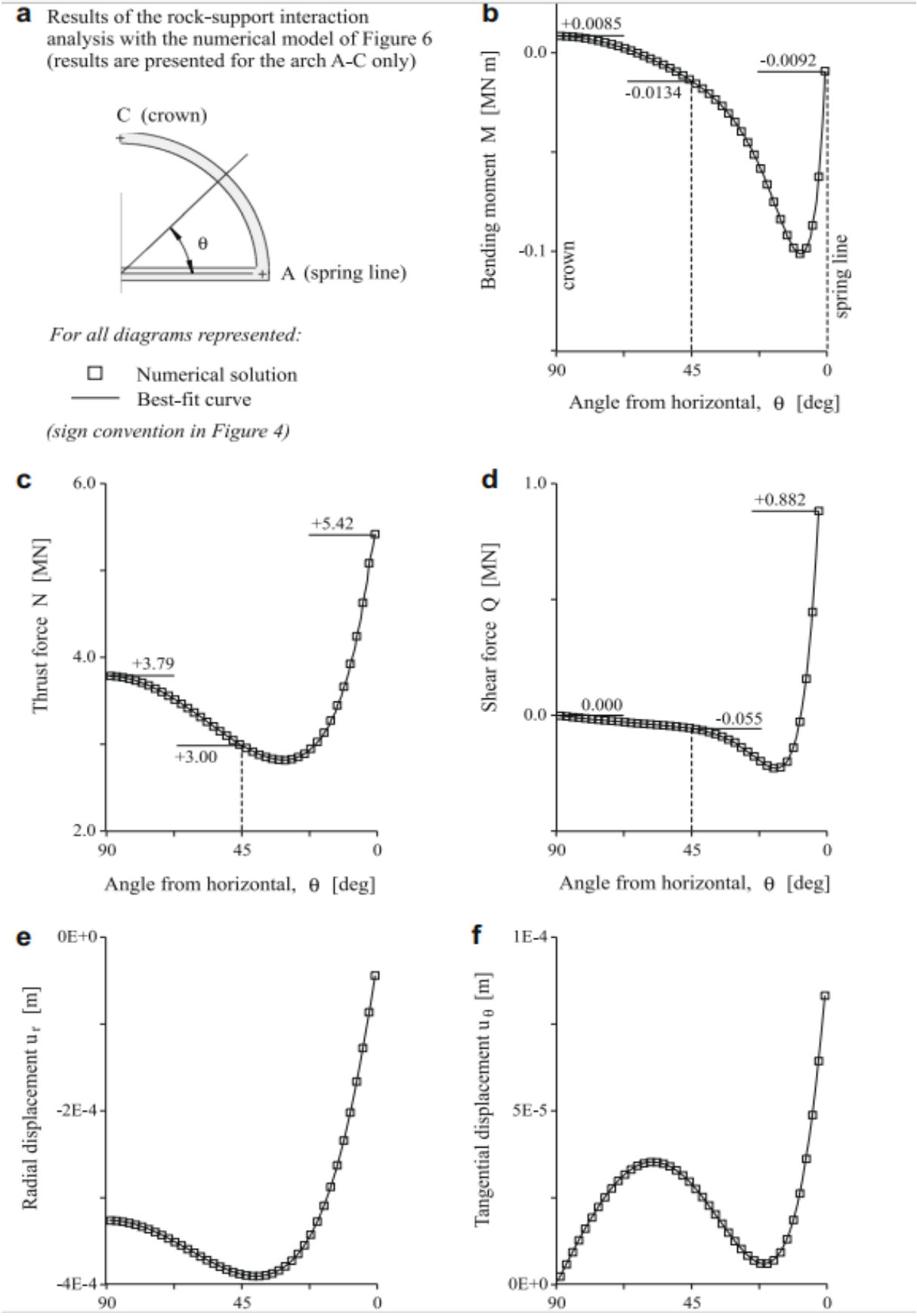

Figure 2-34. Graphical representation of results obtained with the ground-support interaction approach. (a) Description of information represented. Results for (b) bending moment, M, (c) thrust force, N, (d) shear force, Q, (e) radial displacement, u_r and (f) tangential displacement, u_θ (Carranza-Torres & Diederichs, 2009).

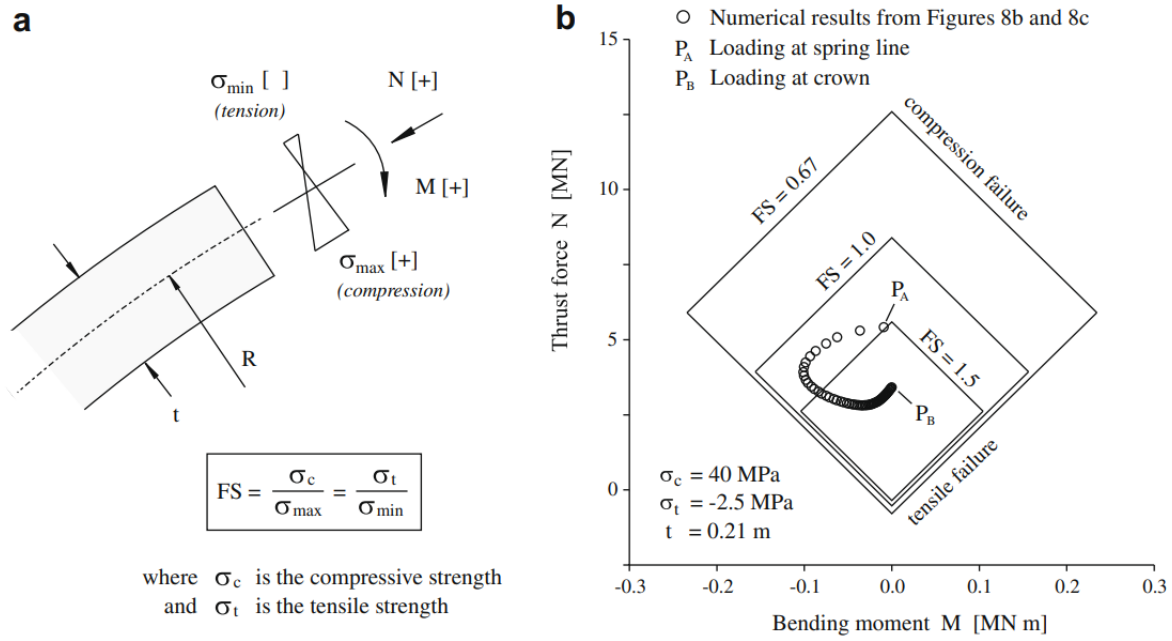

Figure 2-35. (a) Factor of safety (FS) defined in terms of maximum and minimum axial stresses on a section of circular arch. (b) Graphical representation of results from the ground support interaction analysis of the Section, in a thrust–bending moment interaction diagram (Carranza-Torres & Diederichs, 2009).

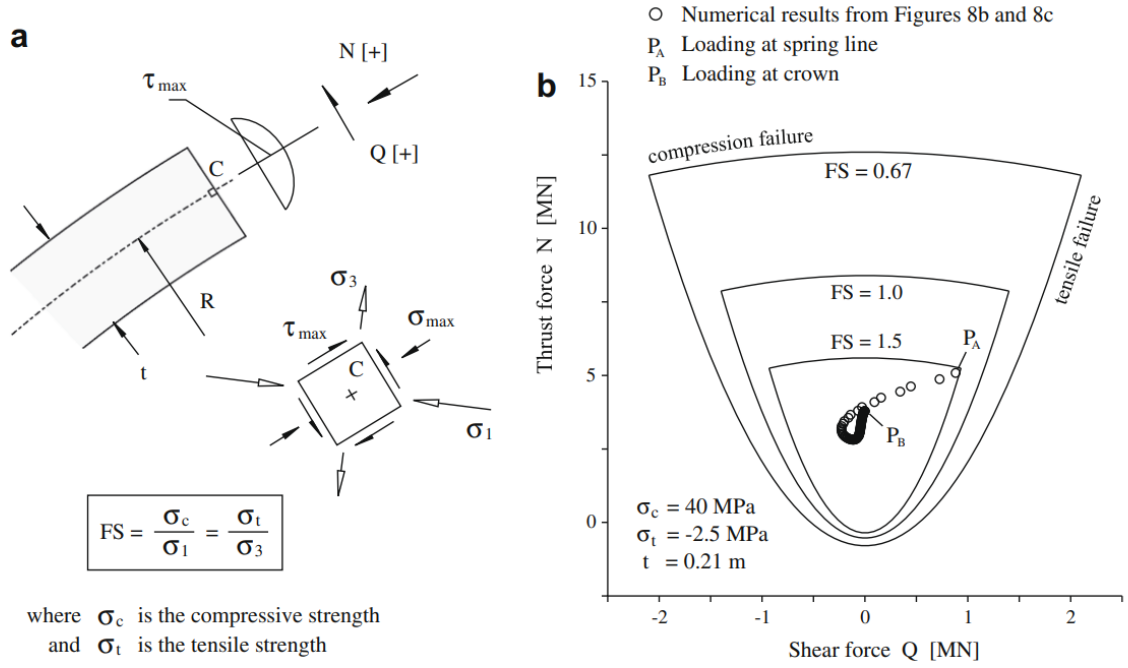

Figure 2-36. (a) Factor of safety (FS) defined in terms of major and minor principal stresses induced by thrust and shear forces on a section of circular arch. (b) Graphical representation of results from the ground-support interaction analysis of the Section, in a thrust–shear force interaction diagram (Carranza-Torres & Diederichs, 2009).

Diagrams and the graphs above indicate the support capacity of the Concrete material in Reinforced concrete lining; This kind of lining includes steel rebars too that can be verified with same approach; results are presented in the following figures.

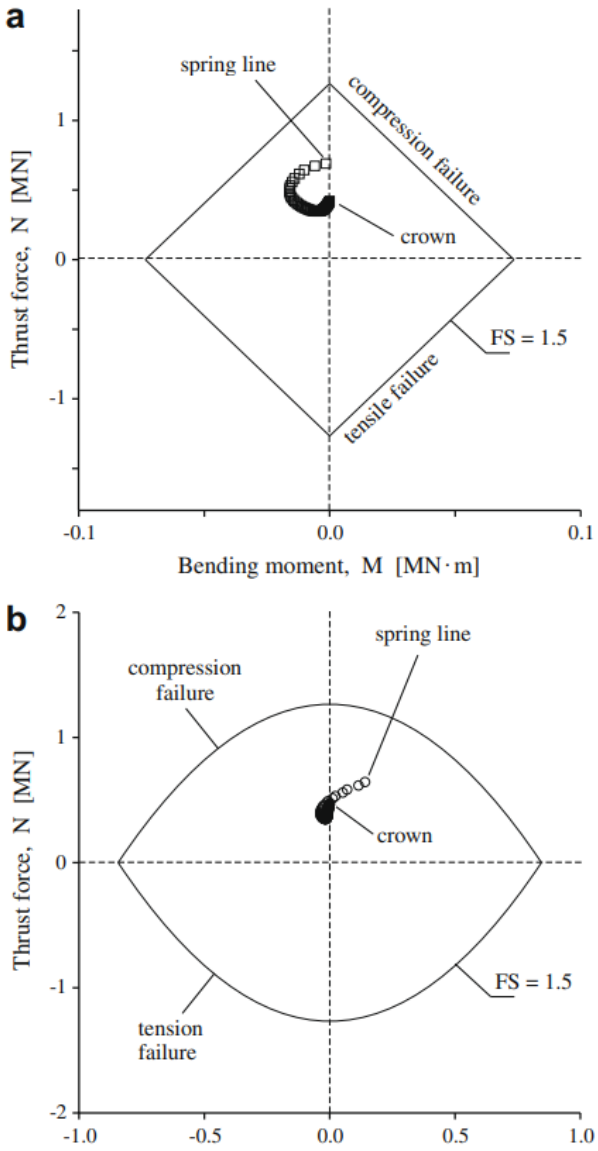

Figure 2-37. Capacity with Safety factor equal to 1.5 for the steel rebars inside the reinforced concrete (Carranza-Torres & Diederichs, 2009).

By using capacity diagrams, it becomes possible to check whether the selected lining system can safely withstand the axial forces, bending moments, and shear forces imposed by the rock mass in a considered value of Safety Factor without failing. Dividing the lining into segments and evaluating the induced loads on each portion provides a conservative assessment, ensuring that every point along the lining is verified even in complex loading conditions.

2.7. Similar Case-Studies in Norway

The development of underground space in Norway, particularly for large-span openings, stems from a long history rooted initially in the hydropower sector and later expanded to urban infrastructure, storage, and public-use facilities. Norway's geology, dominated by Precambrian and Paleozoic hard rocks, favors this underground utilization. The fundamental approach is often associated with the **Norwegian Method of Tunnelling (NMT)**, emphasizing a design that exploits the rock mass's inherent capacity for self-support (NTS, Norwegian Rock Caverns, 2016).

Here are some examples of the similar research and projects that has been done in Norway.

2.7.1. Gjøvik Olympic Ice Hockey Cavern

The Gjøvik Cavern, constructed for the 1994 Winter Olympics, represents one of the world's largest spans for public-use excavations, with a span of 62m (NTS, Norwegian Rock Caverns, 2016).

Figure 2-38. Gjøvik Olympic Ice Hockey cavern (NTS, Norwegian Rock Caverns, 2016)

Geology: The cavern is in a jointed gneiss of fair quality, with an average RQD 67% and Q-values ranging from 1 to 30 (weighted mean of about 9).

Shallow Cover & High Stress: It has a relatively shallow rock cover of only 25 to 50m. Its stability was significantly enhanced by high horizontal stress, which contributed to reduced deformation.

Performance: Predicted maximum deformations were 4 to 8 mm. Measured maximum deformations, taken after the cavern was fully excavated, ranged from 7 to 8 mm closely matching predictions.

Support: Permanent support consisted of 10 cm wet process steel fiber reinforced shotcrete, and systematic intentioned, fully grouted bolting and cable bolting.

2.7.2. Holmestrand Underground Railway Station

The Holmestrand station is unique, featuring a large station hall with a 550 m^2 cross-section and 35 m width, designed to accommodate trains traveling at 250 km/h (NTS, Norwegian Rock Caverns, 2016).

Figure 2-39. Holmestrand underground highway station (NTS, Norwegian Rock Caverns, 2016)

Challenges: The project faced challenges due to the large span, a low rock overburden (as little as 6m in some areas), and the intersection with a major 15m wide fault zone containing clay.

Reinforcement: Due to the low cover and strict waterproofing requirement of per 100 m of tunnel, extensive measures were necessary like Systematic Pre-injection High-pressure grouting (45–90 bar) was used, with long 22.5 m grouting fans to achieve overlap. Long Bolts Rock anchors up to 12 m long, developed in collaboration with a supplier (CT-bolt), were installed.

Excavation through Fault: The major fault zone crossing required reduced blasting rounds 2.5 m spiling (self-drilling hollow bars), lattice girders, and reinforced sprayed concrete lining for stability.

2.7.3. Høvringen Underground Sewage Treatment Plant, Trondheim

Geology: Located in competent gneissic rock with predictable jointing; three caverns with 15 m spans and a total excavated volume of ~10 000 m^3.

Function: Houses trash racks, sand traps, fat skimmers, and later chemical treatment, all underground to reduce environmental impact.

Performance: Over 90% of Trondheim's sewage is treated underground, with no nuisance to the marine environment due to deep outfall and stratification.

Support: Systematic bolting and shotcrete in areas with jointed rock; stable long-term performance with minimal deformation.

Special Feature: Excavated rock was reused in urban construction, improving project sustainability.

Figure 2-40. Høvringen Underground Sewage Treatment Plant, Trondheim (NTS, Norwegian Rock Caverns, 2016)

2.7.4. Industrial and Municipal Caverns

Norwegian expertise extends to a variety of other purposes (NTS, Norwegian Rock Caverns, 2016):

Boliden Odda Waste Disposal: Caverns up to 60 m high and 25 m wide were excavated for storing jarosite residue35. The design evolved over time to increase efficiency by using very high caverns to achieve self-compaction of waste and lower cost per cubic meter. The excavation confirmed a positive water gradient directed into the drained caverns, helping to isolate the waste.

Ulriken Water Treatment Plant: This plant exemplifies the successful underground siting of municipal infrastructure near the city center of Bergen. The construction was complicated by the need to conduct a breakthrough blast underwater to connect the intake line to Lake Svartediket, the water source.

Hydropower (Lysebotn II): This project involves a main cavern 20 m wide and 35 to 40 m high with an overburden of 650m. Due to expected high tangential rock stresses, the support system—consisting of fiber-reinforced shotcrete and end-anchored (flexible) rock bolts—was designed to allow a degree of yielding to prevent overstressing and rock burst intensity, a key adaptation to high in-situ stress regimes.

2.7.5. Core Design and Engineering Principles

Common principles that were presented in the case studies are presented below.

2.7.5.1. The Philosophy of Self-Support

The basic design concept in Norway is to view the rock mass as a self-supporting material. Consequently, the purpose of rock support is to enable and reinforce this self-supporting capability, rather than creating a separate, load-bearing structure to contain a "passive rock mass". This philosophy leads to a preference for flexible support systems (NTS, Norwegian Rock Caverns, 2016).

2.7.5.2. Investigation and Modeling

Detailed investigation is paramount, as deviation from assumed ground conditions is a leading cause of cost and schedule overruns in underground projects (NTS, Norwegian Rock Caverns, 2016).

- **Rock mass classification:** Generally, the Q-system that has been introduced in the previous parts is used and trusted for rock mass classification for Norwegian tunneling projects.
- **Stress Measurement:** In-situ rock stress measurements are critical, especially for large spans and deep excavations. Common methods employed include over-coring (2-D and 3-D) and hydraulic fracturing. High horizontal stress is often a favorable factor for cavern stability, causing reduced deformation.
- **Numerical Modeling:** Finite Element Method (FEM) is employed for complex designs to extrapolate empirical experience and predict rock mass behavior, guiding stability and support design. These models must be continuously calibrated with monitoring data.

2.7.5.3. Cavern Geometry and Layout

The preferred shape for a cavern is generally simple and rounded with an arched roof to promote evenly distributed compressive stresses (NTS, Norwegian Rock Caverns, 2016).

- **Arch Dimension:** A roof arch height of approximately one fifth of the span is commonly chosen for stability.
- **Orientation:** The cavern's longitudinal axis is ideally oriented favorably relative to the major joint systems and the major principal stress direction to maximize stability.
- **Pillar Design:** In multi-cavern layouts, such as for the Lysebotn II power station 17, pillars are typically designed such that vertical separation is no less than the largest span or height of the adjacent caverns, often avoiding separations of less than 20m.

2.7.5.4. Excavation and Support

Excavation is typically performed in stages, starting with the top heading and then proceeding with benching (NTS, Norwegian Rock Caverns, 2016).

- **Primary Support:** Permanent rock reinforcement, largely consistent with NMT, includes systematic bolting and wet process steel fiber reinforced shotcrete.
- **Water Control:** Preventing water ingress is vital, particularly in facilities like water treatment plants or railway stations. Pre-injection (grouting) is the main method, often systematic and using high pressures (e.g., 45–90 bar at Holmestrand) to meet strict waterproofing requirements (e.g., 5 l/min per 100 m).

2.7.5.5. Pre-Excavation Rock Joint Grouting

Pre-excavation rock grouting is a core element of Norwegian tunnelling practice, used to control groundwater inflow and stabilize fractured hard-rock masses during the construction of tunnels, caverns, and hydropower facilities (NTS, Rock Mass Grouting by Norwegian Tunneling Society, 2011).

Norway's granitic and gneissic rocks contain joints, faults, and sheared zones that create highly variable hydraulic conditions, making systematic pre-grouting essential for limiting water ingress and reducing environmental impacts. Cement-based grouts—ranging from standard industrial cement to micro- and ultrafine cements—are the primary materials, supplemented when needed by colloidal nano-silica for fine fissures and chemical resins for acute leakage (NTS, Rock Mass Grouting by Norwegian Tunneling Society, 2011). The procedure typically includes geological and hydrogeological mapping, drilling overlapping grout holes, controlled high-pressure injection, and continuous monitoring through permeability tests and detailed logging. Modern Norwegian practice emphasizes advanced equipment, strict HSE standards, and documentation, with grout pressures reaching up to 100 bar and target permeabilities commonly reduced to 10^{-7}–10^{-8} m/s. Overall, rock-mass grouting in Norway is a highly developed, data-driven, and environmentally focused discipline that sets a benchmark for underground engineering worldwide (NTS, Rock Mass Grouting by Norwegian Tunneling Society, 2011).

Chapter 3. Description of the Case Study

As it was mentioned in Chapter 1. Introduction, this study is inspired by engineering challenges in a tunneling project in Norway; This case study requires excavation of large span Cavern in a poor Rock mass classified with Q-system under high overburden. At the same time of developing this thesis, there was an ongoing tunneling project in Røldal region, Norway and it has been decided to carry out this analysis based on that case study.

3.1. Geometry of Cavern

Geometry of this cavern is almost a semi-oval with a curved invert; Height of this cavern (distance between center of invert and center the crown) is 11 m and the span (width) is 30 m (Figure 3-1).

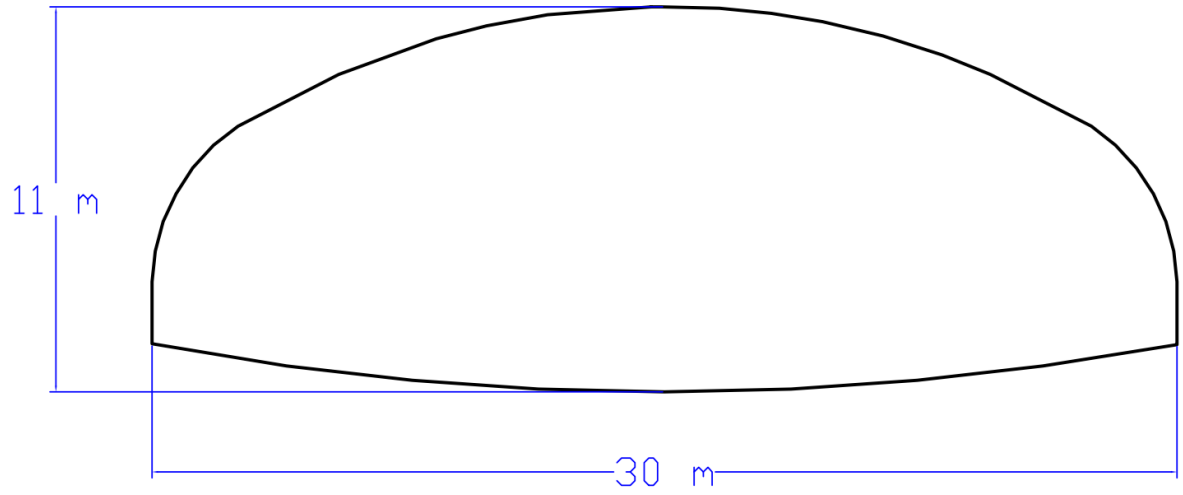

Figure 3-1. Geometry of the Cavern

Although this geometry illustrates an unusual shape for design and construction of a cavern by having a span three times bigger than height, this shape is common geometry of the cavern in tunneling projects in Norway as it was mentioned in Similar Case-Studies in Norway section in Chapter 2.

The Cavern must be excavated with Sequential Excavation Method (SEM) to keep stability and safety of the procedure in controlled condition.

3.2. Geology of the Reference Region

Geological map of the region has been achieved from the existing map that was clipped from the NGU's bedrock map provided in the Geological Survey of the Norway website (NGU, 2025); Following image is clipped from the online bedrock map in the website.

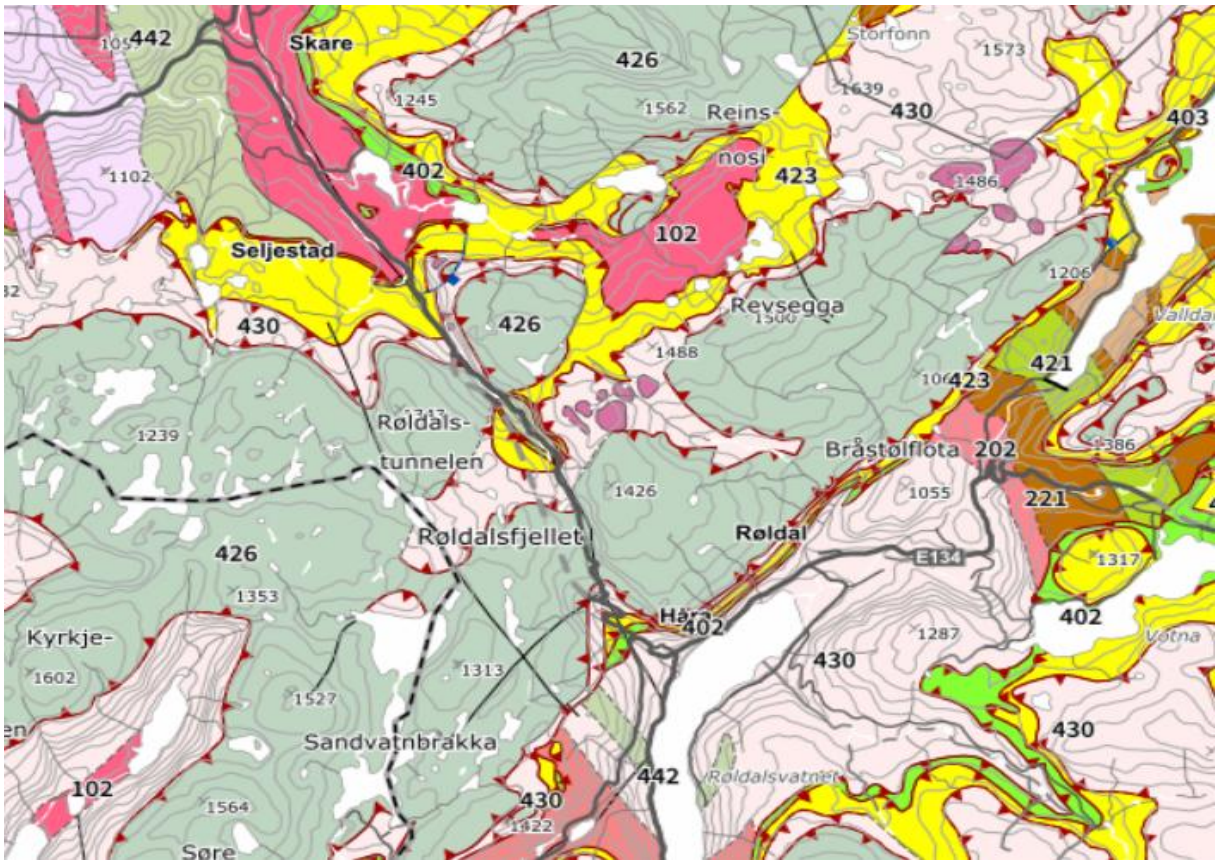

Figure 3-2. Map of bedrock in the region that case study took place; Clipped from Geological Survey of Norway website (NGU, 2025).

Figure 3-3. Legend of the Map provided in Figure 3-2 (NGU, 2025).

As is observed in Figure 3-2 and Figure 3-3, most common rock type is 426 and 430 categories that represent **Gneissic rock**.

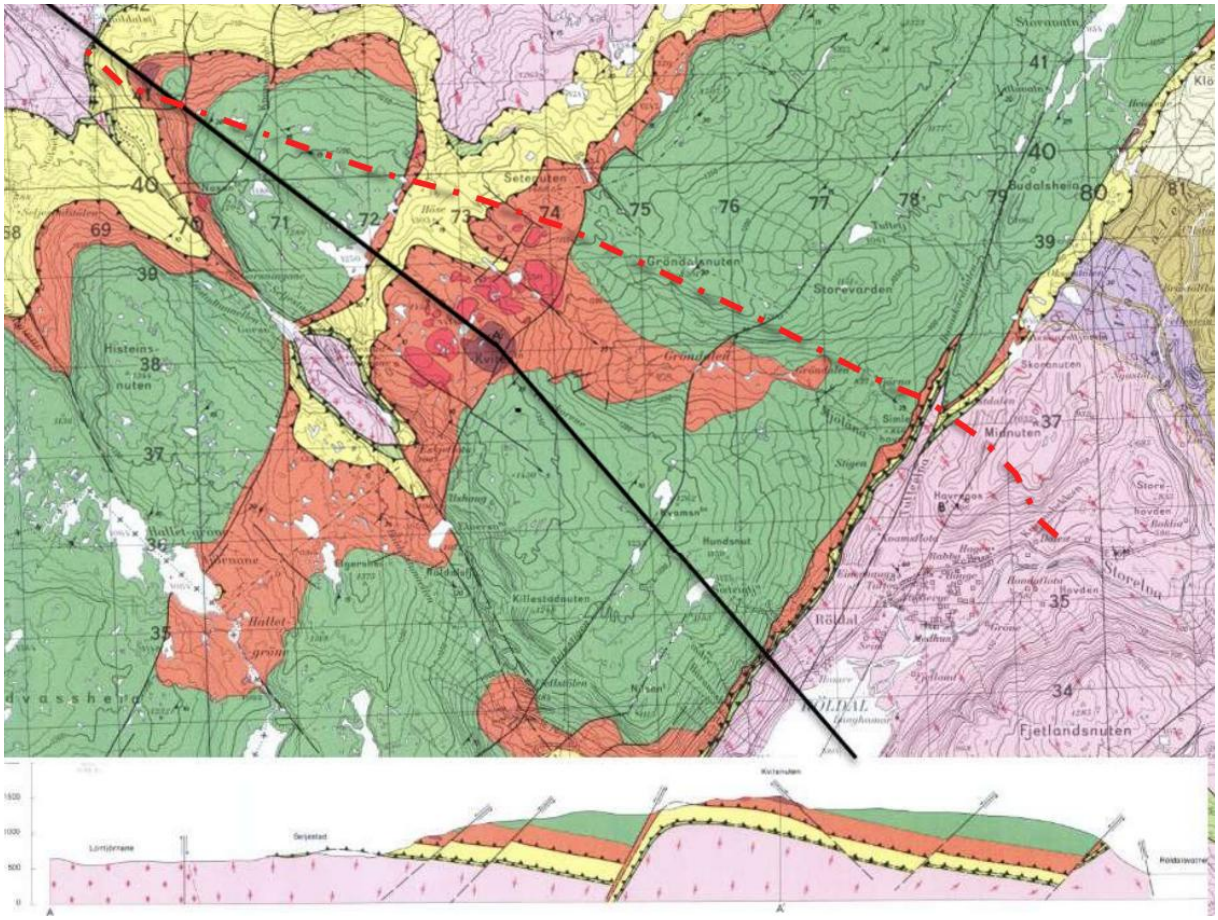

Figure 3-4. clipped from the NGU's bedrock map (NGU, 2025)

Figure 3-4 represents the cross section of the old Røldal tunnel project that was constructed in 1964 indicating in depth higher than 500 the main rock to be excavated is Gneiss. However, there is very limited geological information available, based on the bedrock maps available, it can be approximated that properties of **Gneiss** can be assumed in

The region of the case study lies within a mountainous region with significant topographic variation, the maximum rock cover above the cavern was estimated to be approximately **650 m**. To ensure a conservative and broadly applicable assessment, this maximum value was adopted as the overburden in all evaluations.

3.2.1. In-situ stress Condition

Rock stresses in Scandinavian regions are strongly influenced by ongoing tectonic processes, which often lead to highly variable horizontal-to-vertical stress ratios. Because of this natural variability, stress-related challenges are common in Norwegian tunneling projects. Determining an exact numerical value for the horizontal stress ratio is not possible without detailed laboratory testing or in-situ stress measurements, and therefore a range of stress regimes must be expected.

As previously discussed, the value of k depends heavily on local geological and tectonic conditions. Research conducted in Norway shows a wide spread of stress ratios with depth, as illustrated in the provided figure below (Sanyam & Kirishna, 2025). According to these data, for overburden depths greater than 500 m, the observed k values typically fall between 0.5 and 2.

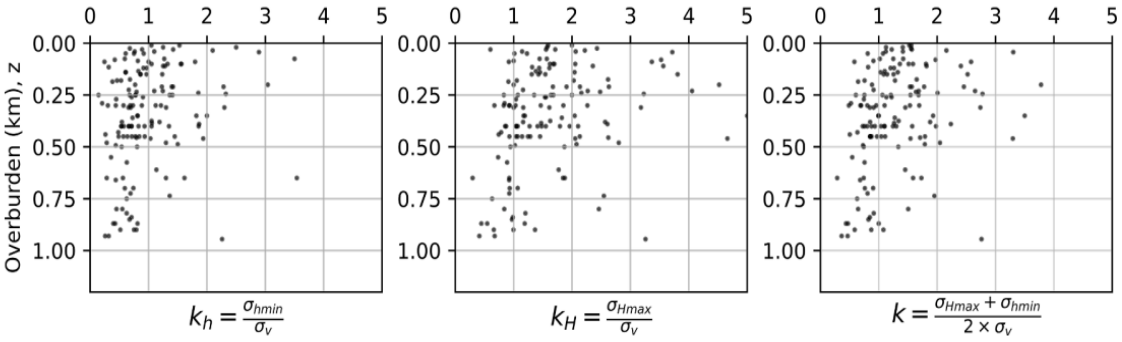

Figure 3-5. Analysis Stress ratio vs Depth in Norway (Sanyam & Kirishna, 2025)

Based on this variability, and to ensure a comprehensive and conservative evaluation applicable to different possible stress conditions, three representative values **0.5, 1, and 2** are adopted in this study.

3.2.2. Rock Mass Classification, Q-system

As it was mentioned in first and second chapter that according to the Norwegian tunneling society regulations, Q-system is implicated in tunneling projects in Norway (NTS, Norwegian Rock Caverns, 2016); In Figure 3-6, the Q-system chart has been classified by different colors to show range of Q value and assumption of RMR values achieved for them using empirical formulas (NGI, 2025).

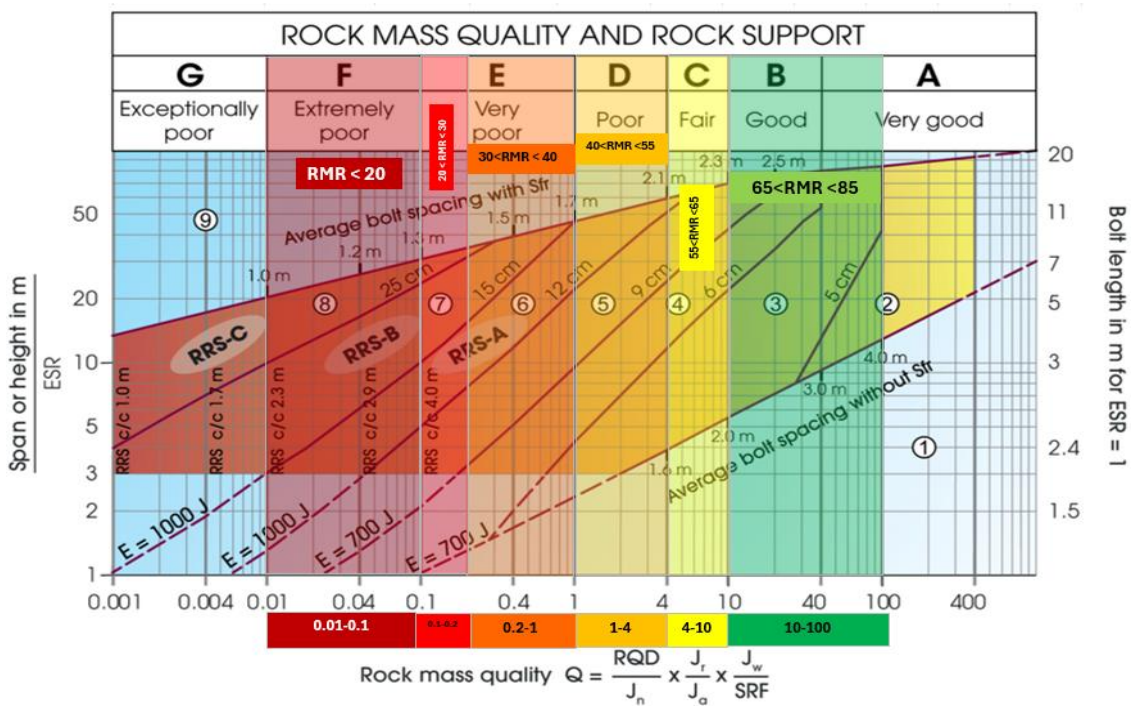

Figure 3-6. Q-system support chart, divided by different color assignments for each range of values (NGI, 2025).

To apply the Q-system properly, the required rock mass parameters must be obtained directly from site investigations. Based on the available geological and geotechnical data for the project area particularly within the zone where the cavern is planned to be excavated the following table presents the values that have been determined (refer to *2.2.1.3. Rock Tunnelling Quality Index, Q*).

$$Q = \frac{RQD}{Jn} \times \frac{Ja}{Jn} \times \frac{Jw}{SRF}$$

Table 3-1. rock mass parameters in Q-system and final Q value

Rock mass	Rock Quality Designation	Joint set number	Joint roughness number	Joint alteration number	Joint Water reduction factor	Stress Reduction Factor	**Rock mass Quality**
	RQD	Jn	Jr	Ja	Jw	SRF	**Q**
	30	12	1.5	2	0.66	1	**1.2**

In support properties, the cavern falls into category 6 of the Q system support suggestion (Figure 3-7).

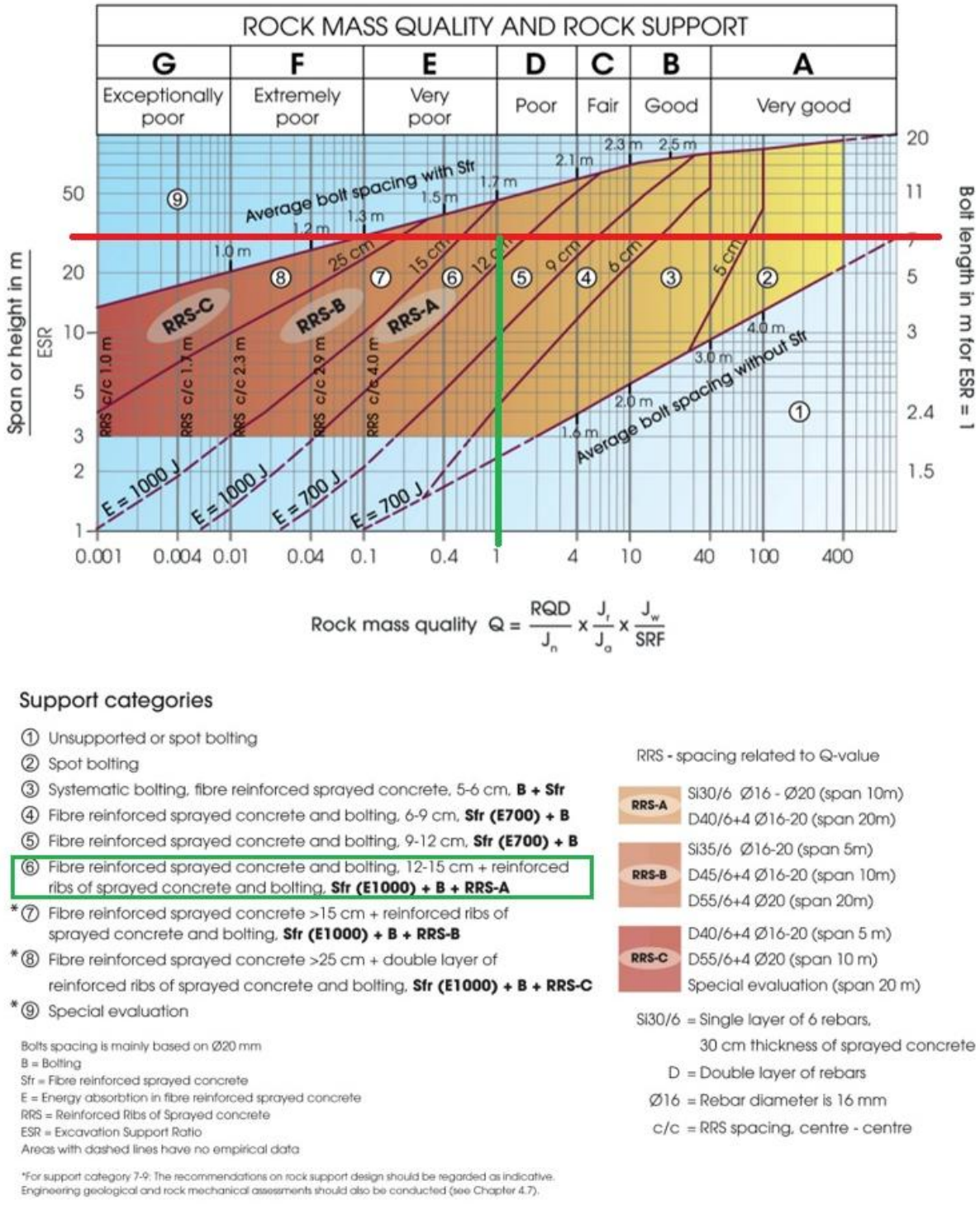

Figure 3-7. Q-system chart for the Cavern

3.2.3. Stress in Rock mass

It is important to note that the unit weight and uniaxial compressive strength (UCS) values adopted in this study have been selected according to preliminary geological data and standardized reference values (Figure 3-8). Specifically, the UCS ranges are derived from the

comprehensive rock strength catalogues developed by NTNU (Norwegian University of Science and Technology) and SINTEF, formally known as The Foundation for Industrial and Technical Research. SINTEF, headquartered in Trondheim, Norway, is one of Europe's largest independent research organizations, established in 1950, and is internationally recognized for its contributions to applied science and engineering (Bruland, 2012).

Uniaxial compressive strength (σ_c) and deformation modulus of rocks

Average values from tests of intact rock samples		**Tests of rocks world-wide**				**Scandinavian rocks tested at SINTEF**			
	ROCK	σ_c MPa	E GPa	E / σ_c	Number of tests	σ_c MPa	E GPa	E / σ_c	Number of tests
Crystalline texture	Dolomite	86	38	443	8	110	49	443	2
	Limestone	107	47	441	81	74	71	961	25
	Marble	133	63	474	20	66	71	1074	4
	Greenschist	-	-	-	-	93	44	472	3
	Clay schist / -stone	68	38	563	2	40	21	537	6
	Micaschist	104	39	374	16	71	30	422	21
	Gneiss	130	53	406	27	130	50	385	107
	Micagneiss	-	-	-	-	89	29	330	5
	Granitic gneiss	-	-	-	-	89	29	330	5
	Granulite	90	41	451	4	-	-	-	-
	Amphibolite	212	101	474	7	107	70	660	16
	Greenstone	281	101	359	1	105	53	503	7
	Quartzite	209	58	276	28	172	56	328	7
	Anorthosite	228	90	395	2	157	86	545	2
	Diorite	173	64	368	6	130	52	403	6
	Gneissgranite	-	-	-	-	117	42	354	5
	Granite	154	48	313	71	169	42	250	20
	Granodiorite	160	51	319	2	171	20	118	2
	Gabbro	228	106	466	5	248	76	306	1
	Norite	229	82	356	8	-	-	-	-
	Olivinestone	-	-	-	-	87	113	1307	5
	Peridotite	197	55	280	1	109	164	1502	1
	Monzonite	110	28	256	8	106	61	580	4
	Andesite	152	31	206	6	-	-	-	-
	Basalt	145	50	347	25	207	82	395	3
	Diabase, dolerite	229	88	384	13	152	81	537	5
	Hyperite	-	-	-	-	245	108	441	2
Clastic texture	Graywacke	81	25	310	12	-	-	-	-
	Sandstone	109	28	257	95	147	28	189	5
	Siltstone	89	31	350	14	-	-	-	-
Very fine-grained rocks	Hornfels	111	74	668	3	-	-	-	-
	Claystone	5	2	301	2	-	-	-	-
	Phyllite	39	26	672	4	61	46	756	12
	Chalk	1	2	1606	2	-	-	-	-
	Marl, marlstone	17	2	133	9	-	-	-	-
	Mudstone	11	1	106	4	-	-	-	-
	Claystone	5	2	301	2	-	-	-	-
Organic rocks - coal		30	3	107	14	-	-	-	-
				Sum of tests =	502			Sum of tests =	281

Figure 3-8. Achieved geomechanically parameters by lab work done by NTNU and SITNEF (Bruland, 2012)

It was decided that the mechanical properties of gneiss would be used in this analysis. Although the typical uniaxial compressive strength of Scandinavian gneiss is around **130 MPa**, no site-specific laboratory tests are available for the rock types present in the study area. For this reason, a conservative approach was adopted by reducing the **UCS** value to **100 MPa** for use in numerical modelling.

GSI value can be calculated as a function of Q value if the Active Stress parameter is eliminated from the calculation of Q; This new value is called Q_{basic} and has been resulted by following formula (Hoek, Support of underground excavations in hard rock. A.A. Balkema, 1995).

$$Q_{basic} = \frac{RQD}{Jn} \times \frac{Ja}{Jn}$$

In this step the GSI value is achievable from this empirical formula (Hoek, Support of underground excavations in hard rock. A.A. Balkema, 1995).

$$GSI = 9\ln(Q_{basic}) + 44$$

Also, RMR will be obtained by following formula using Q value, presented by (Bieniawski, 1989).

$$RMR = 9\ln(Q) + 44$$

Table 3-2 shows the approximated values of RMR and GSI.

Table 3-2. Empirically assigned RMR and GSI values from available Q value

Tunnel Section	**Q**	**Q_{basic}**	**$RMR_{Bieniawski}$**	**GSI_{Hoek} *by* Q_{basic}**
	1.2	*1.9*	45	50

Other relevant parameters that are function of GSI are calculated with following formulas and presented in Table 3-3; Distribution factor is equal to 0 (D=0).

$$m_b = m_i e^{\frac{GSI-100}{28-14D}}$$

$$s = e^{\frac{GSI-100}{9-3D}}$$

$$a = \frac{1}{2} + \frac{1}{6}\left(e^{\frac{-GSI}{15}} - e^{\frac{-20}{3}}\right)$$

$$\sigma_{cm} = \sigma_{ci} \times s^a$$

$$\sigma_t = -\frac{s\sigma_{ci}}{m_b}$$

Table 3-3. GSI relative parameters

Parameter	GSI	D	s	a	UCS intact rock [MPa]	m_i	m_b	σ_{cm} [MPa]	σ_t
value	50	0	0.003	0.5	100	20	3.35	6.02	0.025

As there are no available direct laboratory test on the local rock the values like Elastic modulus of the intact rock was considered 20 GPa based on the range 20 to 60 GPa, that has been proposed by NTNU on the Norwegian rock masses (Bruland, 2012).

$$E_i = 20000\ MPa$$

Based on the equation that was presented by (Diedrichs & Hoek, 2006)

$$E_{rockmass} = E_i \left(0.02 + \frac{1 - \frac{D}{2}}{1 + e^{\frac{60+15D-GSI}{11}}} \right)$$

It can be estimated that the rock mass elasticity young modulus is equal to:

$$E_{rockmass} = 6143\ MPa$$

3.2.4. Rock mass behavior

Because the rock mass quality is poor, it is expected that the ground will behave in an elasto-plastic condition after excavation. This is mainly due to the large span of the cavern and the high overburden, both of which increase the likelihood that in-situ stresses will exceed the rock-mass strength. When this happens, parts of the rock mass may enter the plastic zone, leading to non-elastic deformation around the opening.

Rock mass behavior is analyzed based on Convergence Confinement Method (CCM) according to the formulas presented by **Panet and Guénot in 1982**. (Refer to 2.4.1.3. Convergence-Confinement-Method).

This approach has been done using **GV4 software** to have a model that shows the convergence of the Rock mass by checking the longitudinal distance from the tunnel face, amount of **Convergence (U)** and **Stress Reduction Factor (λ)** can be known and used in further analysis of the model.

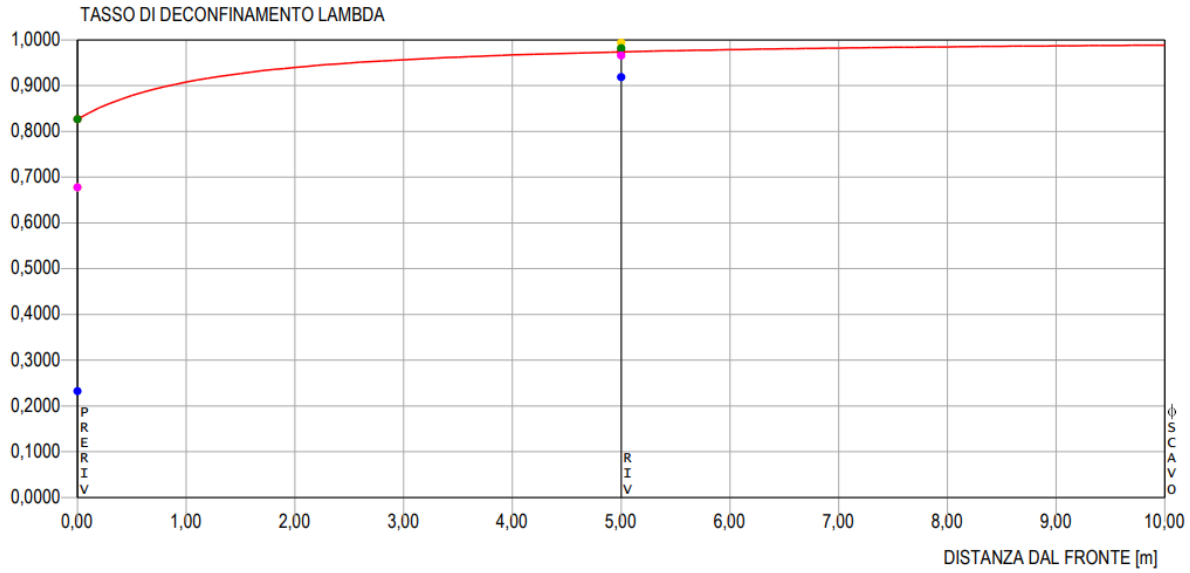

Figure 3-9. Stress reduction factor vs distance from the tunnel face plot

Based on experience in tunneling projects in Norway, 5m will be considered as initial value of excavation advancement in each sequence of excavation therefore by referring to Convergence plot in Figure 3-9, it is estimated to have **at least 97% of Stress Reduction factor** in this point.

$$\lambda = 0.97$$

3.3. Excavation Sequences

Based on the geometry and overall dimensions of the cavern, the excavation must be carried out using the Sequential Excavation Method (SEM). Given the scale and complexity of the opening, a staged approach is essential to maintain stability and control deformation throughout construction. In this section, excavation strategies are introduced. Three distinct excavation styles have been selected for evaluation and numerical modelling. These styles were chosen because they differ significantly in their sequence, geometry, and the way the excavation is initiated and completed. By examining three contrasting approaches, the study aims to capture a broad range of practical scenarios and identify the most suitable method for safe and efficient cavern construction.

Here, these models are presented and introduced.

- **Radial Progressive Enlargement (RPE) – Model A**
- **Side Drifts (SD) – Model B**
- **Top Heading and Bench (TBH) – Model C**

These models are described and their diagrams are presented below.

3.3.1. Model A– Radial Progressive Enlargement (RPE)

Model A represents an excavation strategy where the process begins at the central core of the cavern and then gradually expands outward in all directions. This approach focuses first on creating a stable internal core that can safely carry the initial loads. Once this central portion is secured with primary support, the excavation proceeds outward in a controlled, symmetrical manner. This method helps maintain overall stability during the early stages of construction, reduces the risk of excessive deformation, and allows the support system to be mobilized progressively as the cavern grows to its full span.

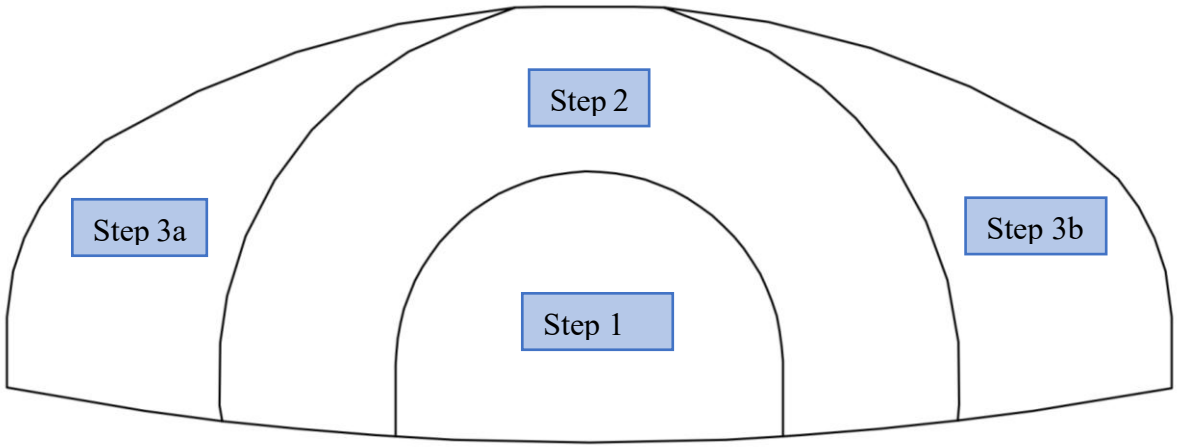

Figure 3-10. Model A – RPE

3.3.2. Model B – Side Drifts (SD)

Model B follows an excavation sequence that begins with the creation of two side drifts, one on the left and one on the right before the central core is removed. This approach resembles the logic behind constructing a protective shell or helmet: side sections are established first to provide initial stability and define the overall boundary of the cavern. Once these side drifts are excavated and initially supported, they act as structural guides that help control deformation and distribute stress more evenly. With the outer framework secured, the central core can then be safely excavated, allowing the cavern to reach its full width while maintaining a stable excavation front throughout the process.

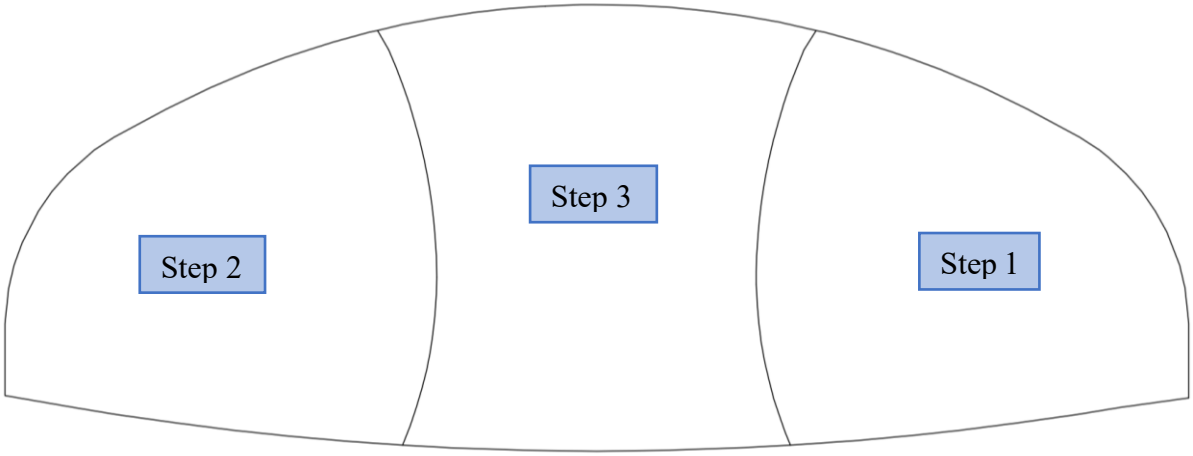

Figure 3-11. Model B – SD

3.3.3. Model C – Top Heading and Bench (TBH)

This model follows a more traditional and structured excavation sequence, beginning with the top heading, which is divided into two distinct phases. This staged approach allows the upper portion of the cavern to be opened gradually, maintaining control over deformation while ensuring that the initial support system can be installed promptly as each section advances. The concept is like shaping the upper dome of a structure—carefully removing material in controlled layers to preserve stability as the geometry develops. Once the top heading is fully excavated and supported, the process continues with a single bench excavation, completing the lower portion of the cavern. This method provides clear, organized progression from top to bottom, offering good control overground behavior and allowing support installation to follow a predictable and efficient sequence.

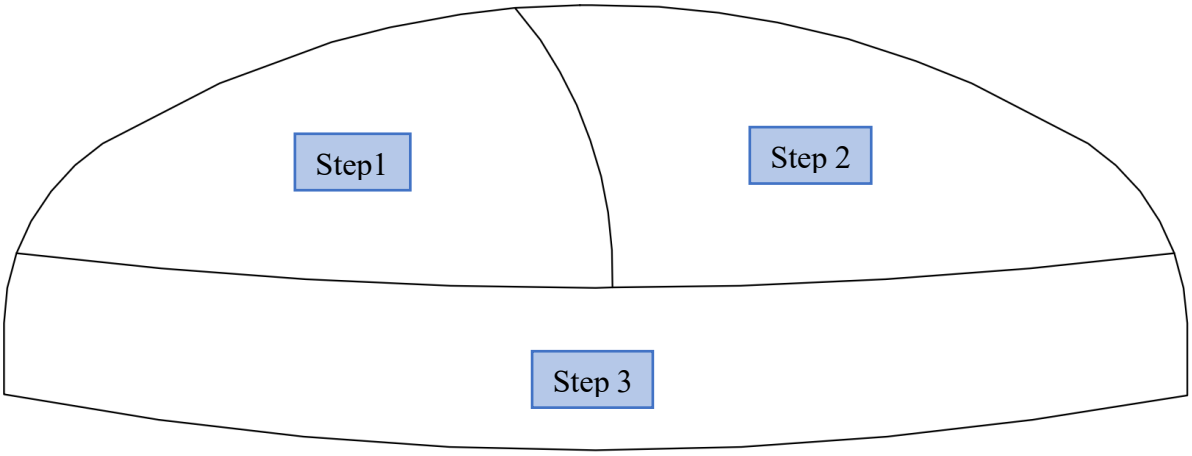

Figure 3-12. Model C – TBH

The styles are evaluated by advanced numerical modeling under three different horizontal-to-vertical stress ratios equal to 0.5, 1 and 2 (refer to 3.2.1. In-situ stress Condition). In total nine models have been created, computed and analyzed in this thesis.

3.4. Support Configurations

Norwegian Geotechnical institute (2025) has selected Q-system as the main reference of rock mass classification and empirical support suggestion.

Type of support and the material utilized in the design of cavern was selected based on Q-system chart and the cavern falls in Category 6 that is described below (Figure 3-7).

Support Category 6:

- Fiber reinforced shotcrete, thickness 15cm
- Reinforced ribs with shotcrete, 40 cm final thickness (including 15cm of first layer shotcrete), 4.5 m of center-to-center spacing, Double row of rebars (6 rebars up, 4 ribs down) with diameter of 20 mm.
- 7m bolts with 1.7m spacing.

Although the existing support layout suggested by Q-system provides a baseline for design, it needs to be adjusted to fit the specific conditions of the case study. Since the cavern will be analyzed under three different horizontal-to-vertical stress ratios, some support parameters such as rock-bolt length and the longitudinal spacing of the RRS must be modified.

The idea is straightforward: as the stress ratio increases, the support must become stronger. For example, a 7-meter rock bolt may work under low stress, but under higher stress ratios it needs to be lengthened to reach elastic zone. Likewise, the RRS spacing should be reduced so that the elements are installed closer together to better handle higher stresses.

The table below summarizes how the support features assumed for each value.

Table 3-4. Support parameters for each stress ratio

Horizontal-to-Vertical stress ratio, k	RRS Spacing (m)	Rock bolt length (m)	
		Roof	Wall
0.5	4.5	7	7
1	3	7	7
2	1.5	12	7

This approach ensures a conservative approach that illustrates under high rock cover or variable stress regimes, preliminary empirical analysis should be revised and adapted, considering specific conditions.

Chapter 4. Methodology

After estimating the necessary Q-system parameters and identifying the appropriate support category, the work focuses on analyzing different excavation styles under varying stress conditions. This chapter introduces the core methodology used to assess ground response, support performance, and interaction across these scenarios.

4.1. Numerical Modeling

This section focusses on modeling the cavern with Finite Element Method (FEM) to evaluate performance of the excavation styles under different stress ratios.

The numerical analysis and modeling were performed using **RS2 (Phase2)**, a comprehensive 2D Finite Element Analysis (FEA) program developed by **Rocscience**.

RS2 is a widely accepted tool in geotechnical engineering for assessing the stability, stress redistribution, and deformation characteristics of both rock and soil masses. The software facilitates the simulation of complex, multi-stage underground excavations, enabling the implementation of advanced constitutive models, such as the Generalized Hoek-Brown and Mohr-Coulomb criteria, along with various support elements. Its core capability lies in accurately modeling the two-dimensional, plane-strain behavior of the rock mass, allowing for the precise analysis of support capacity (thrust and bending moment) and the ultimate prediction of tunnel convergence.

4.1.1. Properties of the Model

In this section, the properties of the material, support, meshing and other features of the model as input is introduced.

4.1.1.1.1. Mesh Properties

Basic model is made in the software; these figures are clipped from RS2 software showing the excavation boundary of the cavern (Figure 4-1) and the mesh setup input

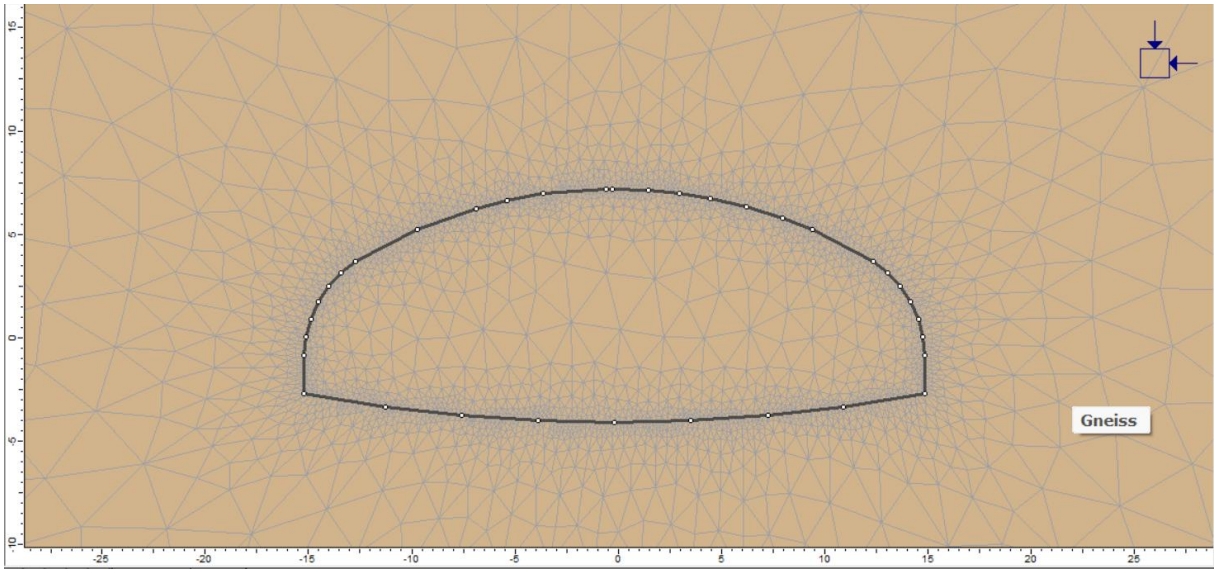

Figure 4-1. Meshed Excavation Boundary of the cavern

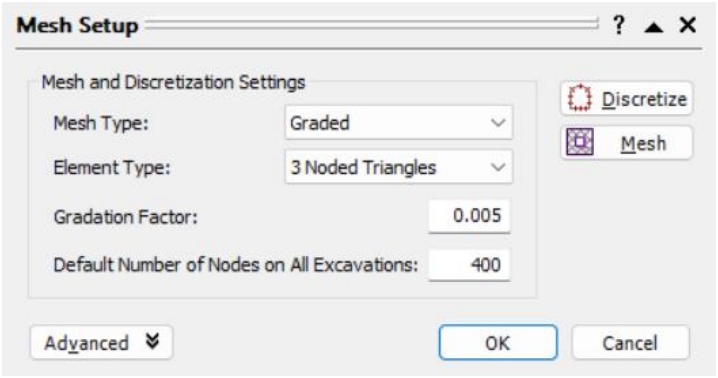

Figure 4-2. Mesh Setup

4.1.1.1.2. Material Properties

Table 4-1 shows the parameters of rock mass to be assigned to the software models.

Table 4-1. Material Properties to be used in RS2

Rock mass	Rock Cover, H [m] w.r.t crown	Rock mass unit weight, γ [MN/m^3]	Intact rock strength, σ_c [MPa]	Elastic Modulus of the Intact Rock [MPa]	Elastic Modulus of the rock mass [MPa]	Q	GSI	s	a	m_i	m_b	Rock mass strength σ_{cm} [MPa]
	650	0,027	100	20000	6143	1.2	50	0.003	0.5	20	3.35	6.02

Material properties of the rock mass have been assigned in the software and are presented in the following figures.

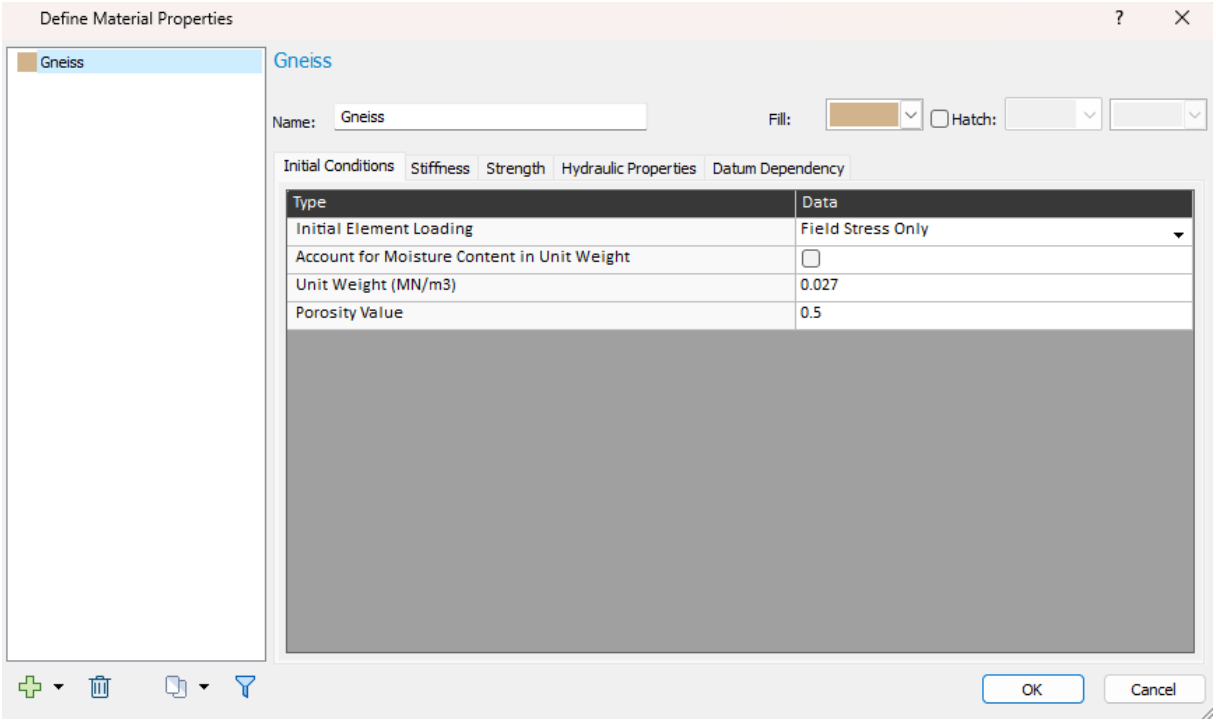

Figure 4-3. Material properties, Initial condition

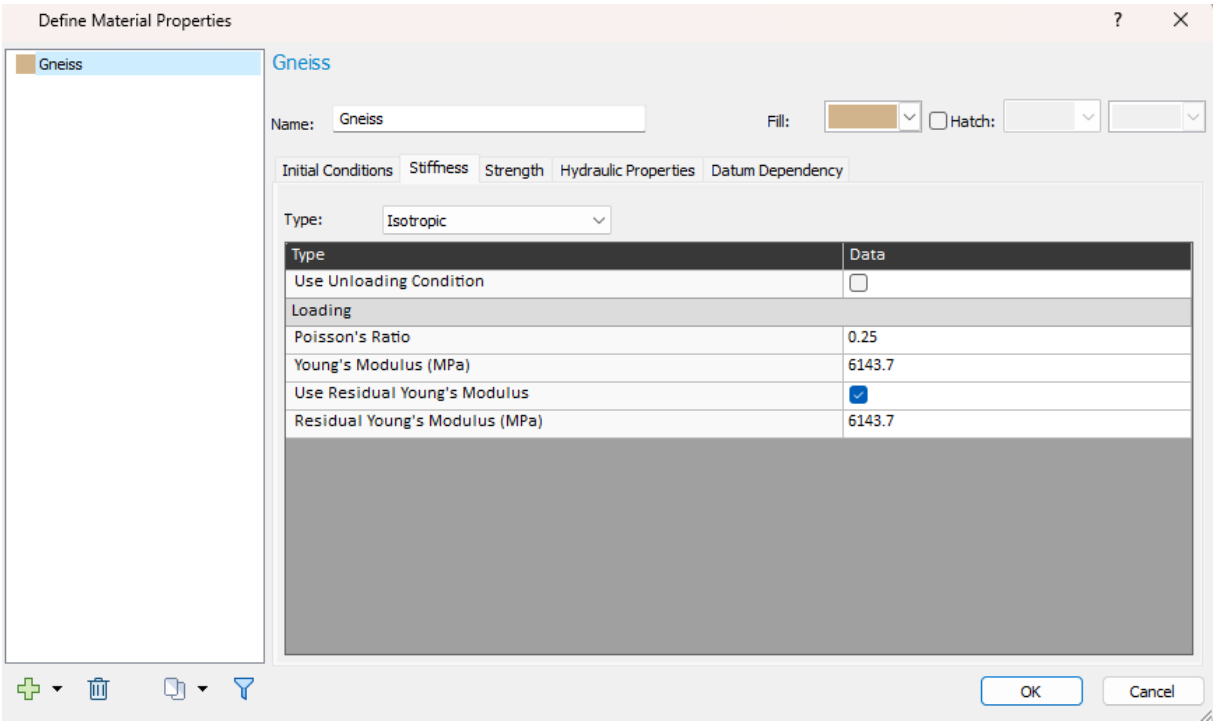

Figure 4-4. Material properties, Stiffness

Young modulus of the rock mass is calculated in the software based on Generalized Hoek-Diederichs equation presented in the Figure 4-4.

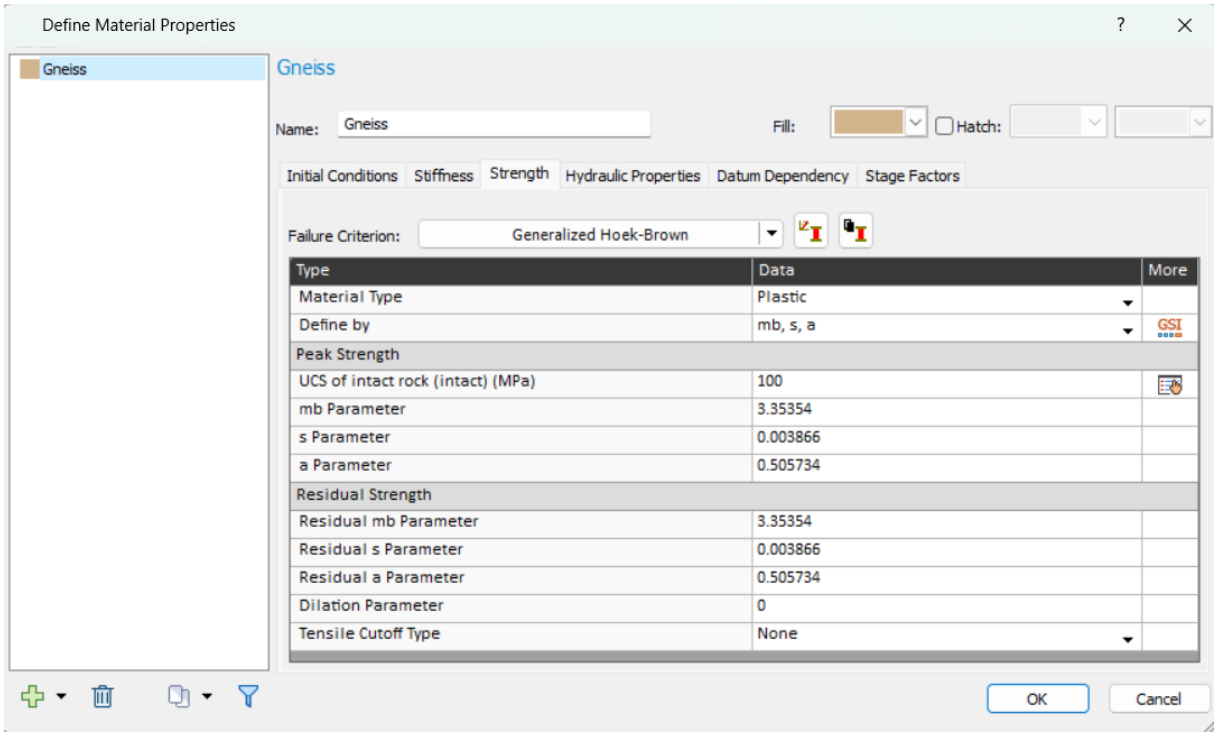

Figure 4-5. Material Properties, Strength

Norwegian tunneling society regulates rock joint grouting for the projects and based on the implication of grouting, the rock mass is considered as drained in the model (Figure 4-6).

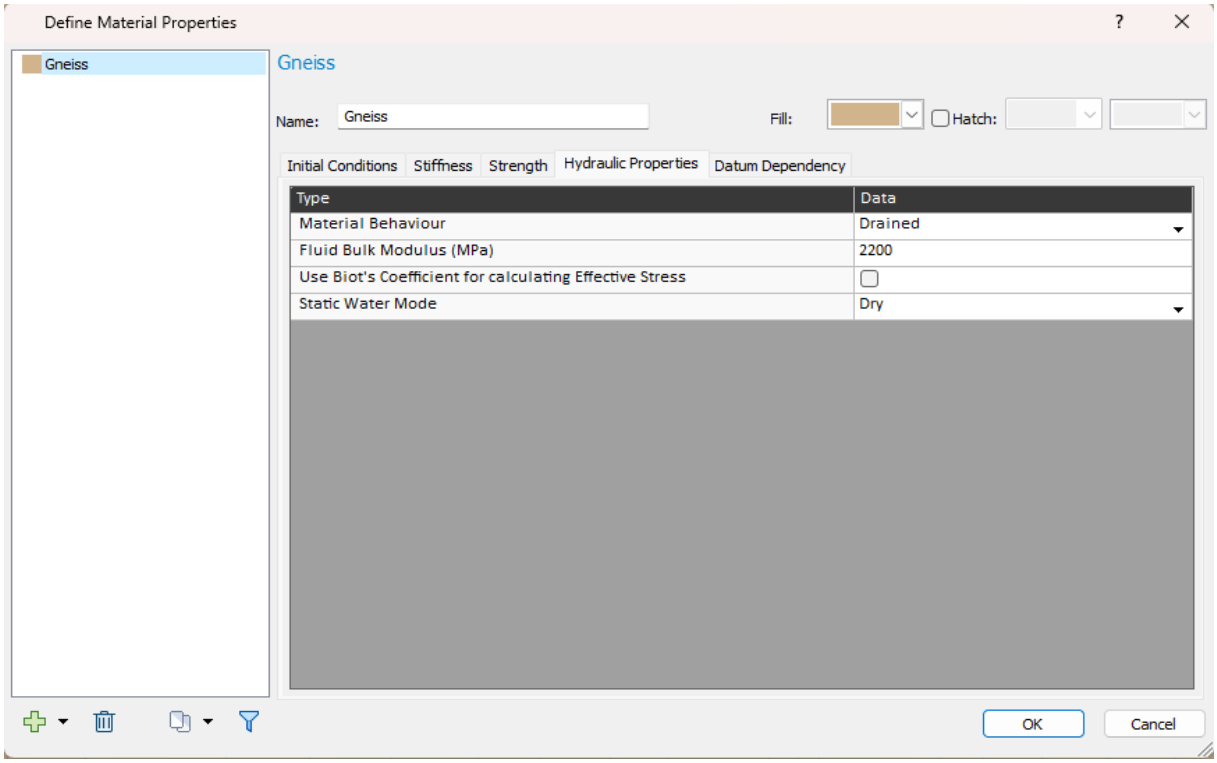

Figure 4-6. Material Properties, Hydraulic Properties

4.1.1.1.3. Field Stress

Field stress properties are assigned based on multiplying rock cover height on the cavern which is 650 m and the unit weight of the rock which is 0.027 MN/m^3 .

$$\sigma_v = \gamma H$$

Horizontal stress will be evaluated by the value of k based on the following formula.

$$\sigma_h = k.\sigma_v$$

It was explained before that the models will be computed with three different values of horizontal to vertical stress ratios which are **0.5, 1 and 2.**

This approach will give three separate results for each model that will be presented in Chapter 5. Results.

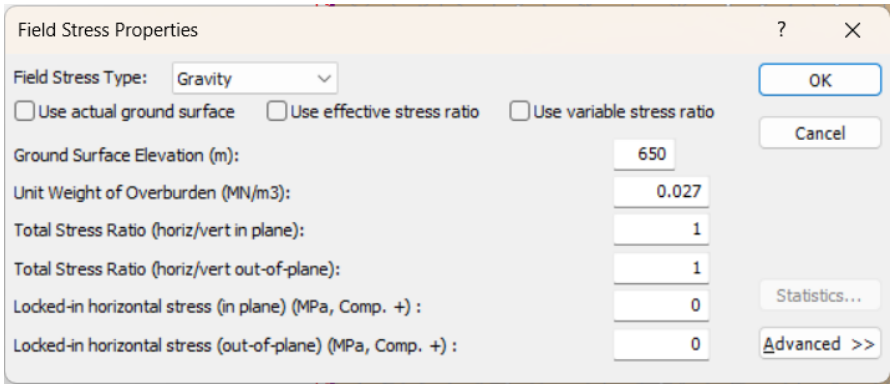

Figure 4-7. Field stress properties, k=1

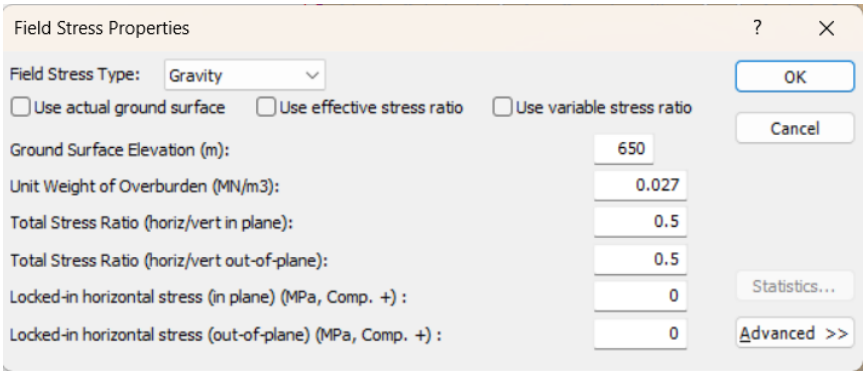

Figure 4-8. Field stress properties, k=0.5

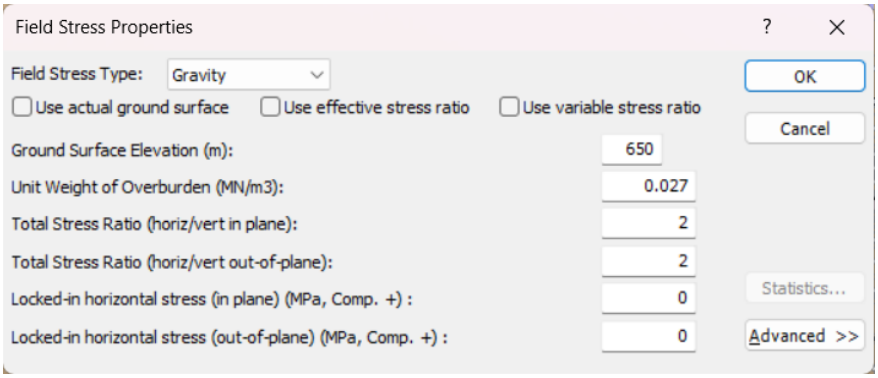

Figure 4-9. Field stress properties, k=2

4.1.1.1.4. Support Properties

Q-chart Support Category 6 is presented below (NGI, 2025).

- Fiber reinforced shotcrete, thickness 15cm
- Reinforced ribs with shotcrete, 40 cm final thickness (including 15cm of first layer shotcrete), 4.5 m of center-to-center spacing, Double row of rebars (6 rebars up, 4 ribs down) with diameter of 20 mm.
- 7m bolts with 1.7m spacing

RS2 software has ability to accept the support features in the section of "Properties" in toolbar.

Reinforced Ribs of Sprayed Concrete : Although it is possible to add different kind of liners in RS2 software but there is no option to select Reinforced Ribs of Sprayed Concrete (RRS) as a liner type in RS2 ; therefore a substitution method has been used from the paper published by Harvard and Nilsen in 2018 that recommend equations to simulate the properties of RRS into a Reinforced Concrete by assigning concrete thickness, rebar spacing and section depth of the reinforced concrete based on the RRS properties (Havard & Nilsen, 2018).

Thickness of equivalent layer of Reinforced Concrete is calculated based on following formula (Havard & Nilsen, 2018).

$$Conceret\ Thickness = \frac{RRS\ total\ thickness * RRS\ width}{RRS\ spacing} + Thickness\ of\ First\ layer$$

Sets of RRS that are being used in Norwegian projects, has 70 cm of width including 50 cm of the steel ribs and 10 cm of concrete on both sides (Figure 4-10).

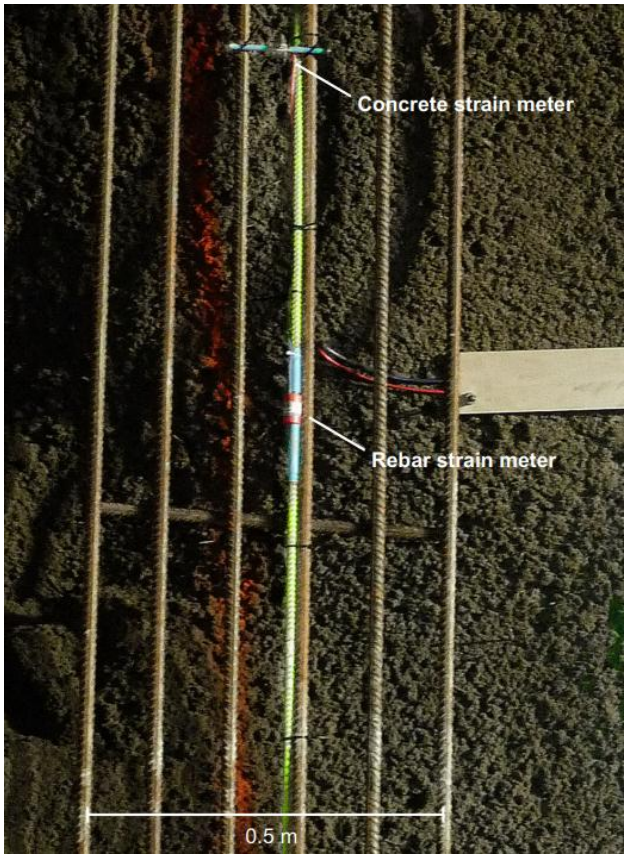

Figure 4-10. RRS figure (Havard & Nilsen, 2018)

$$Conceret\ Thickness = \frac{0.4\ m * 0.7\ m}{4.5\ m} + 0.15\ m = 0.21\ m$$

The spacing between rebars in the equivalent Reinforced concrete is achieved by dividing the RRS spacing to the number of rebars as it is written below (Havard & Nilsen, 2018).

$$Rebar\ Spacing = \frac{RRS\ Spacing}{Number\ of\ rebars} = \frac{4.5}{10} = 0.45\ m$$

Section depth that shows the distance between two layers of rebar will be calculated considering 5 cm of distance from the upper and bottom section of the concrete layer.

$$Rebar\ section\ depth = Concrete\ thickness - 0.1\ m$$

$$Rebar\ section\ depth = 0.21\ m - 0.1\ m = 0.11\ m$$

RS2 is 2D FEM software and based on the principles of numerical modeling it will consider 1 m of third dimension in computation procedure; Therefore, the lining will be considered with 1 m length in the longitudinal view. Figure 4-11 shows the longitudinal section of the Reinforced Concrete.

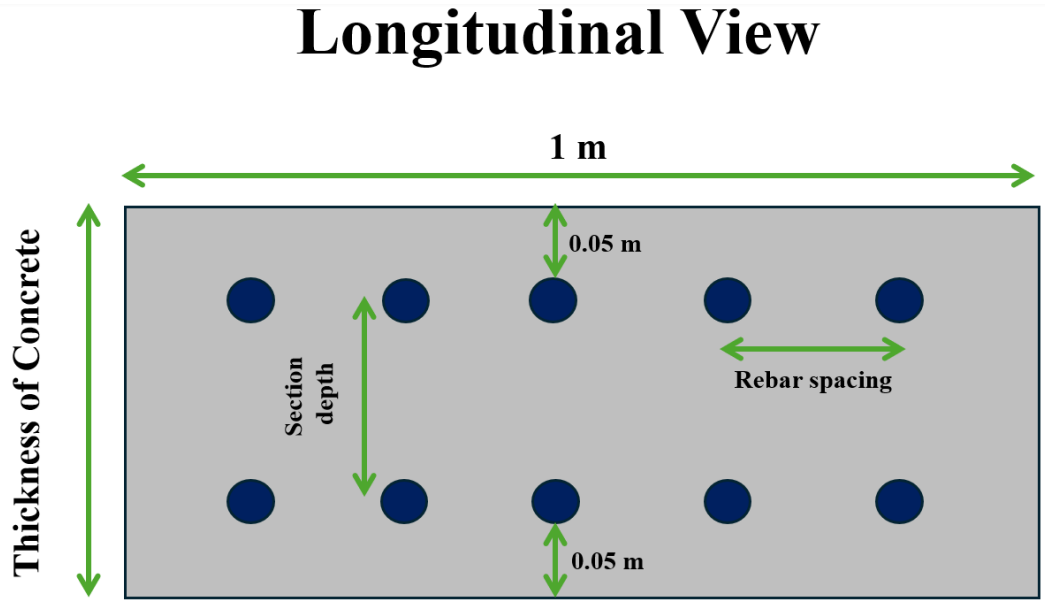

Figure 4-11. Reinforced Concrete longitudinal view

Achieved data will be entered as the liner property of RRS in the software like following figure.

RRS (equivalent reinforced concrete layer)

Name: RRS (equivalent reinforced concrete layer) Color:

Liner Type: Reinforced Concrete

Type	Data	More
Initial Conditions		
Concrete Unit Weight (MN/m3)	0.024	
Include Weight in Stress Analysis	☑	
Reinforcement		
Reinforcement	☑	
Common Type	Rebar(Europe): #20 (diameter=20mm)	
Spacing (m)	0.45	
Section Depth (m)	0.11	
Area (m2)	0.000628	
Moment of Inertia (m4)	1.915e-06	
Young's Modulus (MPa)	210000	
Compressive Strength (MPa)	400	
Tensile Strength (MPa)	400	
Weight (kg/m)	4.94	
Concrete		
Concrete	☑	
Thickness (m)	0.21	
Young's Modulus (MPa)	25000	
Poisson Ratio	0.2	
Compressive Strength (MPa)	40	
Tensile Strength (MPa)	3.5	
Advanced Properties		
Material Type	Elastic	
Sliding Gap	☐	
Beam Element Formulation	Timoshenko	
Axial Strain (+Expansion)	0	
Stage Properties		
Stage Concrete Properties	☐	

Figure 4-12. Properties of equivalent Reinforced concrete that represents RRS in RS2

In 3.4. Support Configurations section it was mentioned that by increasing the horizontal to vertical stress ratios, center to center spacing of the RRS will reduce, therefore, for the models computed with hydrostatic condition (k=1) and high stress regime (k=2) the spacing will decreases and consequently equivalent reinforced concrete features like thickness of concrete and rebar spacing will change; Following table shows properties of reinforced concrete for all stress ratios.

Table 4-2. Equivalent Reinforced Concrete for each stress regimes

Horizontal to Vertical stress ratio, k	**RRS**				**Reinforced Concrete**		
	Smoothing layer thickness (m)	RRS total thickness (m)	RRS width (m)	RRS spacing (m)	Thickness (m)	Rebar spacing (m)	Section depth (m)
0.5	0.15	0.4	0.7	4.5	0.21	0.45	0.11
1	0.15	0.4	0.7	3	0.24	0.3	0.14
2	0.15	0.4	0.7	1.5	0.34	0.15	0.24

Smoothing Layer: Another phase of lining, which is the primary smoothing layer of shotcrete with thickness of 15cm, is defined in the model with the properties indicated in Figure 4-13.

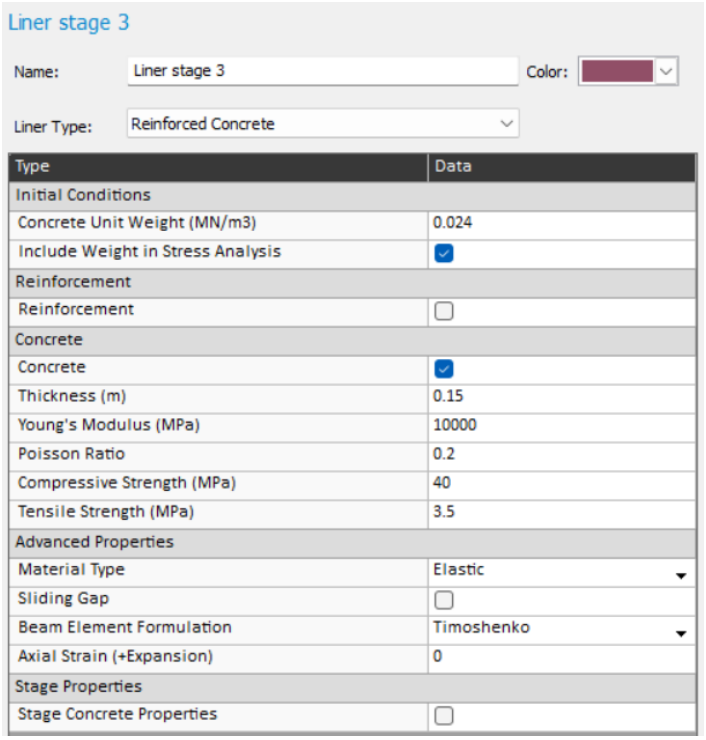

Figure 4-13. Properties of smoothing layer of shotcrete

Smoothing layer shows the fresh shotcrete directly applied after excavation; Young's Modulus of the shotcrete is assigned based on the fresh concrete properties. Shotcrete properties will change through time and study carried out by researchers shows Young's modulus of the concrete as a function of time in a graph presented in following figure. (Smanioto & Neuner, 2022)

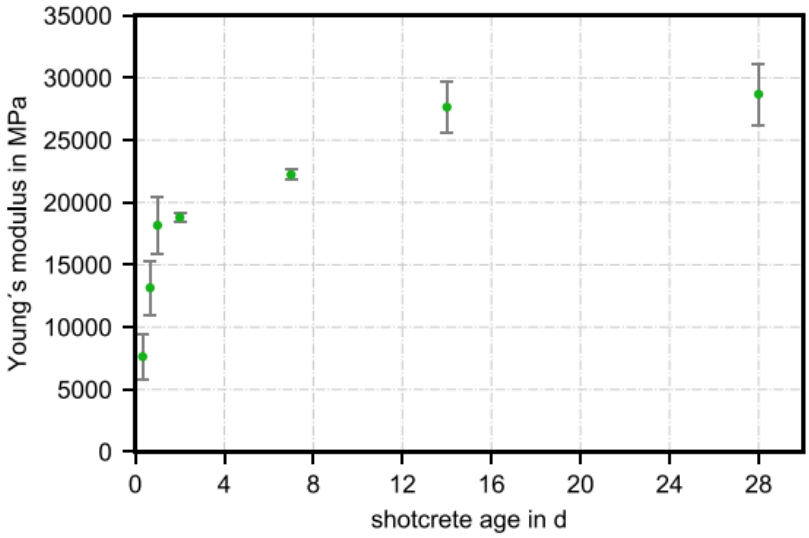

Figure 4-14. Young's Modulus of Shotcrete as function of time after installation (Smanioto & Neuner, 2022)

Layer of shotcrete with thickness of 15 cm is applied on the invert of the cavern; the properties are defined in following figure.

Invert

Name: Invert Color:

Liner Type: Reinforced Concrete

Type	Data
Initial Conditions	
Concrete Unit Weight (MN/m3)	0.024
Include Weight in Stress Analysis	☑
Reinforcement	
Reinforcement	☐
Concrete	
Concrete	☑
Thickness (m)	0.15
Young's Modulus (MPa)	25000
Poisson Ratio	0.2
Compressive Strength (MPa)	40
Tensile Strength (MPa)	3.5
Advanced Properties	
Material Type	Elastic
Sliding Gap	☐
Beam Element Formulation	Timoshenko
Axial Strain (+Expansion)	0
Stage Properties	
Stage Concrete Properties	☐

Figure 4-15. Properties of Shotcrete installed on the invert

Rock Bolts: Length and spacing of the bolts are **7 m** and **1.7 m** respectively and the third-dimension spacing of them is **1.5 m** to be intersected with installed RRS.

In models computed with k = 2 it was decided to lengthen thirteen rockbolts on the crown to 12 m.

Table 4-3. Rock bolts length for each stress ratio

Horizontal-to-Vertical stress ratio, k	Rock bolt length (m)	
	Roof (13 rockbolts)	Wall
0.5	7	7
1	7	7
2	12	7

The properties assigned to the rock bolts in RS2 software are shown in Figure 4-16.

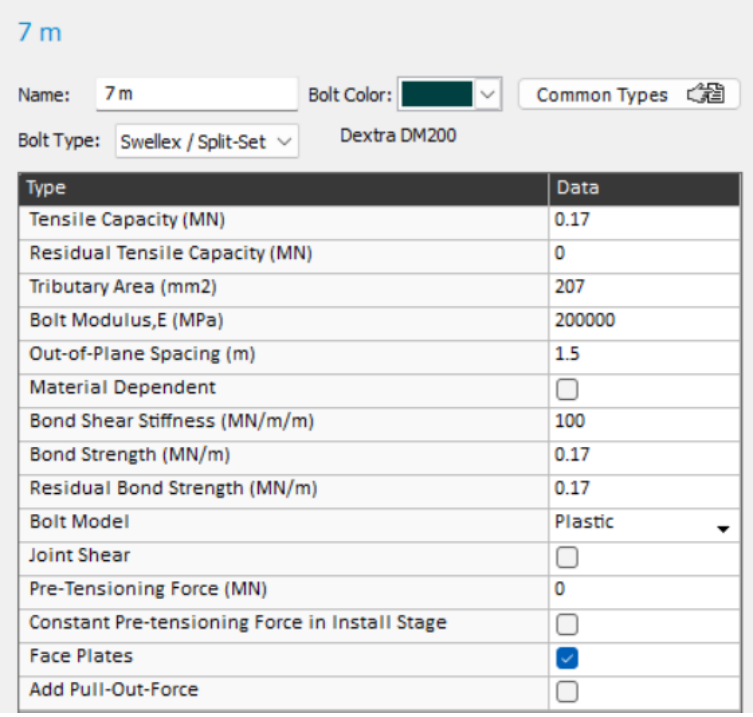

Figure 4-16. Rock bolt properties

4.1.2. Sequences of Excavation

In this section, different styles of excavation sequences will be introduced.

4.1.2.1. Model A – Radial Progressive Enlargement (RPE)

Following figure shows the excavation boundaries of Model A.

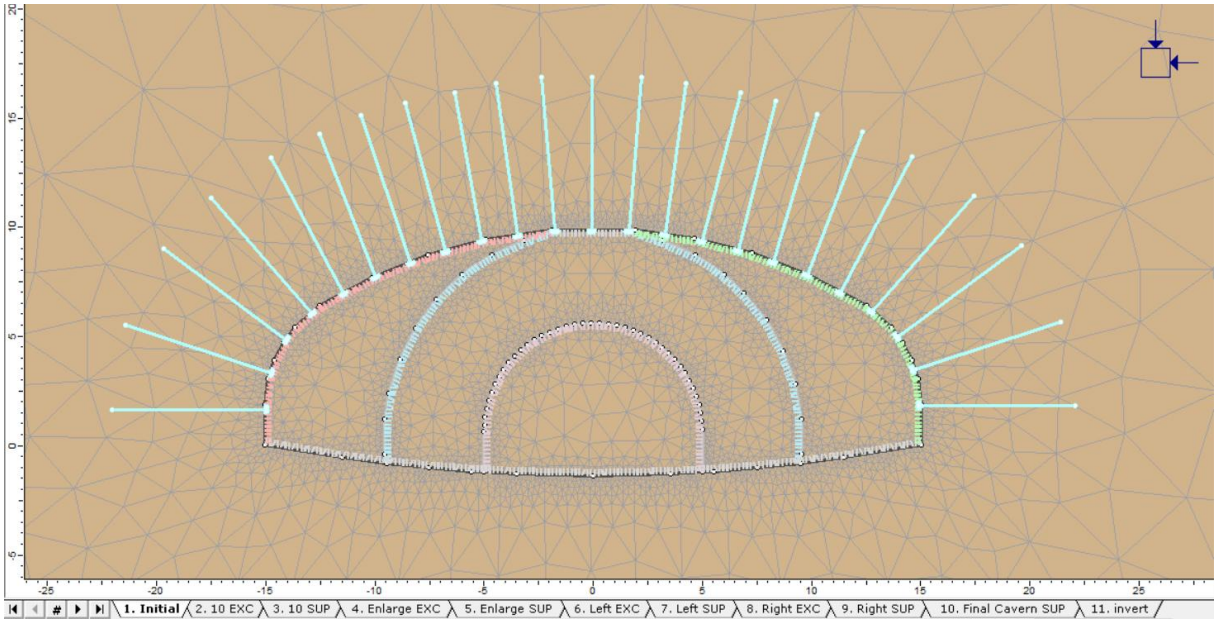

Figure 4-17. Model A

This model has 10 stages that consist of excavation and support installations as described in following figure.

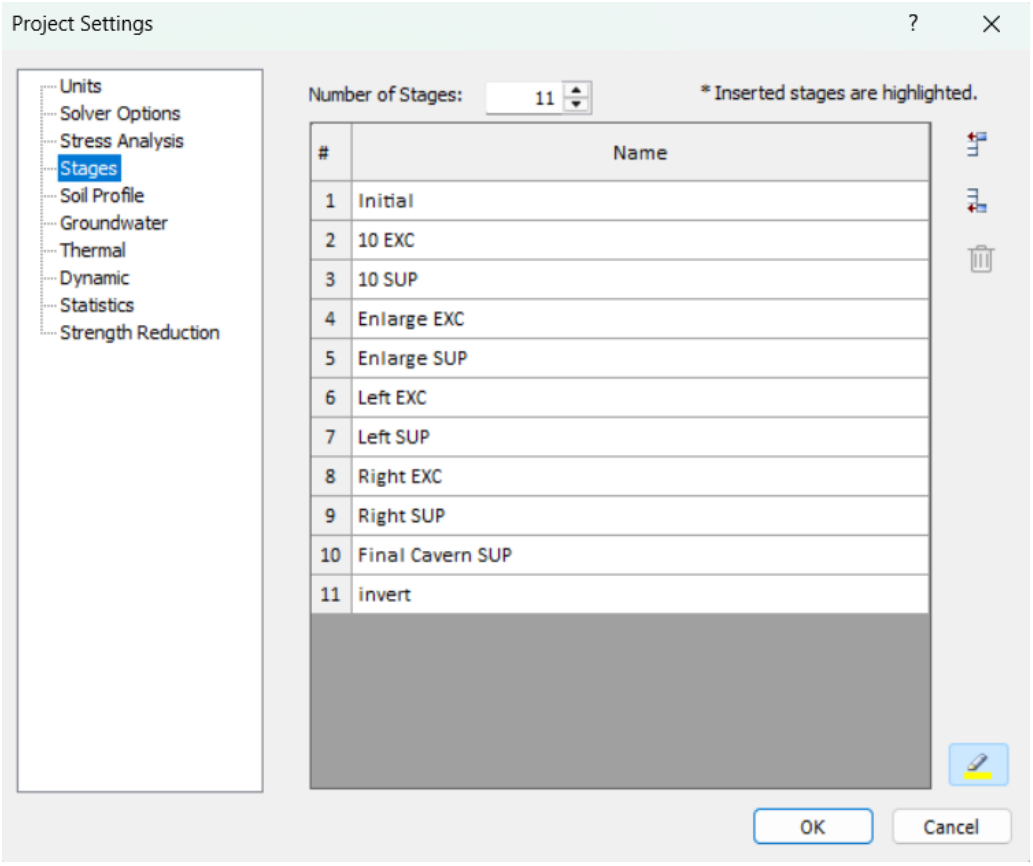

Figure 4-18. Construction stages in Model A

In this model "1st layer shotcrete" is applied in each stage as smoothing layer after the excavation an then after last stage of excavation the RRS is activated as final lining.

Also for indication of the real support activation in the cavern boundaries, a new liner which is Composite liner is applied to the cavern excavation boundaries containing both "1st layer shotcrete"(Liner stage 3, 5, 7 and 9) and "RRS"; These two liners will not be activated at same time because the "1st layer shotcrete" represents only the smoothing layer of shotcrete, but RRS represents first and second layer of lining together as equivalent reinforced concrete.

Activation of each lining will be explained in each stage.

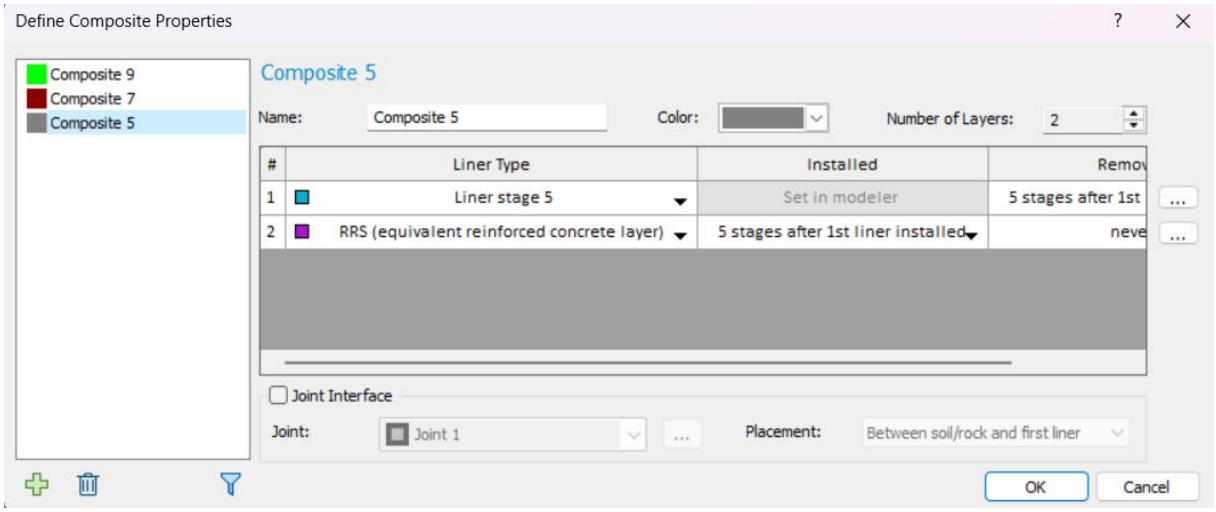

Figure 4-19. Composite stage 5 – Model A

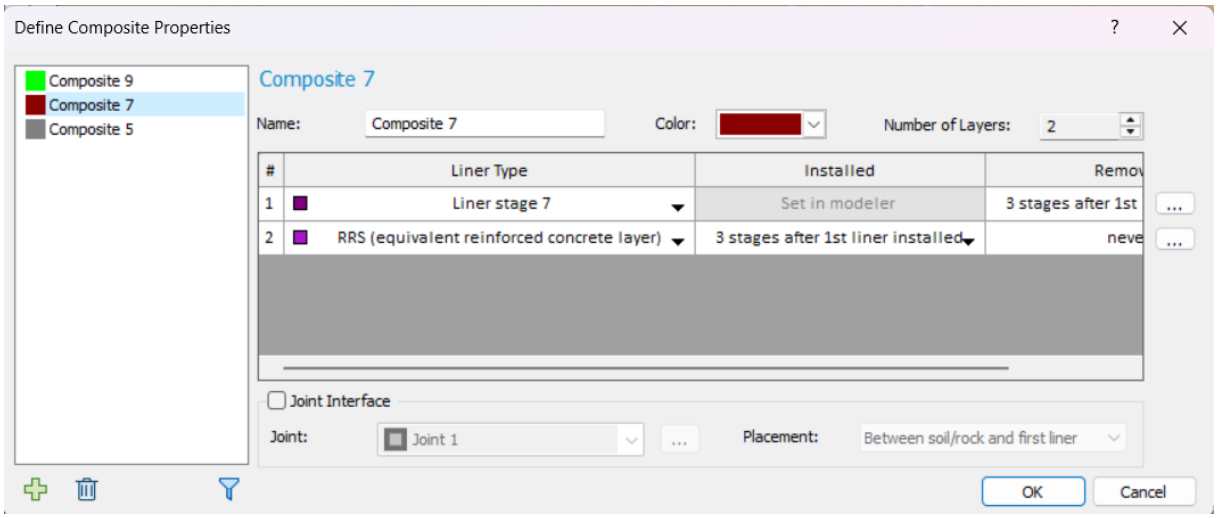

Figure 4-20. Composite stage 7 – Model A

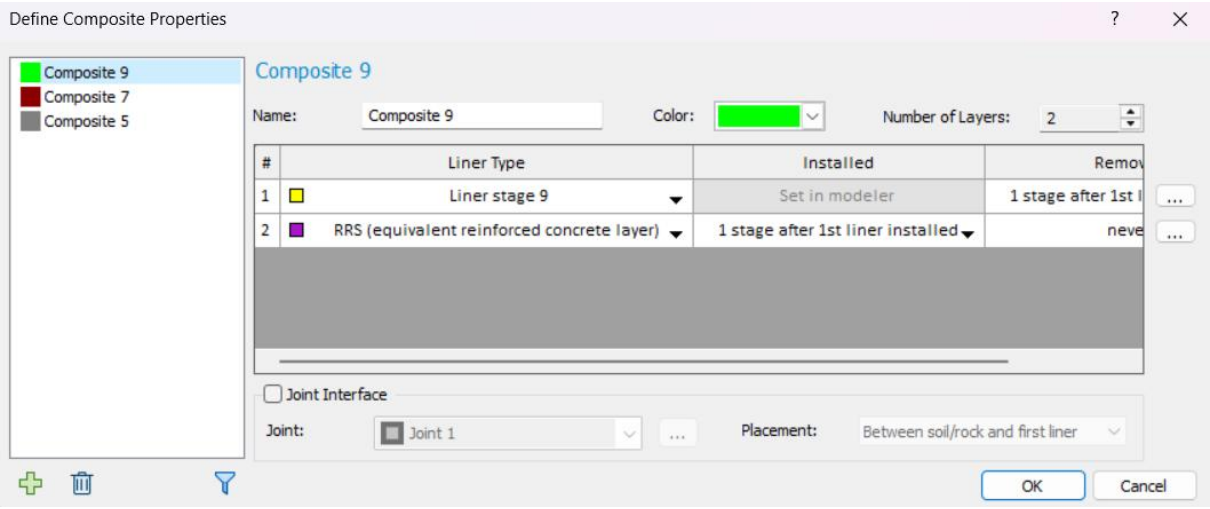

Figure 4-21. Composite stage 9 – Model A

In each stage that a portion is excavated, an Induced stress equal to 3% is applied to the excavation boundary, indicating the stress that should be applied to the liners as a percentage of original primary internal stress in the rock mass before excavation; This shows that after excavation the rock mass relaxation is 97% its original internal pressure at a 5 m distance from the excavation face and then install the support (Read 3.2.4. Rock mass behavior).

- **Stage 1 - Initial:** in this stage nothing has been excavated and rock mass is under its original pressure.

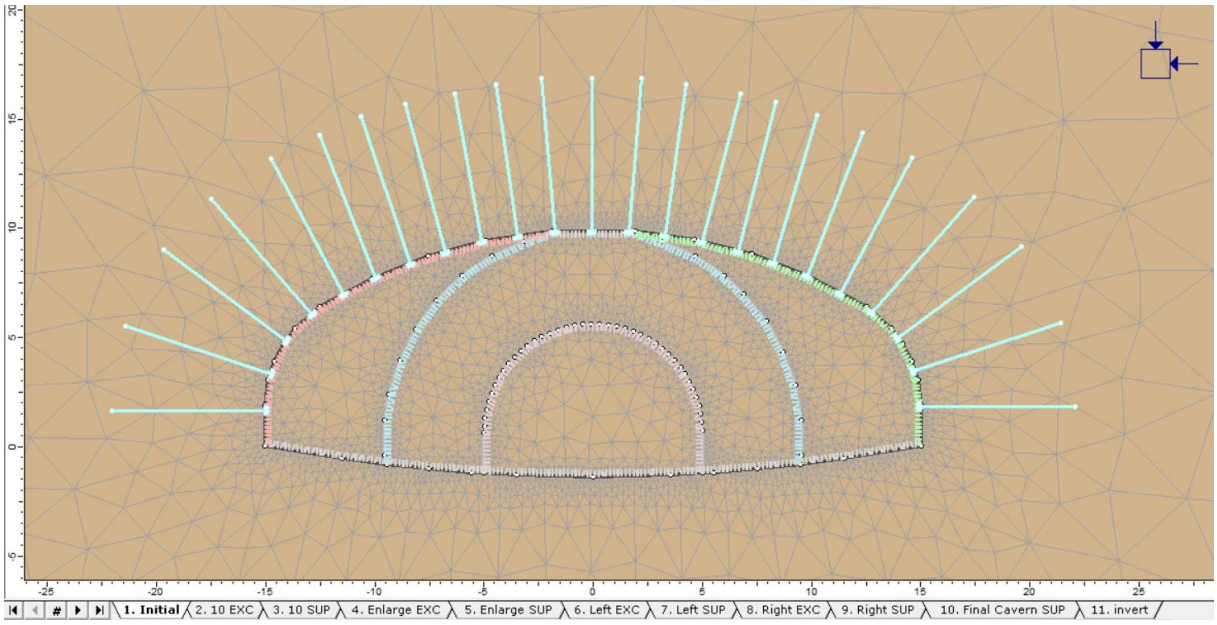

Figure 4-22. Model A-Stage 1

- **Stage 2 - 10 EXC:** in this stage the tunnel is excavated having 10 m span (post-excavation stress is applied as induced stress factor equal to 0.03).

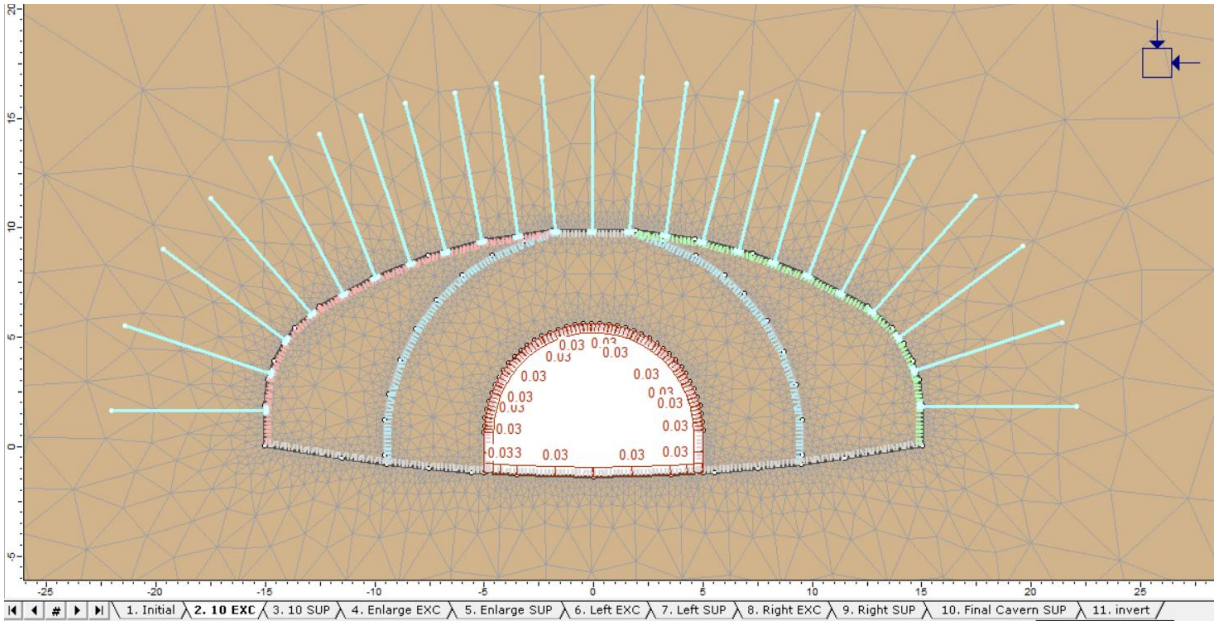

Figure 4-23. Model A-Stage 2

- **Stage 3 - 10 SUP:** 1st layer shotcrete (liner stage 3) is applied to the excavation boundary.

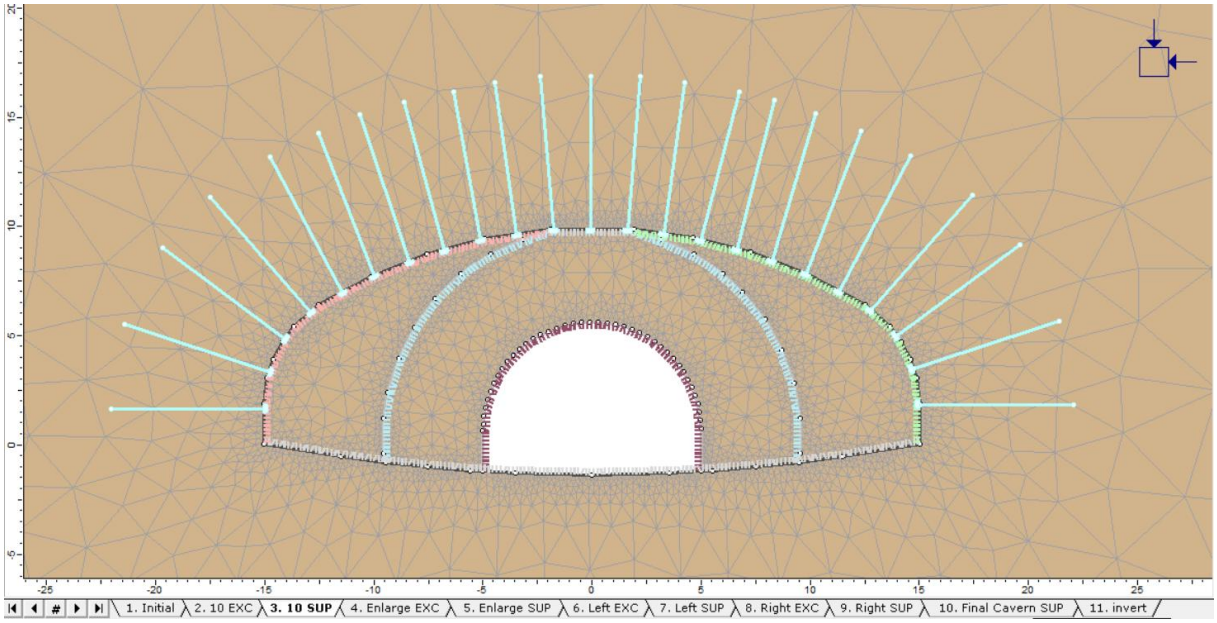

Figure 4-24. Model A-Stage 3

- **Stage 4 - Enlarge EXC:** the ordinary section is enlarged to reach the span of 19 m and maximum height of the cavern (post-excavation stress is applied as induced stress factor equal to 0.03).

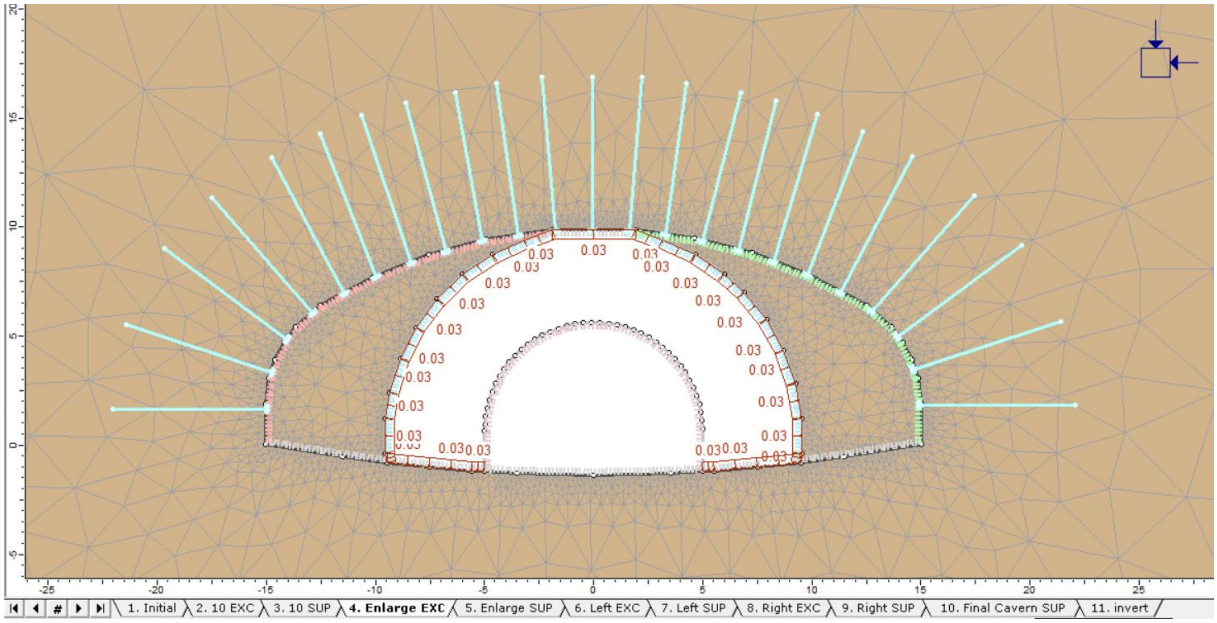

Figure 4-25. Model A-Stage 4

- **Stage 5 - Enlarge SUP:** 1st layer shotcrete (liner stage 5) is applied to the new excavation boundaries, and the part of the roof is supported by three central bolts.

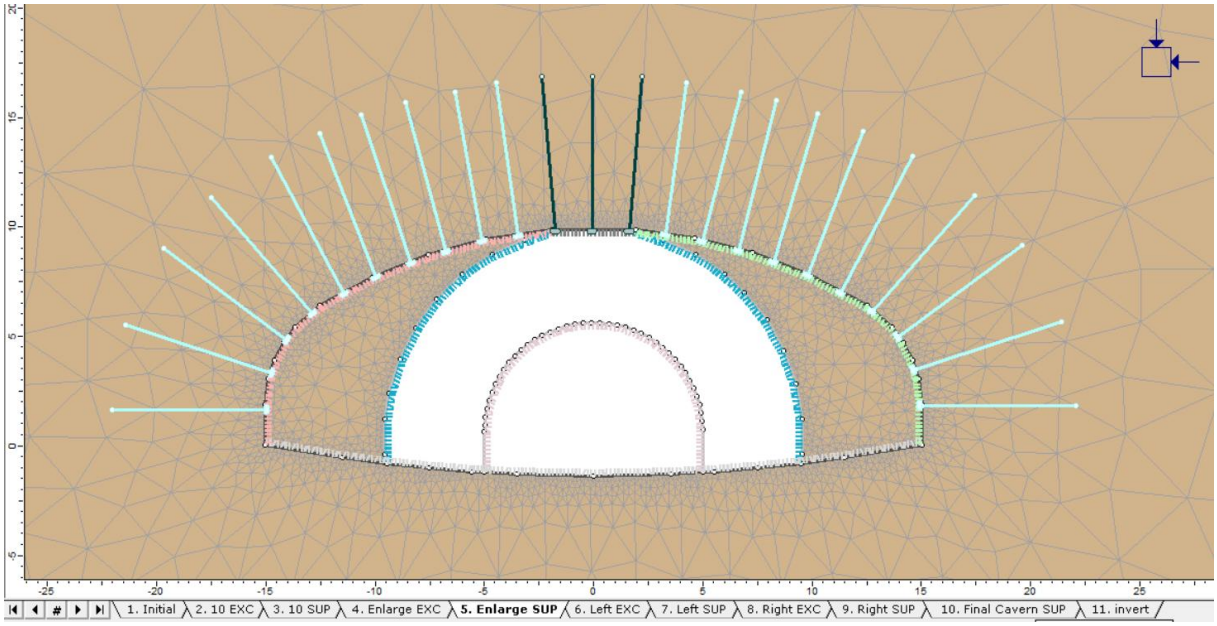

Figure 4-26. Model A- Stage 5

- **Stage 6 - Left EXC:** Slice on the left is excavated reaching the maximum excavation boundary (post-excavation stress is applied as induced stress factor equal to 0.03).

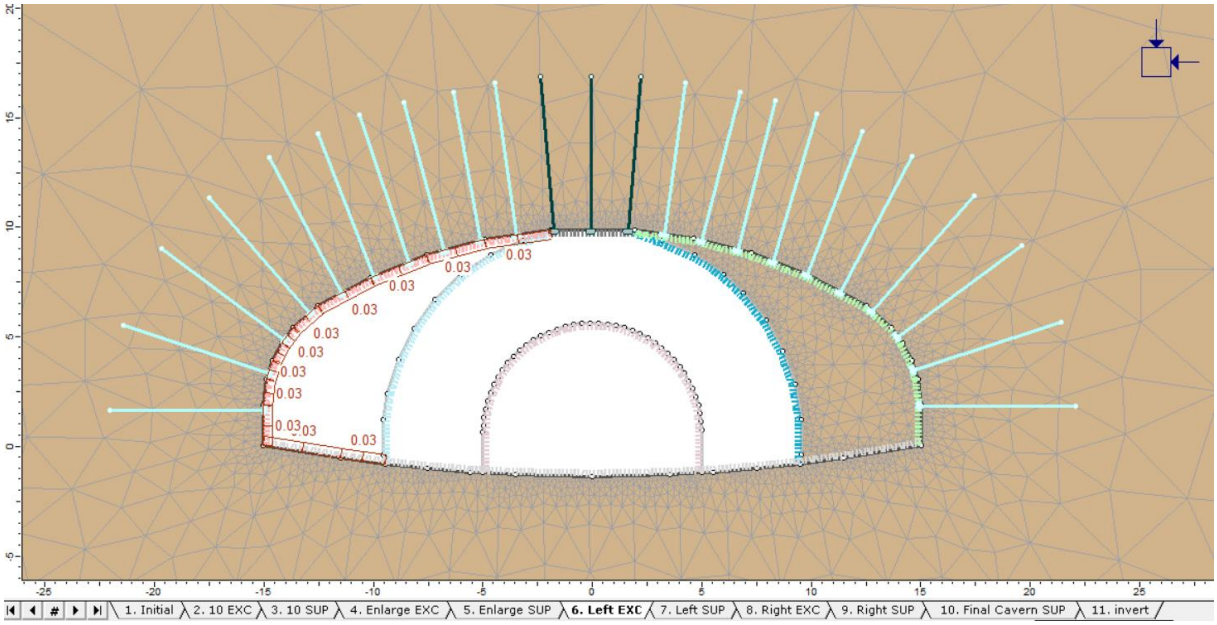

Figure 4-27. Model A- Stage 6

- **Stage 7 - Left SUP:** Slice on the left is supported by rock bolts and the Composite liner (It should be noted that the second layer of composite which is the RRS is not activated in this stage, The Composite liner only indicating the 1st layer shotcrete (Liner stage 7; The RRS is activated in Stage 10).

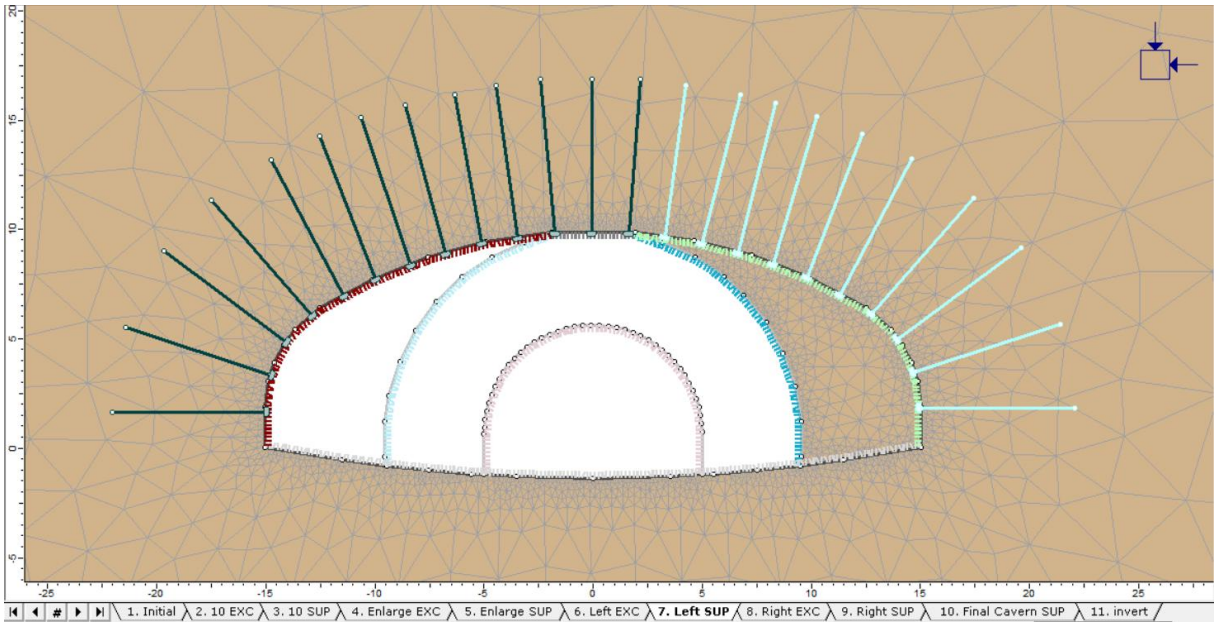

Figure 4-28. Model A- Stage 7

- **Stage 8 - Right EXC:** remained slice on the right is excavated until the maximum excavation boundary (post-excavation stress is applied as induced stress factor equal to 0.03).

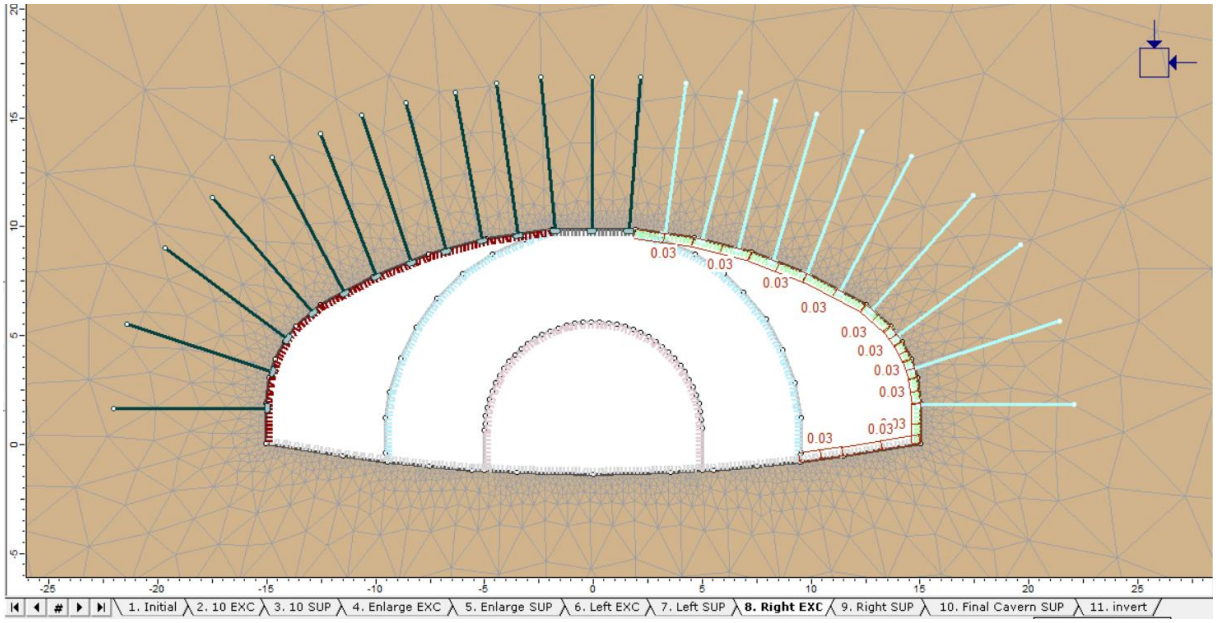

Figure 4-29. Model A-Stage 8

- **Stage 9 - Slice Right SUP:** same support category in stage 7 on the right (It should be noted that the second layer of composite which is the RRS is not activated in this stage, The Composite liner is only indicating the 1st layer shotcrete (liner stage 9); The RRS is activated one stage later); in this stage the cavern has been excavated completely.

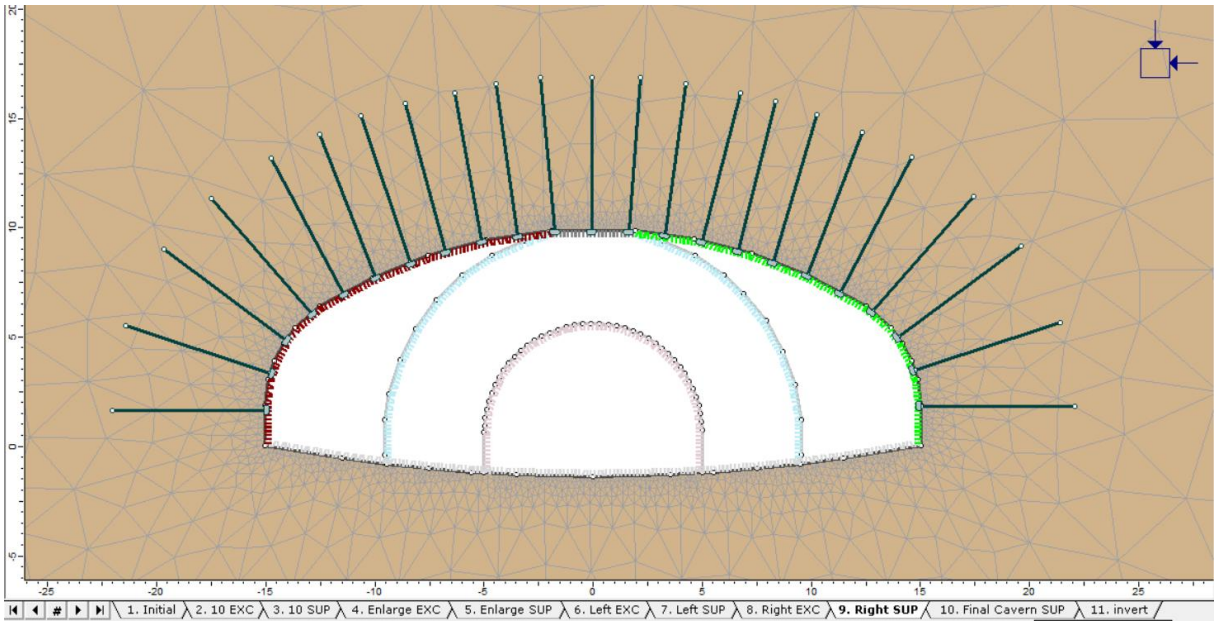

Figure 4-30. Model A-Stage 9

- **Stage 10 – Final cavern SUP:** in this stage the last phase of lining which simulate the RRS as reinforced concrete is activated (only second layer of Composite liner which is the RRS is activated, and all first layers, Liner 3, 5, 7 and 9 are disactivated in this stage).

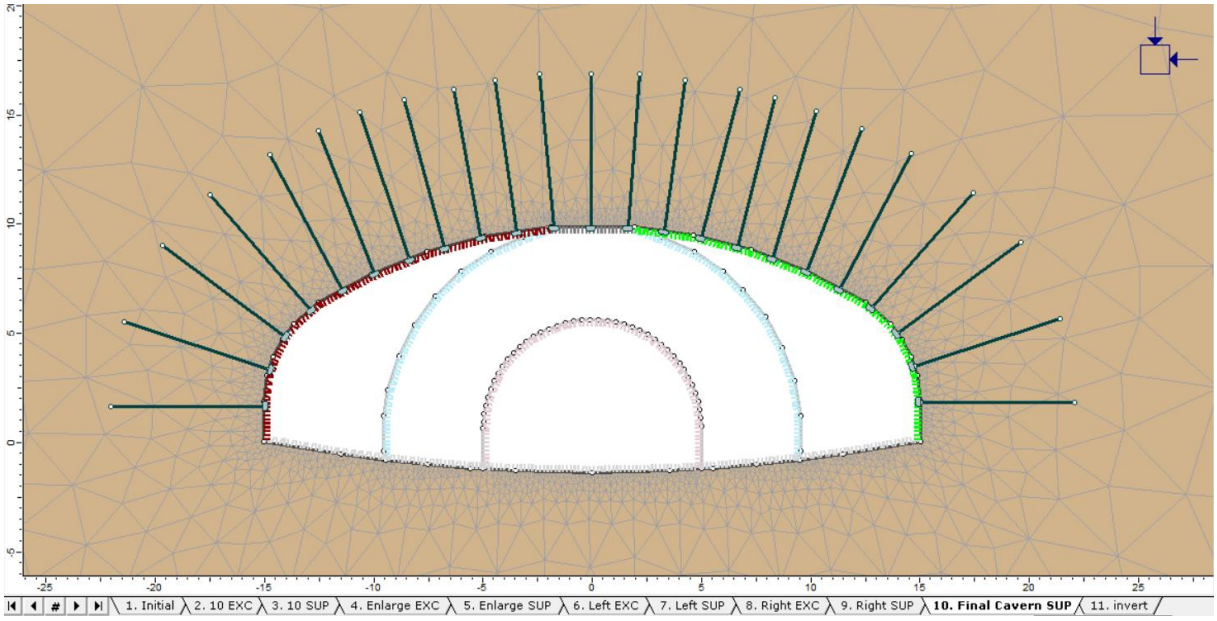

Figure 4-31. Model A-Stage 10

- **Stage 11 – Invert:** final 15cm of shotcrete is applied to the invert.

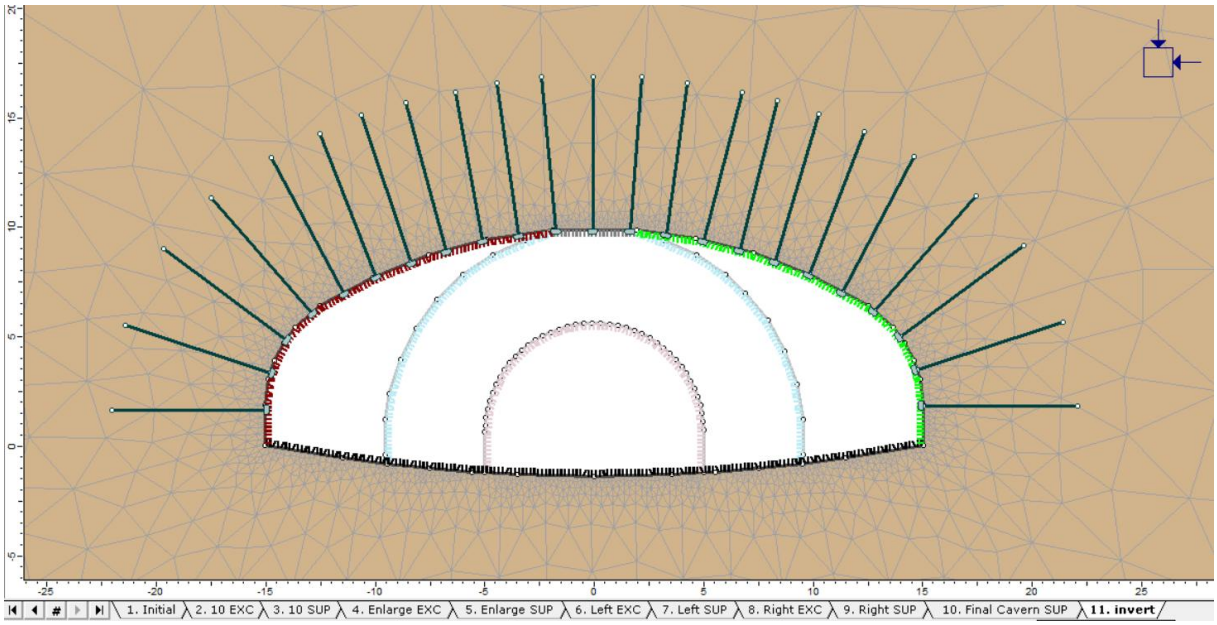

Figure 4-32. Model A- Stage 11

4.1.2.2. Model B – Side Drifts (SD)

This model indicates the sequences of excavation starting from the sides of the cavern and then finish excavation by removing the middle portion.

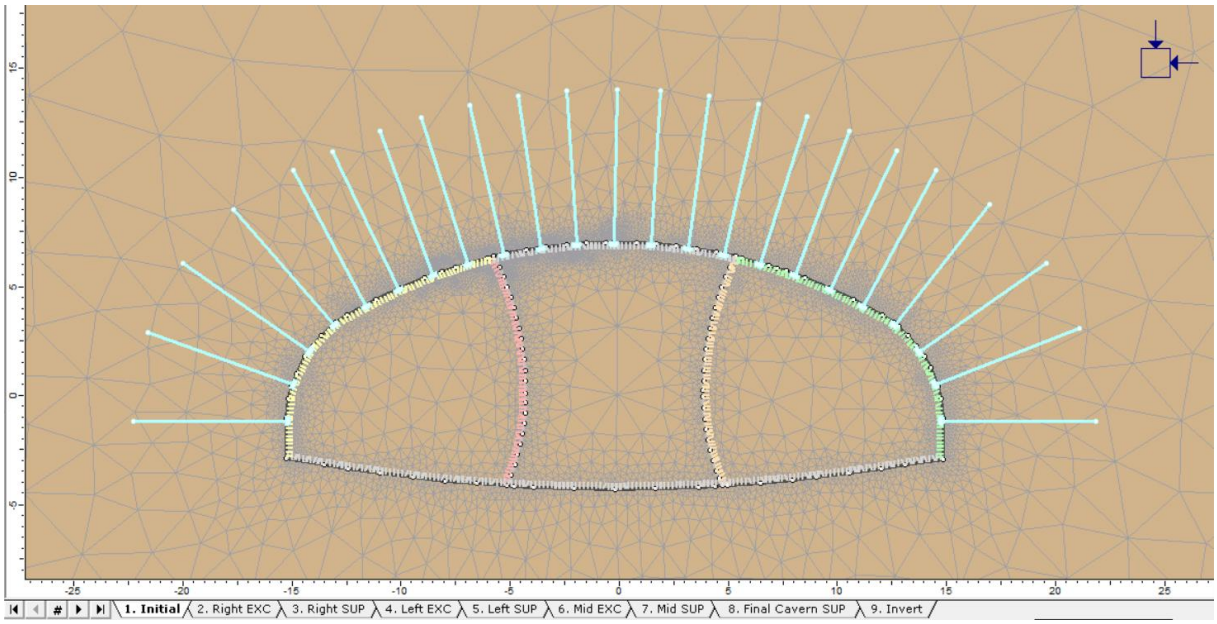

Figure 4-33. Model B

In this model "1st layer shotcrete" is applied in each stage as smoothing layer after the excavation an then after last stage of excavation the RRS is activated as final lining.

There are composite liner applied to the cavern boundaries including 1st layer of shotcrete and RRS; As it was mentioned in Model A these two layers will not be activated at same time; 1st layer of shotcrete is applied directly to the excavation boundaries after each excavation stage until the last stages then RRS will take place which is a simulated reinforced concrete liner representing both 15cm of shotcrete and Reinforced Ribs Sprayed Concrete as a single layer named RRS.

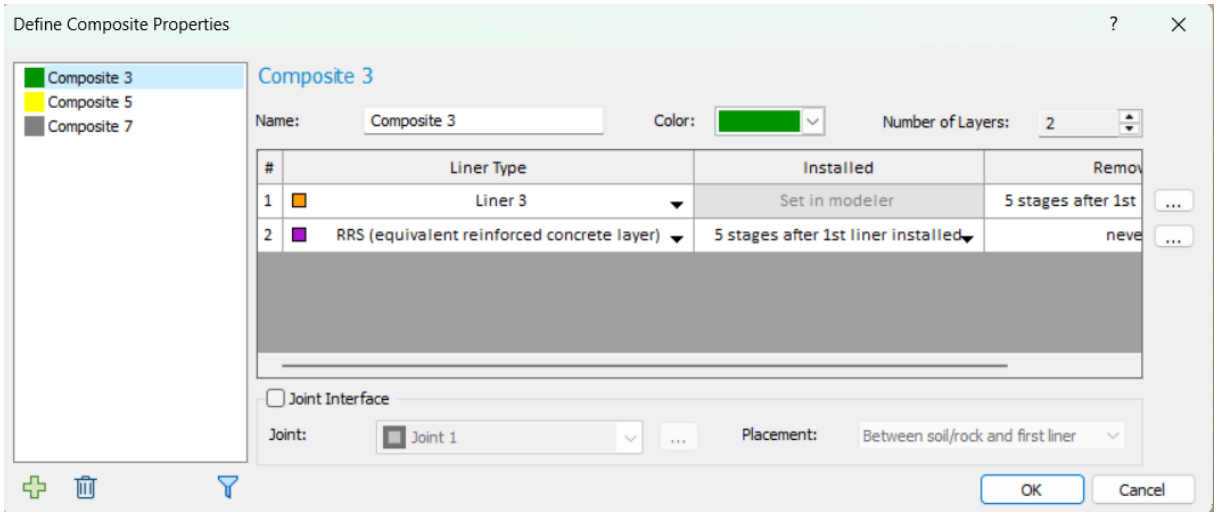

Figure 4-34. Composite 3 – Model B

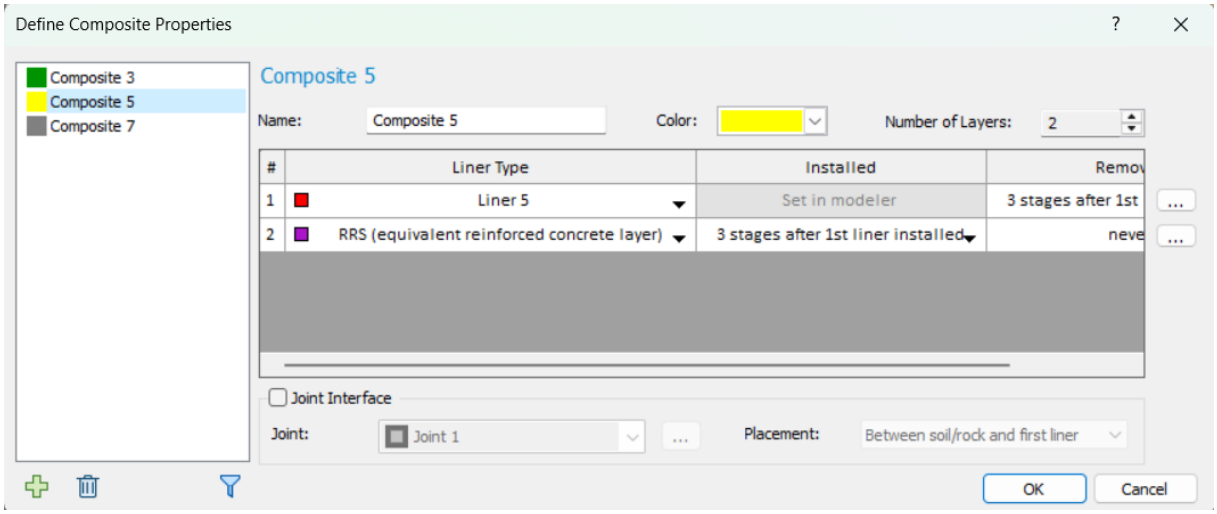

Figure 4-35. Composite 5 – Model B

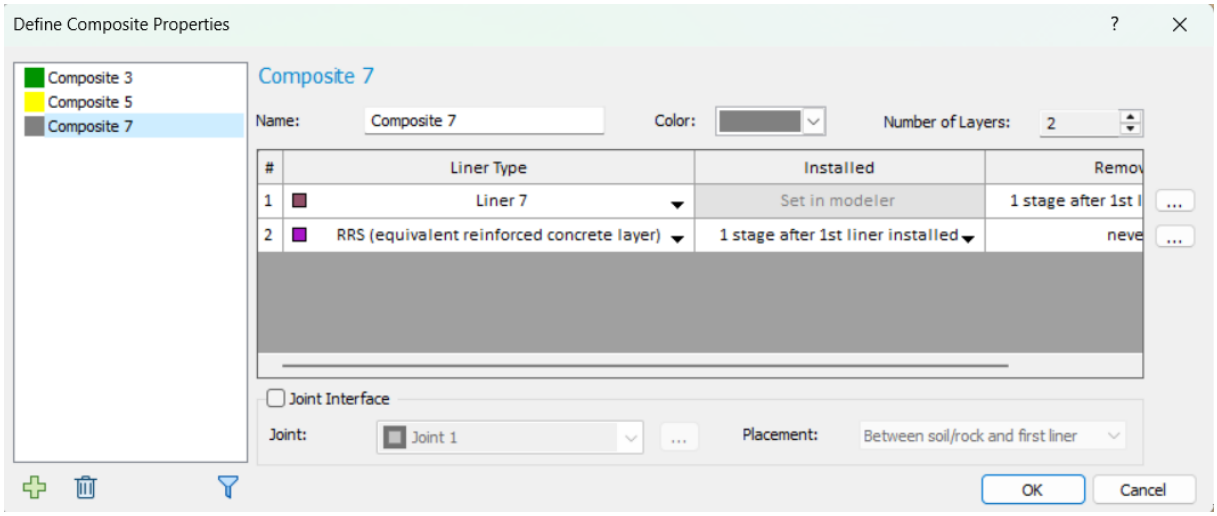

Figure 4-36. Composite 7 – Model B

Following figure shows the construction stages in Model B.

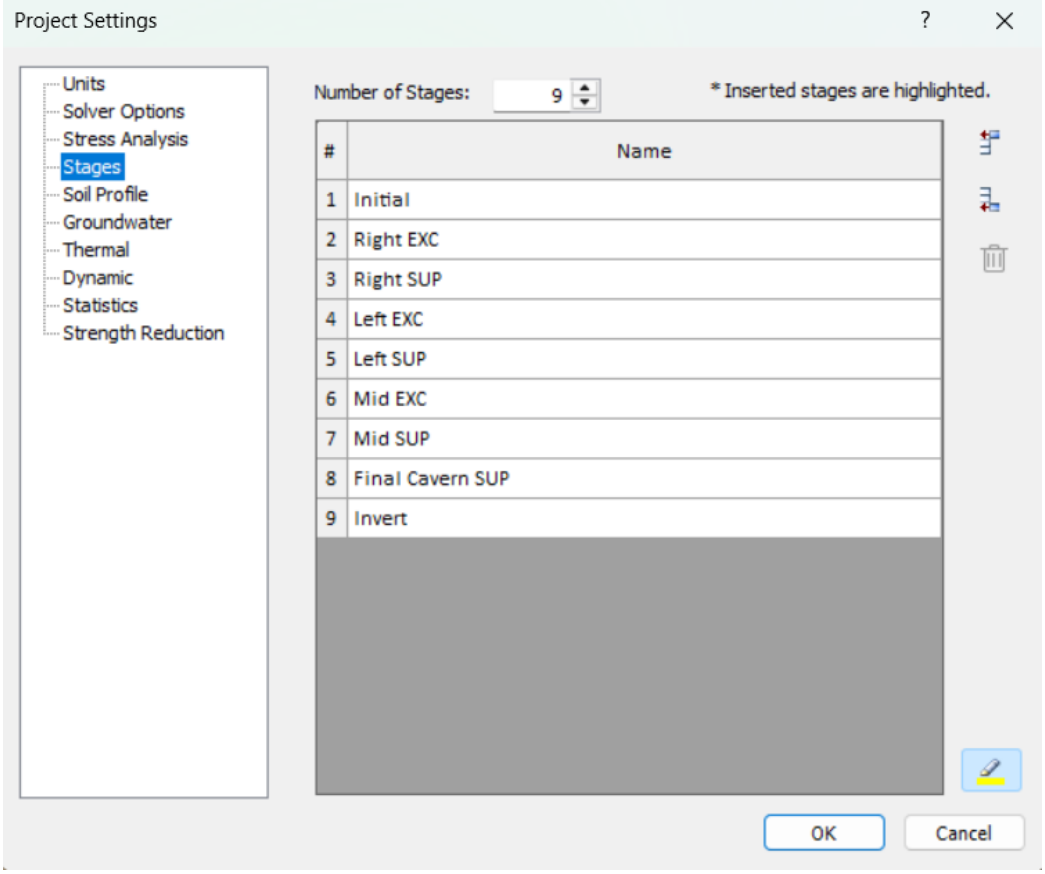

Figure 4-37. Construction Stages in Model B

- **Stage 1 – Initial:** in this stage, nothing has been excavated and the Rock mass is under its natural pressure.

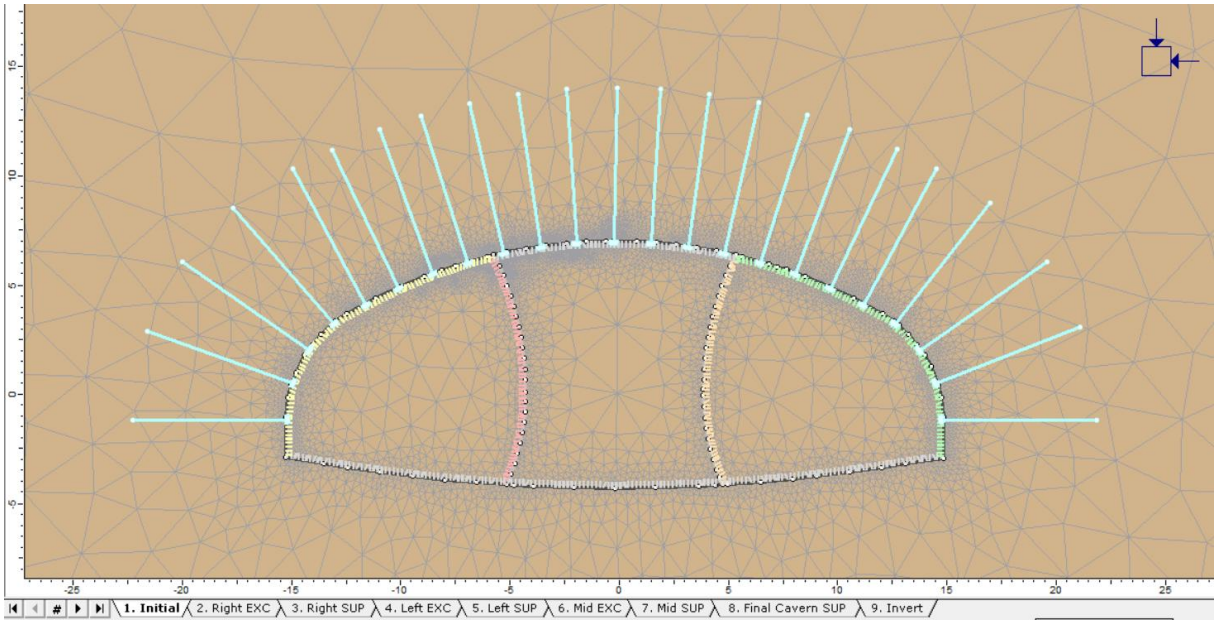

Figure 4-38. Model B-Stage 1

- **Stage 2 – Right EXC:** the portion on the right is excavated (post-excavation stress is applied as induced stress factor equal to 0.03).

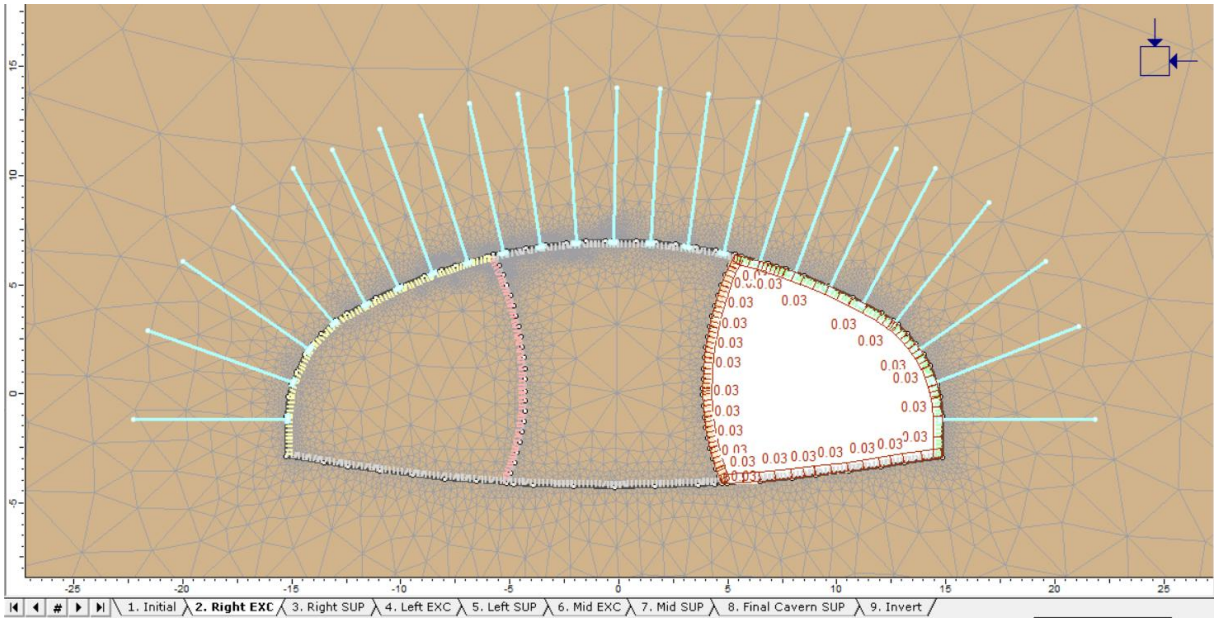

Figure 4-39.Model B-Stage 2

- **Stage 3 – Right SUP:** the excavated boundaries are supported by 1st layer of shotcrete and the rock bolts.

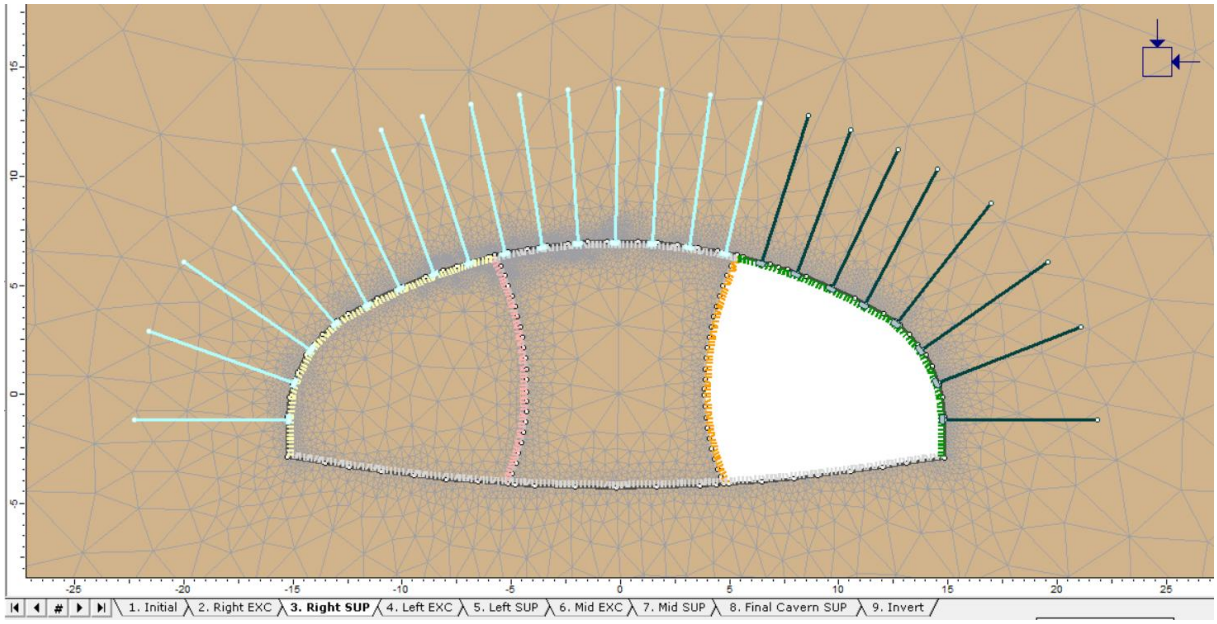

Figure 4-40.Model B-Stage 3

- **Stage 4 – Left EXC:** the portion on the left is excavated (post-excavation stress is applied as induced stress factor equal to 0.03).

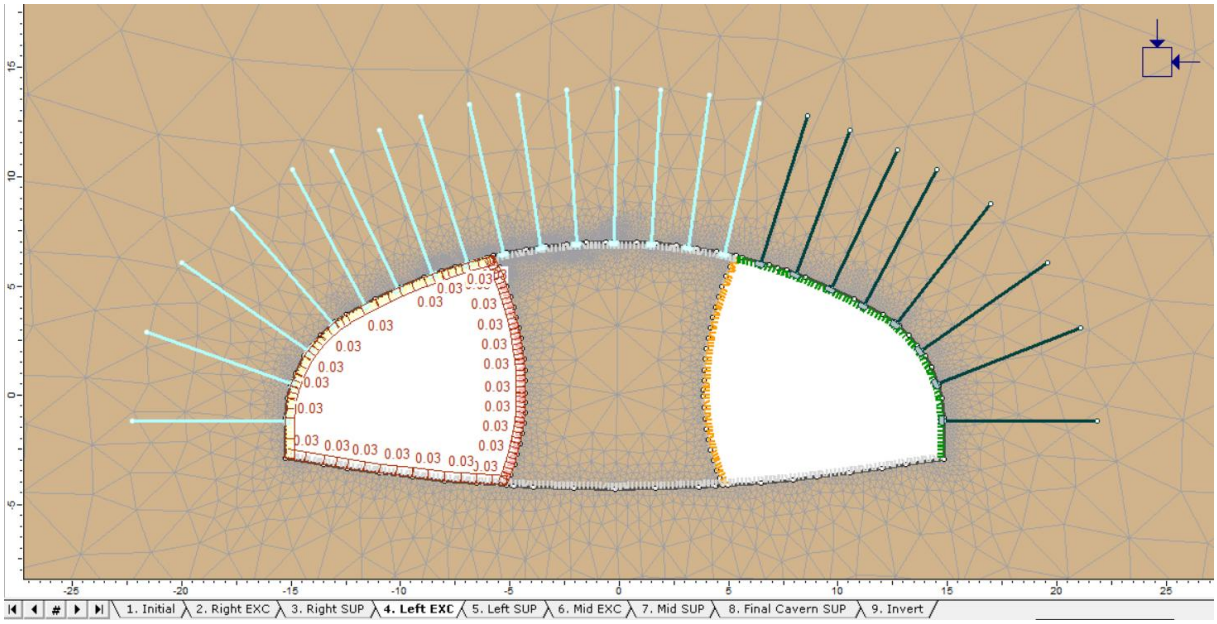

Figure 4-41. Model B-Stage 4

- **Stage 5 – Left SUP:** the excavated boundaries are supported by 1st layer of shotcrete and the rock bolts.

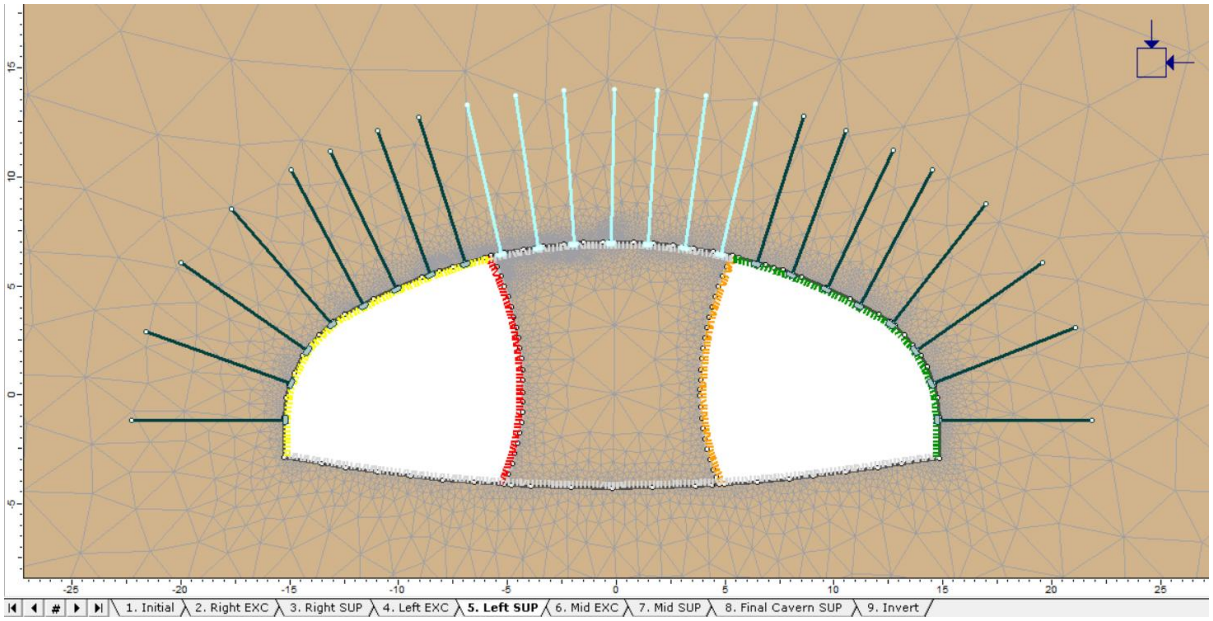

Figure 4-42. Model B-Stage 5

- **Stage 6 – Mid EXC:** the unexcavated portion in the middle is excavated (post-excavation stress is applied as induced stress factor equal to 0.03).

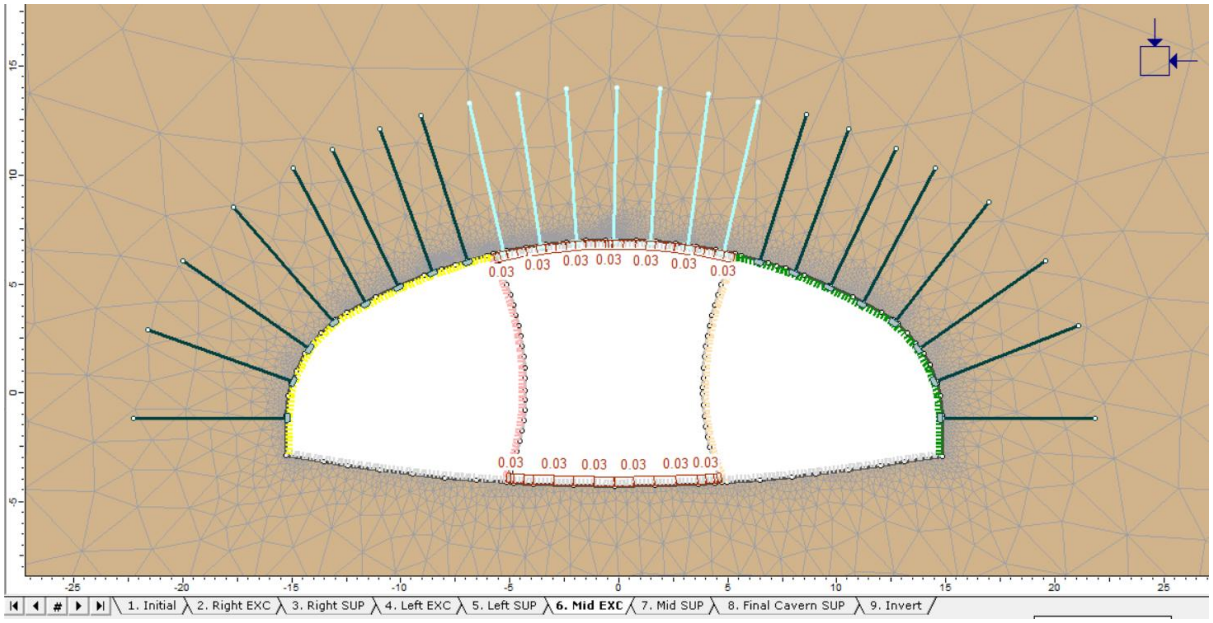

Figure 4-43. Model B-Stage 6

- **Stage 7 – Mid SUP:** excavated boundaries supported by 1st layer of shotcrete and the bolts.

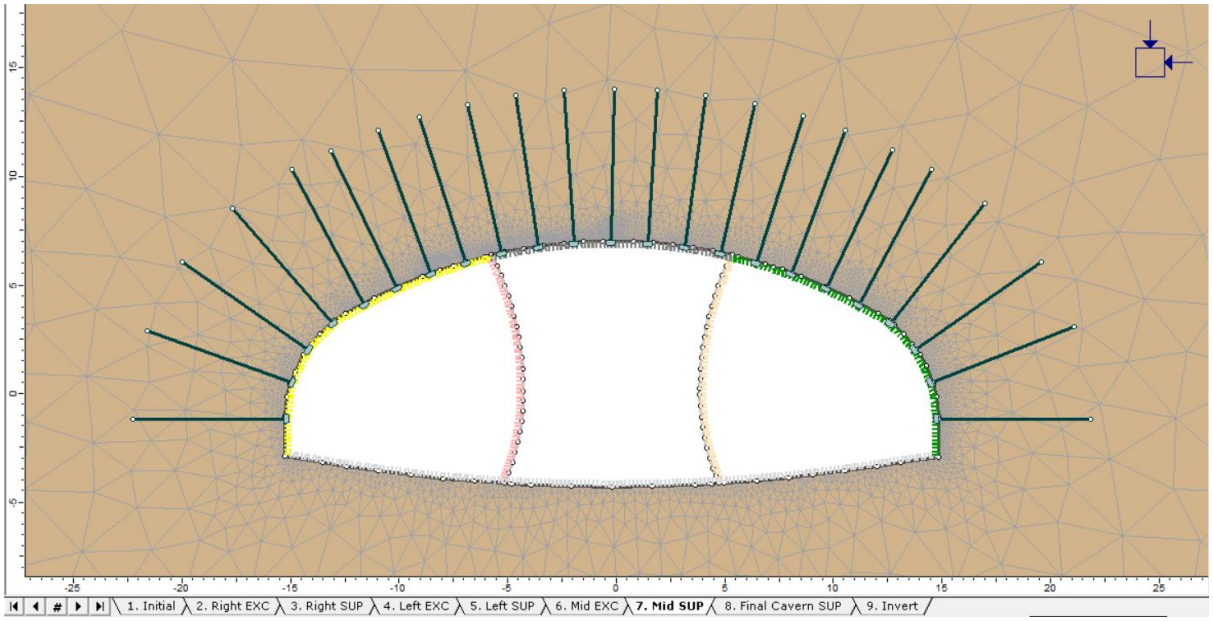

Figure 4-44. Model B-Stage 7

- **Stage 8 – Final Cavern SUP:** RRS is activated as the second layer of composite layer and 1st layer of shotcrete (Liner 3, 5 and 7) are disactivated.

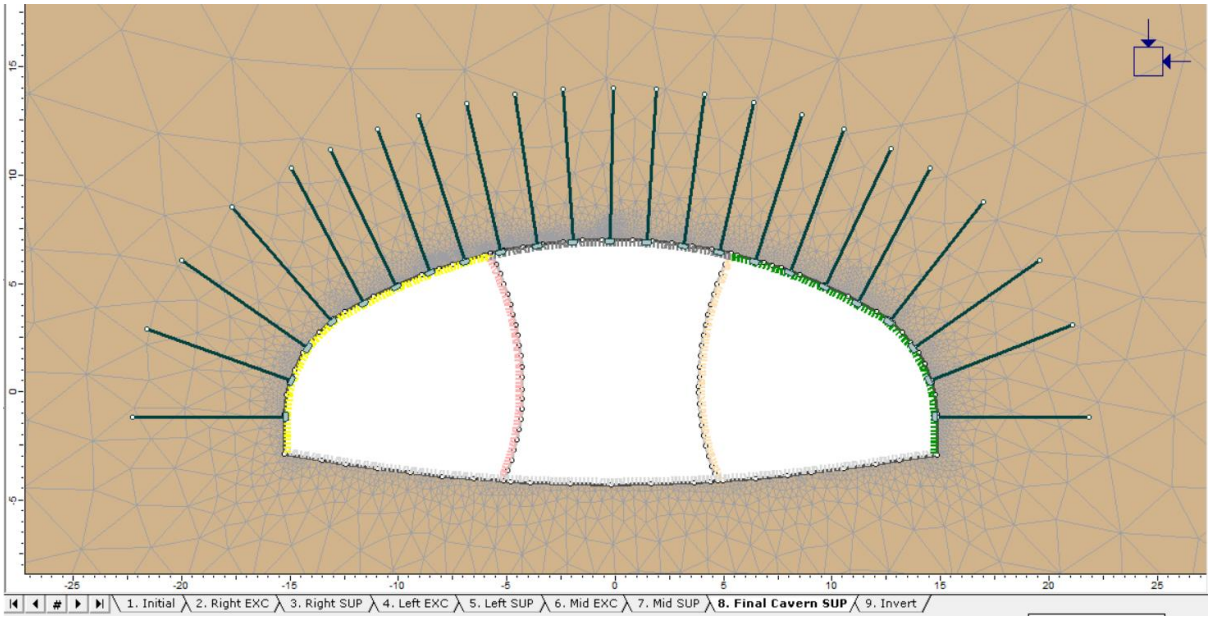

Figure 4-45. Model B-Stage 8

- **Stage 9 – Invert:** 15cm of shotcrete is applied to the invert.

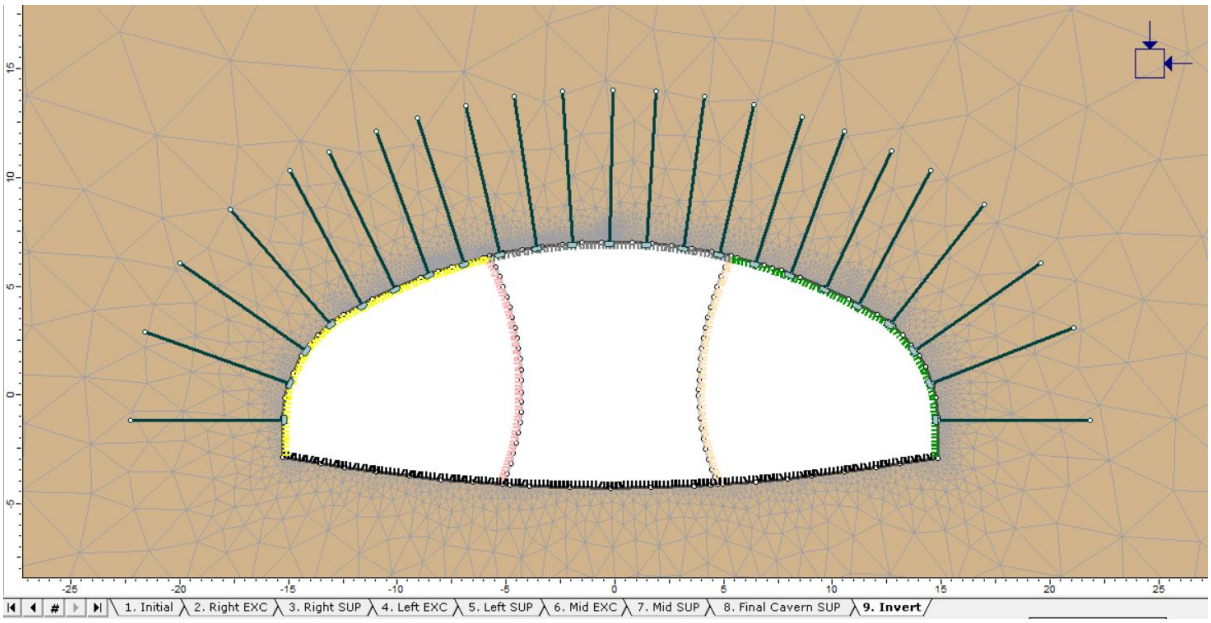

Figure 4-46. Model B - Stage 9

4.1.2.3. Model C – Top Heading and Bench (TBH)

This model follows an excavation sequence, beginning with the top heading, which is divided into two distinct phases and a bench.

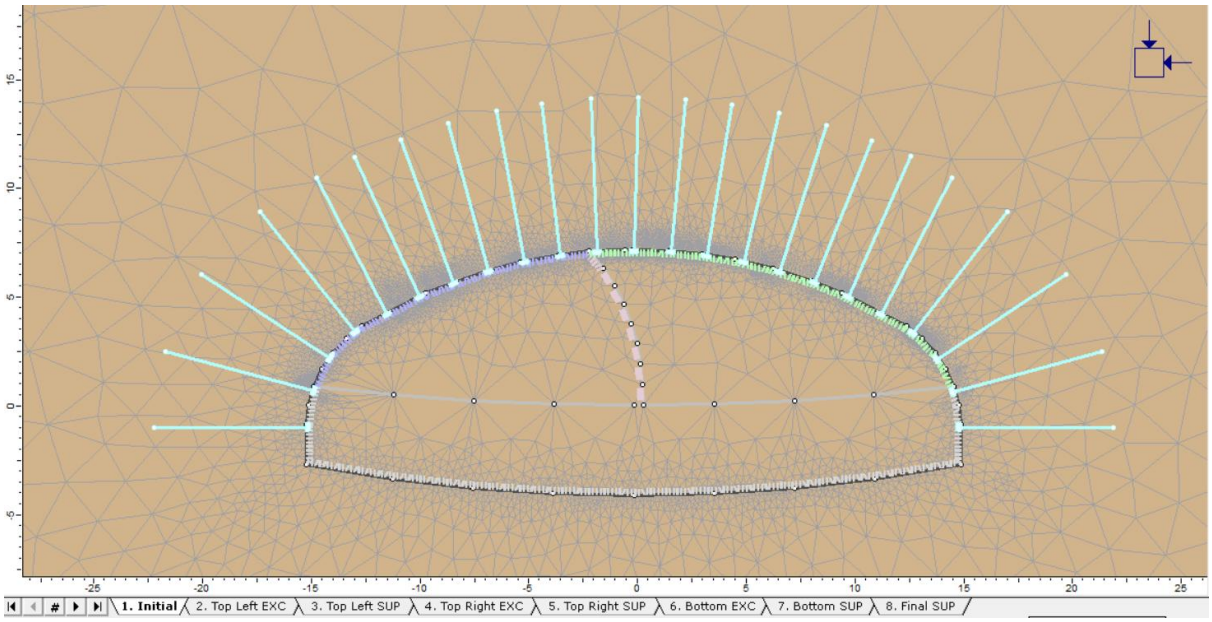

Figure 4-47. Model C

As was mentioned in the introduction of Model A and B, each portion will be excavated and supported based on the same procedure, first 15cm of 1st layer of shotcrete as the primary support along the rock bolts then in the end the RRS will take place in the last stage.

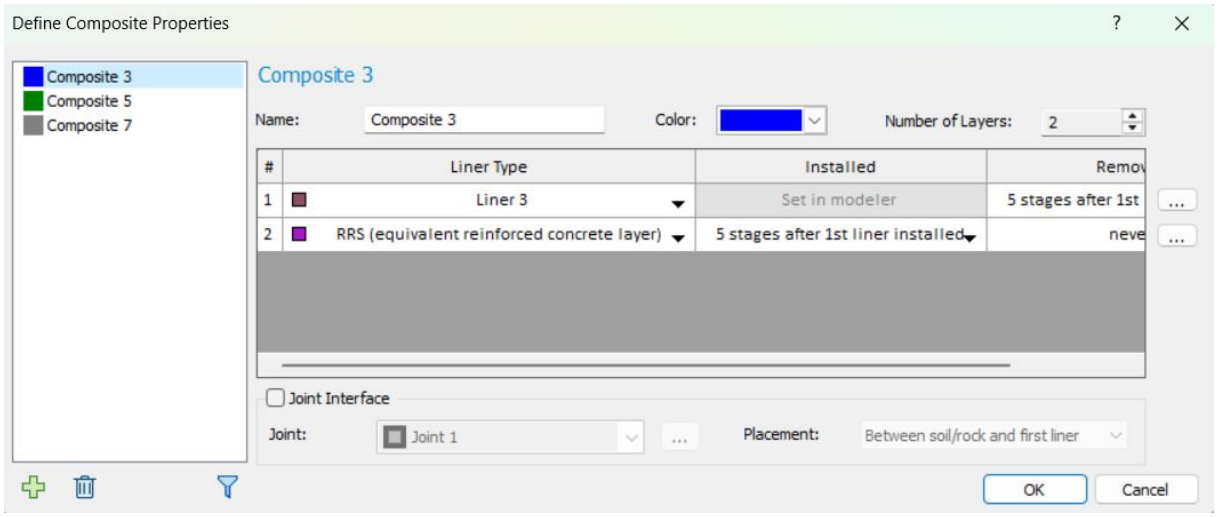

Figure 4-48. Composite 3– Model C

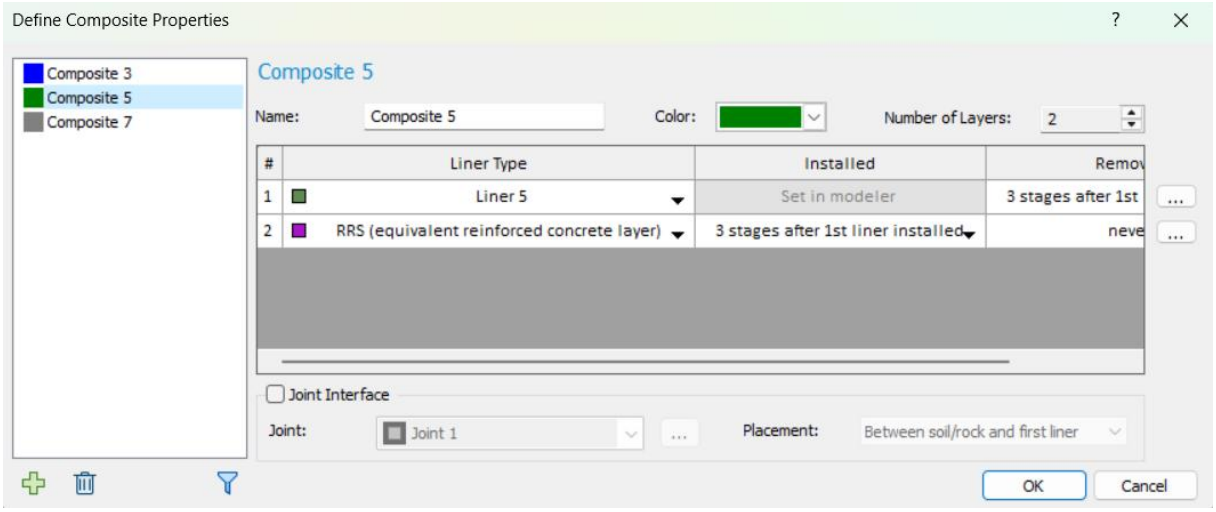

Figure 4-49. Composite 5 – Model C

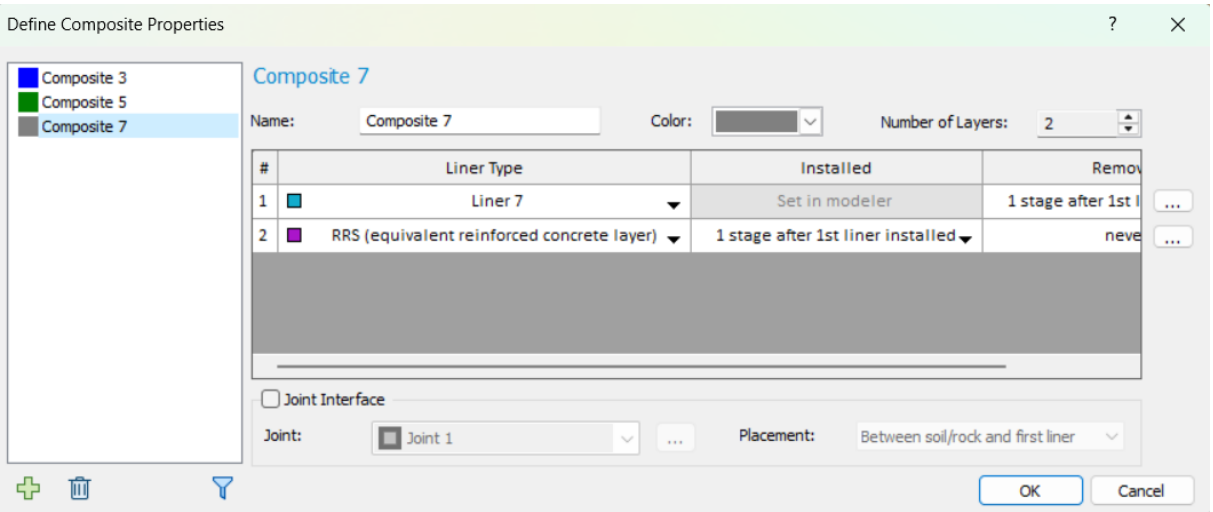

Figure 4-50. Composite 7 – Model C

Following figure (Figure 4-51) shows the number of stages for model C.

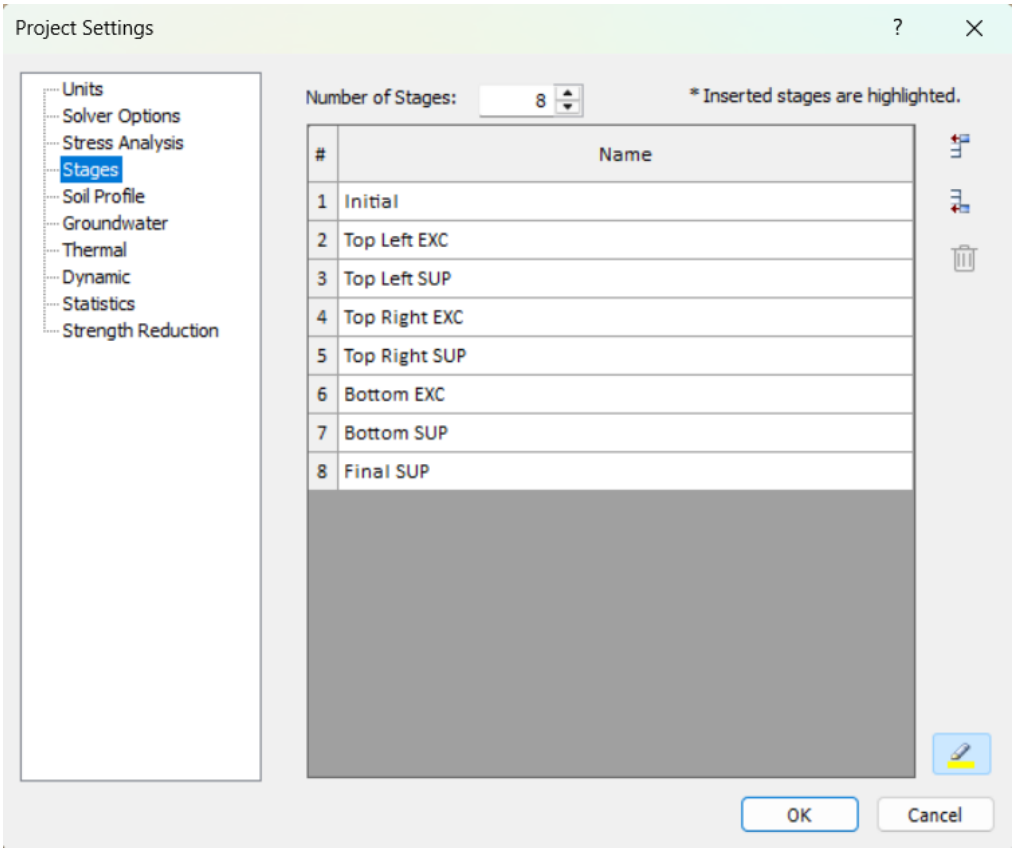

Figure 4-51. Stages in Model C

- **Stage 1 – Initial:** Nothing has been excavated; rock mass is under its natural pressure.

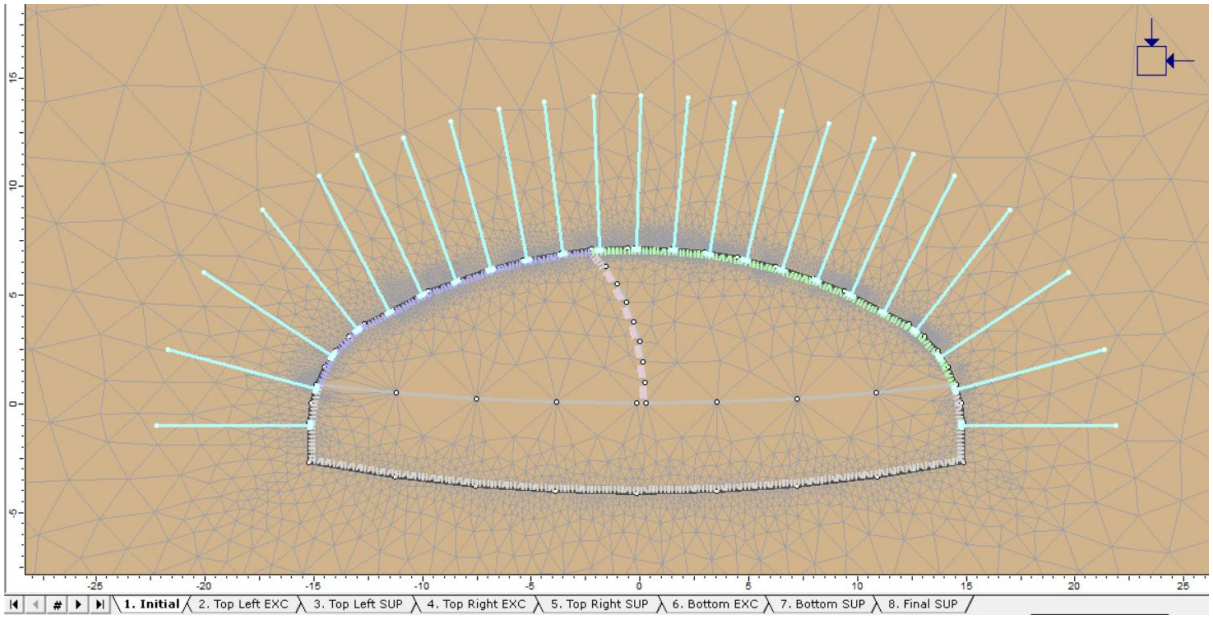

Figure 4-52. Model C-Stage 1

- **Stage 2 – Top Left EXC:** Portion in the top left is excavated (post-excavation stress is applied as induced stress factor equal to 0.03).

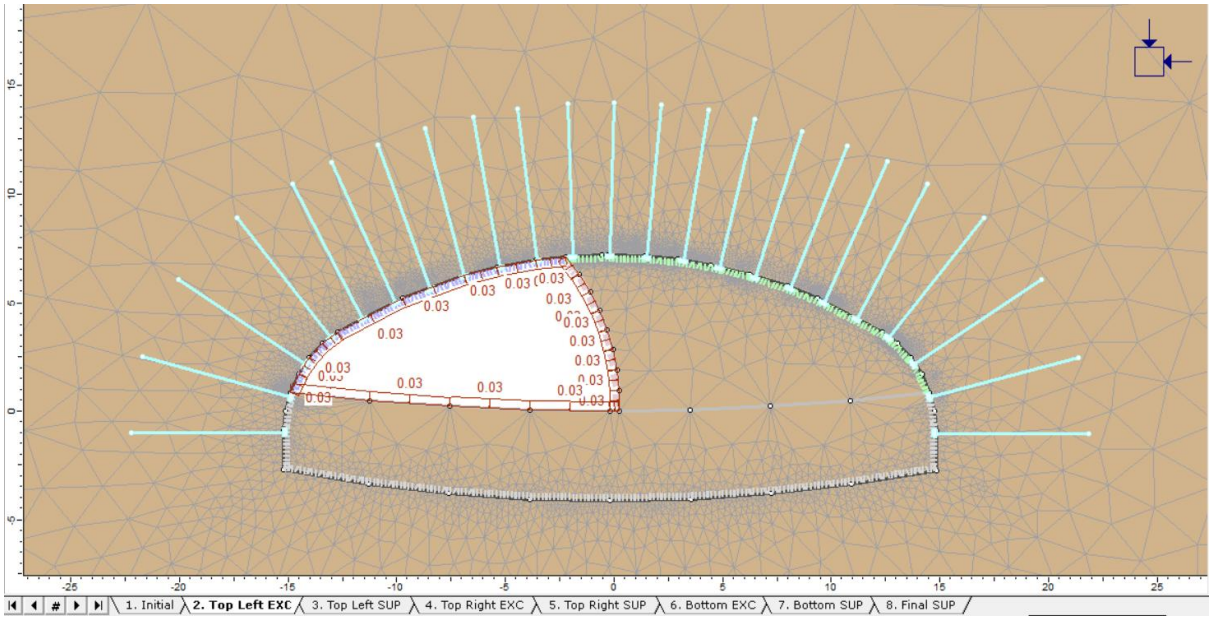

Figure 4-53. Model C-Stage 2

- **Stage 3 – Top Left SUP**: excavation boundary is supported with 1st layer of shotcrete and rock bolts.

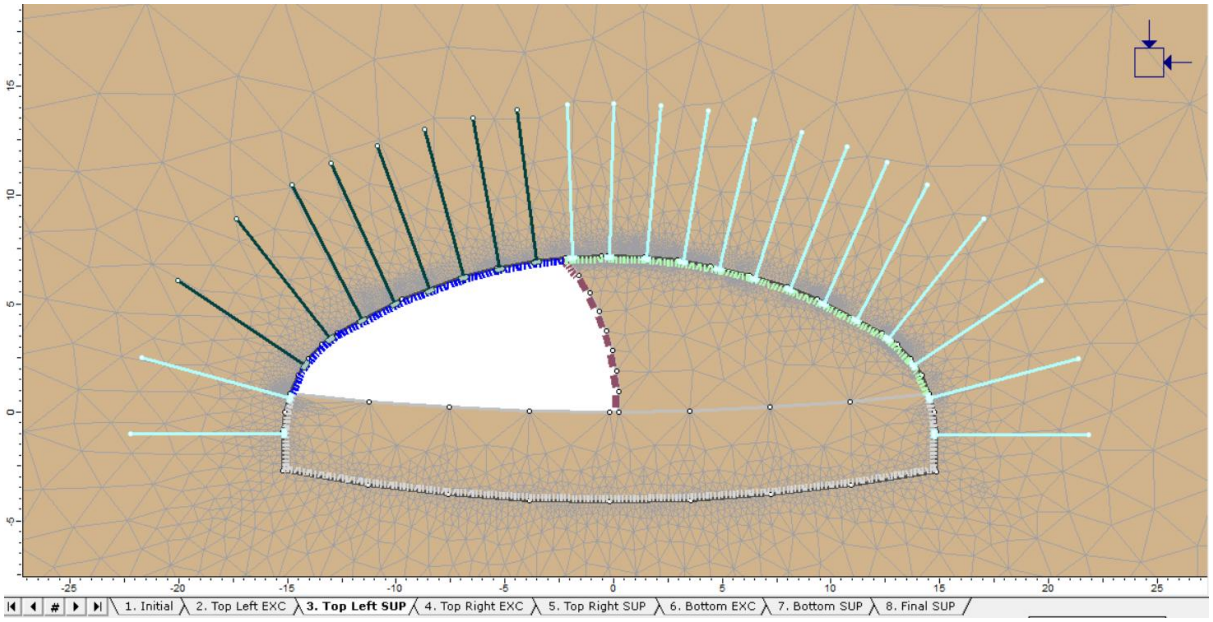

Figure 4-54. Model C-Stage 3

- **Stage 4 – Top Right EXC:** Slice in the top right is excavated (post-excavation stress is applied as induced stress factor equal to 0.03).

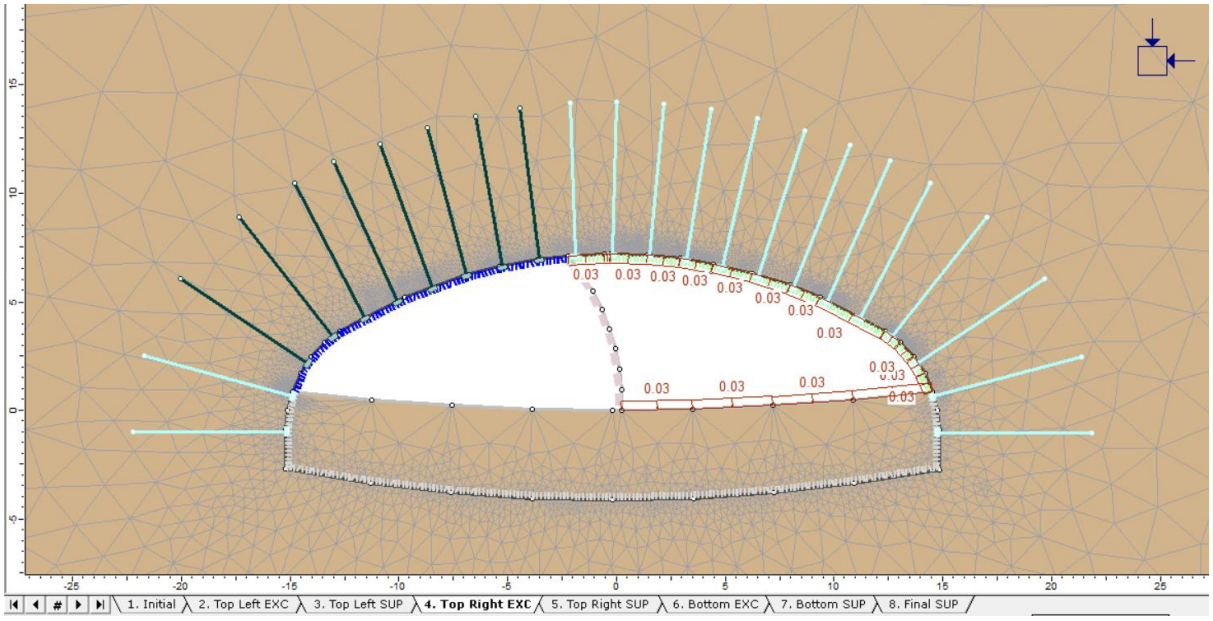

Figure 4-55. Model C-Stage 4

- **Stage 5 – Top Right SUP:** Top right portion is supported with shotcrete and bolts.

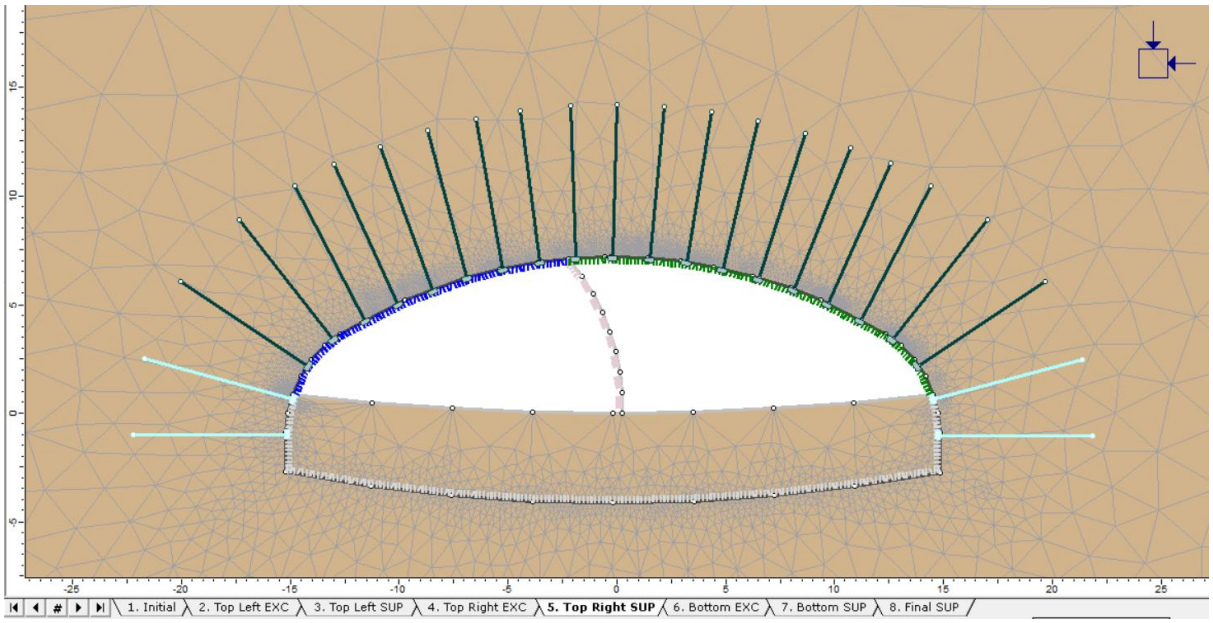

Figure 4-56. Model C-Stage 5

- **Stage 6 – Bottom EXC:** Last portion which is the bottom of the cavern is excavated (post-excavation relaxation stress is applied as induced stress factor equal to 0.03).

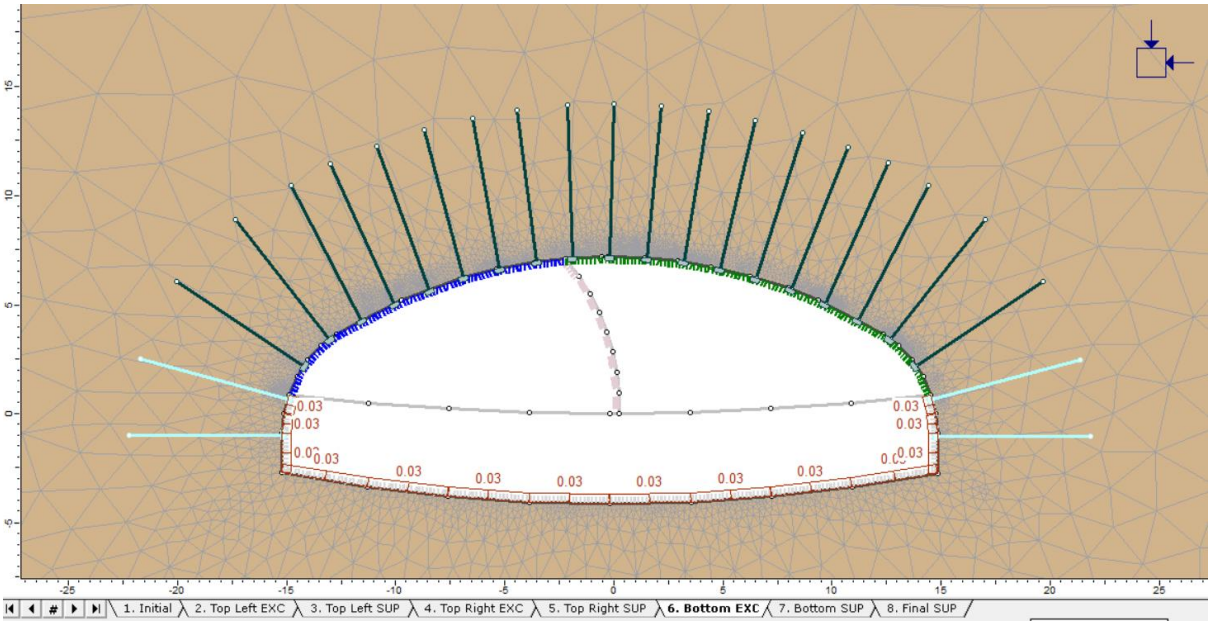

Figure 4-57. Model C-Stage 6

- **Stage 7 – Bottom SUP:** remained part of the walls and the invert is supported by 15cm 1st layer of shotcrete and bolts.

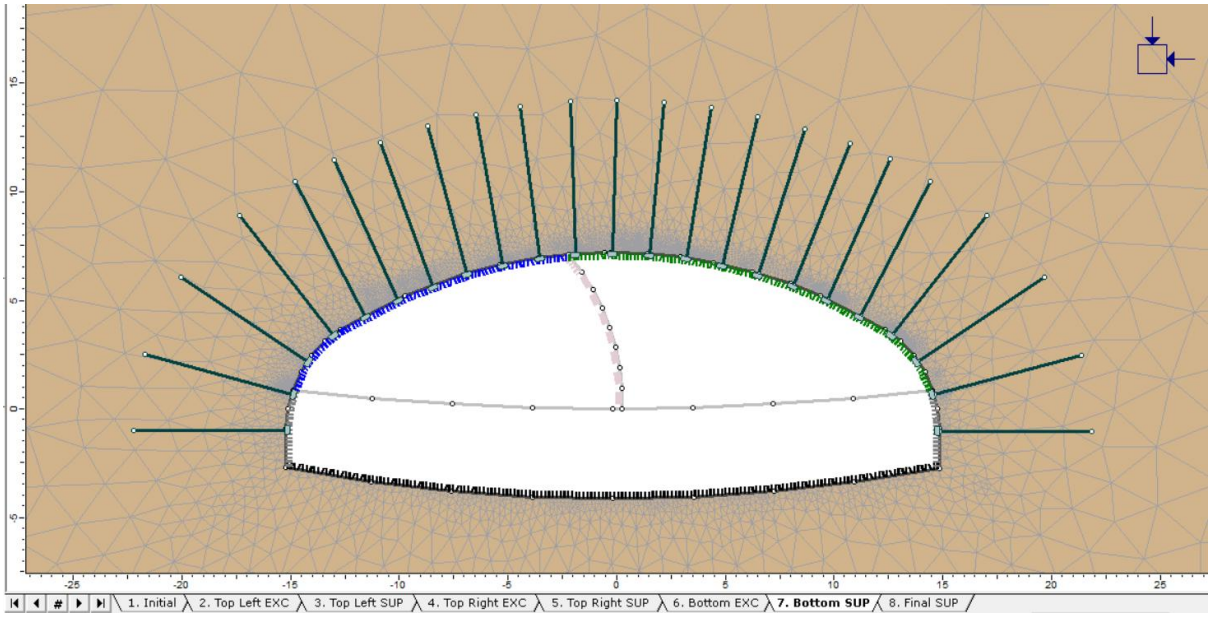

Figure 4-58. Model C-Stage 7

- **Stage 8 – Final Cavern SUP:** RRS is activated and simultaneously 1st layer of shotcrete (Liner 3, 6 and 7) is disactivated.

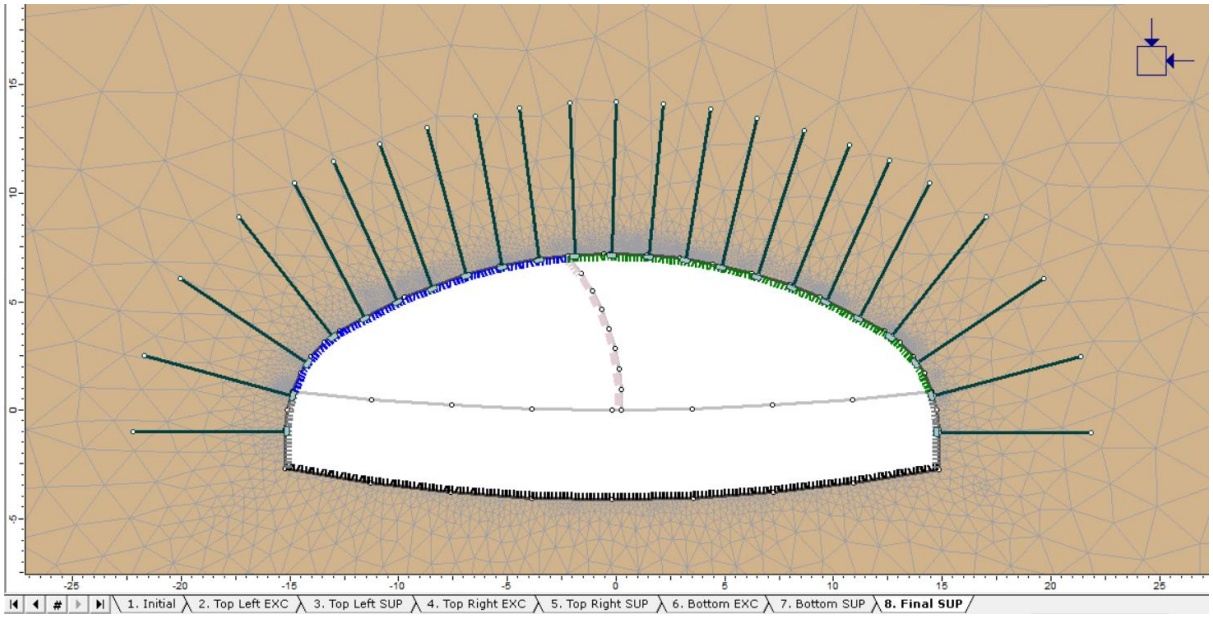

Figure 4-59. Model C - Stage 8

4.1.3. Output overview

This section focused that which outputs of numerical modeling are introduced, and which parameters are included in the investigation.

Displacement: This section will introduce the amount of deformation of the rock mass specifically on the cavern boundary with colored contour lines around the cavern.

Plastic Zone: After each stage of excavation and support a plastic zone will be developed around the excavation boundaries.

Axial Force on Bolts: Rock-bolts must withstand axial forces to keep the stability of the rock mass after excavation; in this section the axial forces acting on the rock-bolts are presented.

Axial Force and Bending Moment on RRS: final lining will be subjected to ground reaction forces which will be shown as axial force and bending moment on the RRS.

Support Capacity, RRS: this section is introducing the capacity of the final lining in M-N-T domain considering four different amount of Safety Factors (FS =1, 2, 3 and 4) based on the Carranza-Torres method that was explained in Chapter 2 (2.6.2. Carranza-Torres & Diederichs Domain)

Support Capacity, Rock-bolts: in this section, number of yielded bolts, their place and type of force acting on them are presented.

Chapter 5. Results

In this chapter the outputs of each model will be presented.

After computing the models, the results in interpretation tool of the **RS2** software can be seen.

Each model interpretation is presented with three different **Horizontal/Vertical stress ratio (k = 0.5, k = 1, k = 2).**

It should be noted that the corner points between the sidewalls and the invert were excluded from the analysis in all nine numerical models. This decision was made to focus on the primary structural zones of interest which are the crown, sidewalls, and invert where the stress redistribution and lining response are most critical. In finite element modelling, very small elements around sharp geometric corners can artificially amplify axial forces, bending moments, and shear forces due to numerical singularities associated with abrupt changes in geometry. These localized peaks do not represent the actual mechanical behaviour of the lining but are instead artefacts of the mesh and corner geometry. Therefore, neglecting these sharp corners provides a more realistic and physically meaningful interpretation of the lining forces and moments

5.1. Model A (RPE)

This model was introduced in Chapter 3 which simulates gradual radial expansion from the center to the final dimension of the Cavern. The results are presented in further sections with different stress ratios.

5.1.1. Model A – k = 0.5

This section is to present results of computation of Model A with stress ratio of 0.5.

5.1.1.1. Total Displacement

As a result of Finite Element Method modeling on the cavern, a contoured line set shows amount of displacement.

Maximum amount of displacement is placed in the invert and around 8.1 cm (Figure 5-1).

Direction of all displacement vectors are almost vertical except in the walls that are directed to outside of the excavation boundaries.

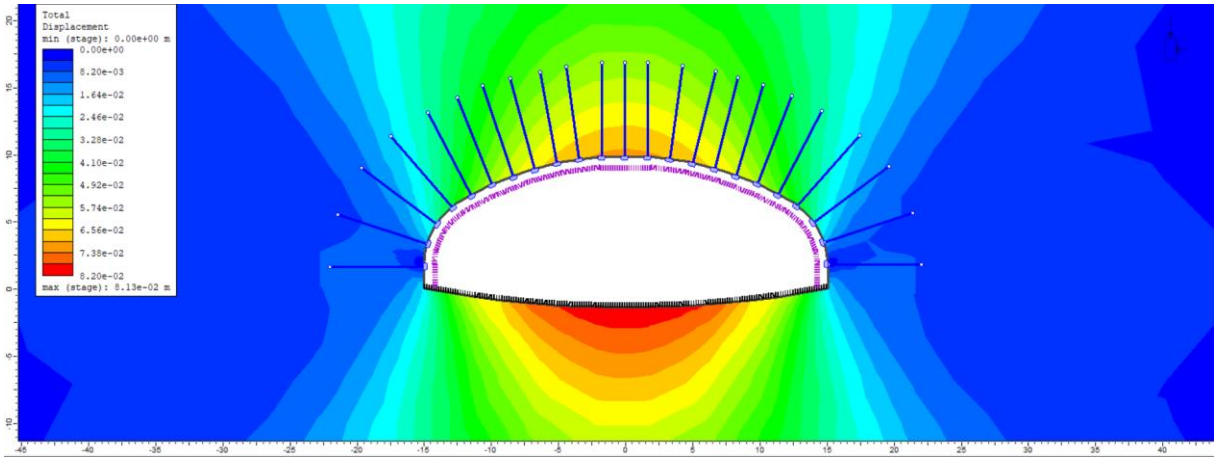

Figure 5-1. Total displacement - Model A, k = 0.5

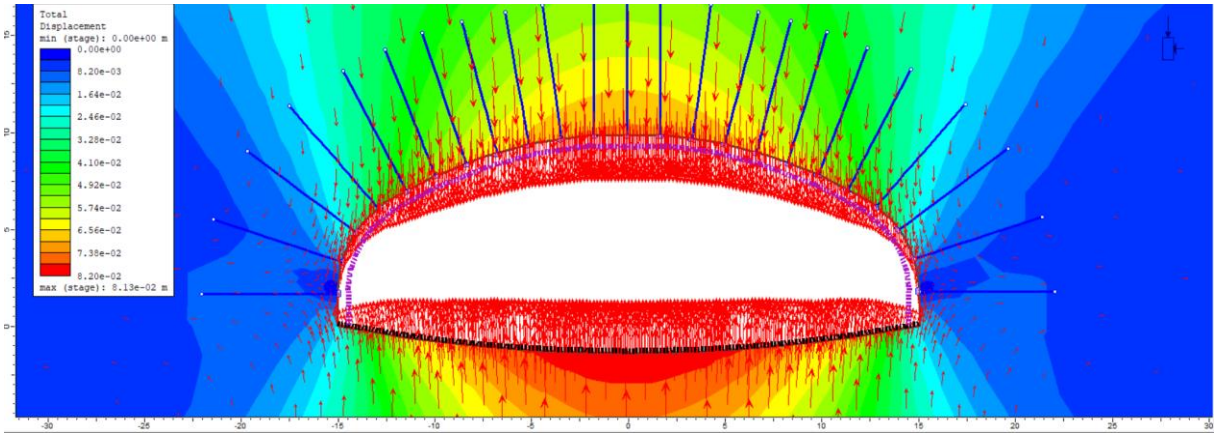

Figure 5-2. Deformation vectors and direction - Model A, k = 0.5

5.1.1.2. Plastic Radius around the cavern

It is important to visualize the behavior of Rock mass around the cavern and recognize the furthest points that act plastic around the excavation boundaries. Following figures show the percentage of plastic behavior around the cavern after each construction stage. Highest length plastic radius is almost 4 m in the last stage.

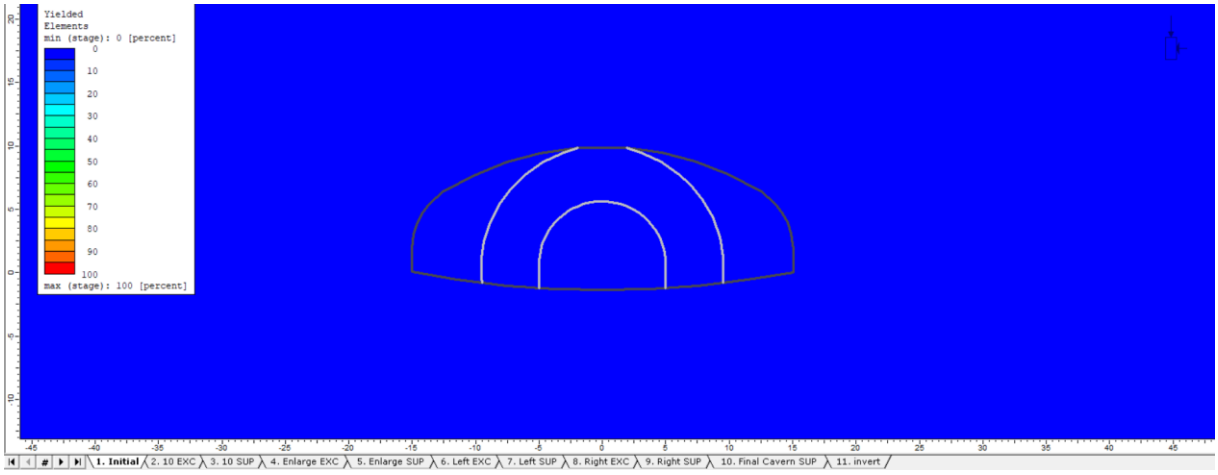

Figure 5-3. Yielded elements, Stage 1 - Model A, k = 0.5

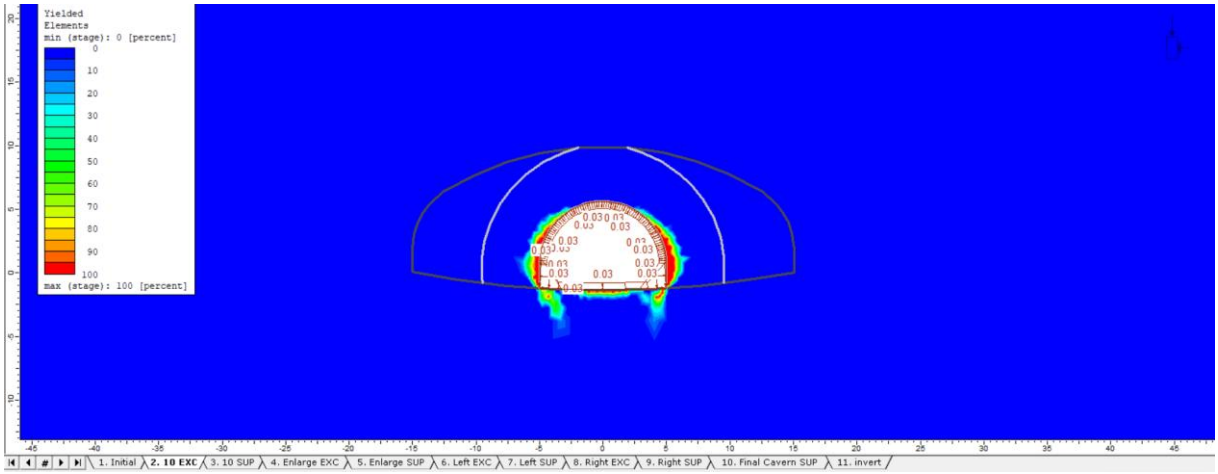

Figure 5-4. Yielded elements, Stage 2 - Model A, k = 0.5

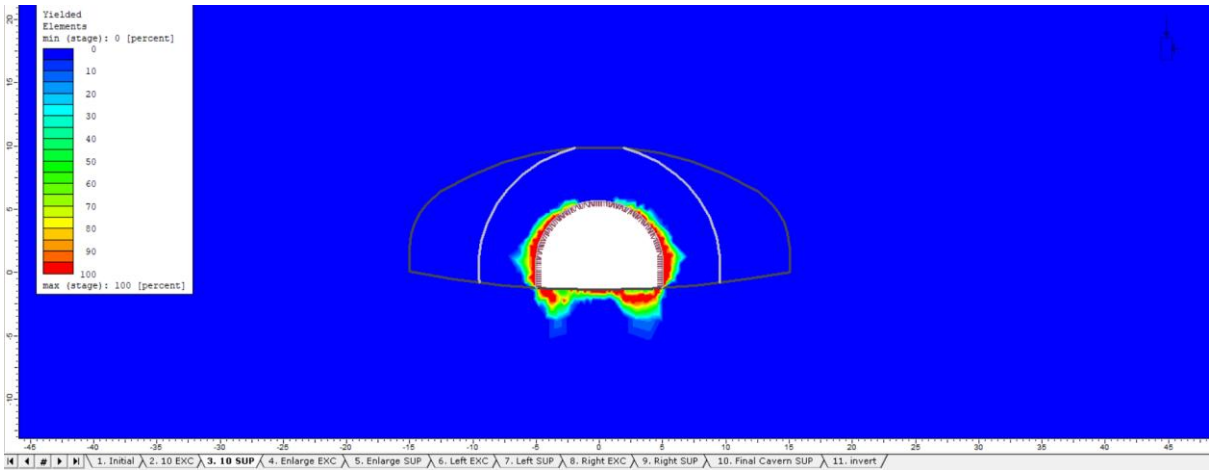

Figure 5-5. Yielded elements, Stage 3 - Model A, k = 0.5

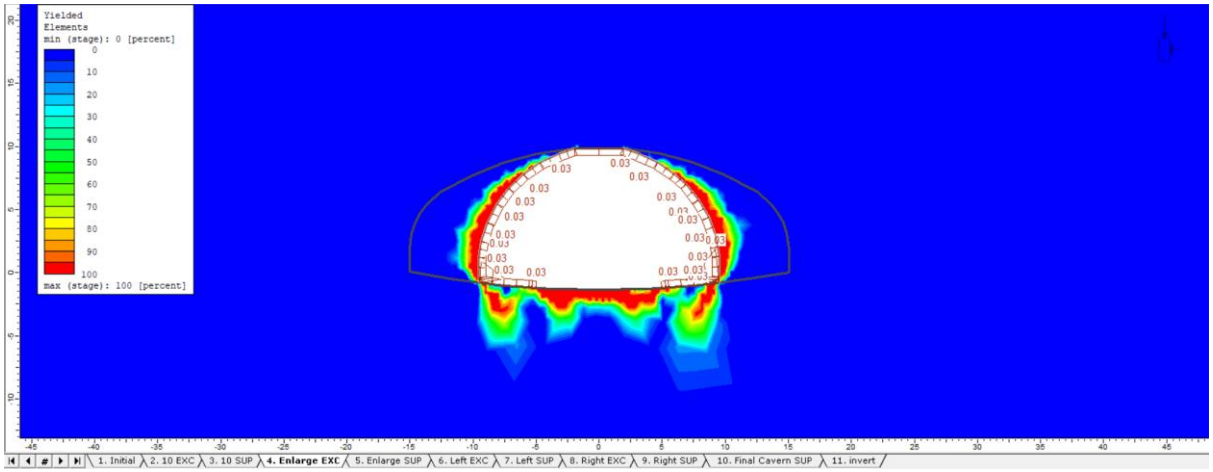

Figure 5-6. Yielded elements, Stage 4 - Model A, k = 0.5

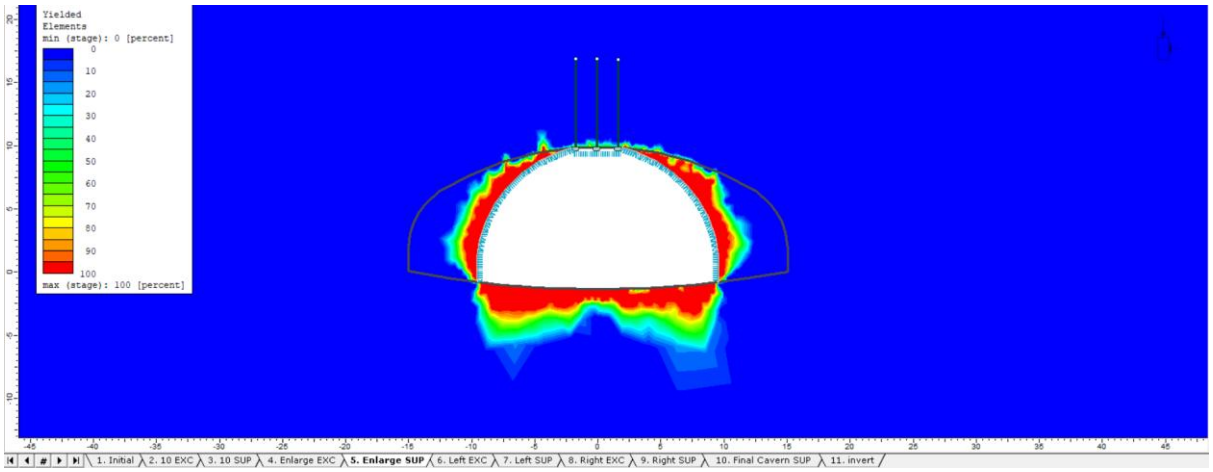

Figure 5-7. Yielded elements, Stage 5 - Model A, k = 0.5

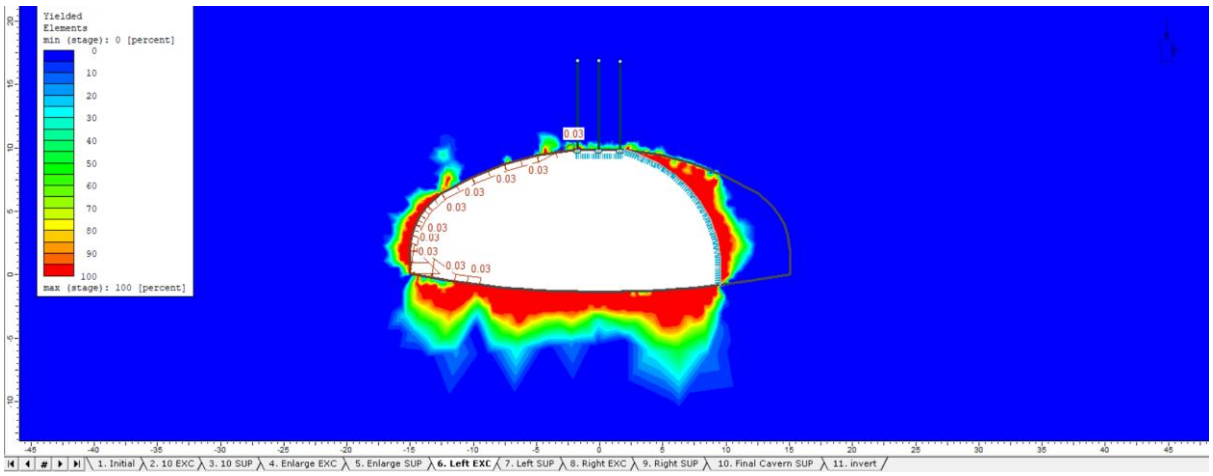

Figure 5-8. Yielded elements, Stage 6 - Model A, k = 0.5

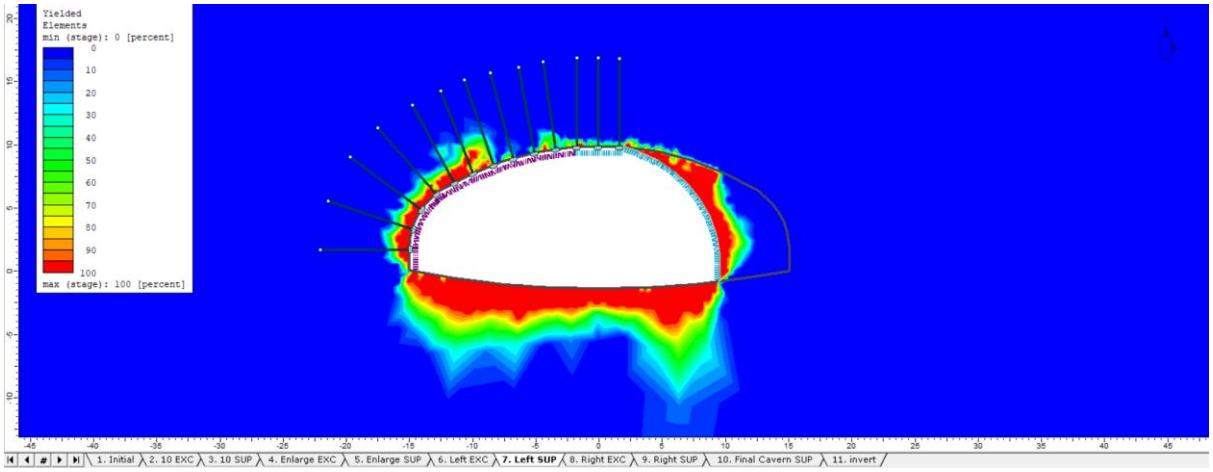

Figure 5-9. Yielded elements, Stage 7 - Model A, k = 0.5

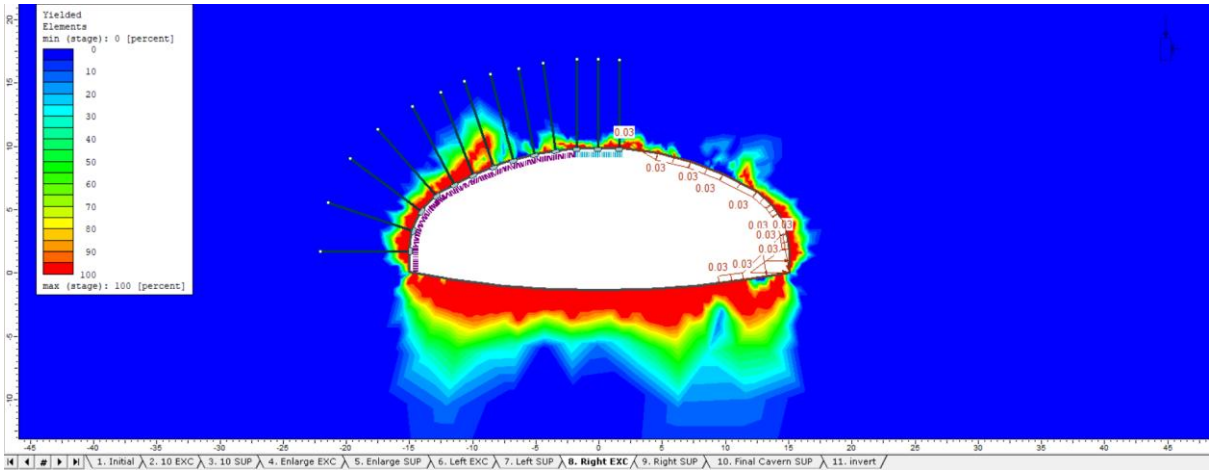

Figure 5-10. Yielded elements, Stage 8 - Model A, k = 0.5

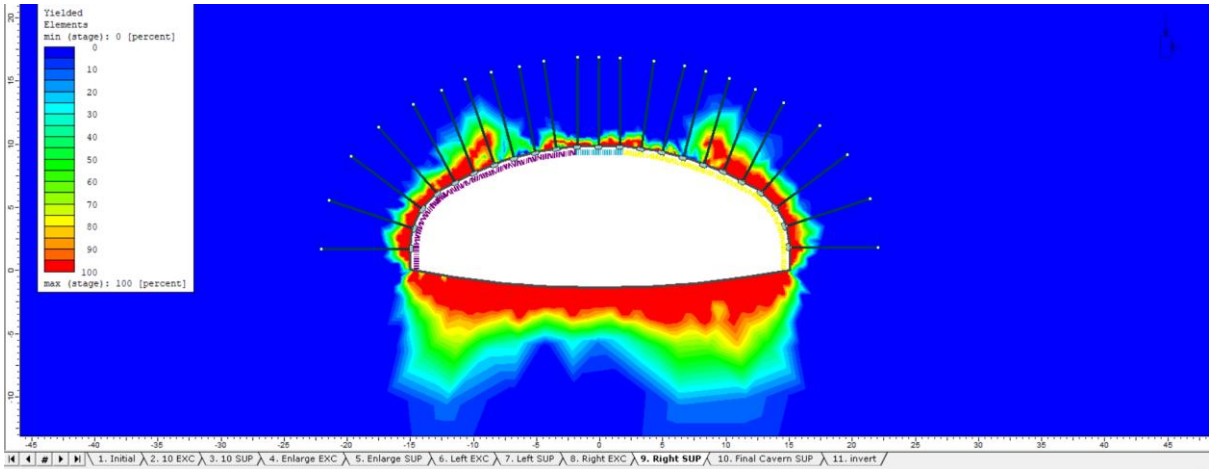

Figure 5-11. Yielded elements, Stage 9 - Model A, k = 0.5

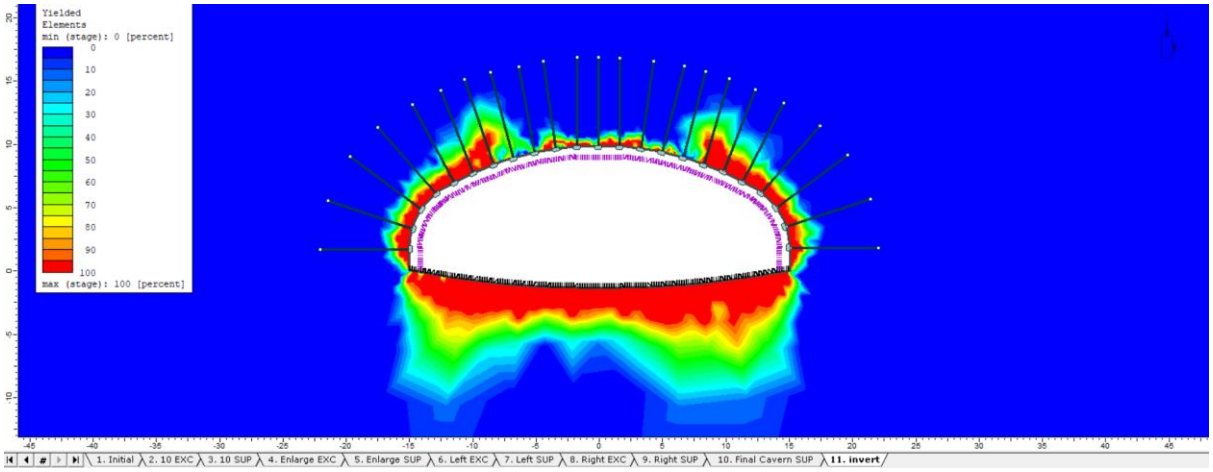

Figure 5-12. Yielded elements, Stage 10 & 11 - Model A, k = 0.5

It is also possible to visualize the plastic points and their type (tension or shear) around the cavern.

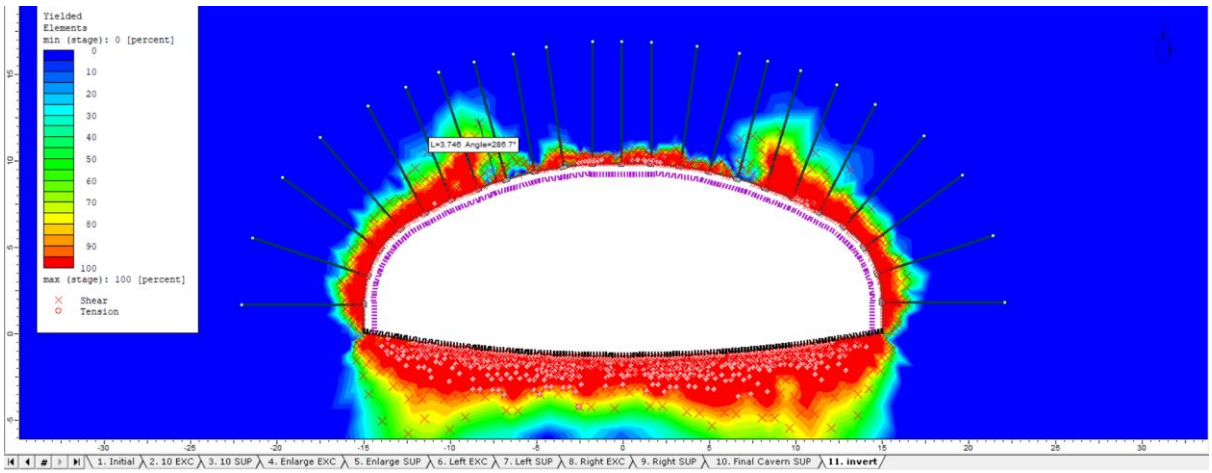

Figure 5-13. Plastic Points - Model A, k = 0.5

5.1.1.3. Axial Force on Rock Bolts

Maximum axial force acting on bolts is 0.06 MN. Axial force acting on the Rock bolts are presented in the following figure.

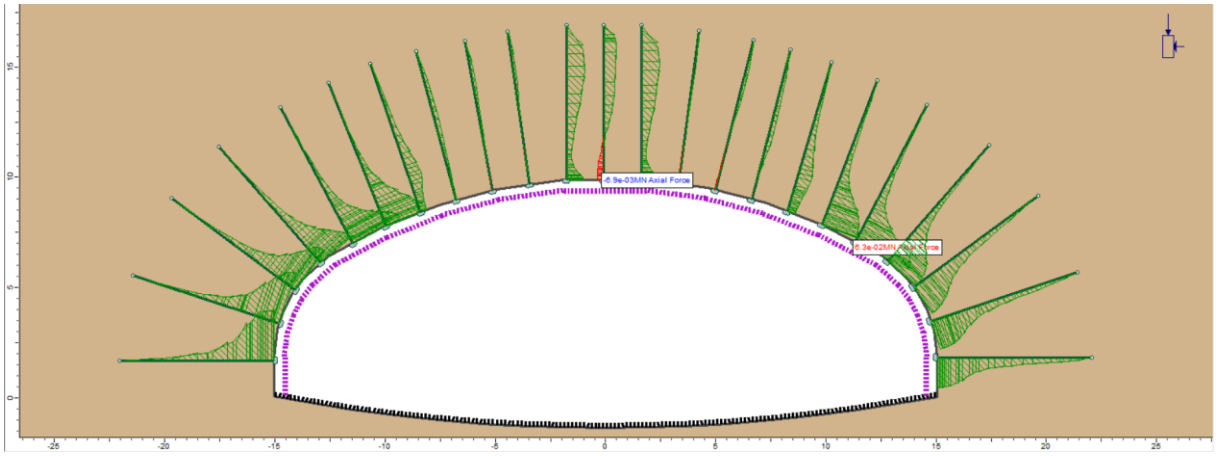

Figure 5-14. Axial Force on Rock Bolts - Model A, k = 0.5

5.1.1.4. Axial Force and Bending Moment on RRS

In this section maximum axial force and bending moment on the RRS is presented in following picture (Green Hatch shows positive values as compression and Red Hatch shows tension with negative values); Maximum compression is positioned between roof and walls around 1.7 MN. Also, there are negative values showing tension in the roof with maximum amount of 0.6 MN.

It should be noted that the corner points between the walls and invert are neglected from analysis in all models.

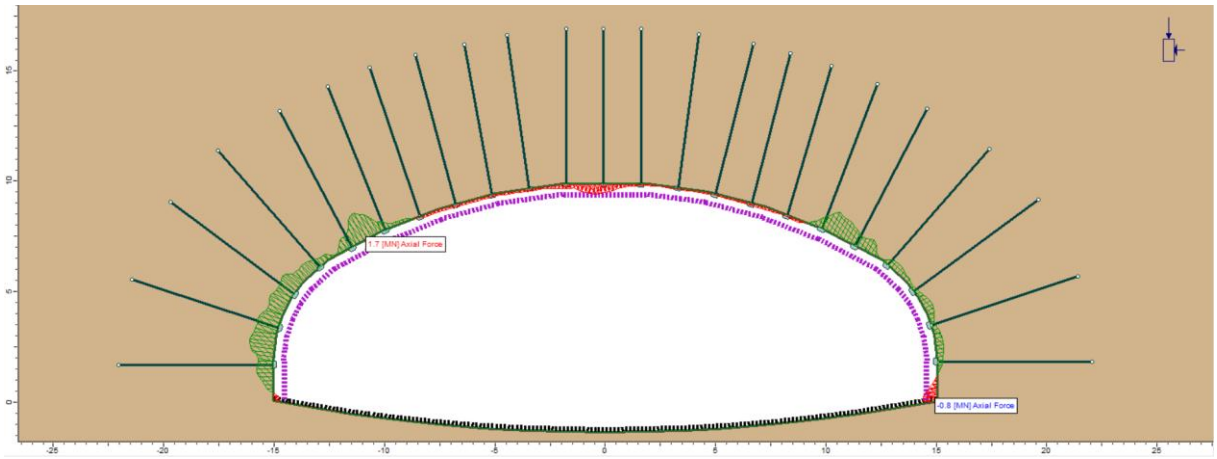

Figure 5-15. Axial Force on the RRS - Model A, k = 0.5

Also Bending moment on RRS can be visualized. Maximum Bending moment is 0.017 MNm between crown and the left wall of the cavern (Figure 5-16).

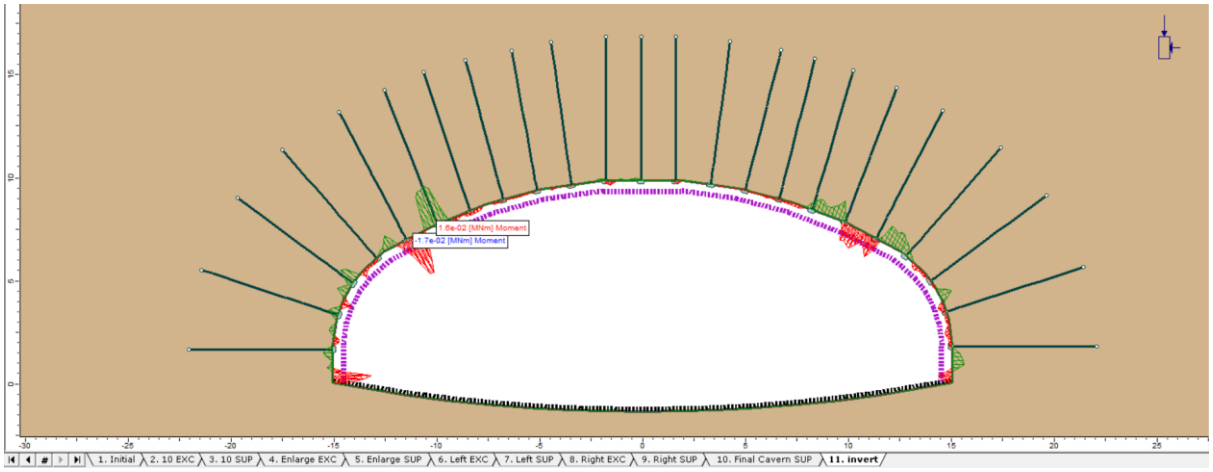

Figure 5-16. Bending Moment on the RRS - Model A, k = 0.5

5.1.1.5. Structural verifications, Rock Bolts

After displaying the yielded bolts on the last stage of the model, no yielded bolts were found.

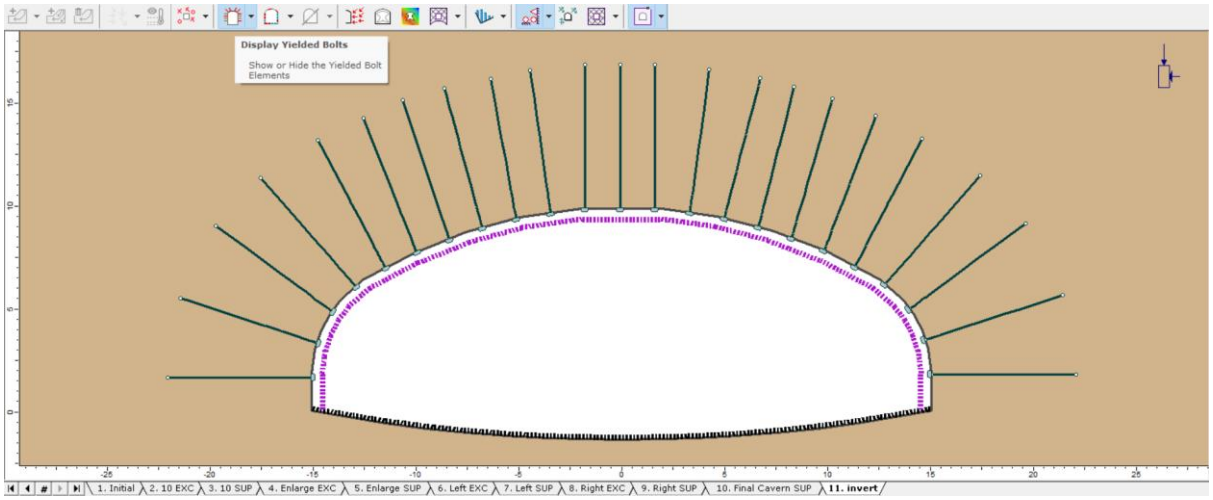

Figure 5-17. Displayed yielded bolts - Model A, k = 0.5

5.1.1.6. Support Capacity, RRS

This set of results contains most important parameters to be used for comparison of the models. Bending Moment-Axial Force and Shear Force-Axial Force dominium with four amounts of safety factors including 1, 2, 3 and 4 has been added to the plot and each point of the lining has been analyzed based on the Carranza-Torres method for support capacity verifications (2.6.1.1. Carranza-Torres & Diederichs Support Capacity Domain).

After plotting the points, it can be checked that which points fall into which value of safety factor as they are presented in the following figures (structural reactions of the corner points of the liner are excluded from the charts).

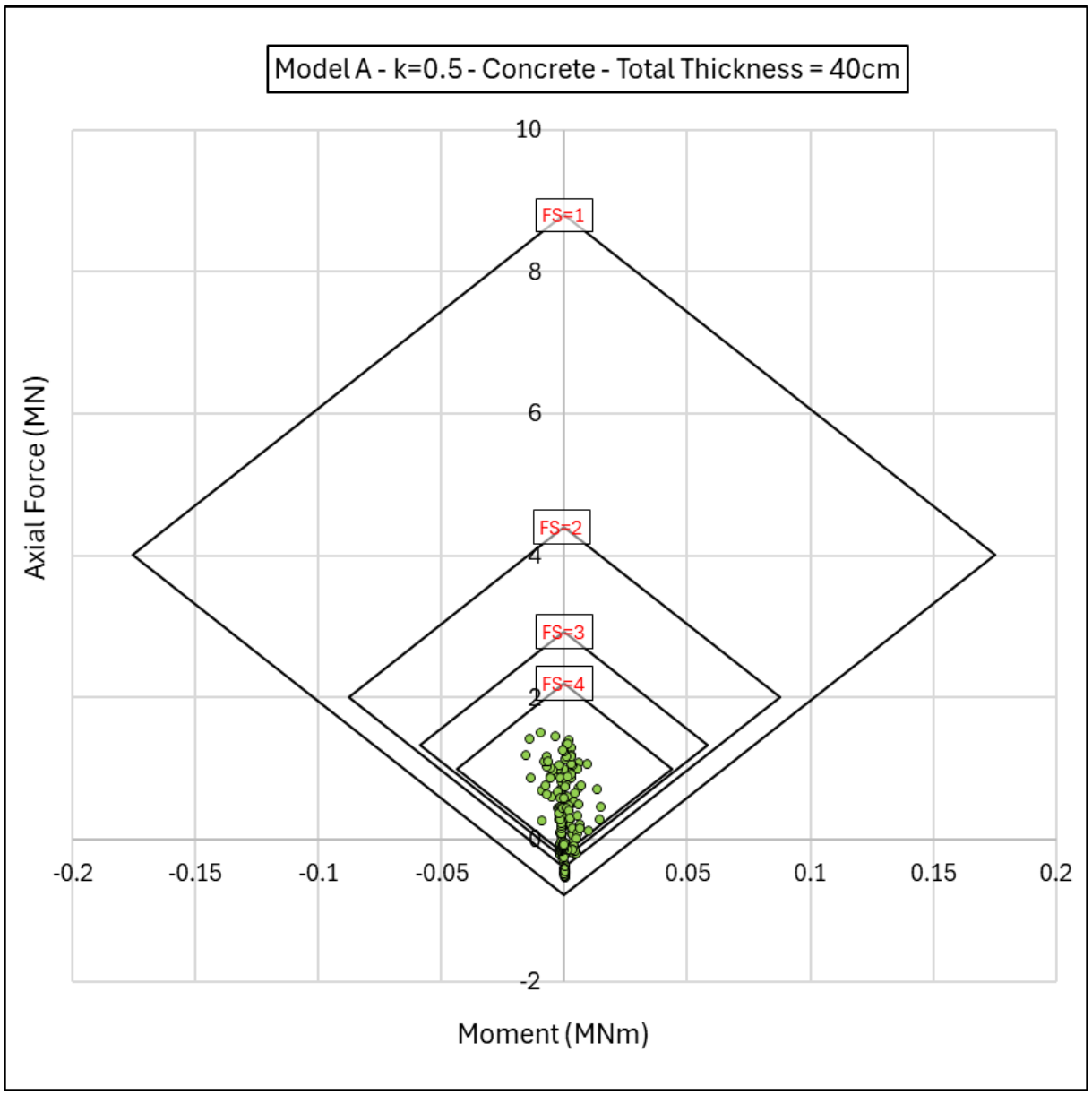

Figure 5-18. Axial Force-Moment plot of the concrete - Model A, k = 0.5

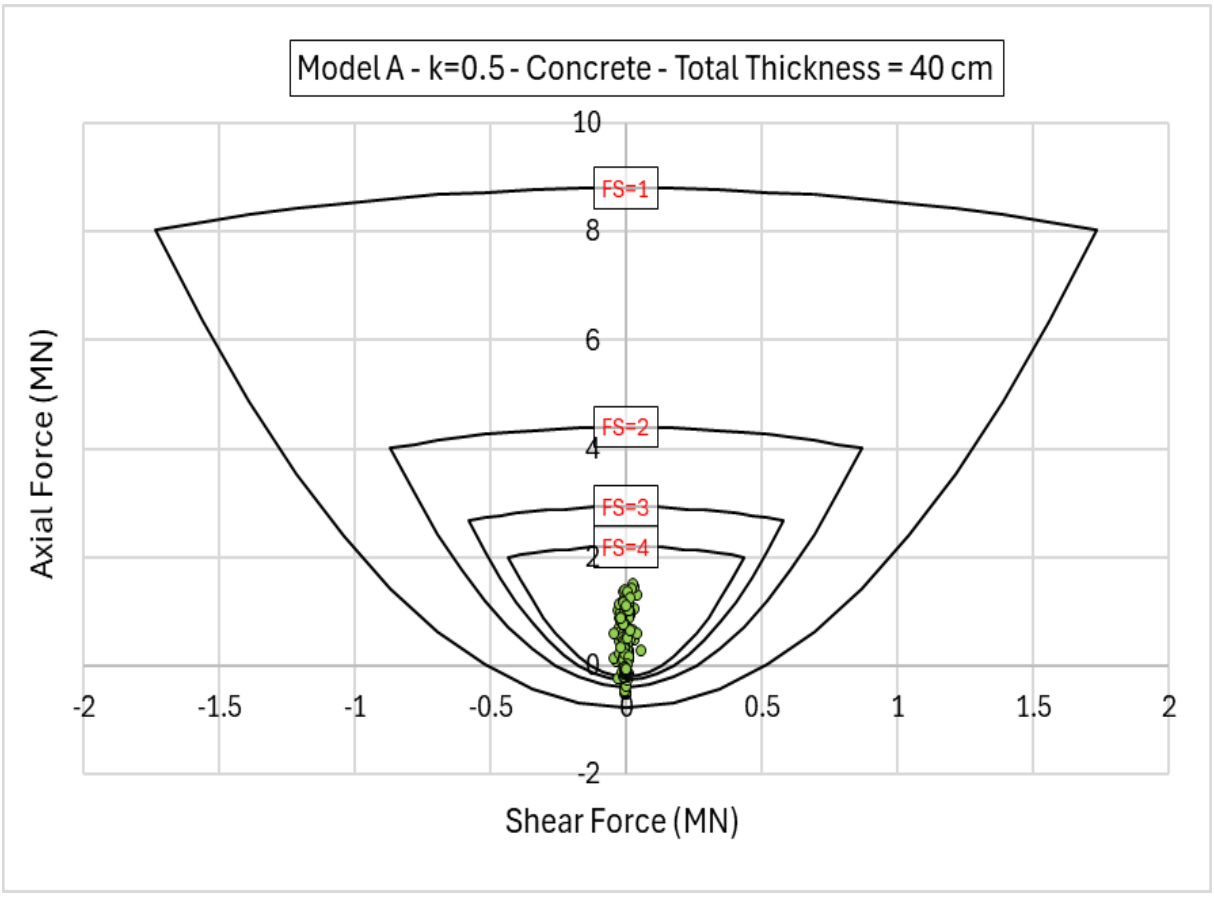

Figure 5-19. Axial Force-Shear Force of the concrete - Model A, k = 0.5

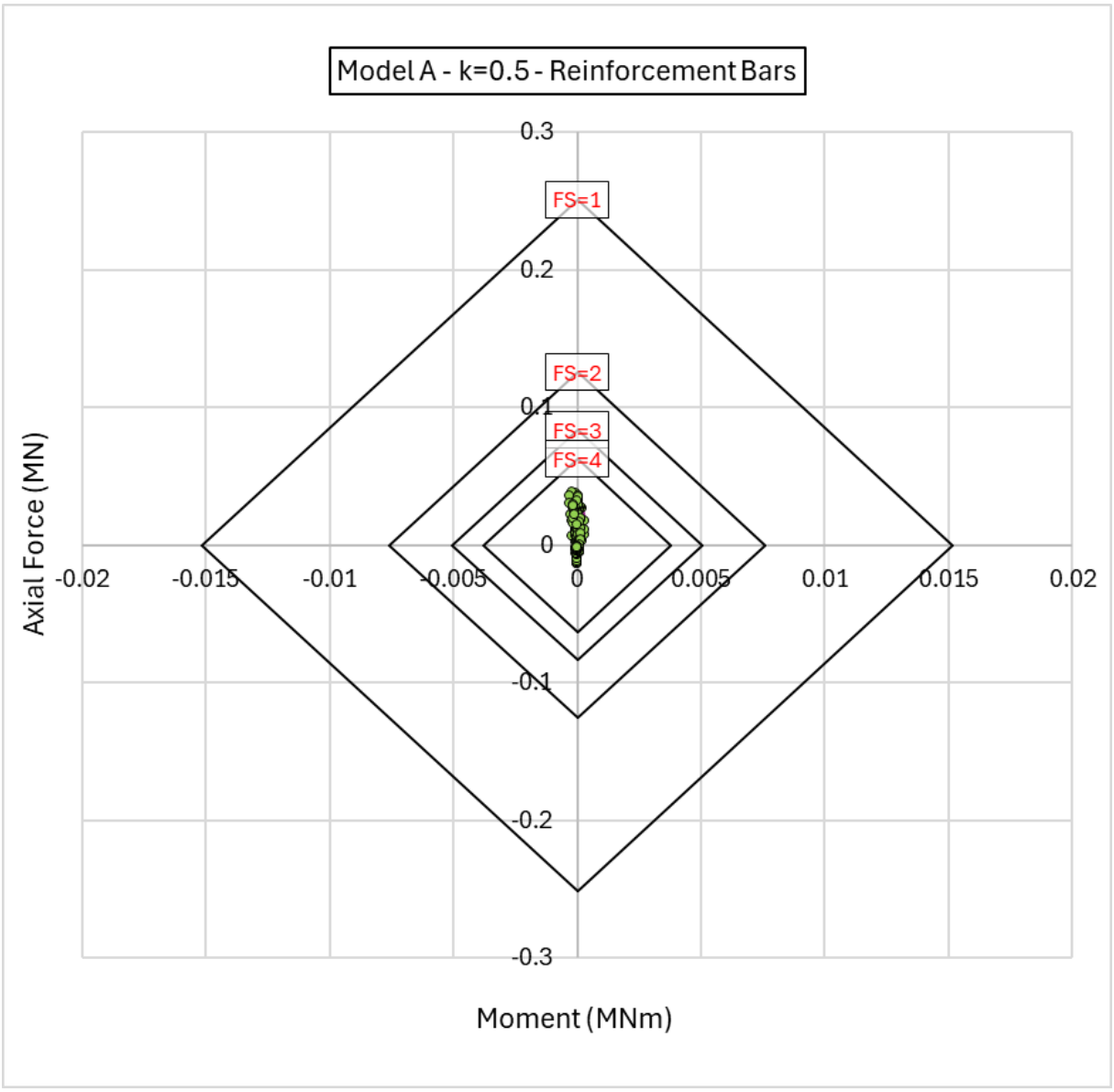

Figure 5-20. Axial Force-Moment on steel Rebars - Model A, k = 0.5

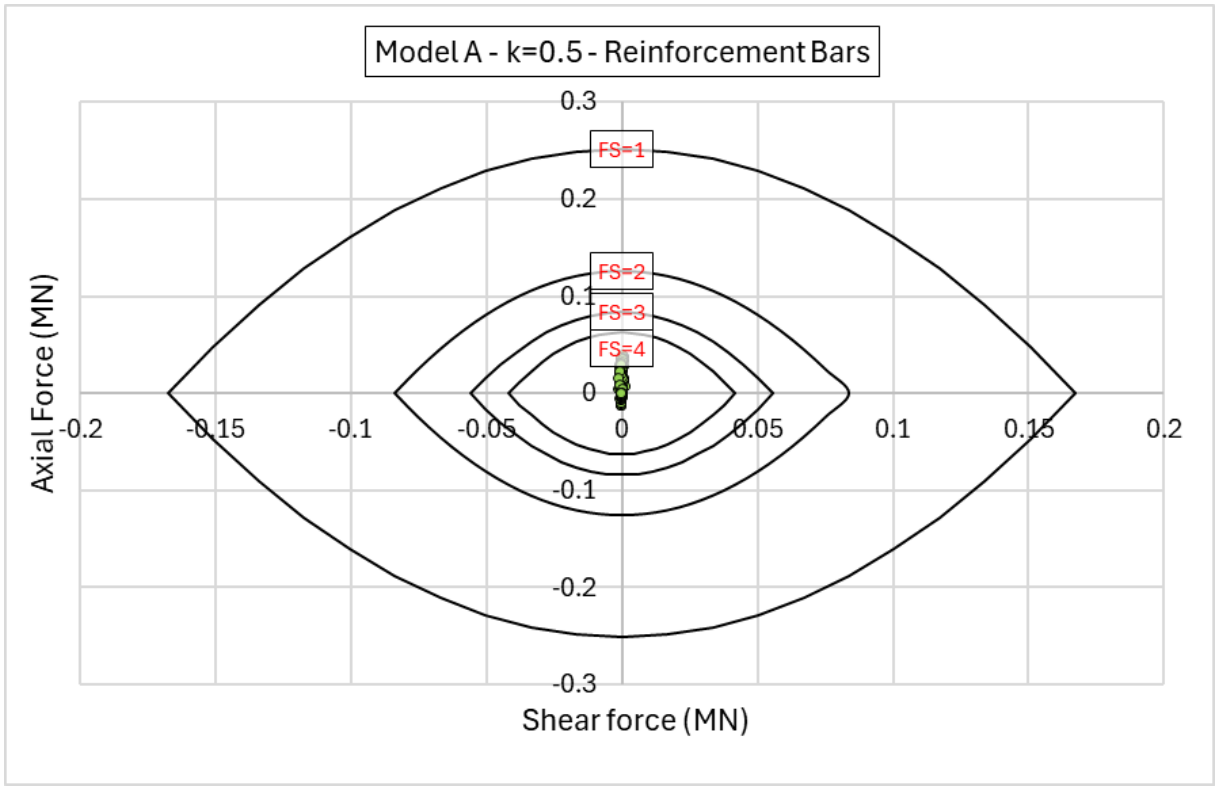

Figure 5-21- Axial Force-Shear Force of the steel Rebars - Model A, k = 0.5

5.1.1.7. Summary of the Results

In this section, a table containing important results from Model A, k=0.5, has been made to summarize presented information. Following table illustrates the features of this model.

Table 5-1. Summary of results - Model A, k=0.5

Model A – k = 0.5	
Maximum displacement at the walls [cm]	2.5
Maximum displacement at the roof [cm]	7.4
Maximum total displacement [cm]	8.1
Maximum radius measured for the plastic zone [m]	4
RRS properties	40 cm thickness c/c spacing 4.5 m
Maximum Compression on RRS [MN]	1.7
Maximum Tension on RRS [MN]	0.6
Min-Max Factor of Safety for RRS	Min: 1.3 Max: Higher than 4
Quantity of rock bolts and their lengths [m]	23 Rock Bolts 7m
Rock bolt tributary area [mm^2]	207
Maximum axial force on rock bolts [MN]	0.063
Number of Yielded bolts and their location	0
Rock Bolt Deformation [cm]	3

In summary, plastic zone is progressively increased around each excavation step concentrated in the side walls until the last stage that reaches 4m far from the excavation borders.

Rock bolts are 7m and their endpoint is in the elastic zone; they are not yielded and they have maximum deformation of 3cm.

RRS liners are being compressed on the walls with highest axial force of 1.7 MN. RRS in the roof are under total tension that reaches 0.6 MN of axial force.

Support capacity plots for concrete show an acceptable performance but there are lots of points under tension in the roof with lowest safety factor of 1.3 compression points have safety factor higher than 4.

5.1.2. Model A – k = 1

This section is to present results of computation of Model A with stress ratio equal to 1.

5.1.2.1. Total Displacement

Maximum displacement is 7.9 cm placed in the invert (Figure 5-22).

Deformation vectors have compressive effect directed to the center of cavern in every point around the cavern; Most of them are vertical.

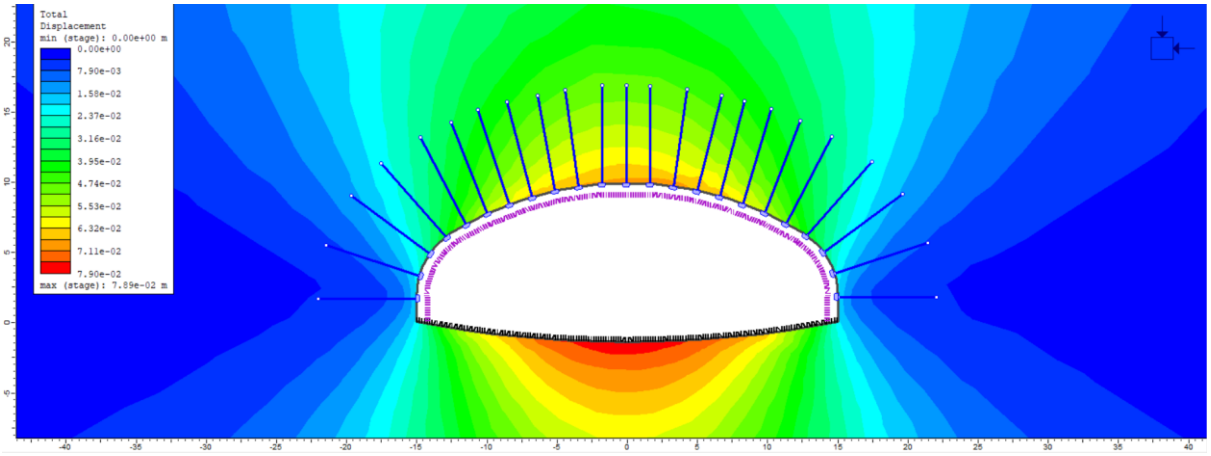

Figure 5-22. Total displacement - Model A, k=1

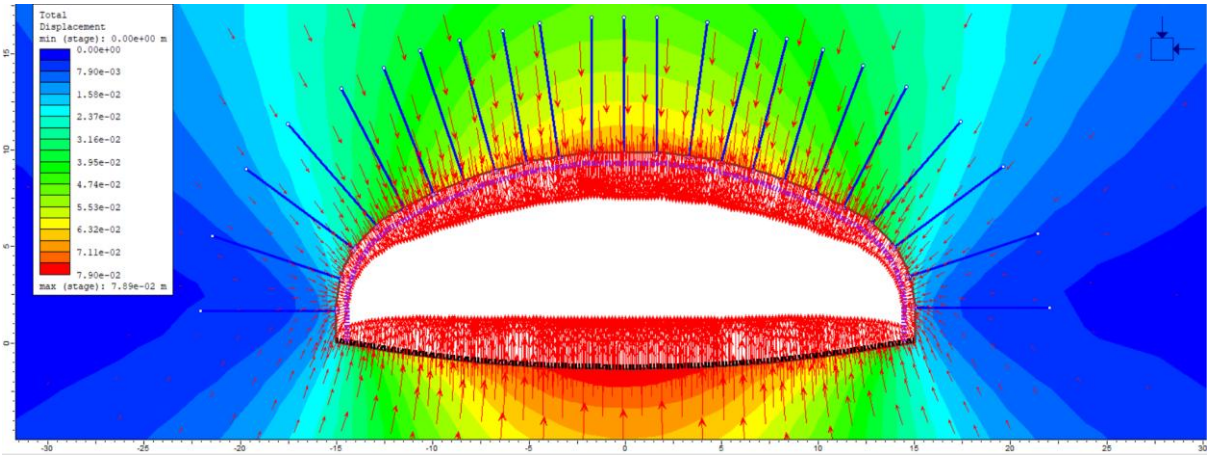

Figure 5-23. Deformation vectors and direction - Model A, k=1

5.1.2.2. Plastic Radius around the cavern

Plastic radius around the cavern is 4m on average in the final stage; Following figures show plastic behavior around excavation boundaries in each stage.

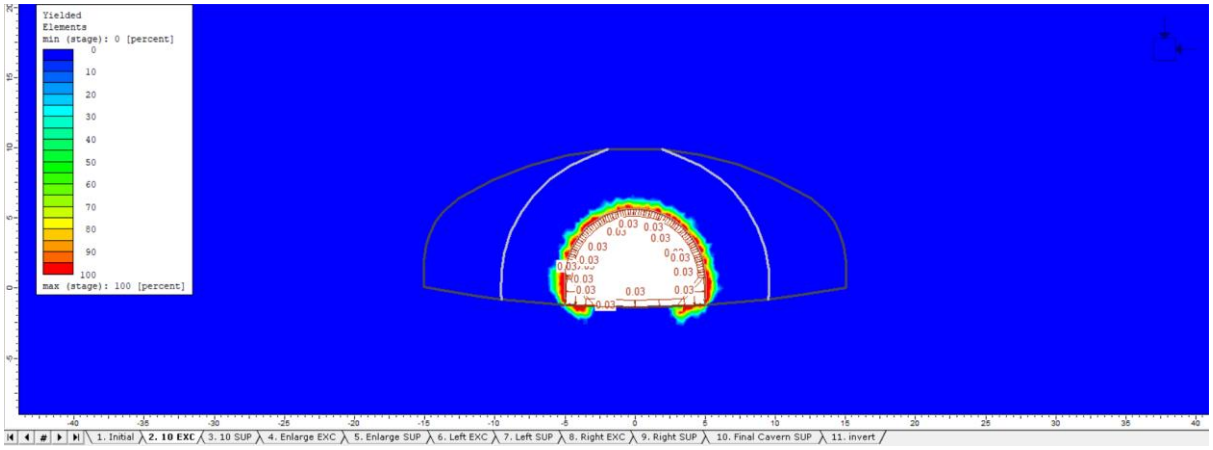

Figure 5-24. Yielded elements, Stage 2 - Model A, k=1

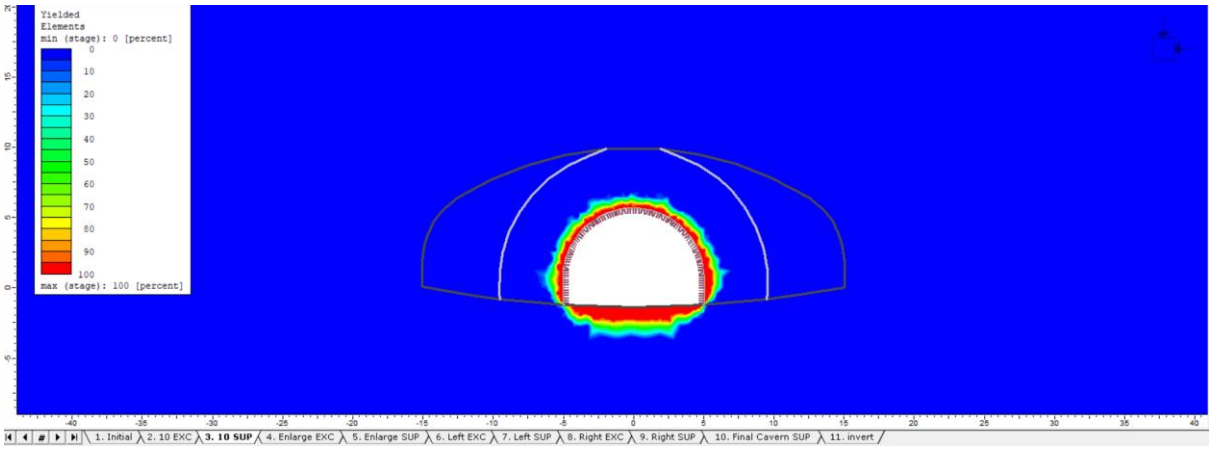

Figure 5-25. Yielded elements, Stage 3 - Model A, k=1

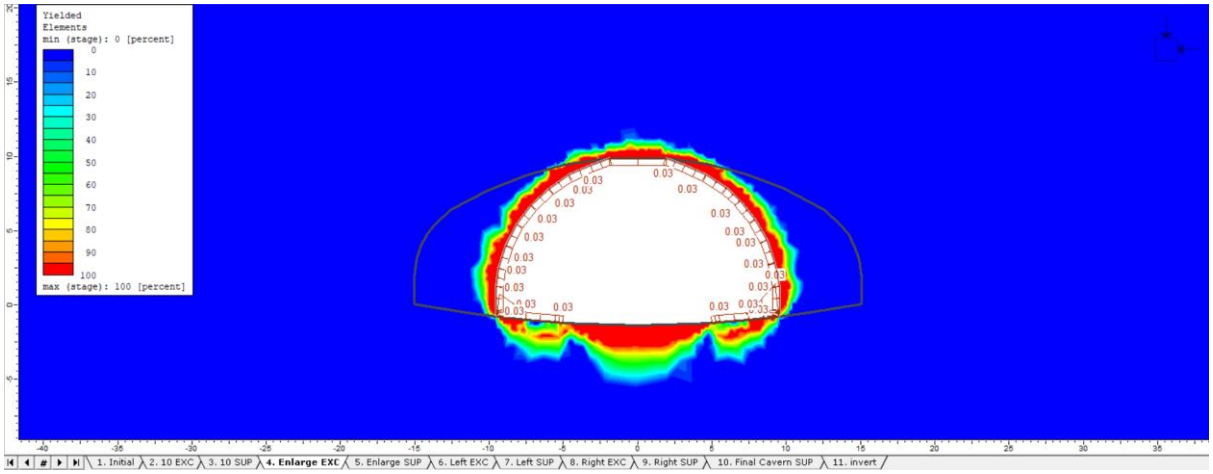

Figure 5-26. Yielded elements, Stage 4 - Model A, k=1

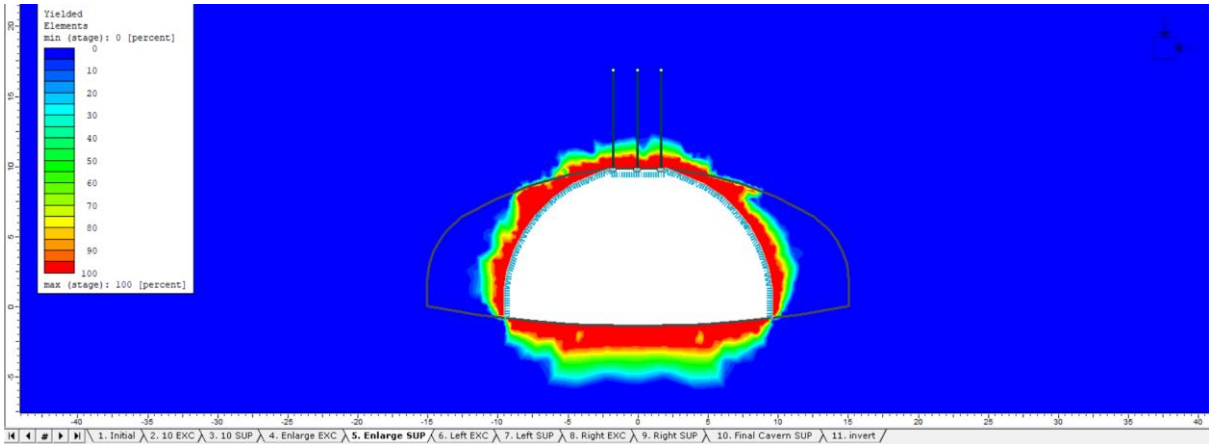

Figure 5-27. Yielded elements, Stage 5 - Model A, k=1

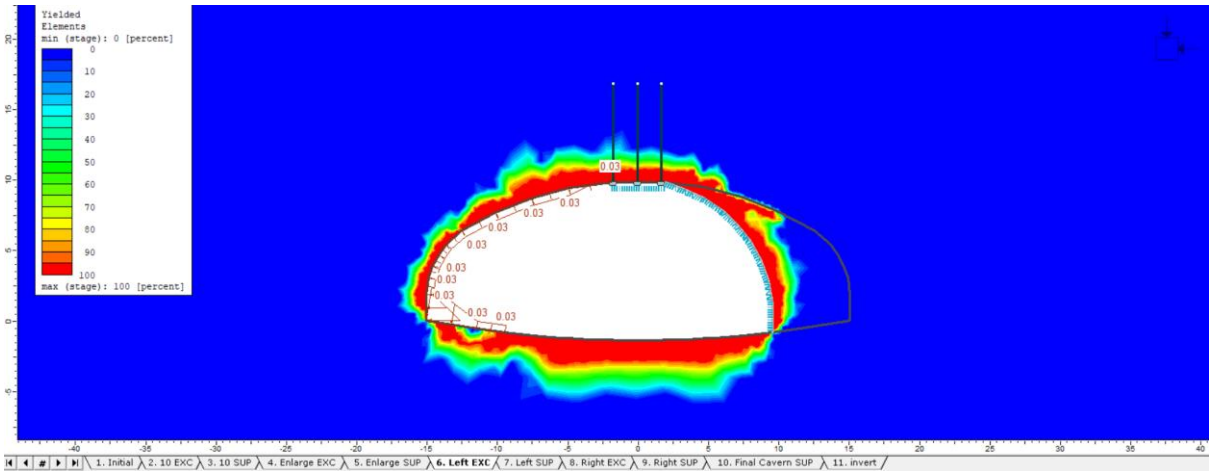

Figure 5-28. Yielded elements, Stage 6 - Model A, k=1

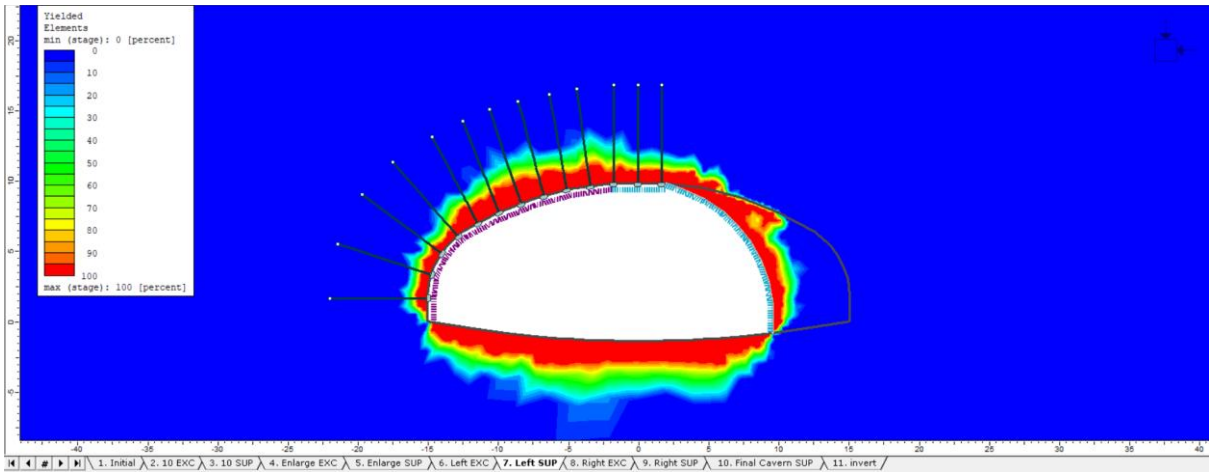

Figure 5-29. Yielded elements, Stage 7 - Model A, k=1

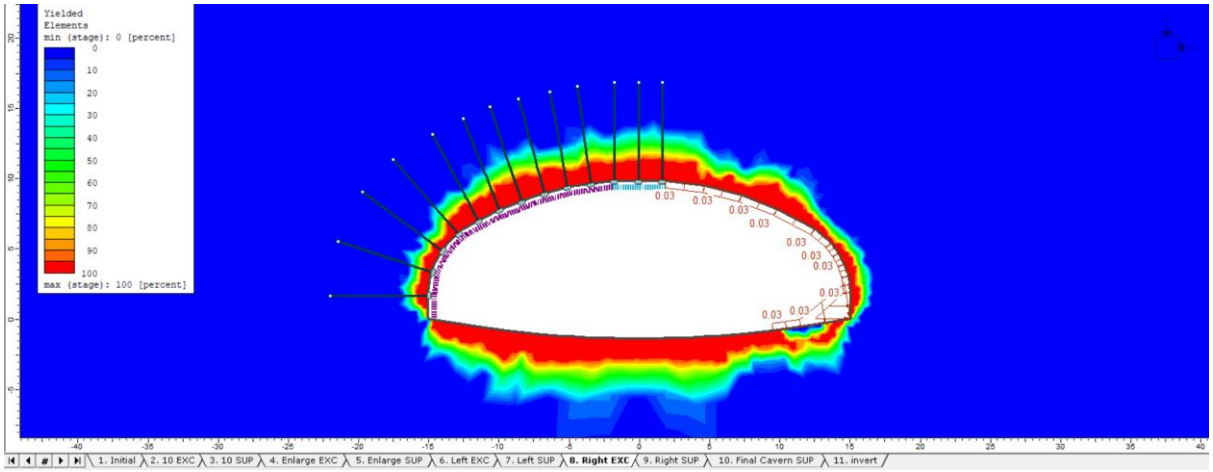

Figure 5-30. Yielded elements, Stage 8 - Model A, k=1

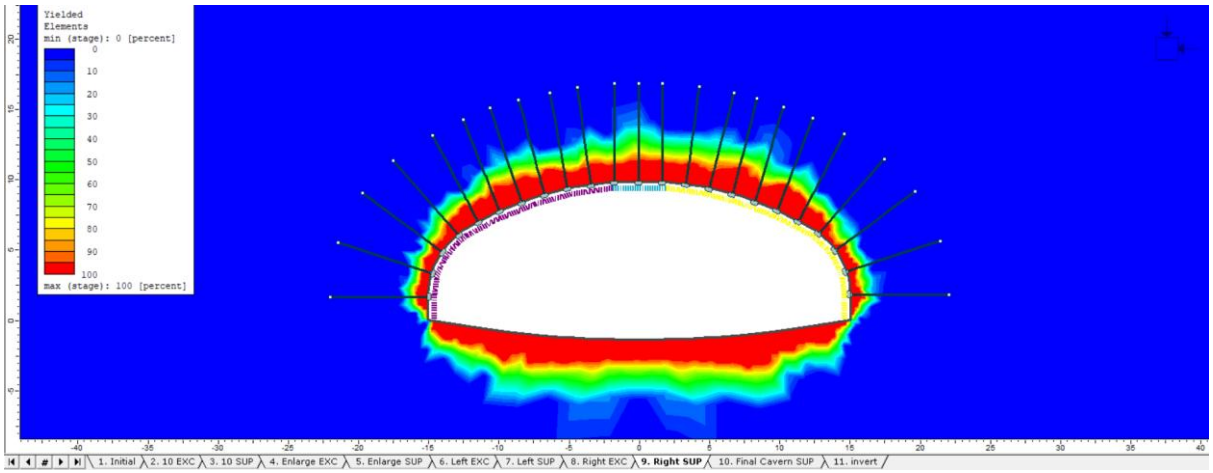

Figure 5-31. Yielded elements, Stage 9 - Model A, k=1

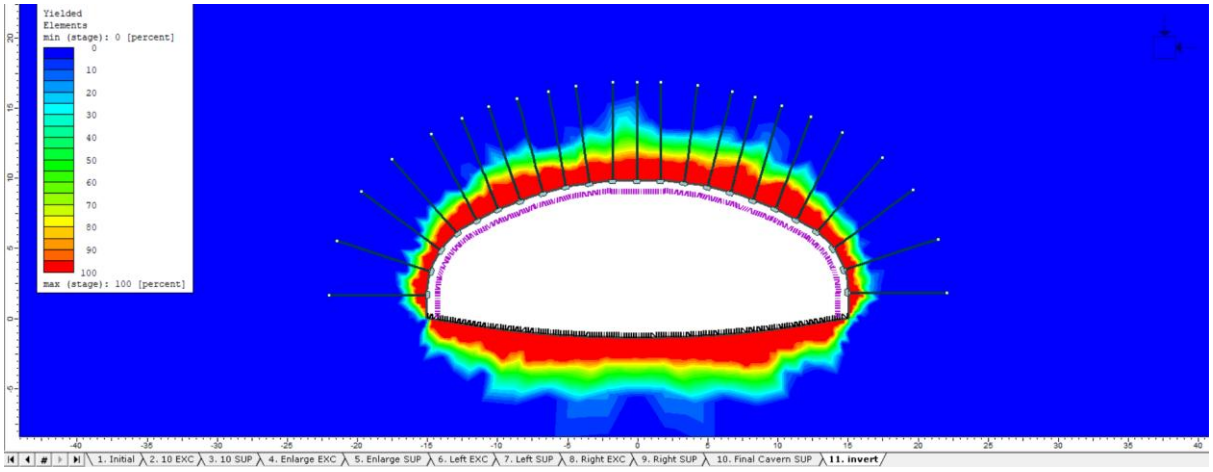

Figure 5-32. Yielded elements, Stage 10 & 11 - Model A, k=1

Plastic points, shear or tension are presented in the following figure. Furthest point is 3.5 m distanced from the excavation boundary (Figure 5-33).

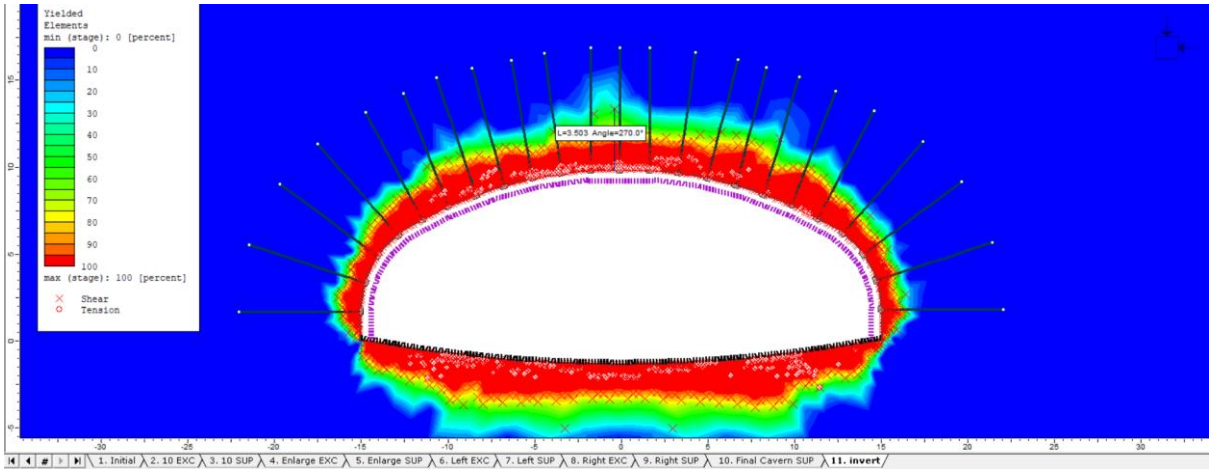

Figure 5-33. Plastic Points - Model A, k=1

5.1.2.3. Axial Force on Bolts

Maximum axial force acting on bolts is 0.1 MN.

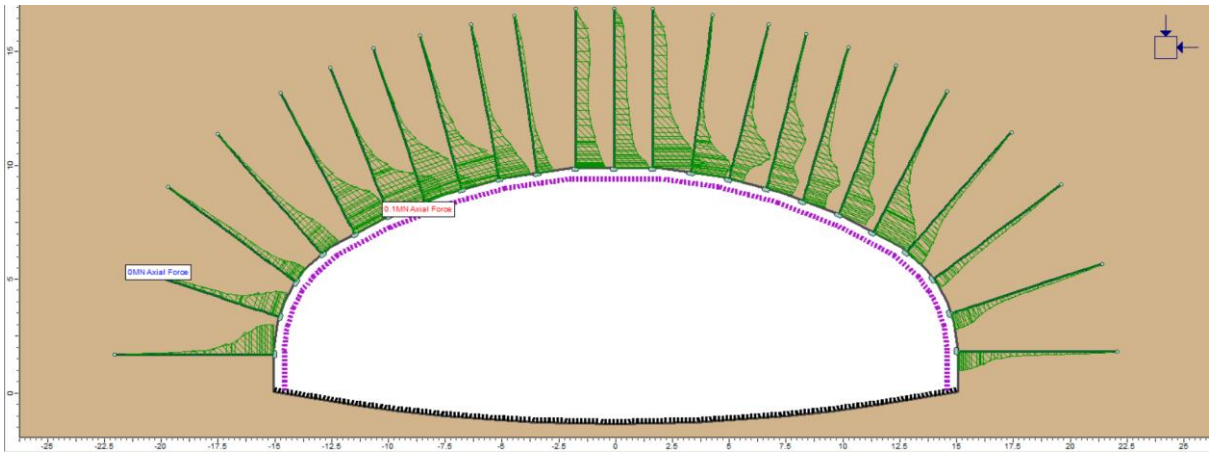

Figure 5-34. Axial Force on Bolts - Model A, k=1

5.1.2.4. Axial Force and Bending Moment on RRS

Maximum compressive axial force is 1.9 MN on the walls; there are some points under tension, and the maximum tension value is -0.4 MN (Figure 5-35). Maximum Bending moment is 0.0024 MNm (Figure 5-36).

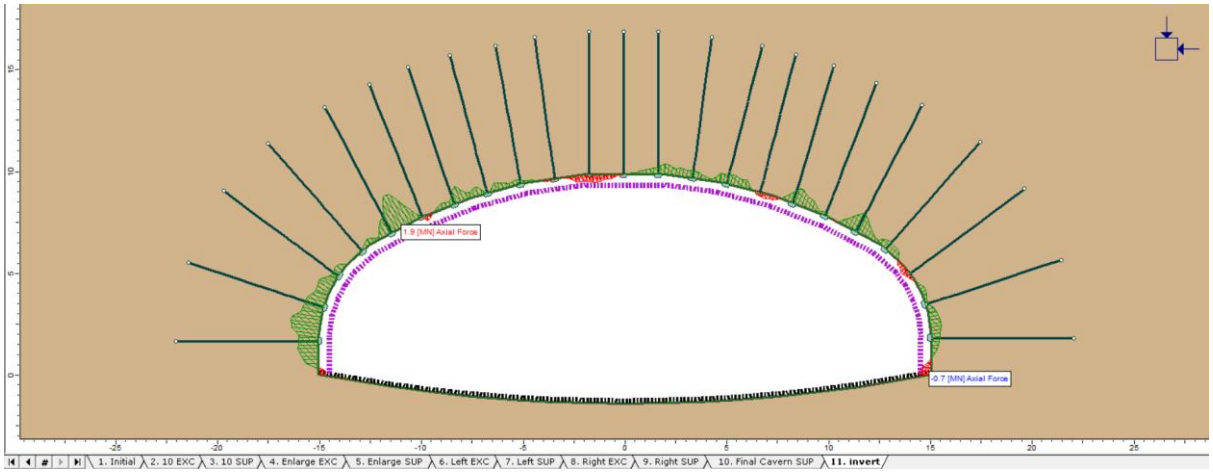

Figure 5-35. Axial Force on RRS - Model A, k=1

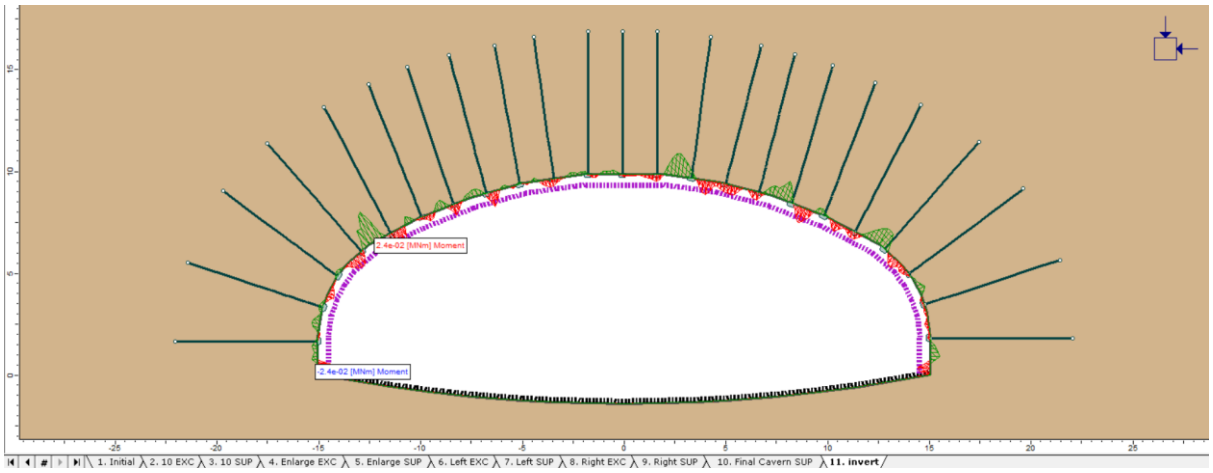

Figure 5-36. Bending Moment on RRS - Model A, k=1

5.1.2.5. Support Capacity, Rock Bolts

No yielded bolts are present in the last stage.

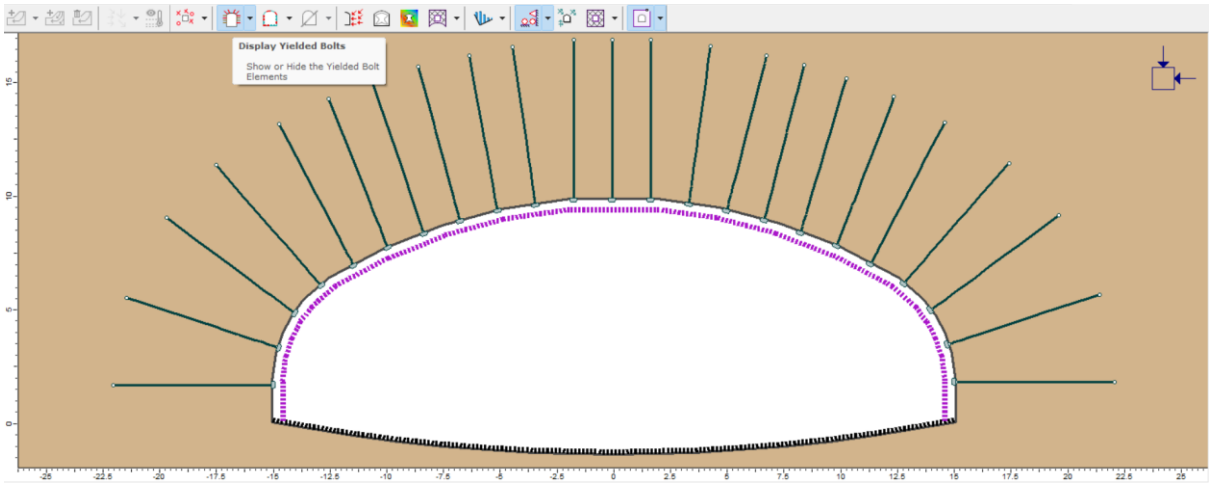

Figure 5-37. Displayed yielded bolts - Model A, k=1

5.1.2.6. Support Capacity, RRS

The following plots show the capacity of final lining, axial force and bending moment acting on it.

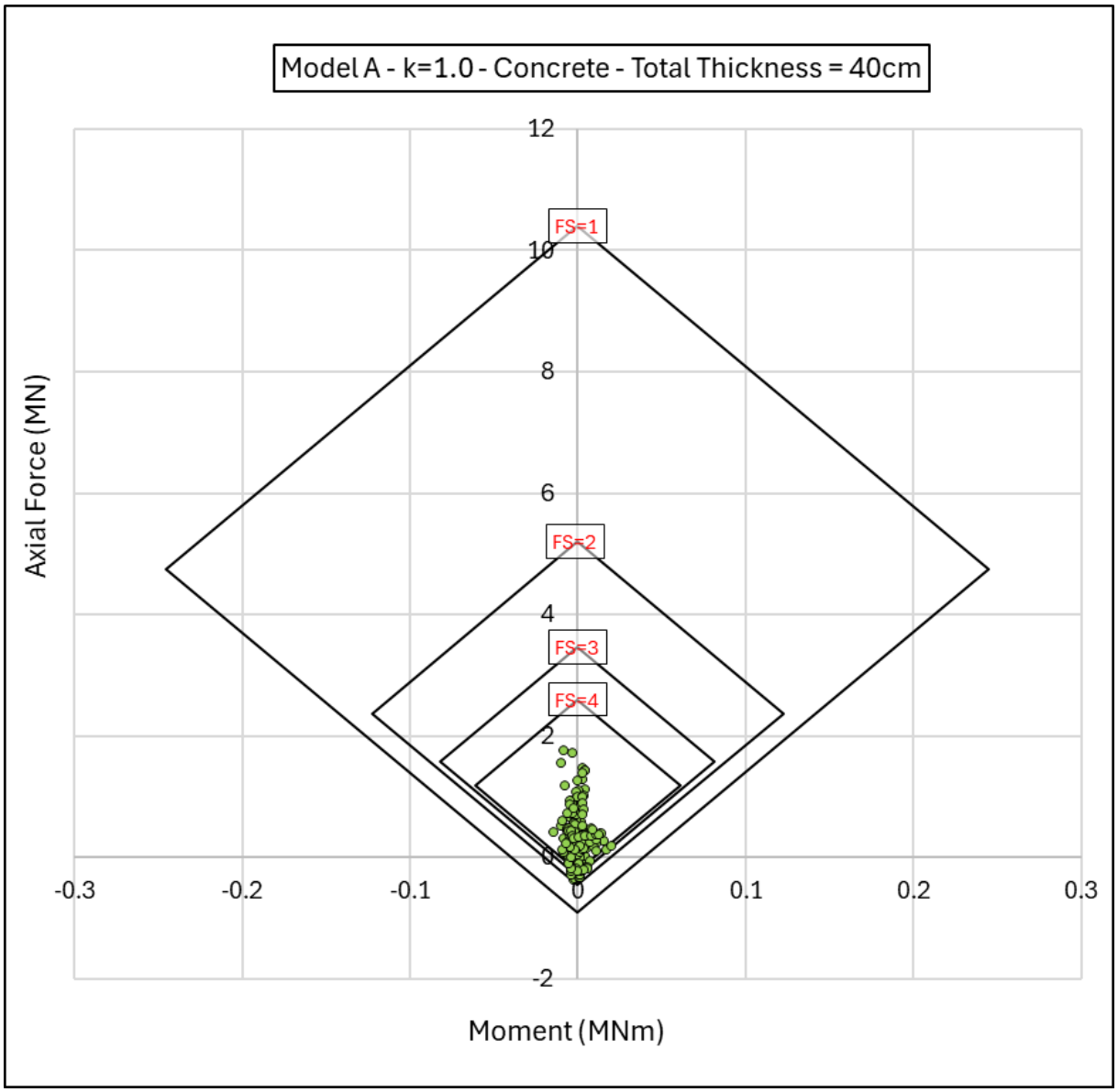

Figure 5-38. Axial Force-Moment plot of Concrete - Model A, k=1

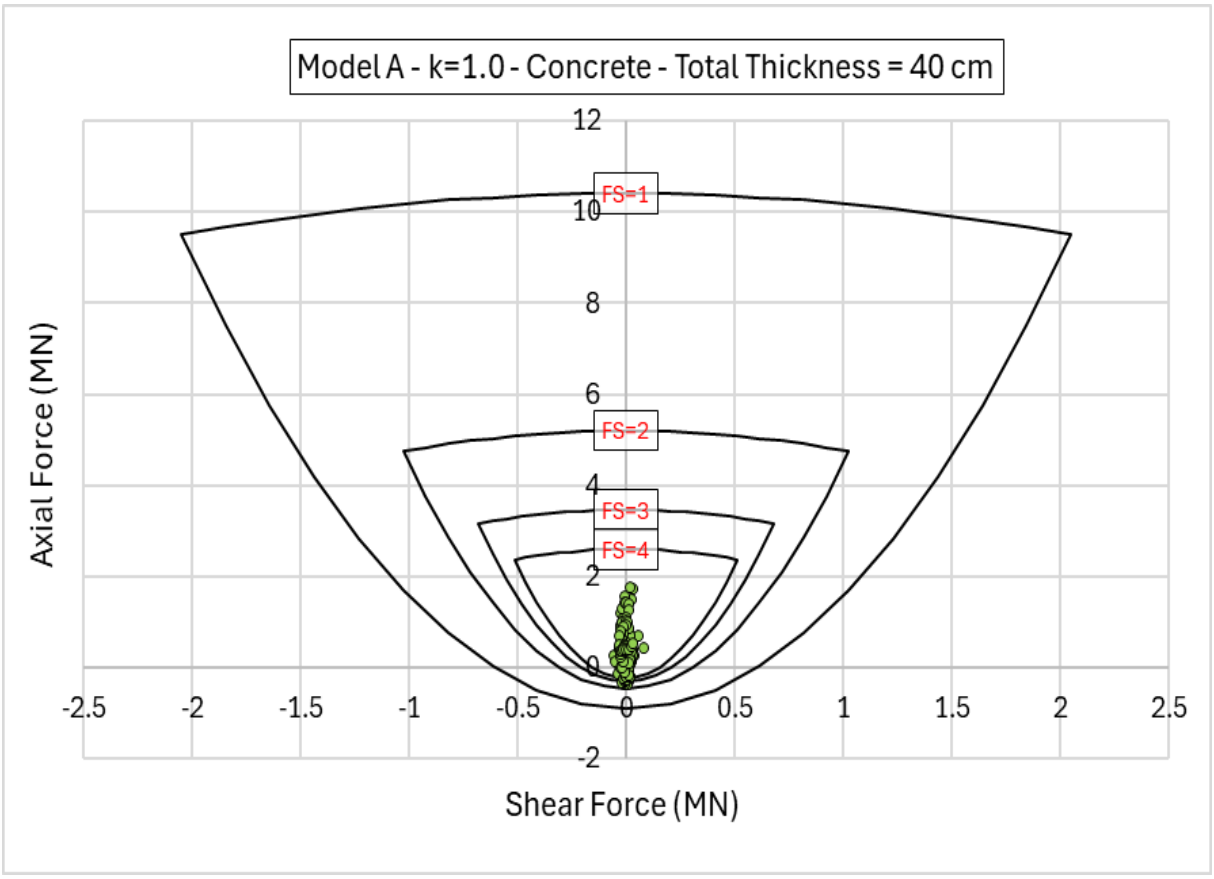

Figure 5-39. Axial Force - Shear Force plot of Concrete - Model A, k=1

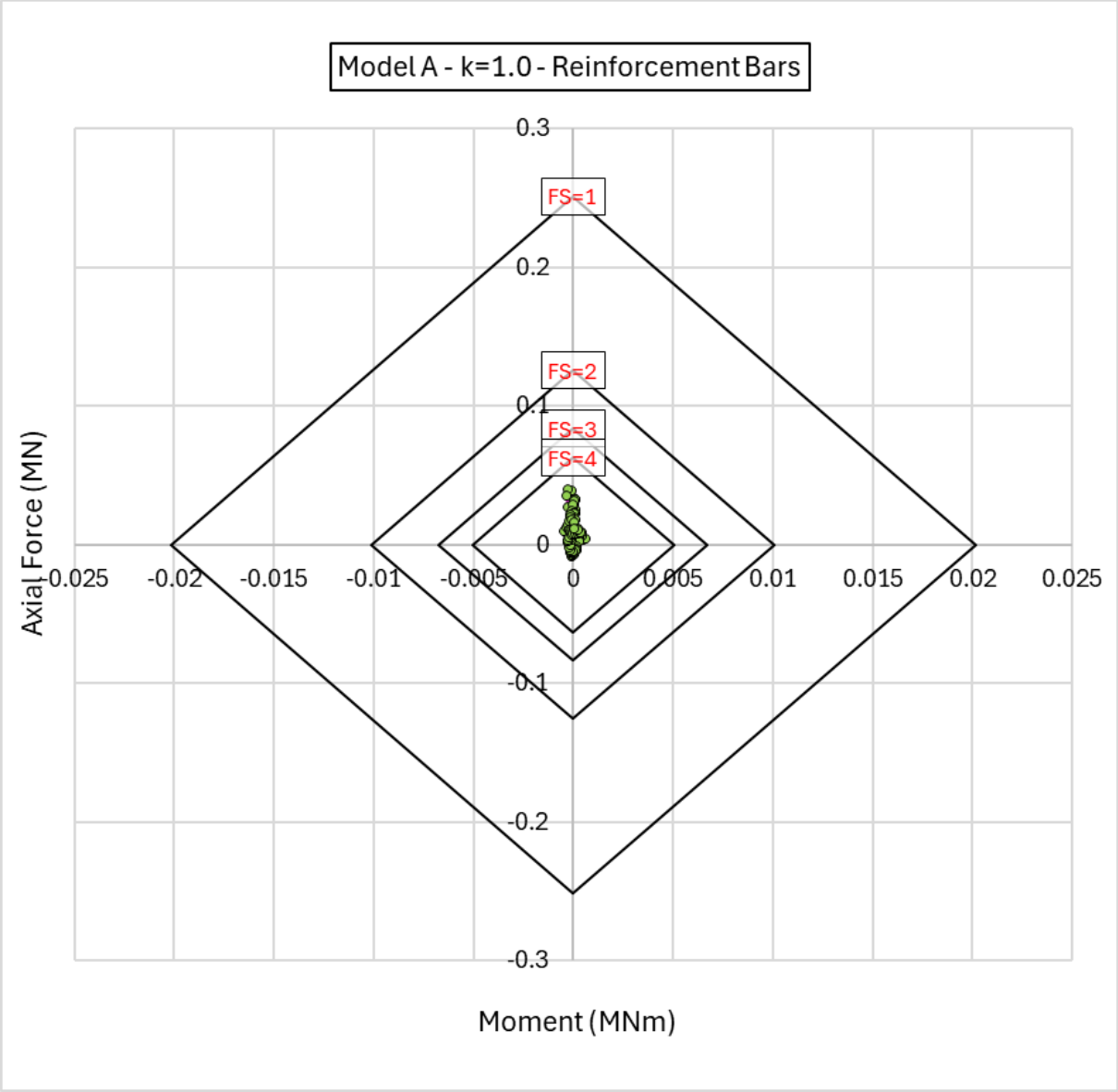

Figure 5-40. Axial Force-moment plot of the steel rebars - Model A, k=1

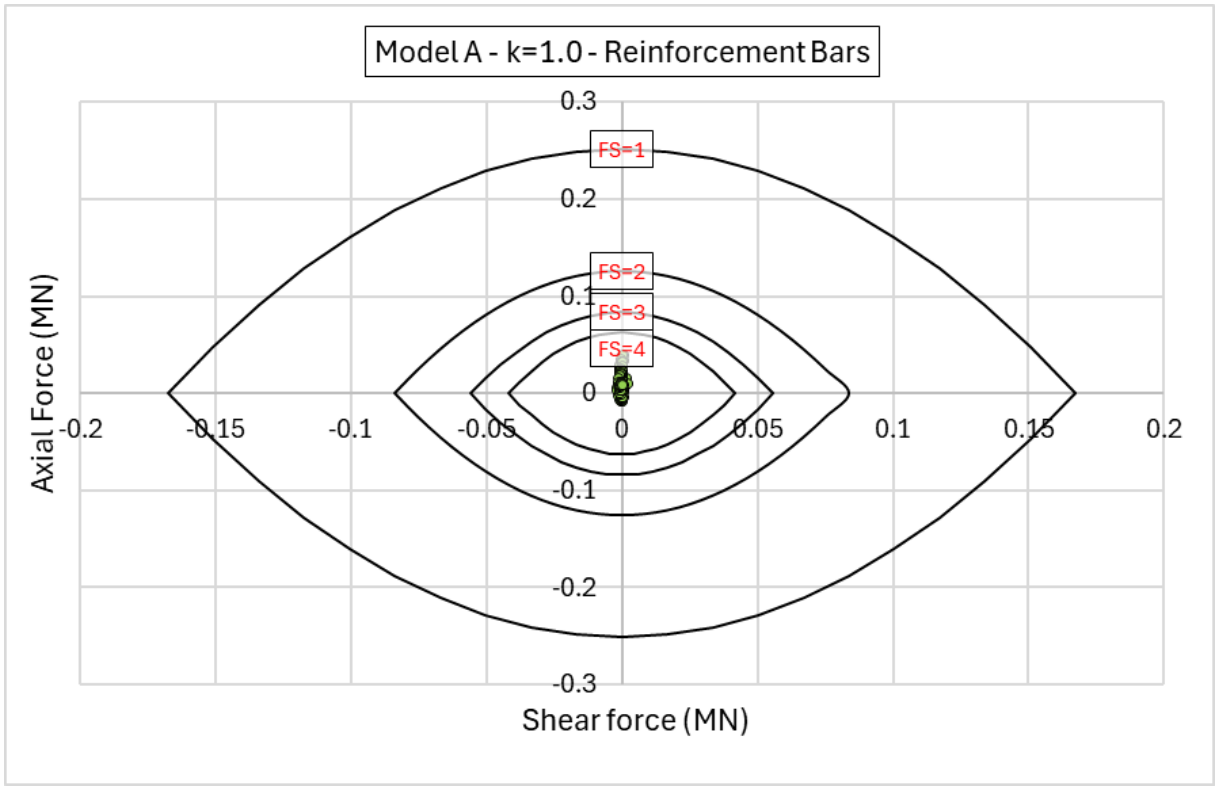

Figure 5-41. Axial Force-Shear Force plot of steel rebars - Model A, k=1

5.1.2.7. Summary of the Results

Table 5-2 shows summarized key output of this model computation.

Table 5-2. Summary of results - Model A, k = 1

Model A – k = 1	
Maximum displacement at the walls [cm]	4
Maximum displacement at the roof [cm]	7.5
Maximum total displacement [cm]	7.9
Maximum radius measured for the plastic zone [m]	4
RRS properties	40 cm thickness c/c spacing 3 m
Maximum Compression on RRS [MN]	1.9
Maximum Tension on RRS [MN]	0.4
Min-Max Factor of Safety for RRS	Min: 1.7 Max: higher than 4
Quantity of rock bolts and their lengths [m]	23 Rock Bolts 7m
Rock bolt tributary area [mm^2]	207
Maximum axial force on rock bolts [MN]	0.1
Number of Yielded bolts and their location	0
Rock Bolt Deformation [cm]	3.5

In summary, plastic zones progressively increased around each excavation step equally balanced around the excavation boundaries until the last stage that reaches 4m far from the cavern.

Rock bolts are 7m and their endpoint is in the elastic zone; they are not yielded and they have maximum deformation of 3.5 cm.

RRS liners are generally being compressed with highest axial force of 1.9 MN except for some points in the roof under total tension that reaches 0.6 MN of axial force.

Support capacity plots for concrete show very good performance even though there are few points under tension in the roof with lowest safety factor of 1.7 but the compression points has amount of safety factor significantly higher than 4.

5.1.3. Model A – k = 2

Model A is computed again with stress ratio equal to 2.

5.1.3.1. Total Displacement

Maximum displacement in this Model is almost 10.7 cm concentrating in the center of invert and roof.

Deformation vectors are mostly horizontal directed to the center of the cavern around the excavation boundaries.

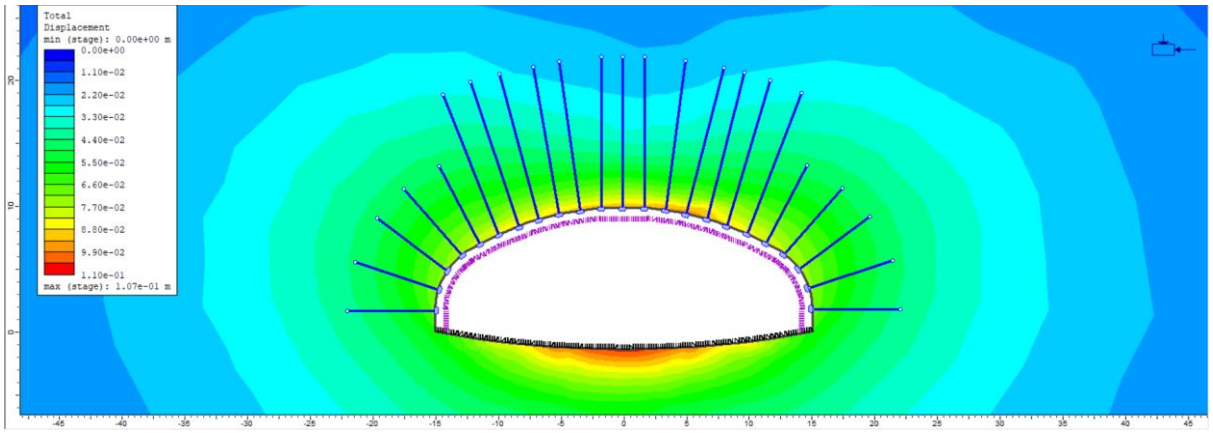

Figure 5-42. Total displacement - Model A, k=2

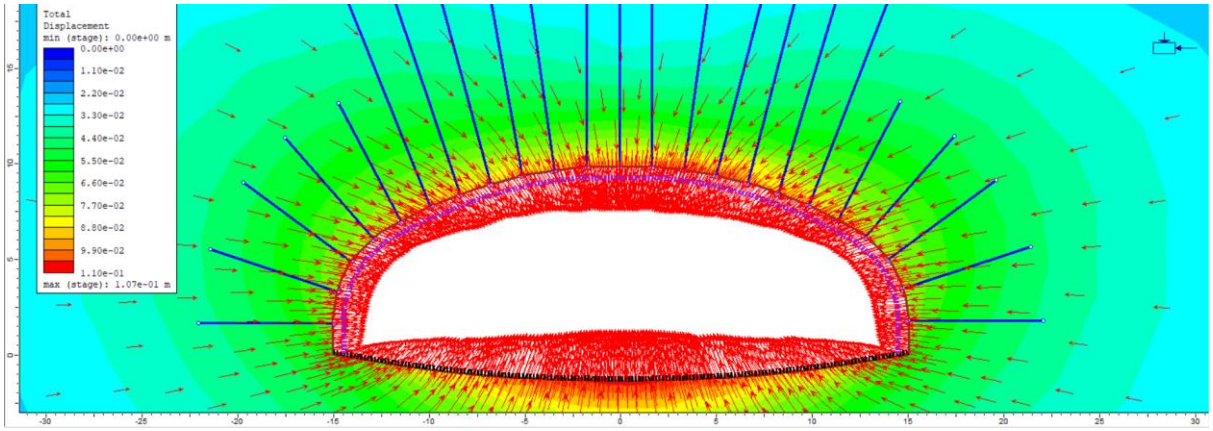

Figure 5-43. Deformation vectors and direction - Model A, k=2

5.1.3.2. Plastic Radius around the cavern

Plastic radius can reach almost 10m up the roof.

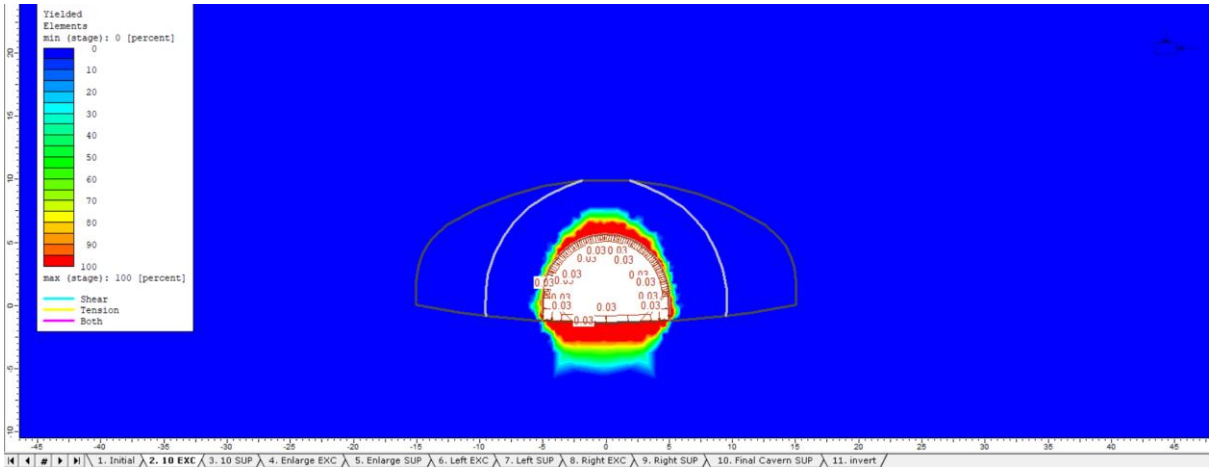

Figure 5-44. Yielded elements, Stage 2 - Model A, k=2

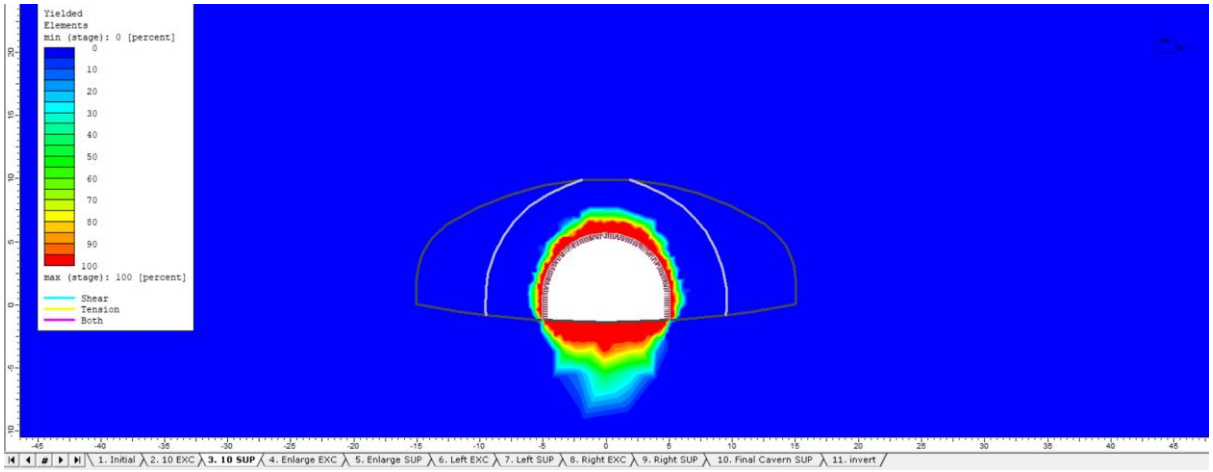

Figure 5-45. Yielded elements, Stage 3 - Model A, k=2

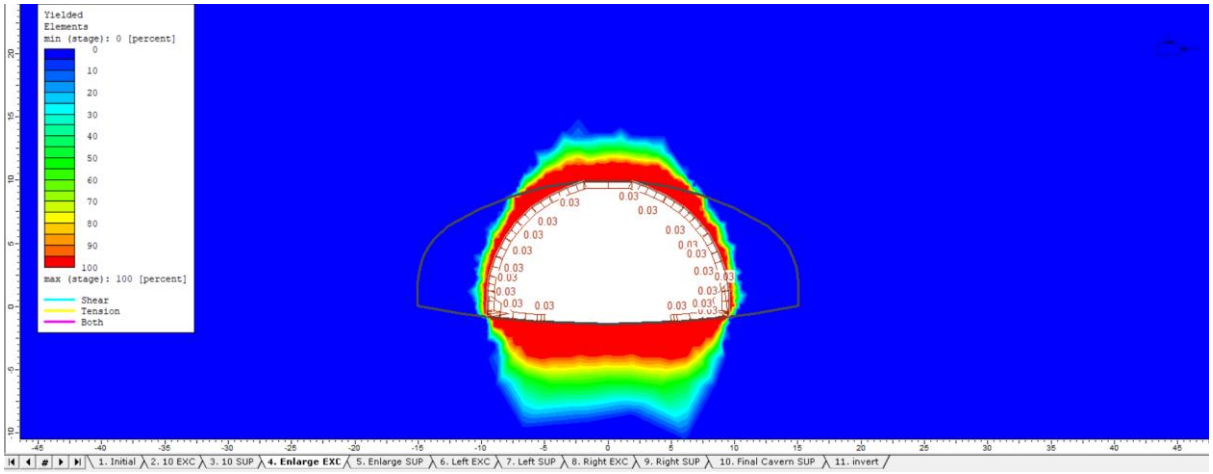

Figure 5-46. Yielded elements, Stage 4 - Model A, k=2

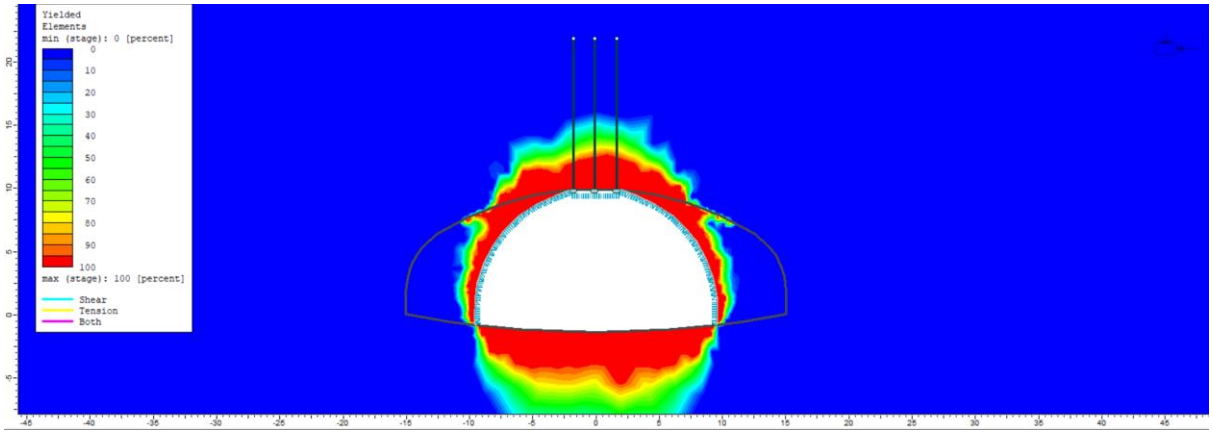

Figure 5-47. Yielded elements, Stage 5 - Model A, k=2

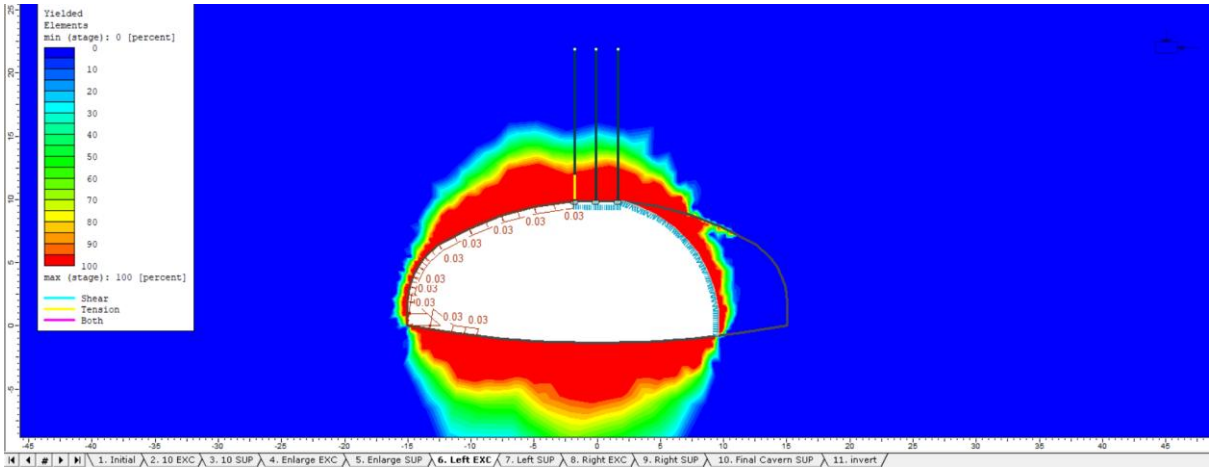

Figure 5-48. Yielded elements, Stage 6 - Model A, k=2

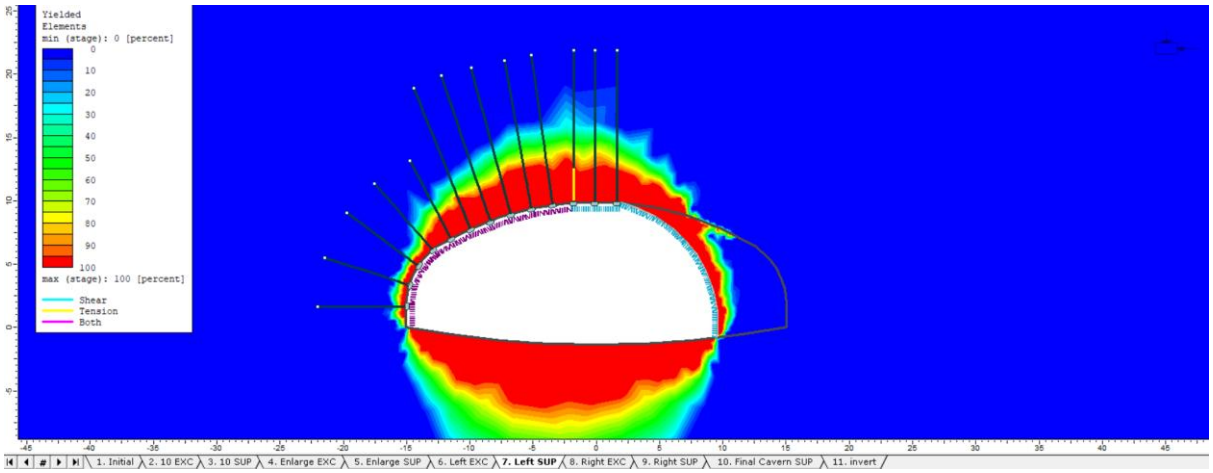

Figure 5-49. Yielded elements, Stage 7 - Model A, k=2

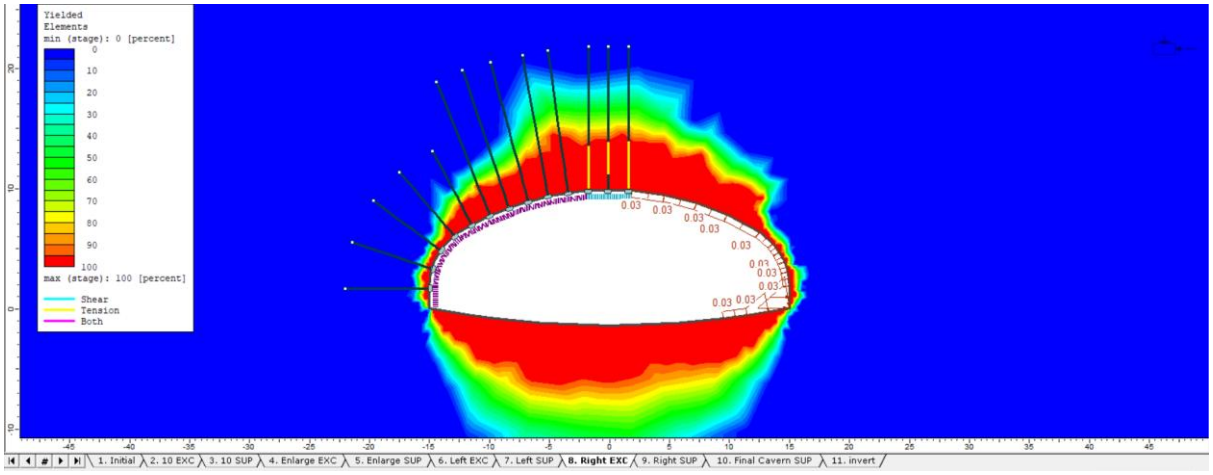

Figure 5-50. Yielded elements, Stage 8 - Model A, k=2

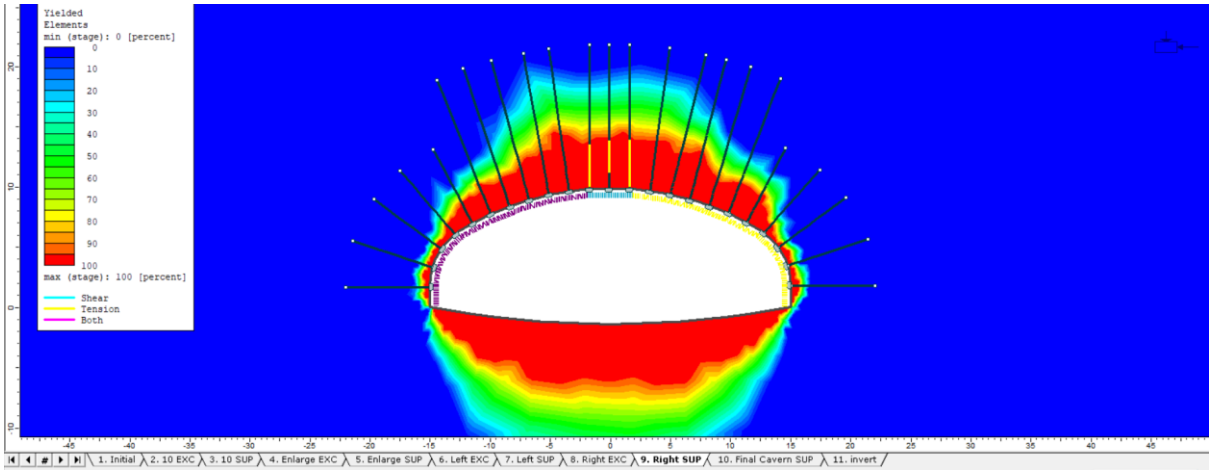

Figure 5-51. Yielded elements, Stage 9 - Model A, k=2

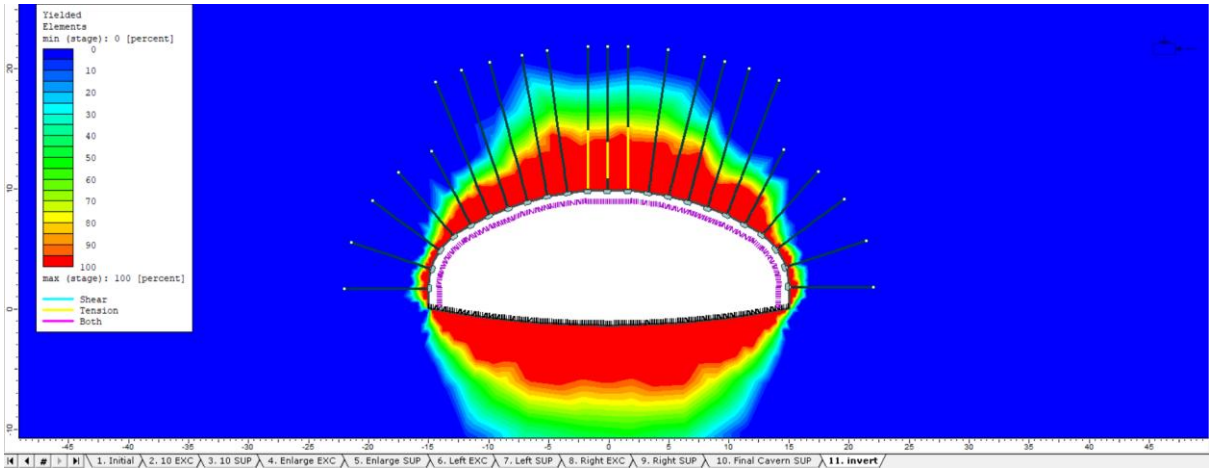

Figure 5-52. Yielded elements, Stage 10 & 11 - Model A, k=2

Maximum distance between the excavation boundary and the plastic points is almost 6.3 m as is shown in Figure 5-53.

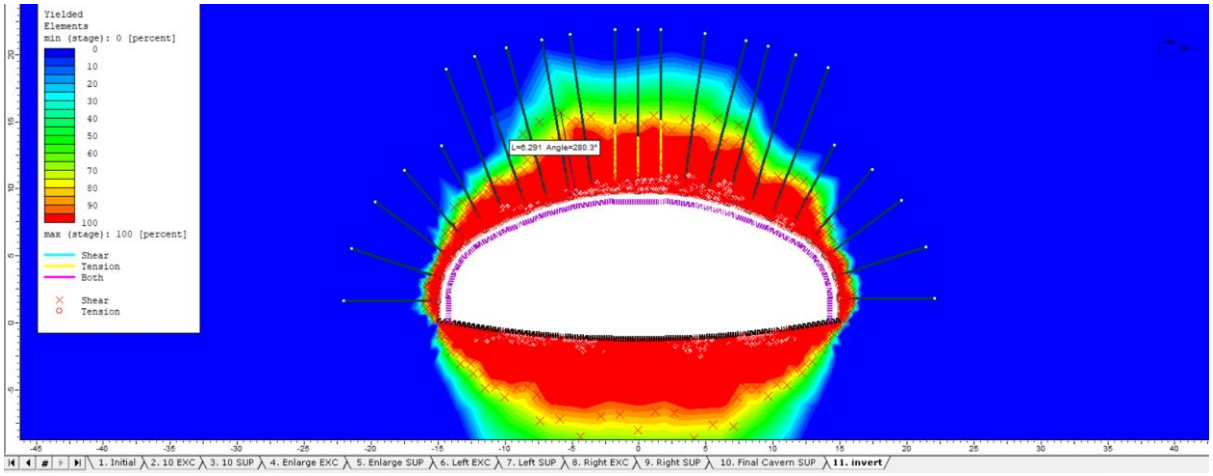

Figure 5-53. Plastic Points - Model A, k=2

5.1.3.3. Axial Force and Bending moment on RRS

In this model axial force is maximumly 1.9 MN and compresses the lining in the roof; there are also some tension forces 0.3 MN in the walls.

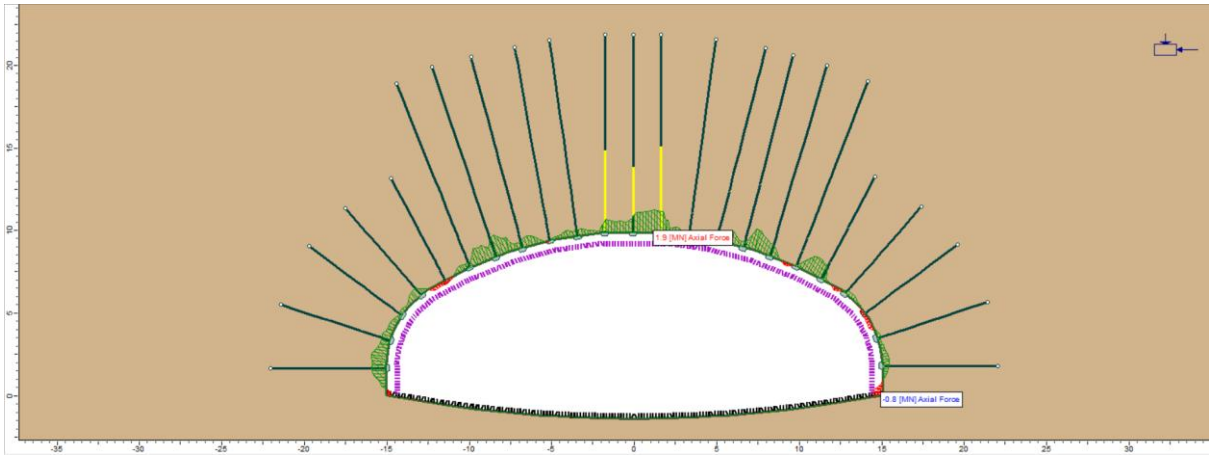

Figure 5-54. Axial Force on RRS - Model A, k=2

Bending Moment reaches 0.03 MNm.

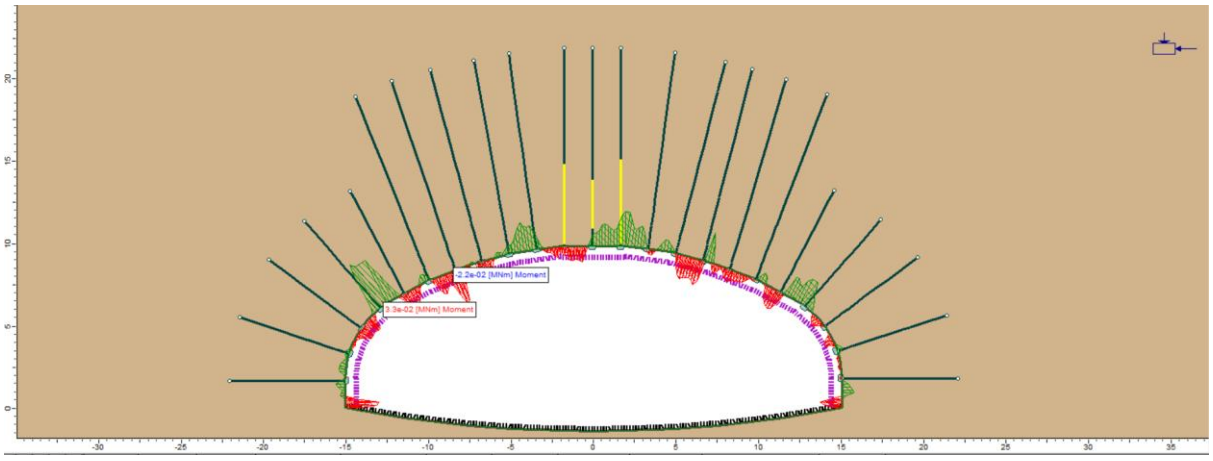

Figure 5-55. Bending Moment on RRS - Model A, k=2

5.1.3.4. Axial Force on Bolts

Axial forces are high and, in some bolts, there are two sets of force acing on them based on their high length; Maximum axial force on a bolt is 0.2 MN.

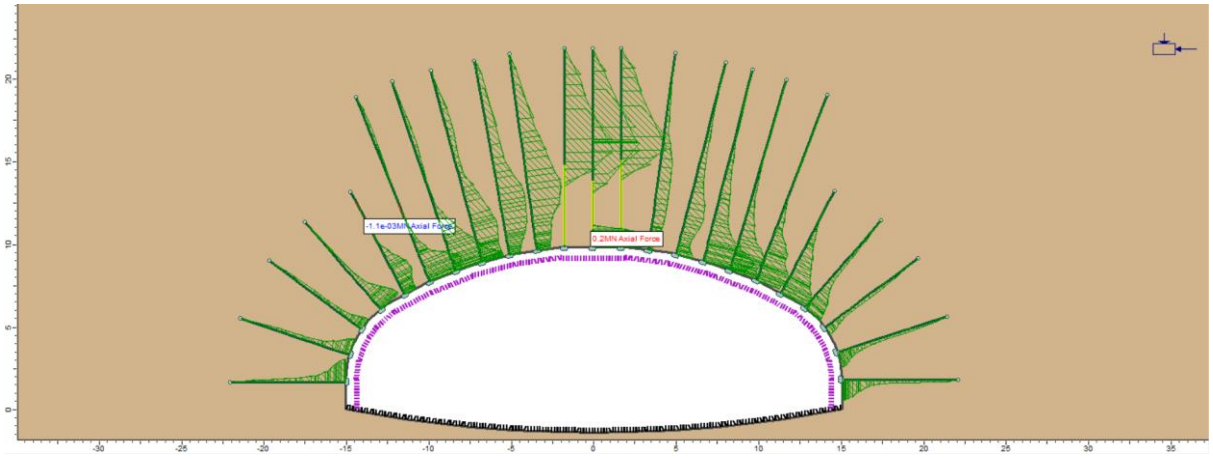

Figure 5-56. Axial Force on rock bolts - Model A, k=2

5.1.3.5. Support Capacity, Rock Bolts

As it was expected some bolts are yielded and their number is three; They are generally affected by tension near the excavation boarder. Following figure shows the yielded bolts.

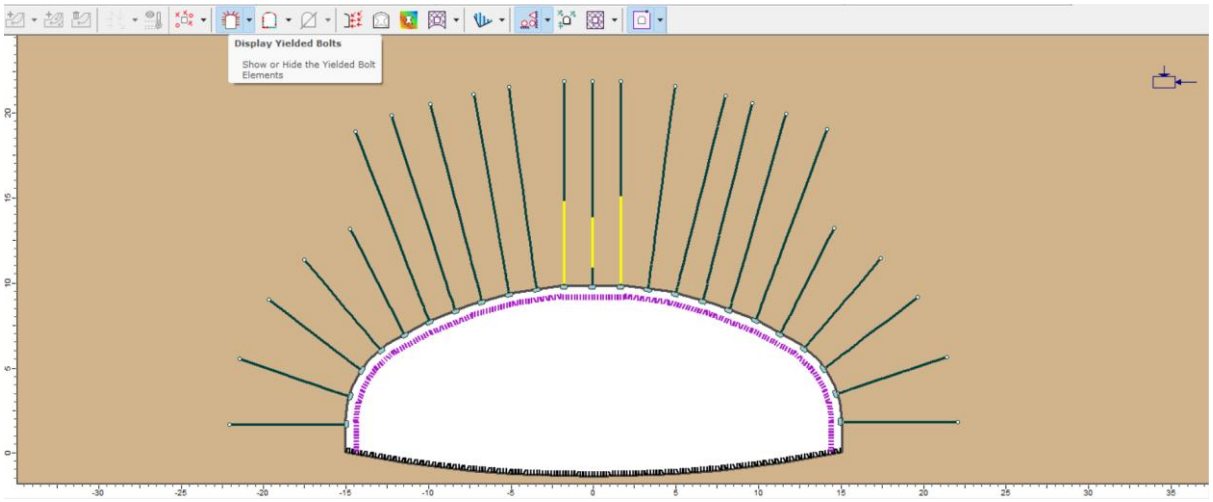

Figure 5-57. Displayed yielded bolts - Model A, k=2

5.1.3.6. Support Capacity, RRS

Following plots show the capacity of RRS in this model.

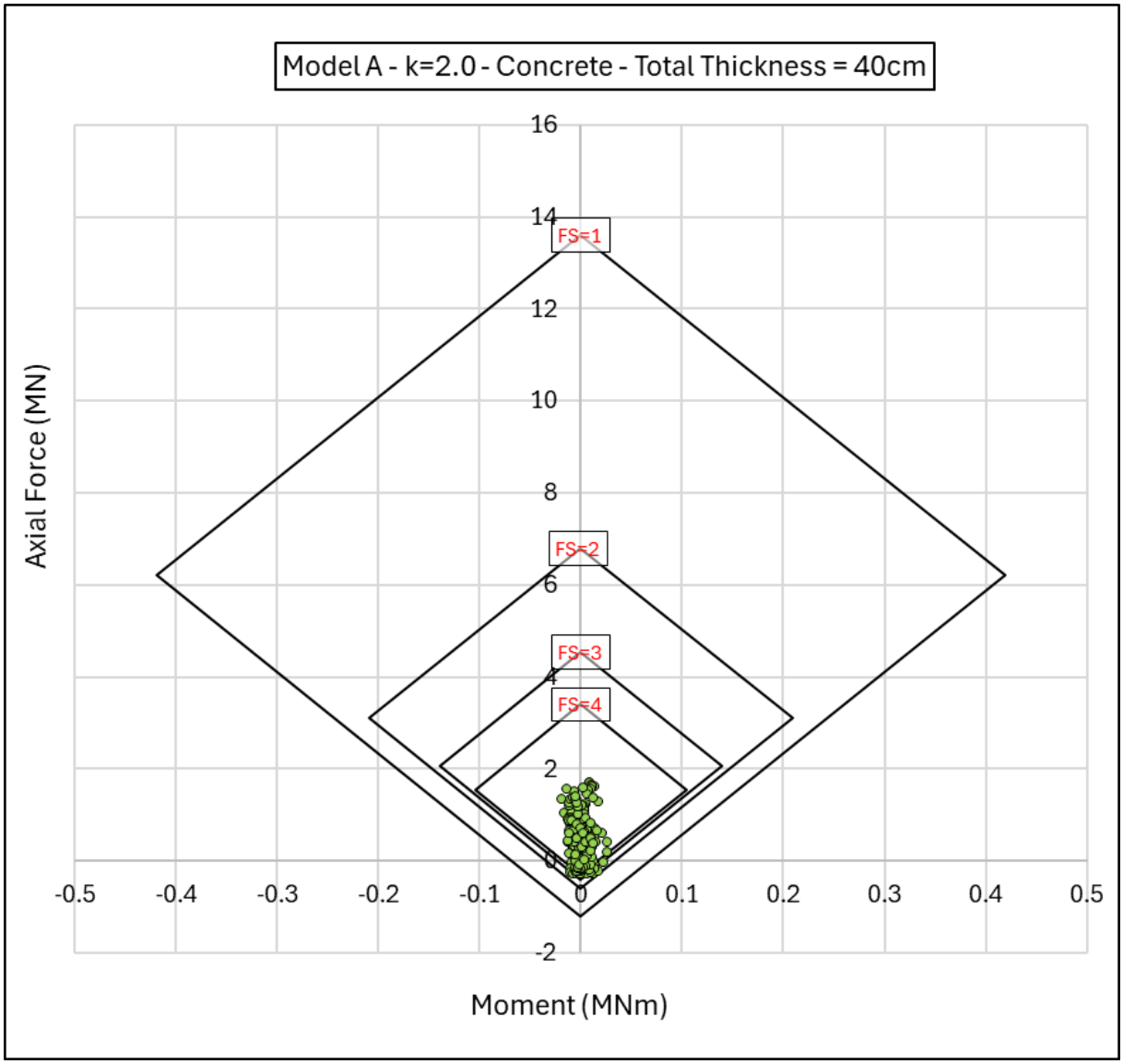

Figure 5-58. Axial Force-Moment Plot of the RRS - Model A, k=2

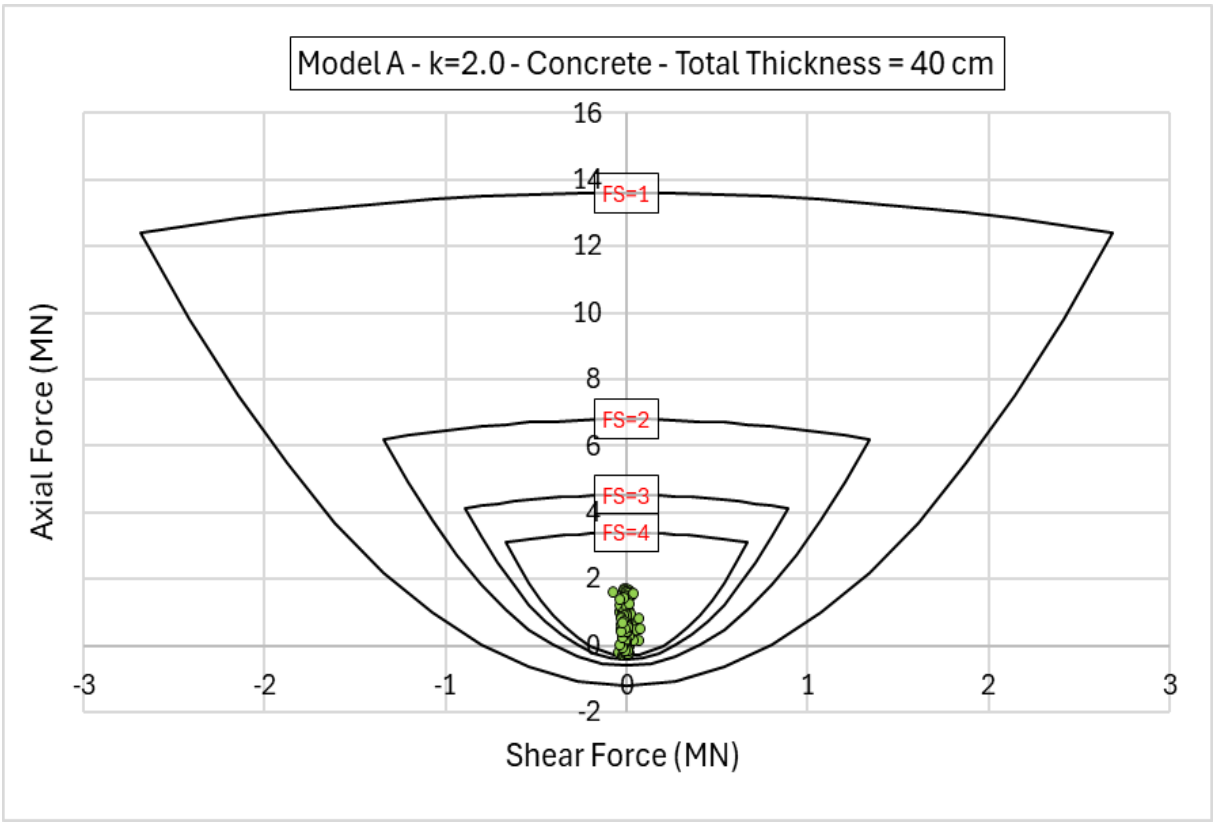

Figure 5-59. Axial Force-Shear Force plot of RRS - Model A, k=2

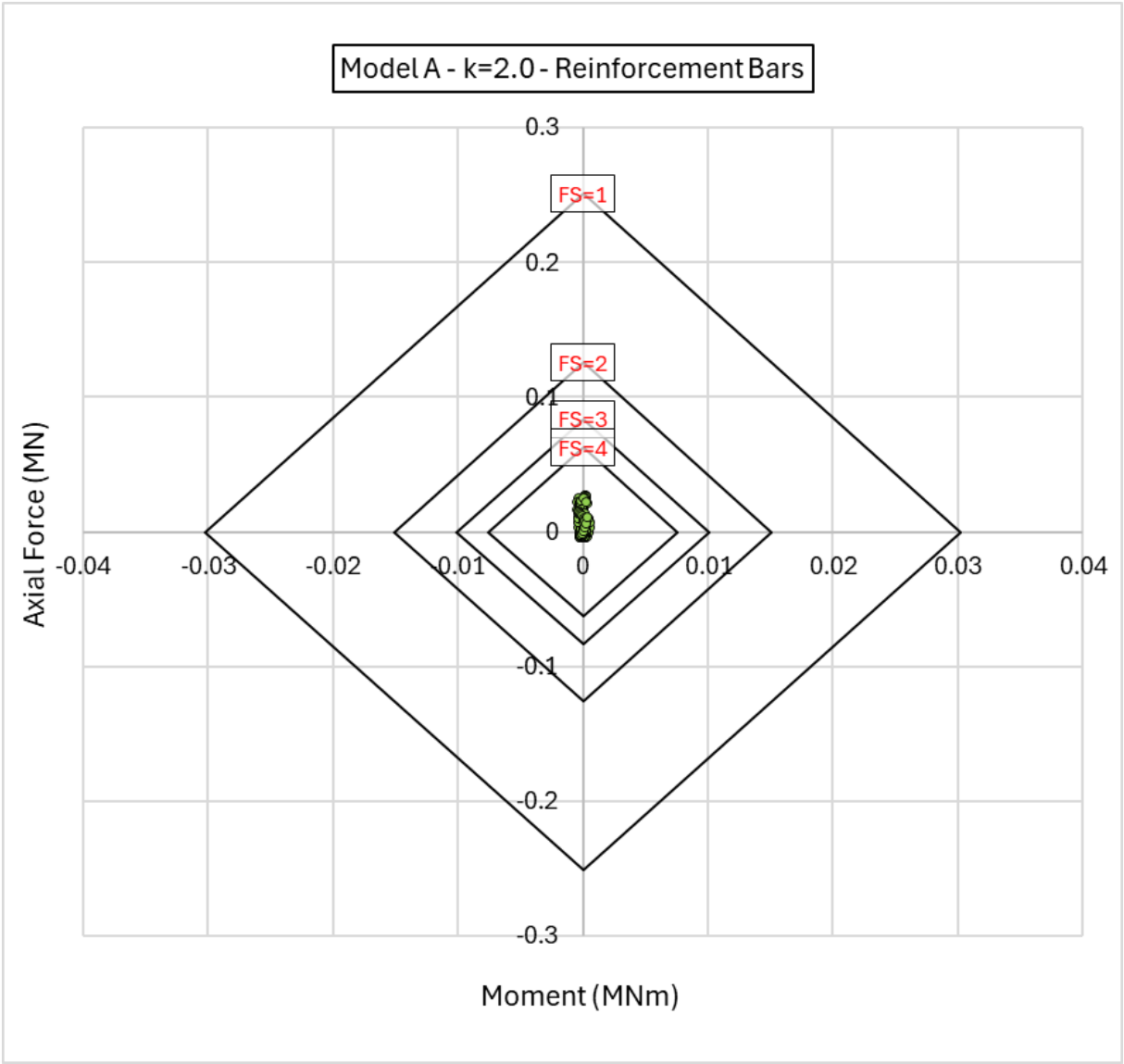

Figure 5-60. Axial Force - Moment plot of steel rebars - Model A, k=2

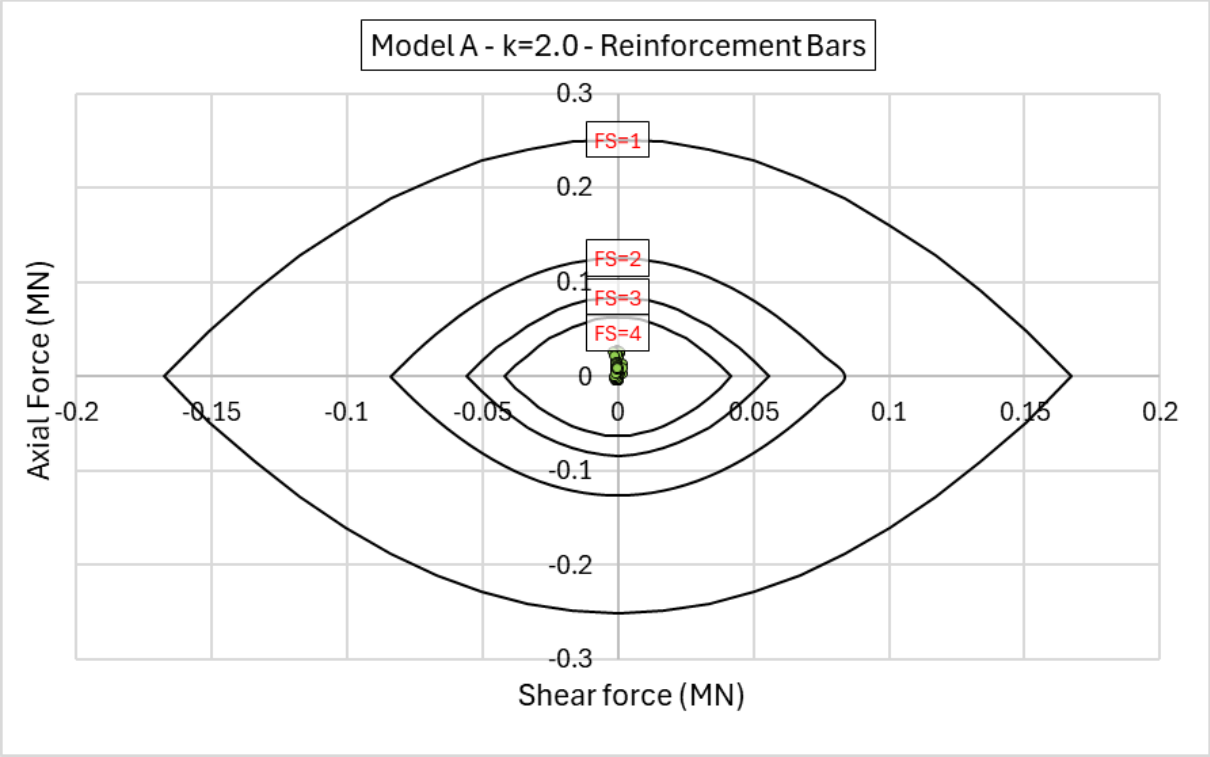

Figure 5-61. Axial Force-Shear Force plot of steel rebars - Model A, k=2

5.1.3.7. Summary of Results

Following table shows a summary of results for Model A with stress ratio higher than 2.

Table 5-3. Summary of results - Model A, k = 2

Model A – k = 2	
Maximum displacement at the walls [cm]	6
Maximum displacement at the roof [cm]	10
Maximum total displacement [cm]	10.7
Maximum radius measured for the plastic zone [m]	10
RRS properties	40 cm thickness c/c spacing 1.5 m
Maximum Compression on RRS [MN]	1.9
Maximum Tension on RRS [MN]	0.3
Min-Max Factor of Safety for RRS	Min: 2.2 Max: Higher than 4
Quantity of rock bolts and their lengths [m]	23 Rock Bolts 13 Rock Bolts 12 m 10 Rock Bolts 7 m
Rock bolt tributary area [mm^2]	207
Maximum axial force on rock bolts [MN]	0.2
Number of Yielded bolts and their location	3 rock bolts (Center of the crown)
Rock Bolt Deformation [cm]	5.7

In summary, plastic zones progressively expand around each excavation step concentrated on the crown of the excavation boundaries until the last stage that reaches 10 m far from the cavern.

Rock bolts on the sidewalls are 7 m, and have 12 m of length in the roof; Their endpoint is in the elastic zone; five bolts are yielded with maximum deformation of 5.8 cm.

RRS liners are generally compressed with highest axial force of 1.9 MN except for some points in the around the walls under tension that reaches 0.3 MN of axial force.

Support capacity plots for concrete show good performance even though there are few points under tension in the roof with lowest safety factor of 2.2.

5.2. Model B (SD)

Model B simulates the sequences of excavation starting from sides on right and left then the central portion in the last stage.

5.2.1. Model B – k = 0.5

Results of computation of Model B with stress ratio of 0.5 are presented below.

5.2.1.1. Total Displacement

Displacement contours are concentrated on the center of the roof and the invert; Maximum amount of displacement is 8.1 cm. Direction of deformations are vertical, except in the walls.

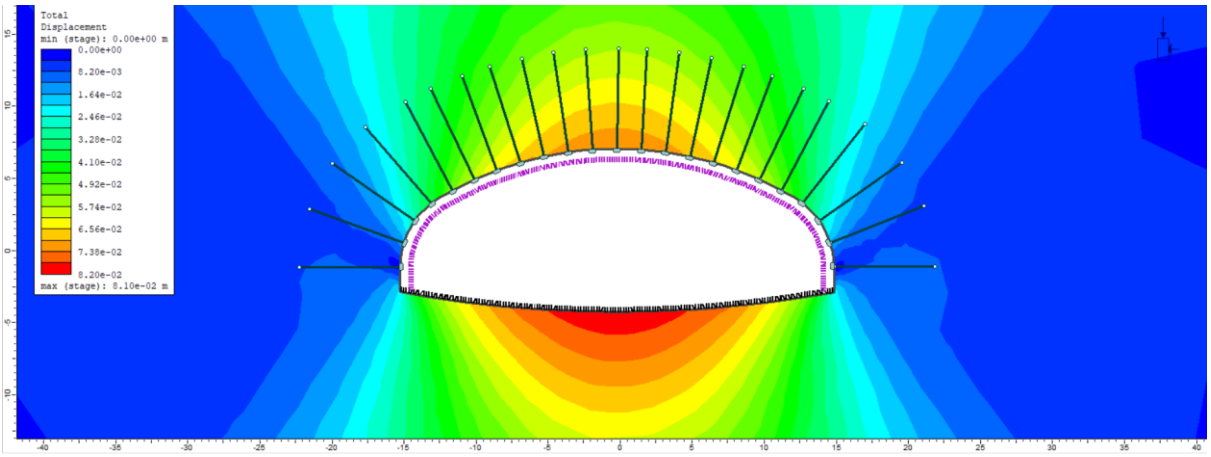

Figure 5-62. Total displacement - Model B, k=0.5

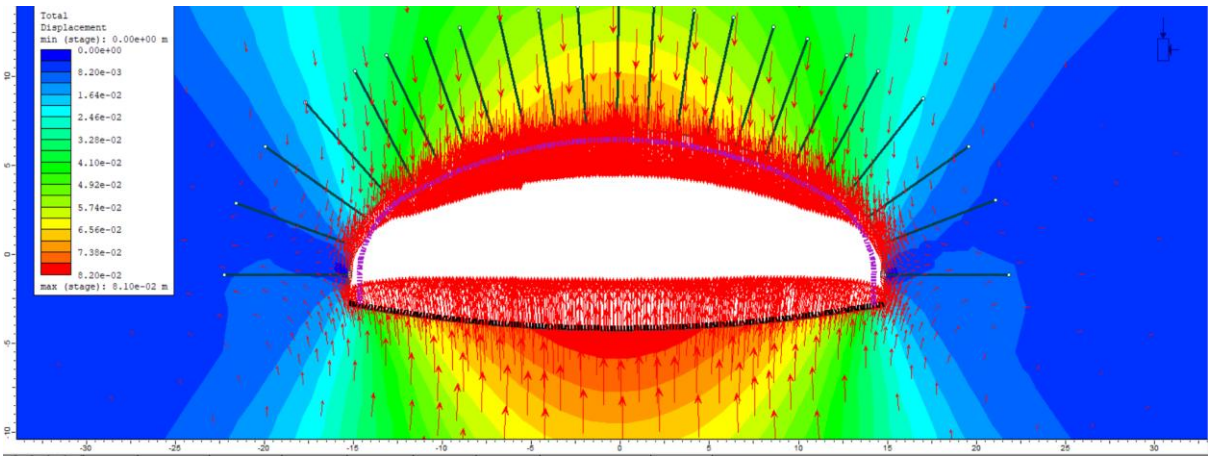

Figure 5-63. Deformation vectors and displacement - Model B, k=0.5

5.2.1.2. Plastic Radius around the cavern

Yielded elements reach almost up to 5 m from the cavern boundary, and they are concentrated on right wall and the left wall.

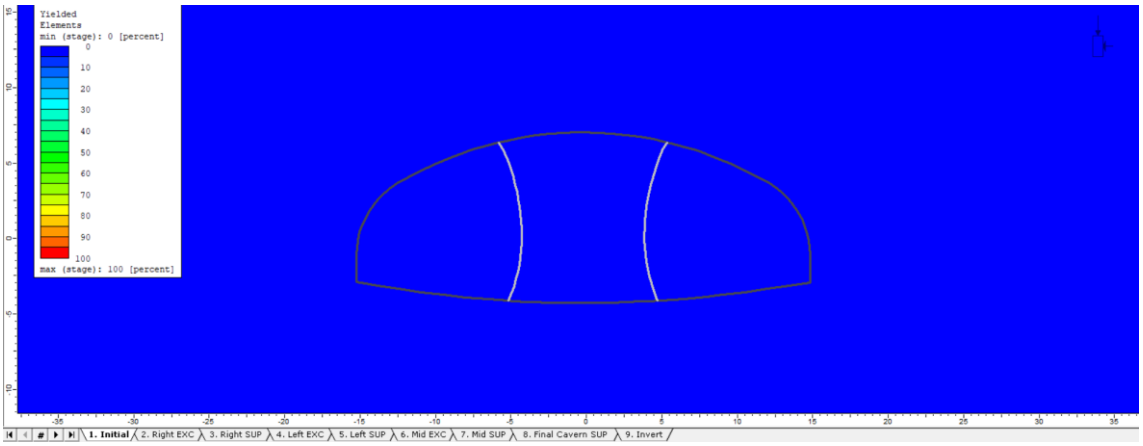

Figure 5-64. Yielded elements, Stage 1 - Model B, k=0.5

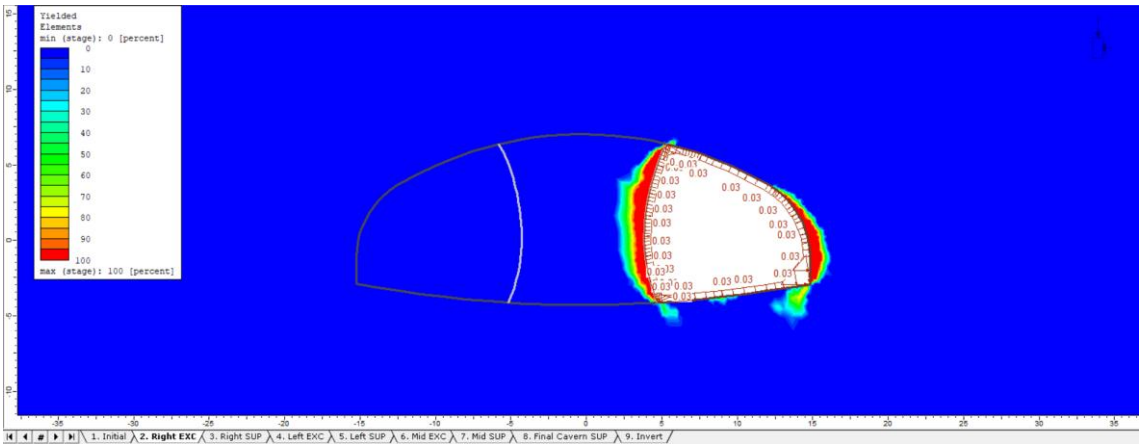

Figure 5-65. Yielded elements, Stage 2 - Model B, k=0.5

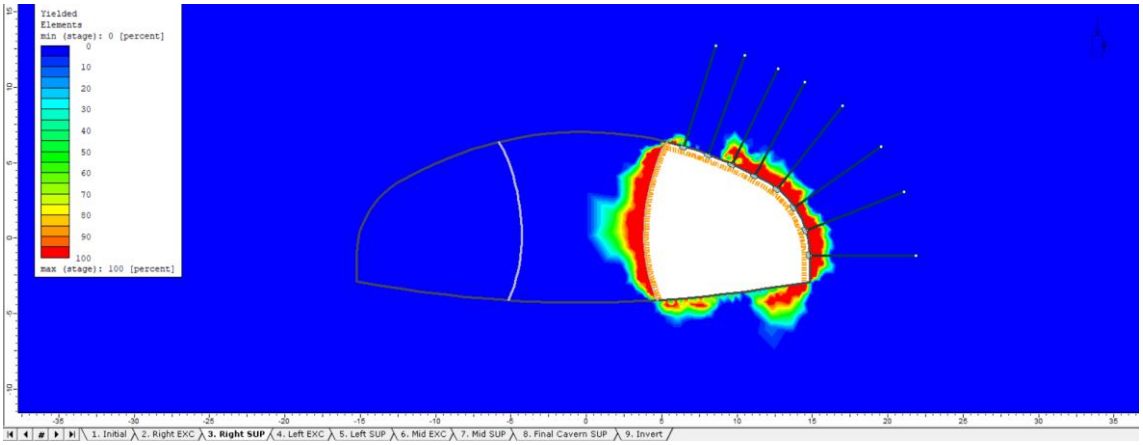

Figure 5-66. Yielded elements, Stage 3 - Model B, k=0.5

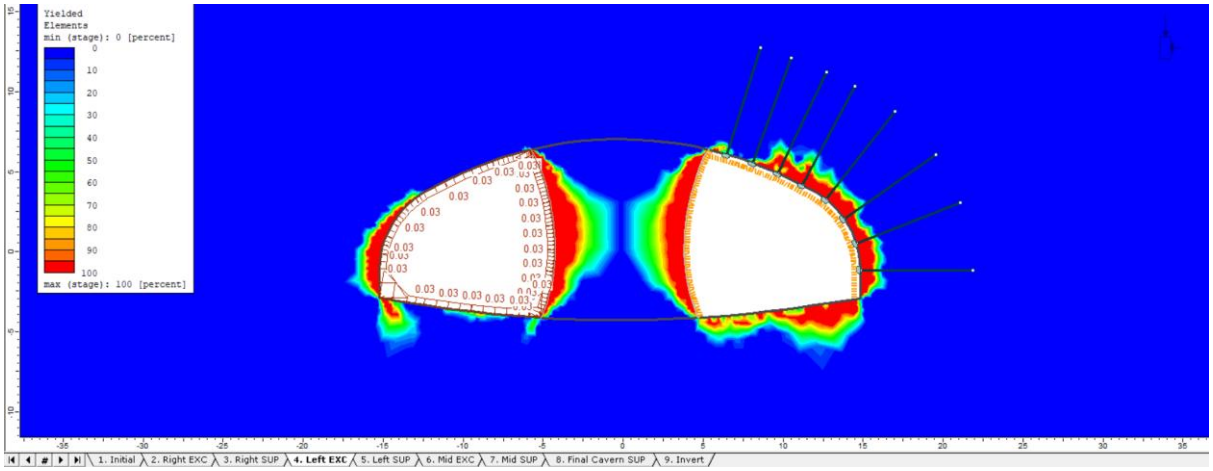

Figure 5-67. Yielded elements, Stage 4 - Model B, k=0.5

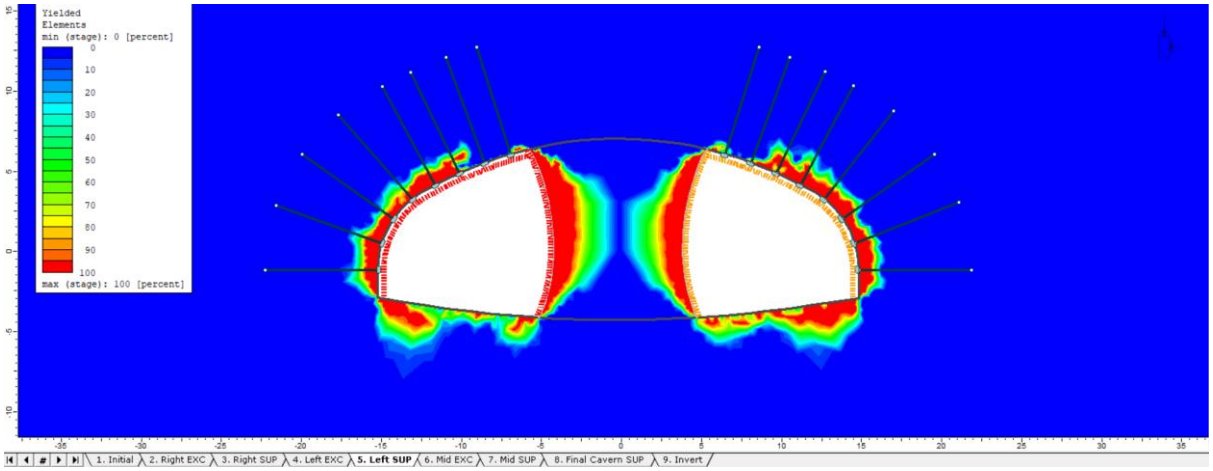

Figure 5-68. Yielded elements, Stage 5 - Model B, k=0.5

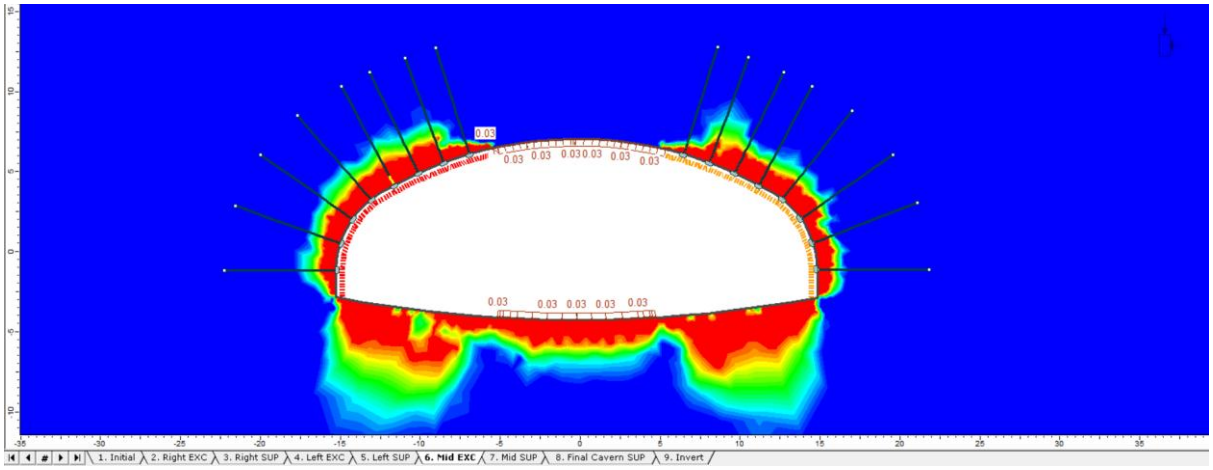

Figure 5-69. Yielded elements, Stage 6 - Model B, k=0.5

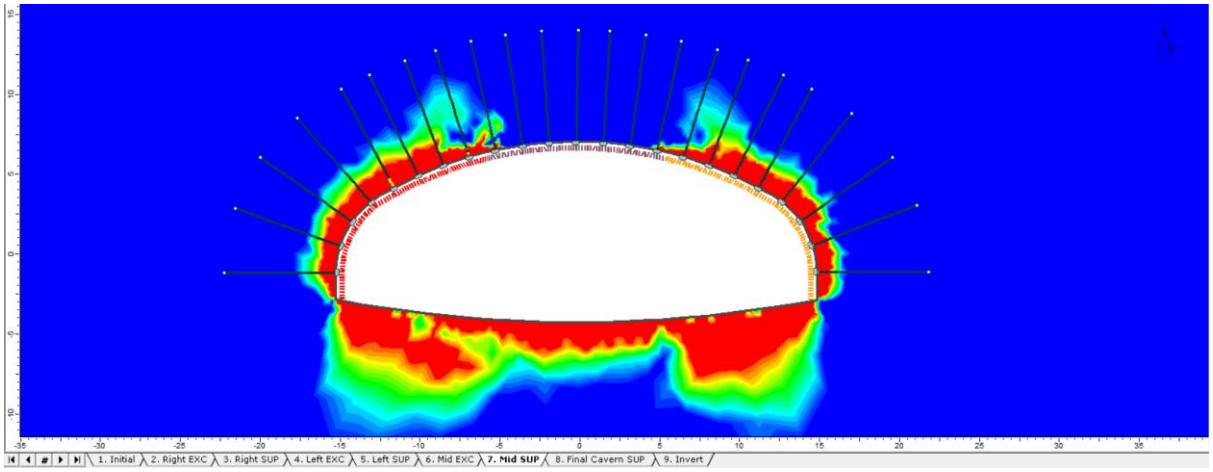

Figure 5-70. Yielded elements, Stage 7 - Model B, k=0.5

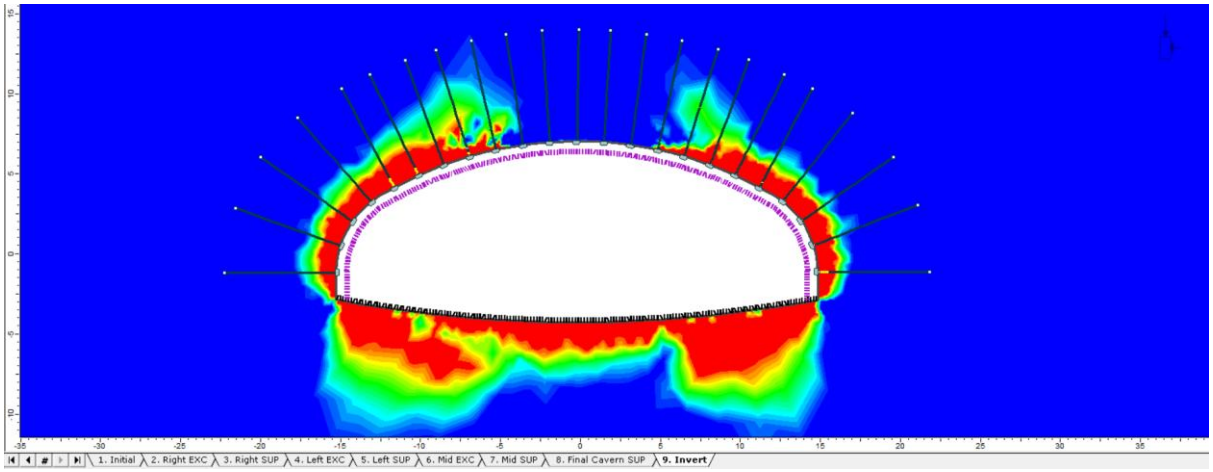

Figure 5-71. Yielded elements, Stages 8 & 9 - Model B, k=0.5

The furthest plastic point is almost placed 4 m distance from excavation boundary.

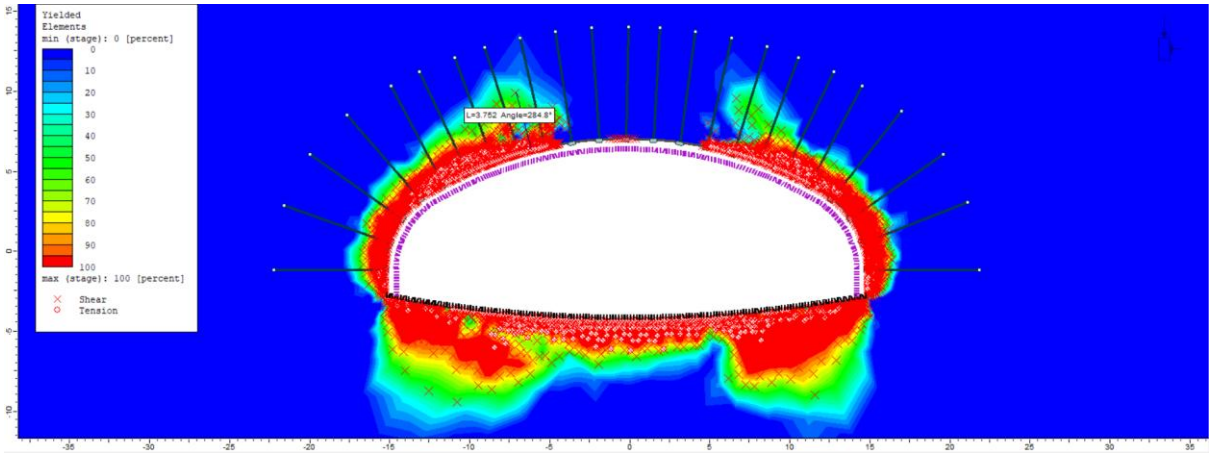

Figure 5-72. Plastic Points - Model B, k=0.5

5.2.1.3. *Axial Force on Bolts*

The rock Bolts on the walls face highest amount of axial force which is maximumly 0.2 MN (Figure 5-73).

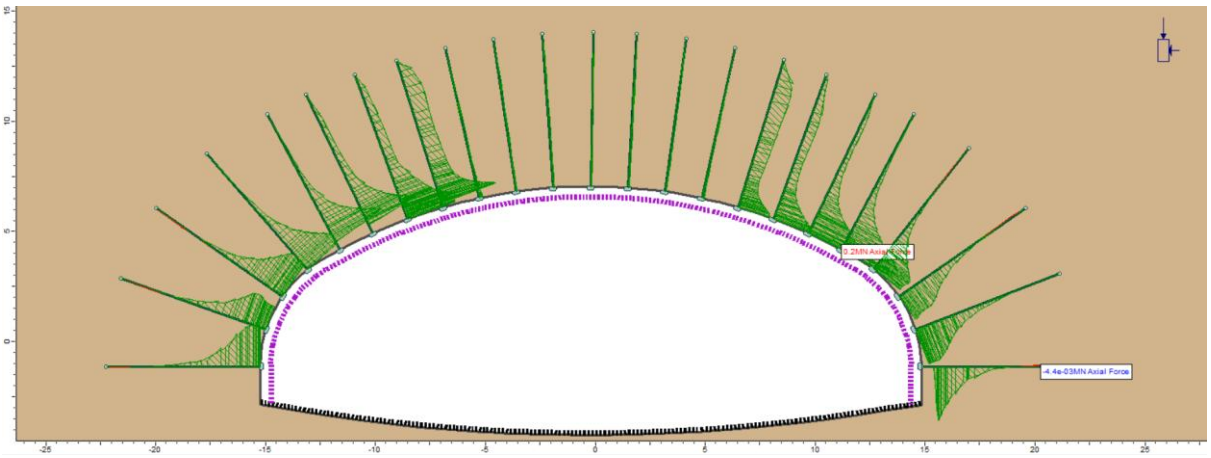

Figure 5-73. Axial force on rockbolts - Model B, k=0.5

5.2.1.4. *Axial Force and Bending Moment on RRS*

Maximum axial force is 5.4 MN and compressing the lining in the walls; Also, there is tension force in the roof with maximum value of 0.6MN. Highest Bending moment is 0.032MNm.

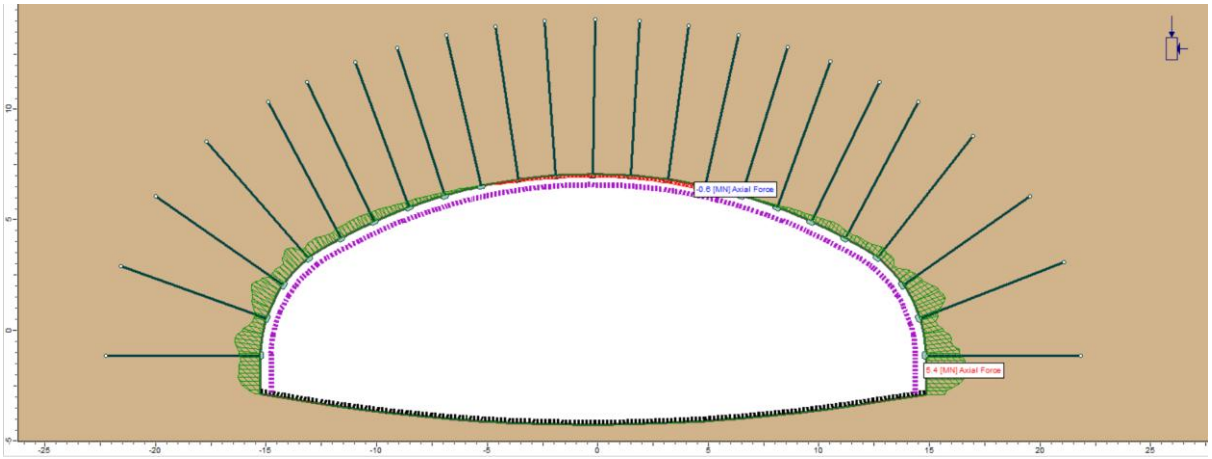

Figure 5-74. Axial Force on RRS - Model B, k=0.5

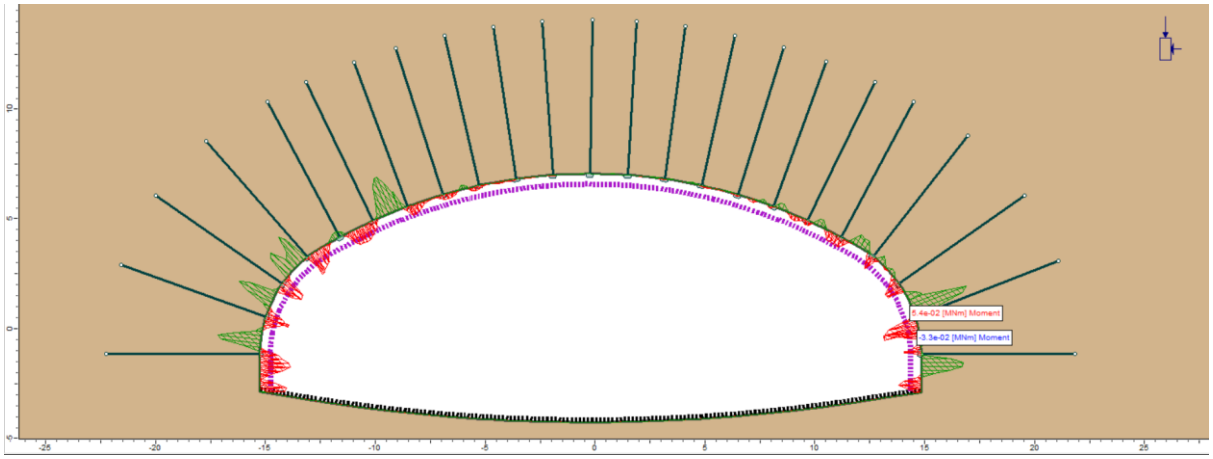

Figure 5-75. Bending Moment on RRS - Model B, k=0.5

5.2.1.5. Support Capacity, Rockbolts

There are three yielded bolts in the last stage.

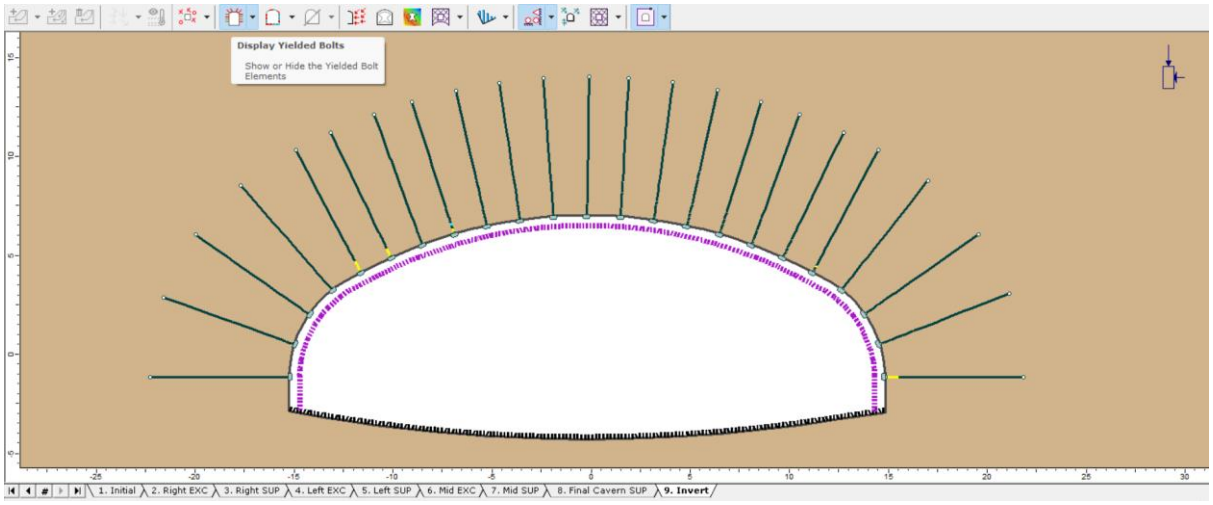

Figure 5-76. Displayed yielded bolts - Model B, k=0.5

5.2.1.6. Support Capacity, RRS

Following figures show the support capacity of concrete and rebars in RRS.

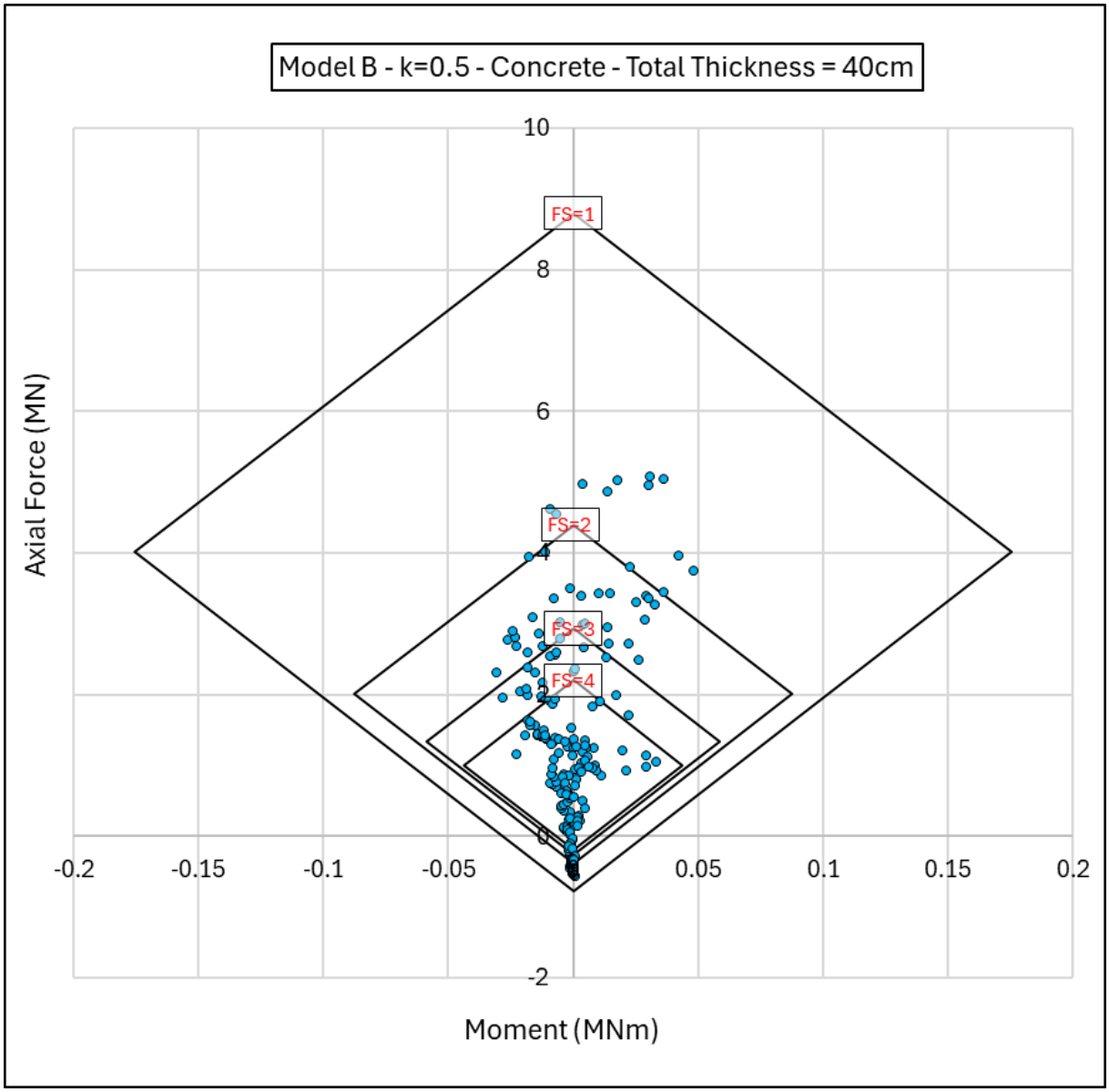

Figure 5-77. Axial Force-Moment plot of concrete - Model B, k=0.5

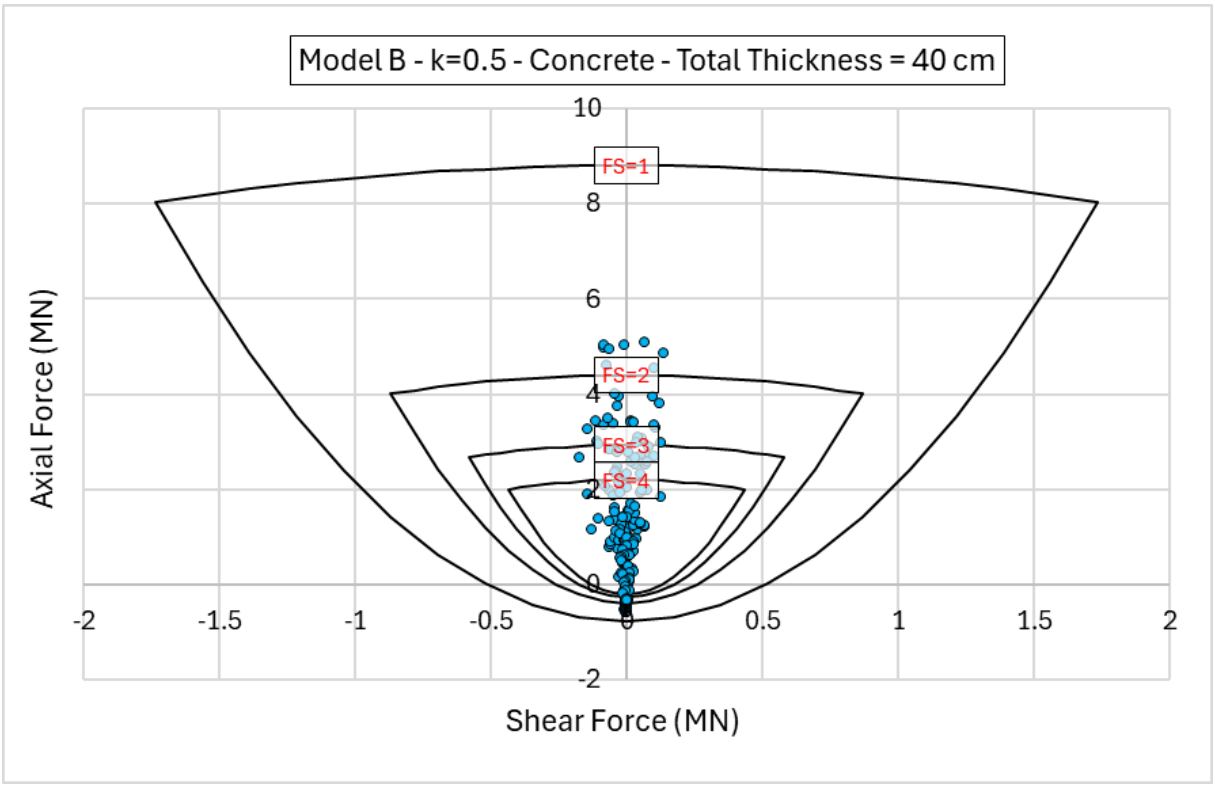

Figure 5-78. Axial Force-Shear Force plot of concrete - Model B, k=0.5

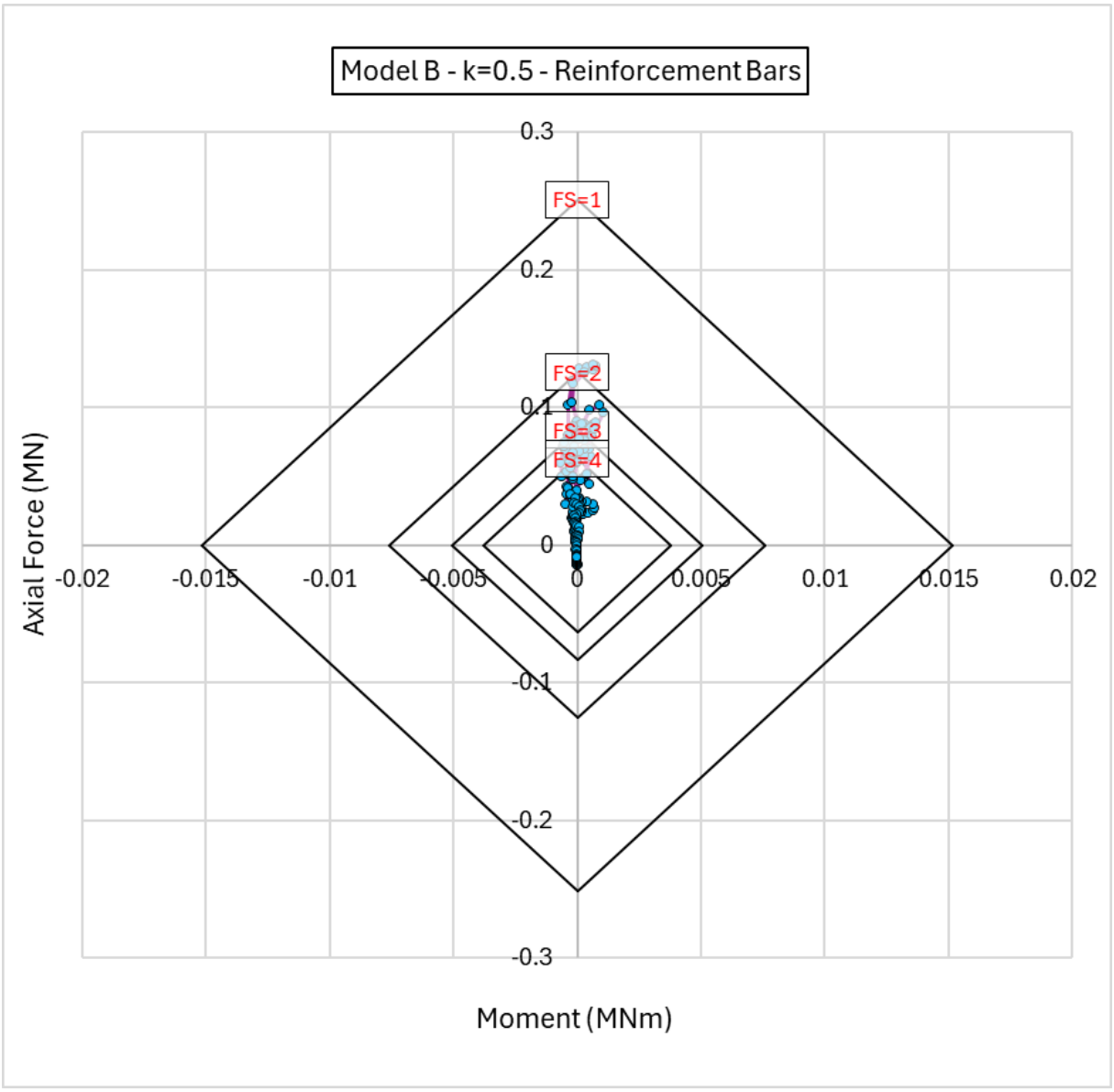

Figure 5-79. Axial Force-Moment plot of steel rebars - Model B, k=0.5

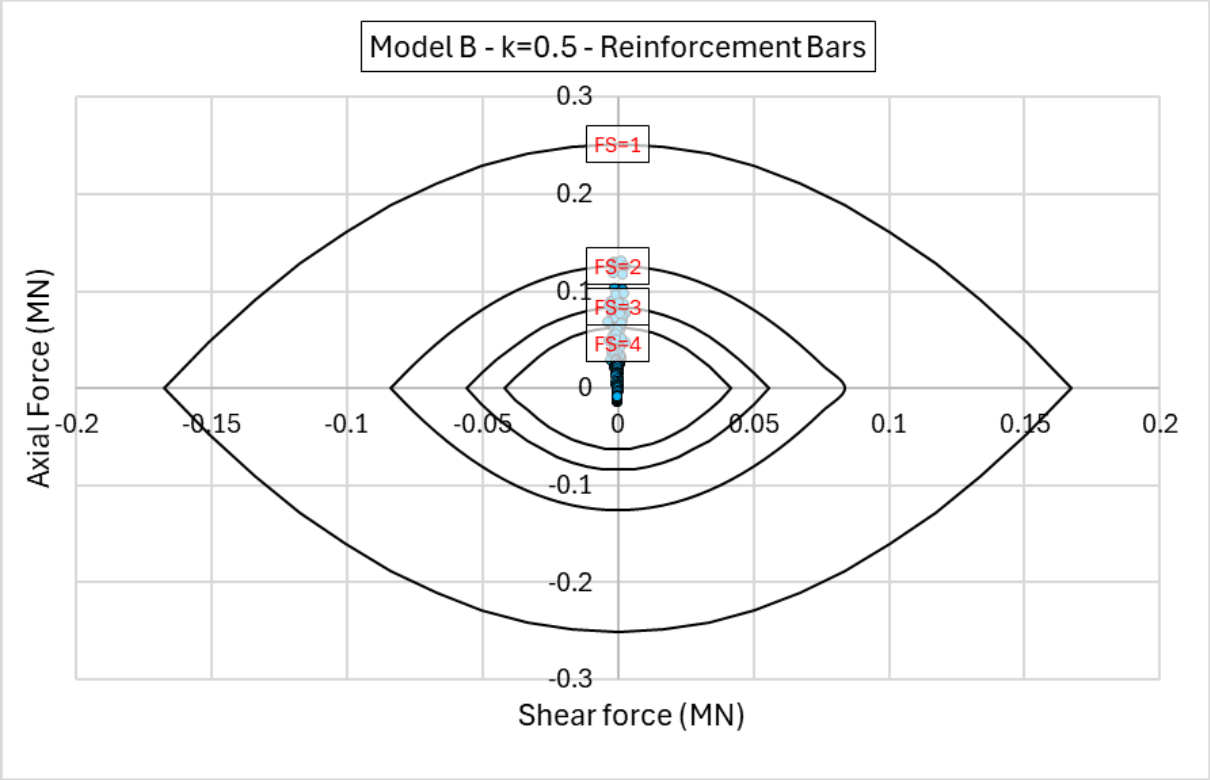

Figure 5-80. Axial Force-Shear Force plot of steel rebars - Model B, k=0.5

5.2.1.7. Summary of Results

A summary of achieved results that were presented before is indicated in this section.

Table 5-4. Summary of Results - Model B, k = 0.5

Model B – k = 0.5	
Maximum displacement at the walls [cm]	4
Maximum displacement at the roof [cm]	7.3
Maximum total displacement [cm]	8.1
Maximum radius measured for the plastic zone [m]	5
RRS properties	40 cm thickness c/c spacing 4.5 m
Maximum Compression on RRS [MN]	5.4
Maximum Tension on RRS [MN]	0.6
Min-Max Factor of Safety for RRS	Min: 1.2 Max: Higher than 4
Quantity of rock bolts and their lengths [m]	23 Rock Bolts - 7m
Rock bolt tributary area [mm^2]	207
Maximum axial force on rock bolts [MN]	0.2
Number of Yielded bolts and their location	3 (Sidewall)
Rock Bolt Deformation [cm]	4.2

In summary, plastic zone is progressively increased around each excavation step concentrated in the side walls until the last stage that reaches 5.5 m far from the excavation borders.

Rock bolts are 7m and their endpoint is in the elastic zone; there are three yielded bolts, and they have maximum deformation of 4.2 cm.

RRS liners are being compressed on the walls with high axial force of 5.4 MN. RRS in the roof is under tension with 0.6 MN of axial force that covers the crown.

Support capacity plots for concrete show unacceptable performance with high compression and tension; lowest amount of safety factors is 1.2 for the points under tension in the crown.

5.2.2. Model B – k = 1

In this section, results of Model B computation under hydrostatic pressure are presented.

5.2.2.1. Total Displacement

Maximum Displacement is 8.1 cm in the center of invert and the roof. Deformation vectors are mostly vertically directed to the center of cavern.

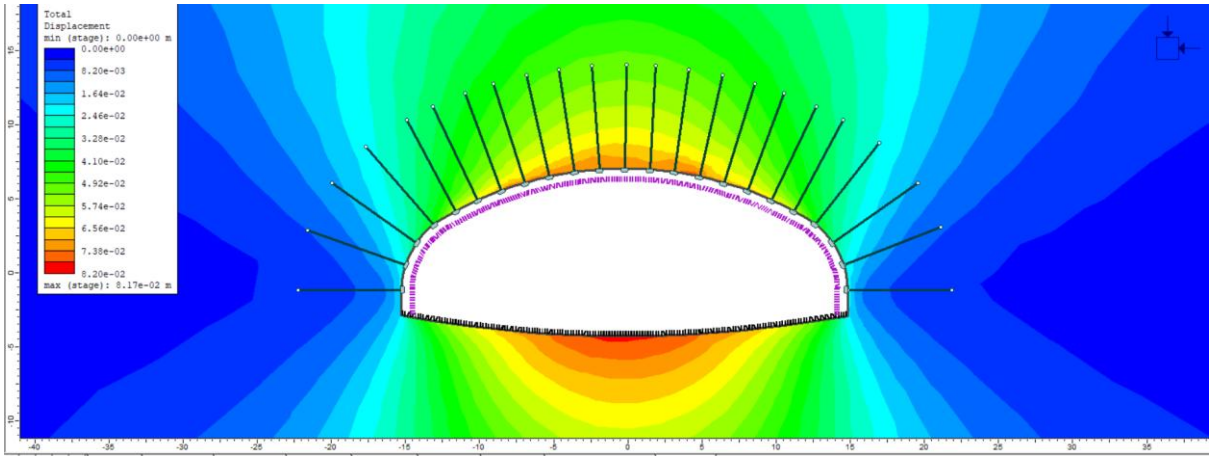

Figure 5-81. Total Displacement - Model B, k=1

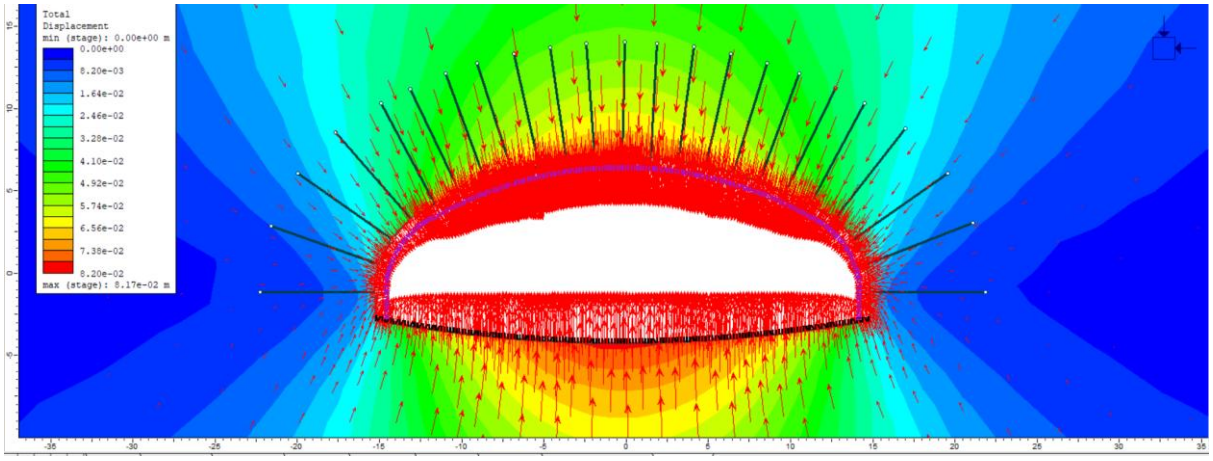

Figure 5-82. Deformation vectors and direction - Model B, k=1

5.2.2.2. Plastic Radius around the cavern

Maximum plastic radius around the cavern in the final stage is 5 m.

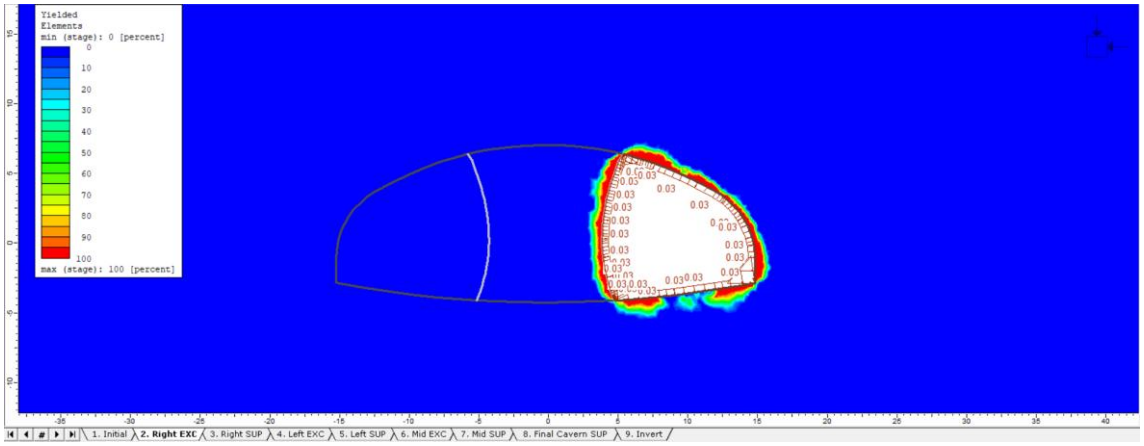

Figure 5-83. Yielded elements, Stage 2 - Model B, k=1

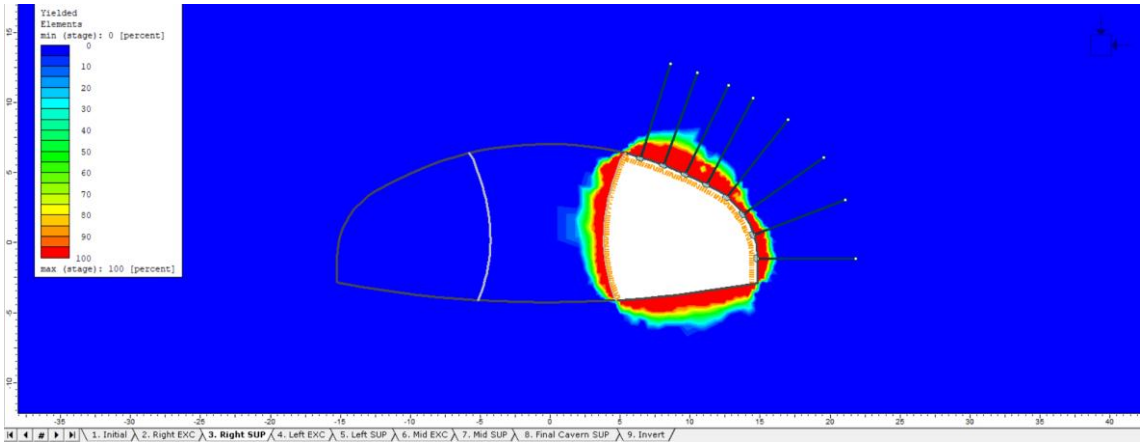

Figure 5-84. Yielded elements, Stage 3 - Model B, k=1

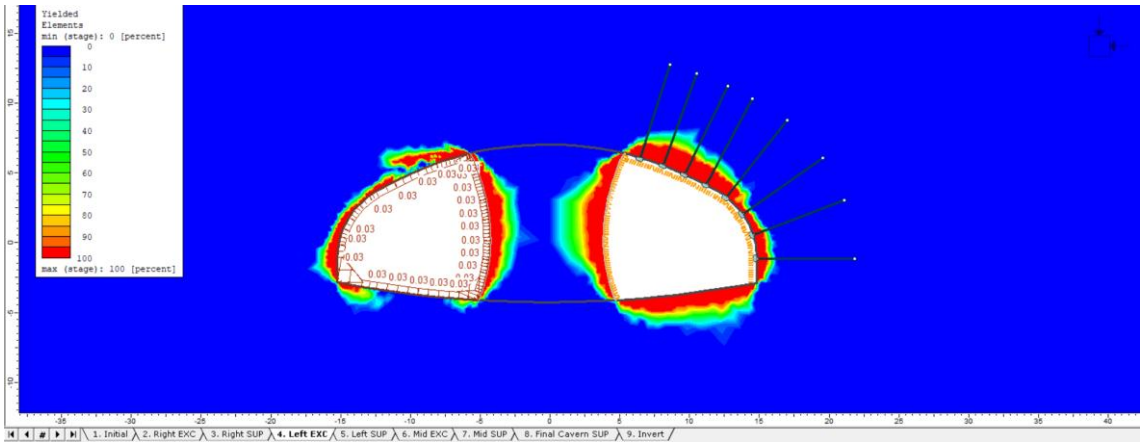

Figure 5-85. Yielded elements, Stage 4 - Model B, k=1

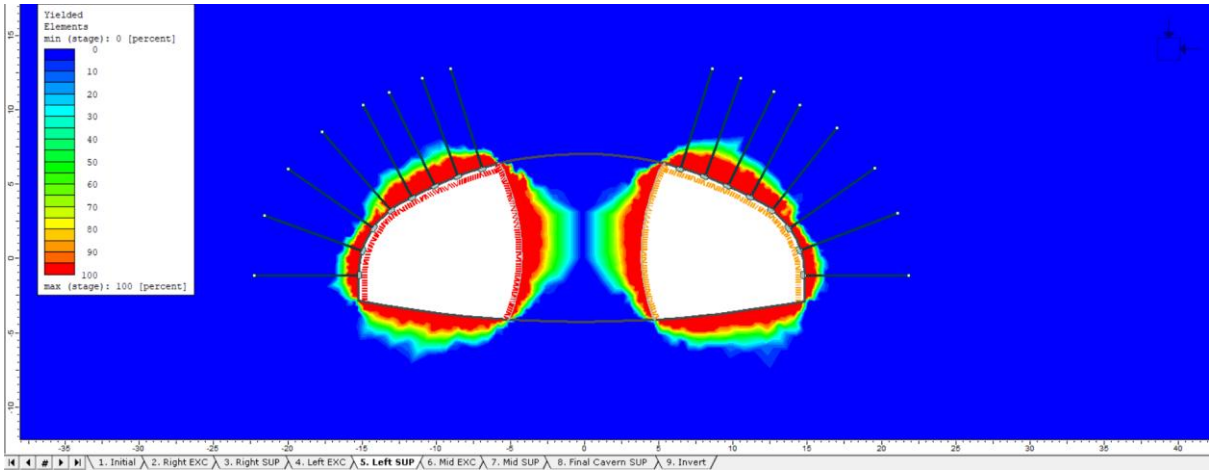

Figure 5-86. Yielded elements, Stage 5 - Model B, k=1

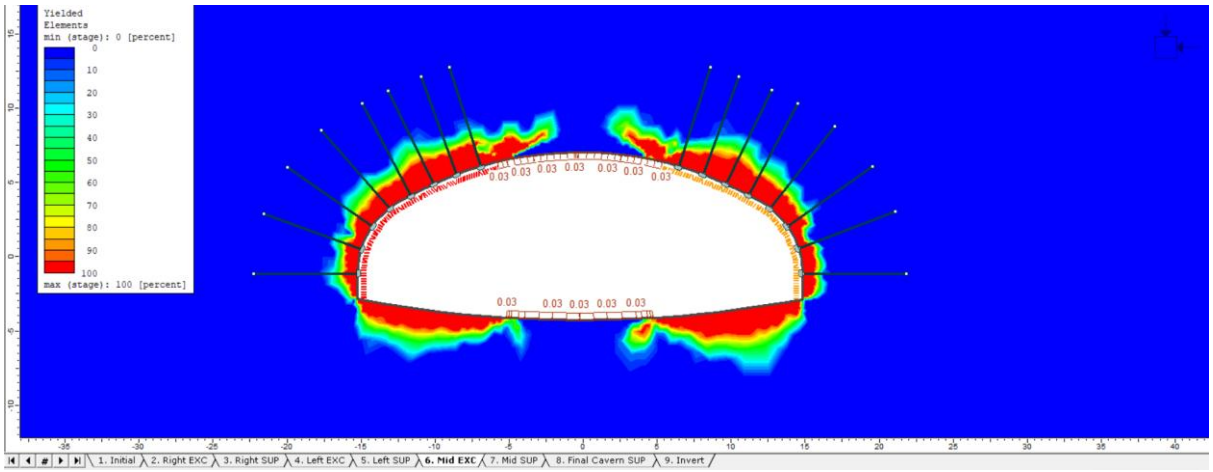

Figure 5-87. Yielded elements, Stage 6 - Model B, k=1

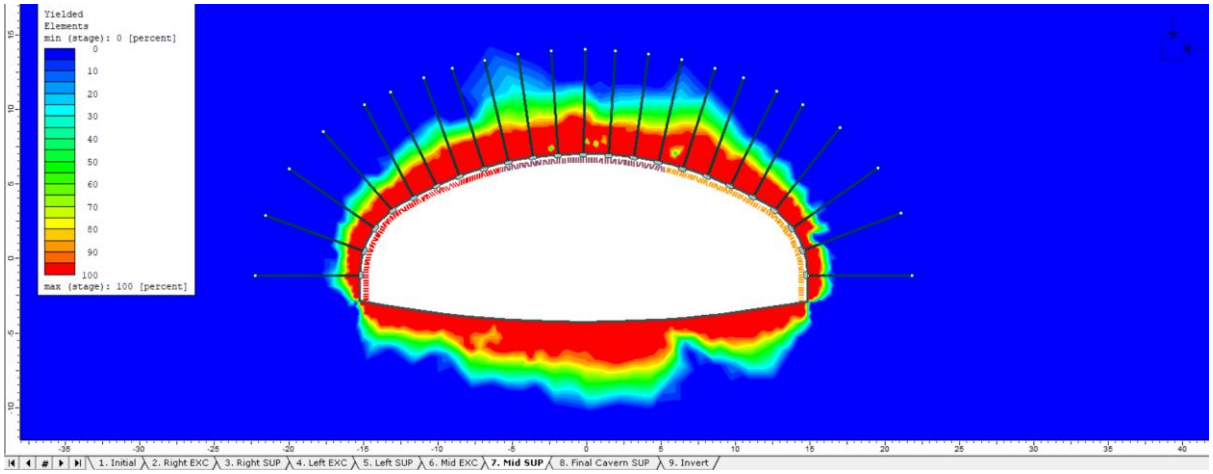

Figure 5-88. Yielded elements, Stage 7 - Model B, k=1

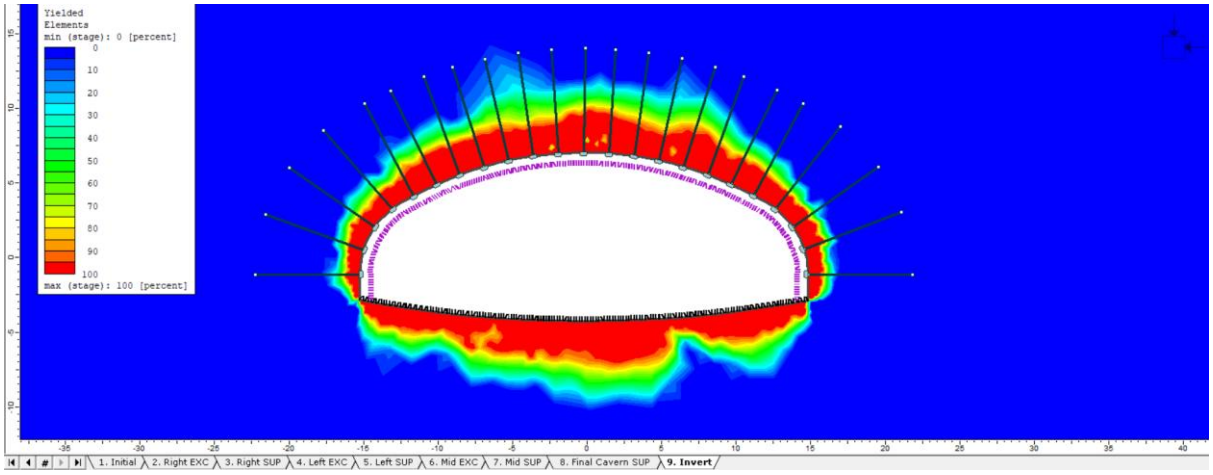

Figure 5-89. Yielded elements, Stage 8&9 - Model B, k=1

Plastic points placed around the cavern with maximum distance equal to 4 m from the excavation boundary.

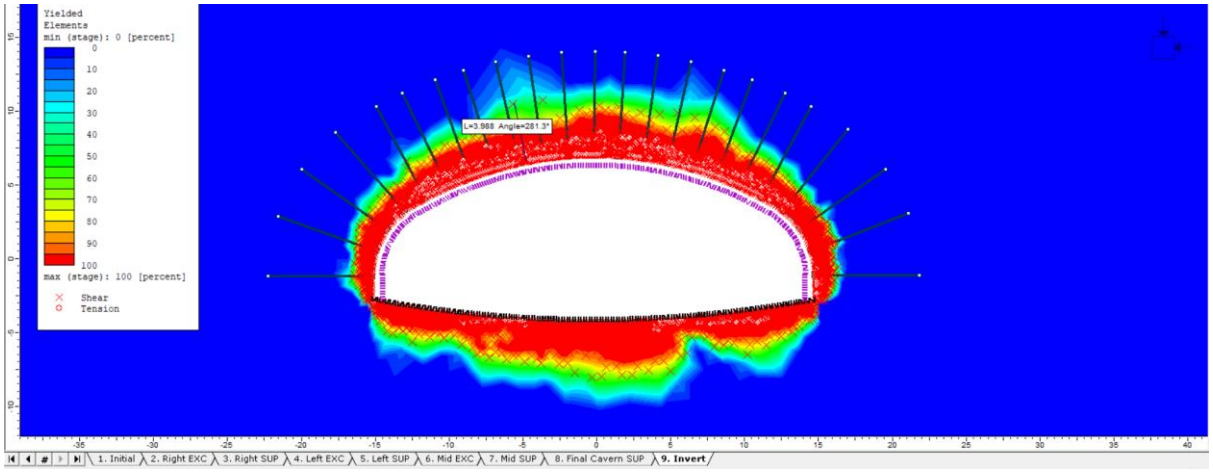

Figure 5-90. Plastic Points - Model B, k=1

5.2.2.3. *Axial Force on Rockbolts*

Maximum axial force acting on bolts is 0.2MN.

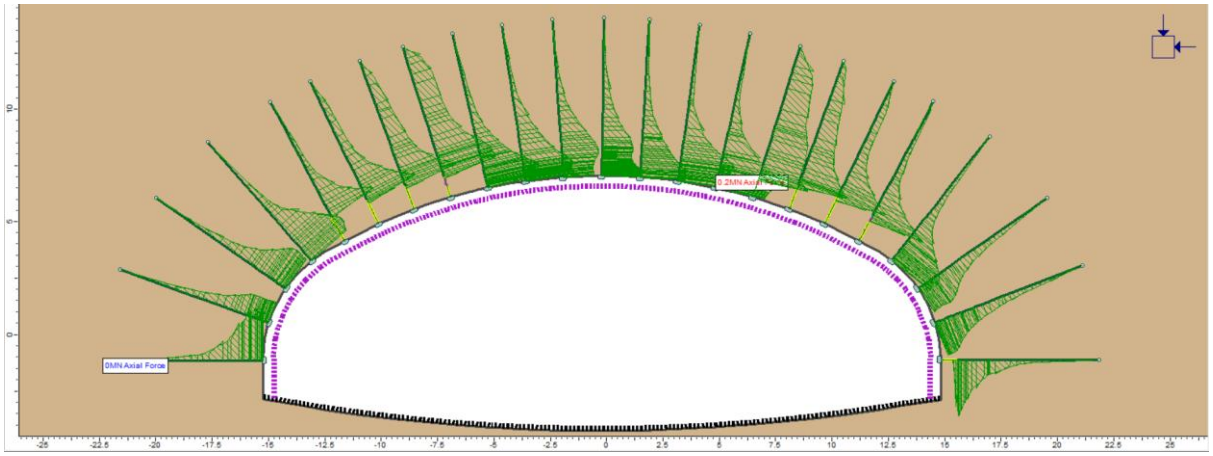

Figure 5-91. Axial Force on bolts - Model B, k=1

5.2.2.4. *Axial Force and Bending Moment on RRS*

Maximum axial force is 5.9 MN acting on the sidewalls; very few number of points under tension that can be negligible.

Bending Moment is maximumly 0.062 MNm.

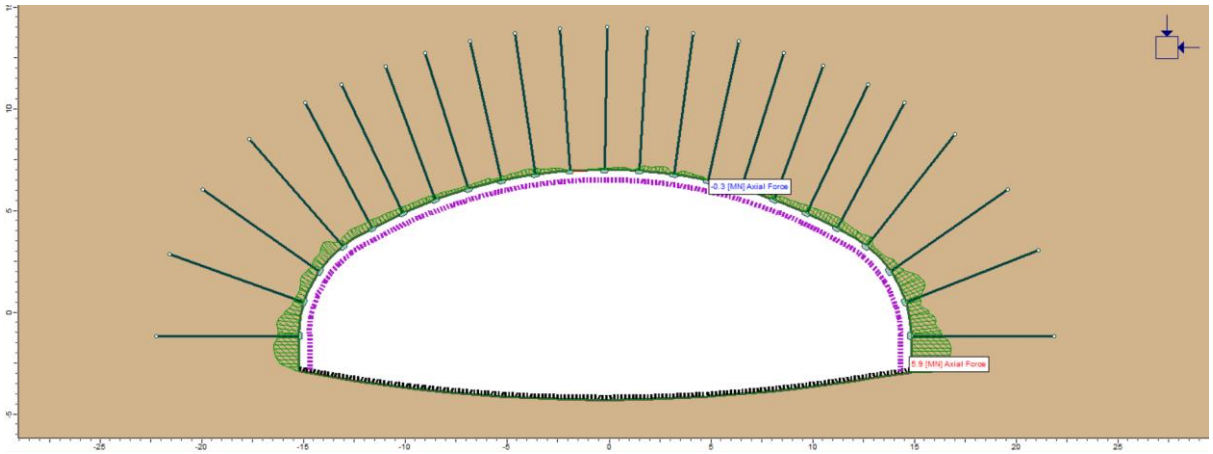

Figure 5-92. Axial Force on RRS - Model B, k=1

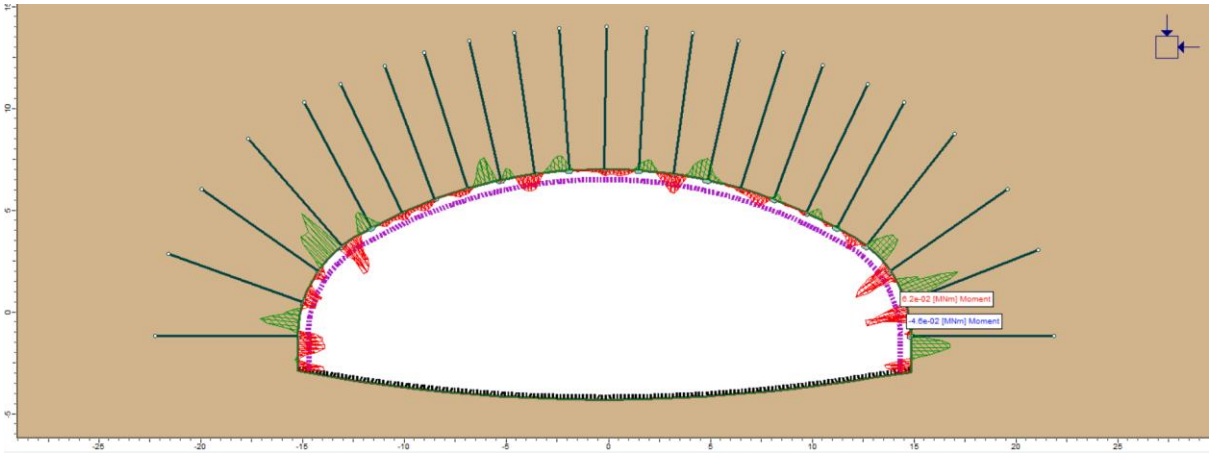

Figure 5-93. Bending Moment of RRS - Model B, k=1

5.2.2.5. Support Capacity, Rockbolts

There are nine yielded bolts mostly affected by tension.

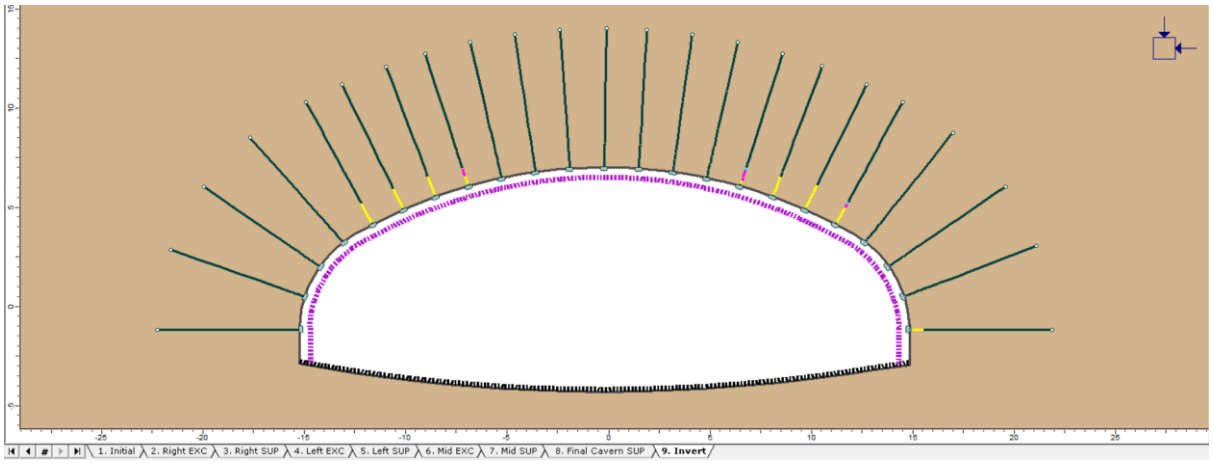

Figure 5-94. Displayed yielded bolts - Model B, k=1

5.2.2.6. Support Capacity, RRS

Plots showing the capacity of concrete and rebars in the RRS are presented below.

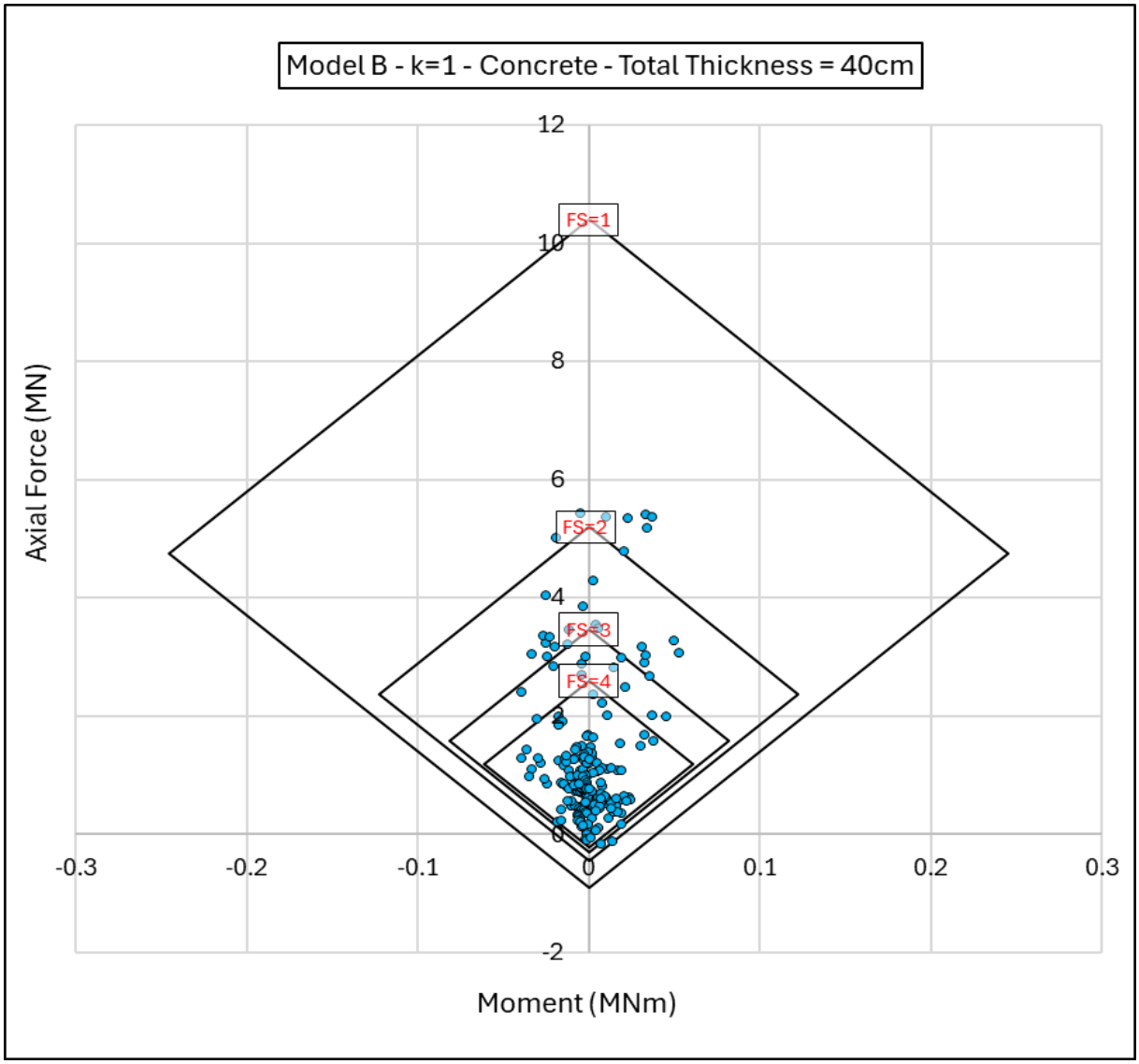

Figure 5-95. Axial Force-Moment plot of concrete - Model B, k=1

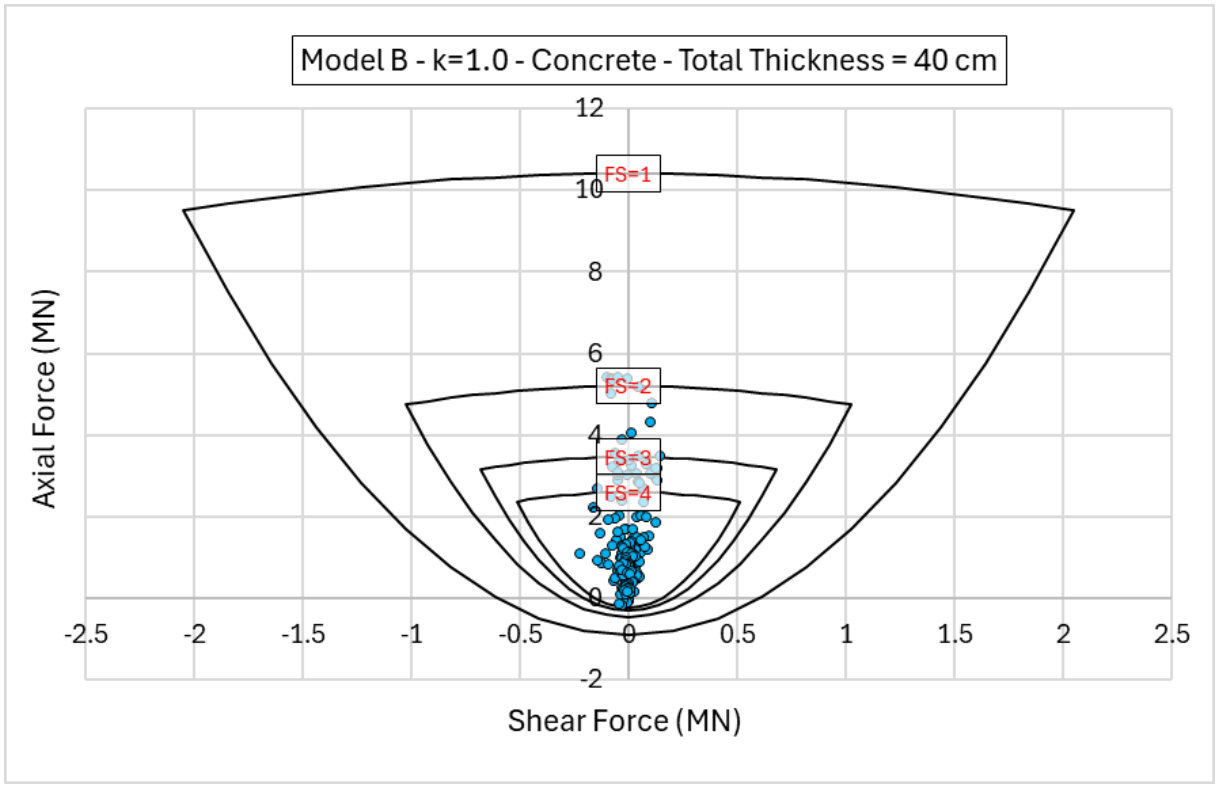

Figure 5-96. Axial Force-Shear Force plots of concrete - Model B, k=1

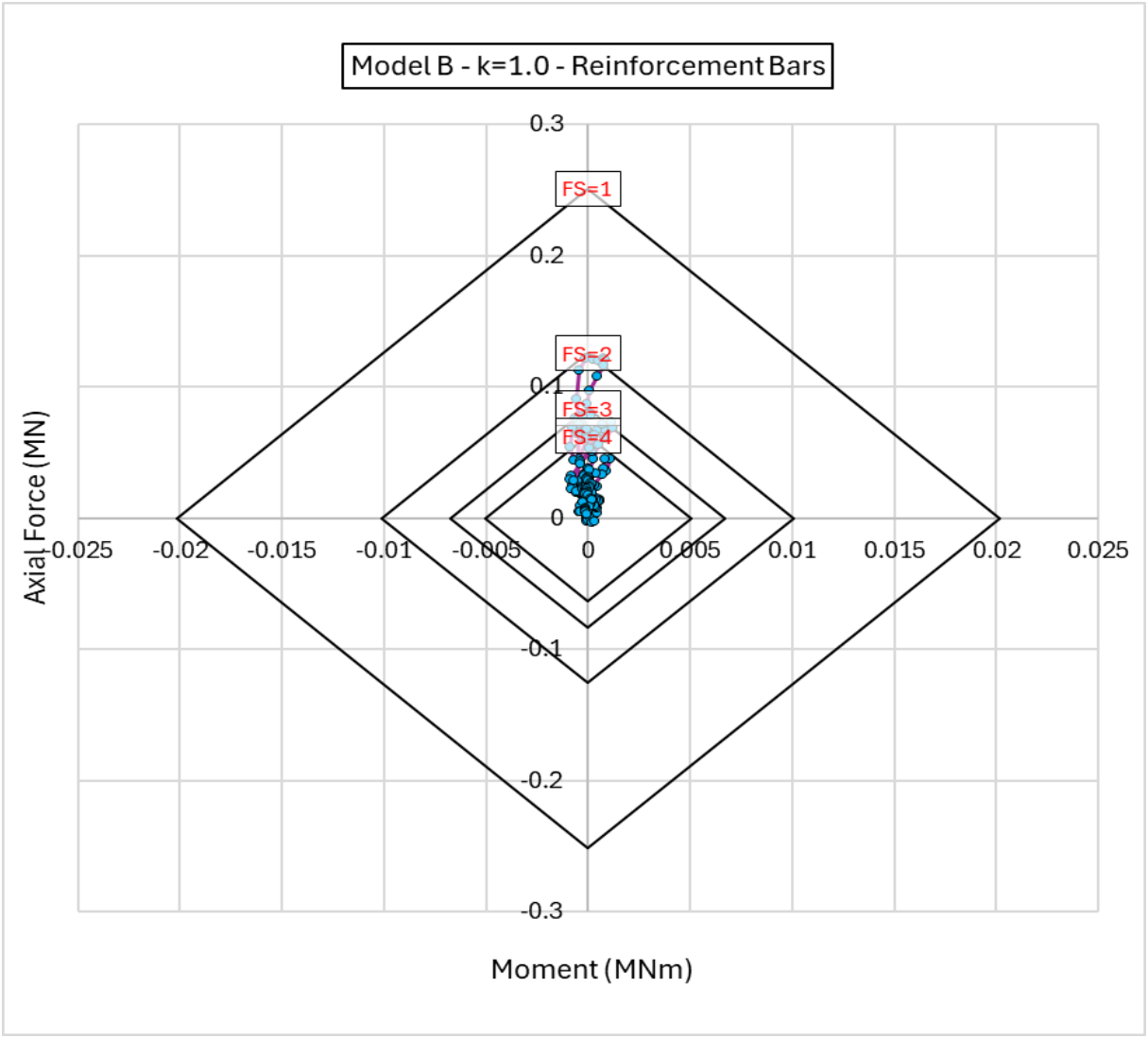

Figure 5-97. Axial Force-Moment plot of Steel Rebars - Model B, k=1

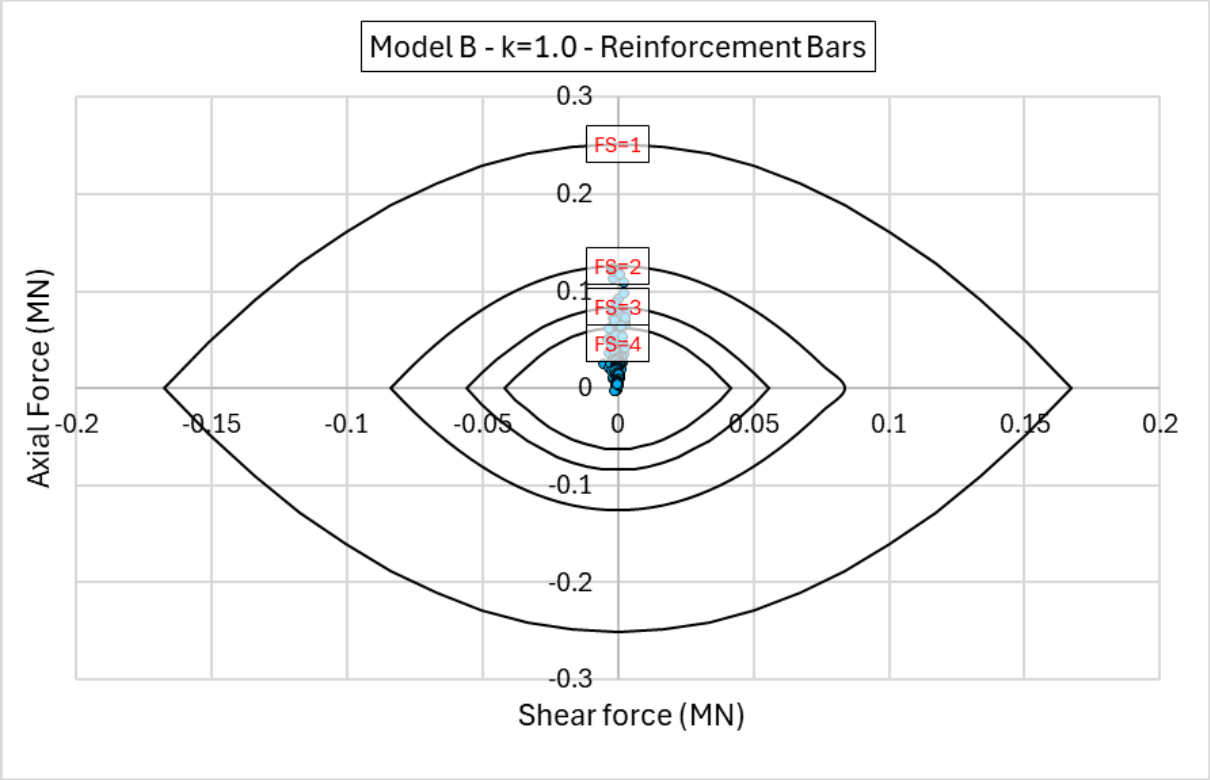

Figure 5-98. Axial Force-Shear Force plot of Steel Rebars - Model B, k=1

5.2.2.7. Summary of Results

Obtained results after computation of Model B under hydrostatic stress regime is presented below.

Table 5-5. Summary of Results - Model B, k = 1

Model B – k = 1	
Maximum displacement at the walls [cm]	3.5
Maximum displacement at the roof [cm]	7.7
Maximum total displacement [cm]	8.1
Maximum radius measured for the plastic zone [m]	5
RRS properties	40 cm thickness c/c spacing 3 m
Maximum Compression on RRS [MN]	5.9
Maximum Tension on RRS [MN]	0.3
Min-Max Factor of Safety for RRS	Min: 1.5 Max: higher than 4
Quantity of rock bolts and their lengths [m]	23 Rock Bolts 7m
Rock bolt tributary area [mm^2]	207
Maximum axial force on rock bolts [MN]	0.2
Number of Yielded bolts and their location	9 (between crown and walls)
Rock Bolt Deformation [cm]	5

In summary, plastic zones progressively increased around each excavation step equally balanced around the excavation boundaries until the last stage that reaches 5 m far from the cavern.

Rock bolts are 7m and their endpoint is in the elastic zone; there are nine yielded bolts, and they have maximum deformation of 5 cm.

RRS liners are generally being compressed with high axial force equal to 5.9 MN except for very few points between roof and walls under tension that reaches maximumly to 0.3 MN of axial force.

Support capacity plots for concrete show acceptable performance even though there are very few points under tension between the roof and walls with lowest safety factor of 1.5.

5.2.3. Model B – k = 2

Model B was computed with stress ratio equal to 2 and following results are achieved.

5.2.3.1. Total Displacement

Highest amount of displacement is 11.2 cm and is concentrated on the center of invert and roof. Generally, deformation vectors are directed horizontally, expect the middle of the roof that are almost vertically directed to the center of cavern.

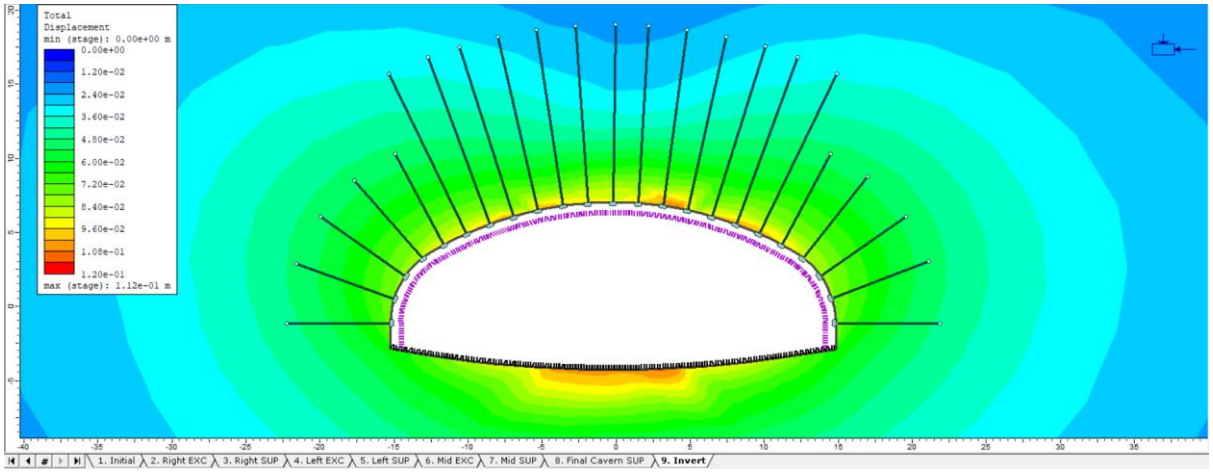

Figure 5-99. Total displacement - Model B, k=2

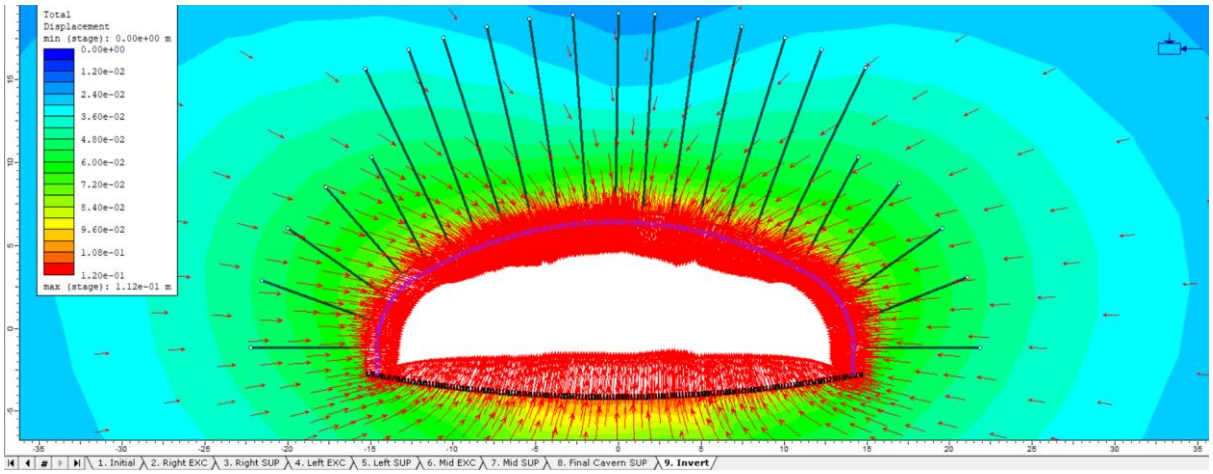

Figure 5-100. Deformation vectors and directions - Model B, k=2

5.2.3.2. Plastic Radius around the cavern

Plastic radius reaches almost 10 m up the roof.

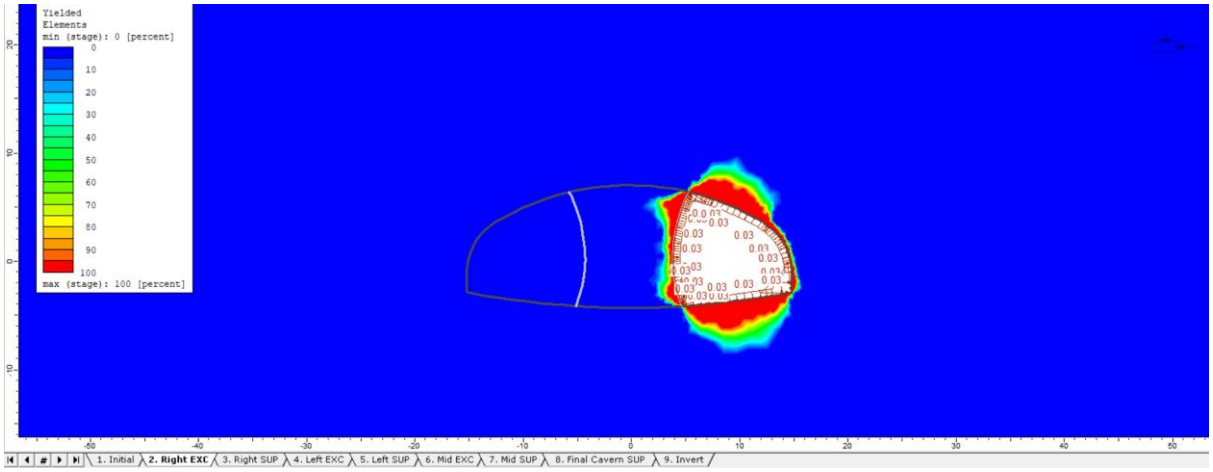

Figure 5-101. Yielded elements, Stage 2 - Model B, k=2

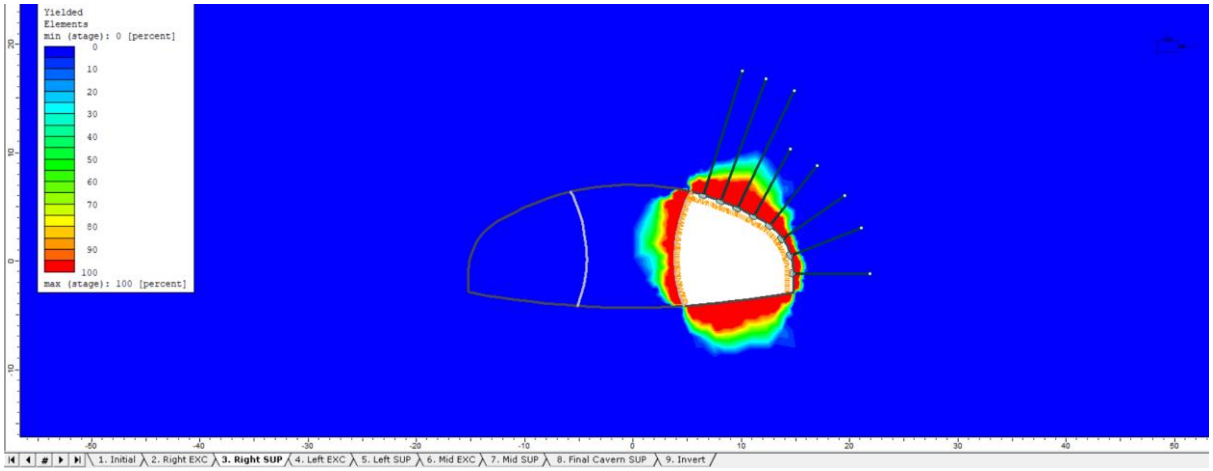

Figure 5-102. Yielded elements, Stage 3 - Model B, k=2

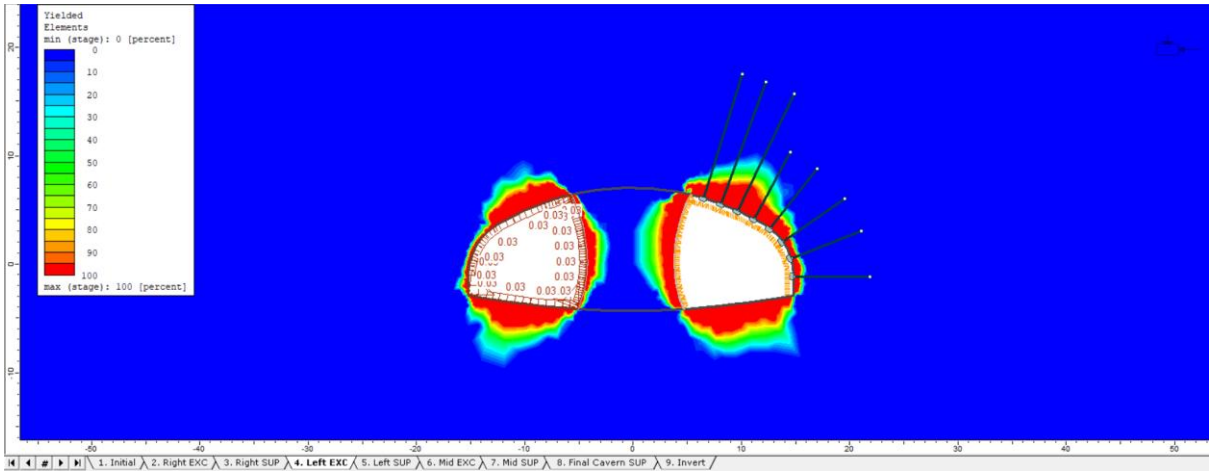

Figure 5-103. Yielded elements, Stage 4 - Model B, k=2

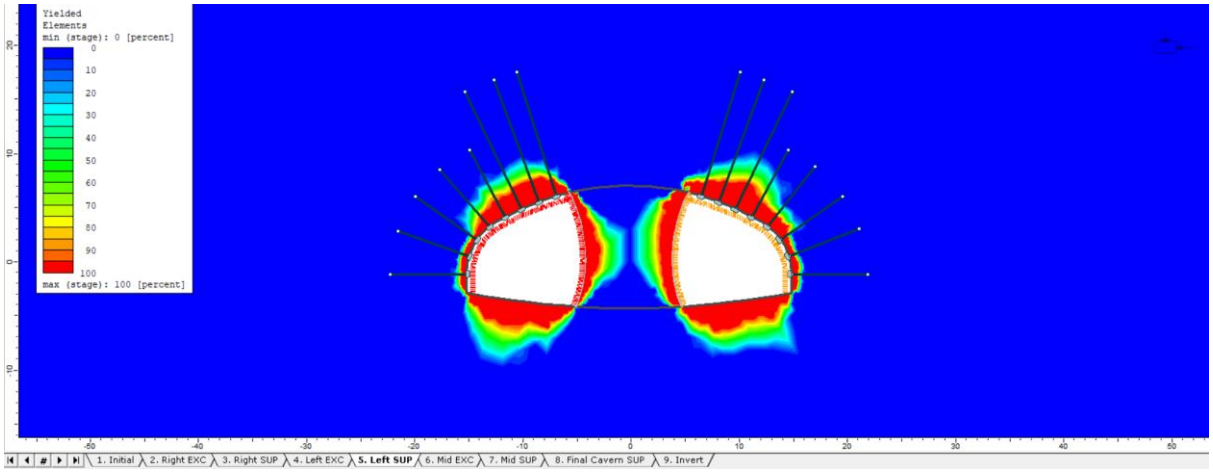

Figure 5-104. Yielded elements, Stage 5 - Model B, k=2

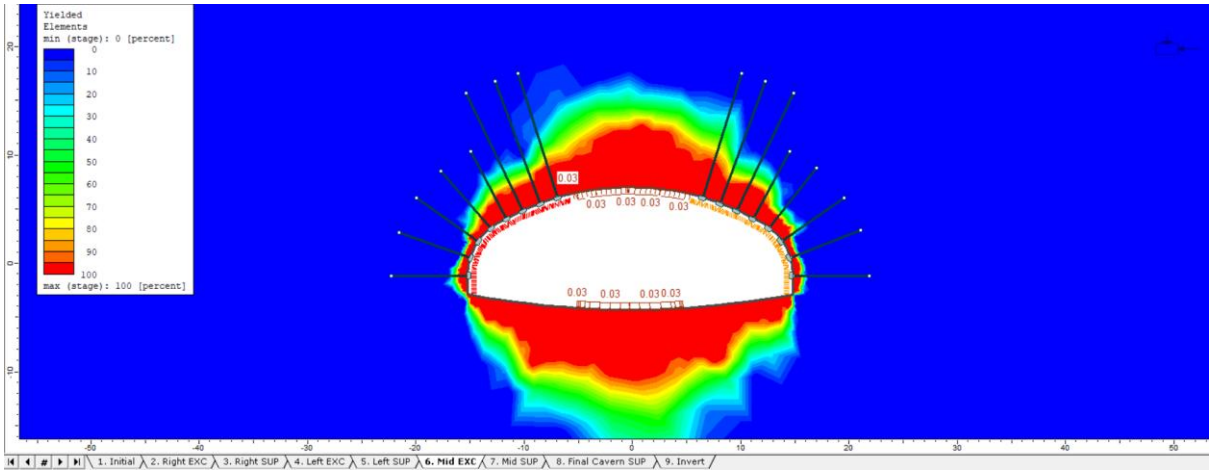

Figure 5-105. Yielded elements, Stage 6 - Model B, k=2

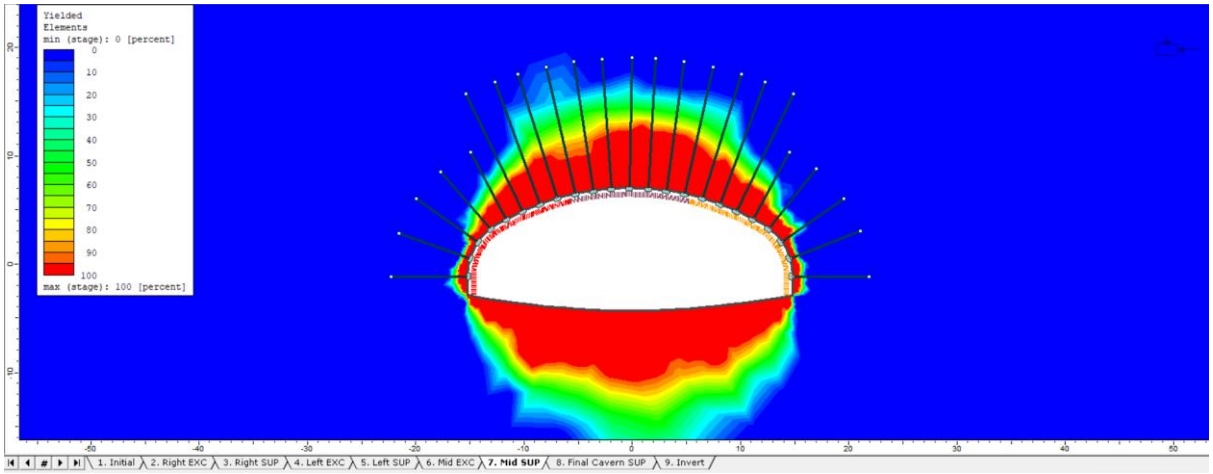

Figure 5-106. Yielded elements, Stage 7 - Model B, k=2

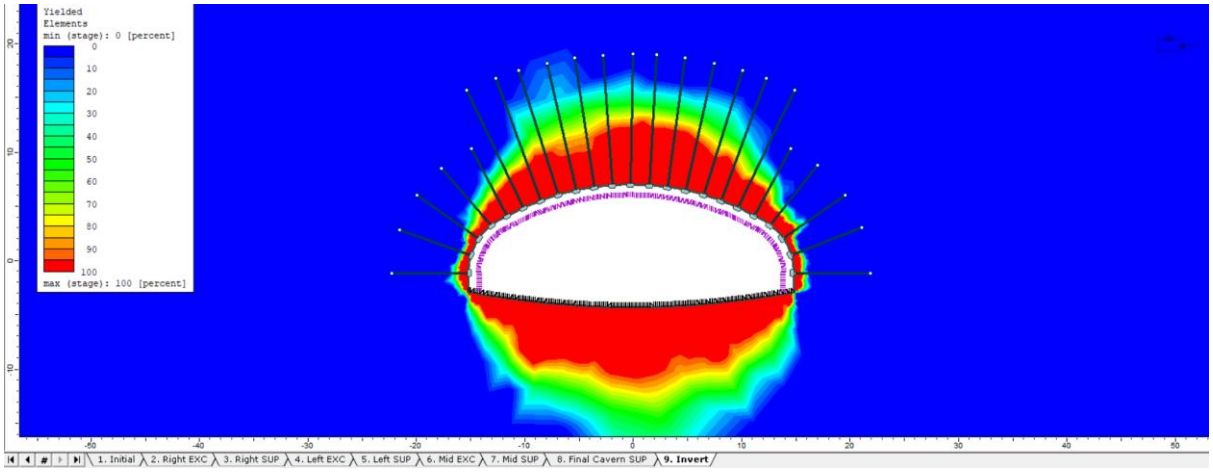

Figure 5-107. Yielded elements, Stage 8&9 - Model B, k=2

Most of the plastic points are concentrated on the center of the roof and reach almost a distance of 7 m.

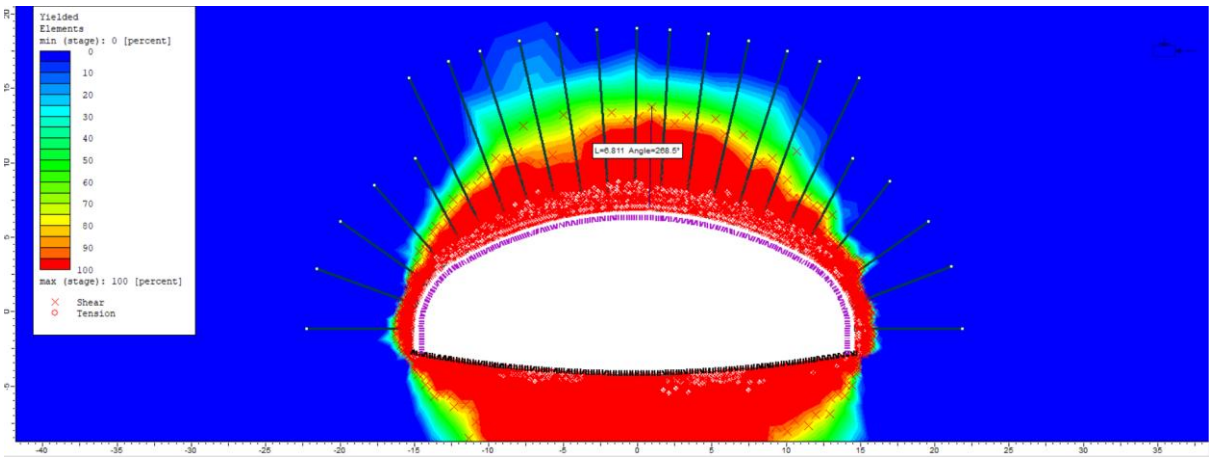

Figure 5-108. Plastic Points - Model B, k=2

5.2.3.3. *Axial Force on Rock Bolts*

Axial force acting on rock bolts reaches up to 0.2 MN.

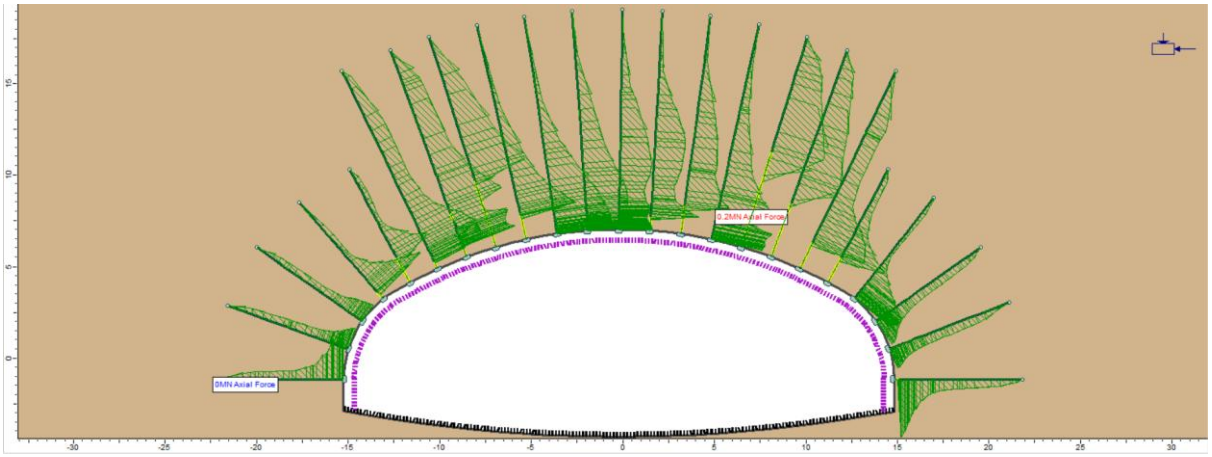

Figure 5-109. Axial Force on Rock bolts - Model B, k=2

5.2.3.4. *Axial Force and Bending Moment on RRS*

Highest value of axial force is 5.3 compressing RRS in walls. Tension points are placed in the corner which are neglected from the analysis. There is also bending moment with highest value of 0.08 MNm.

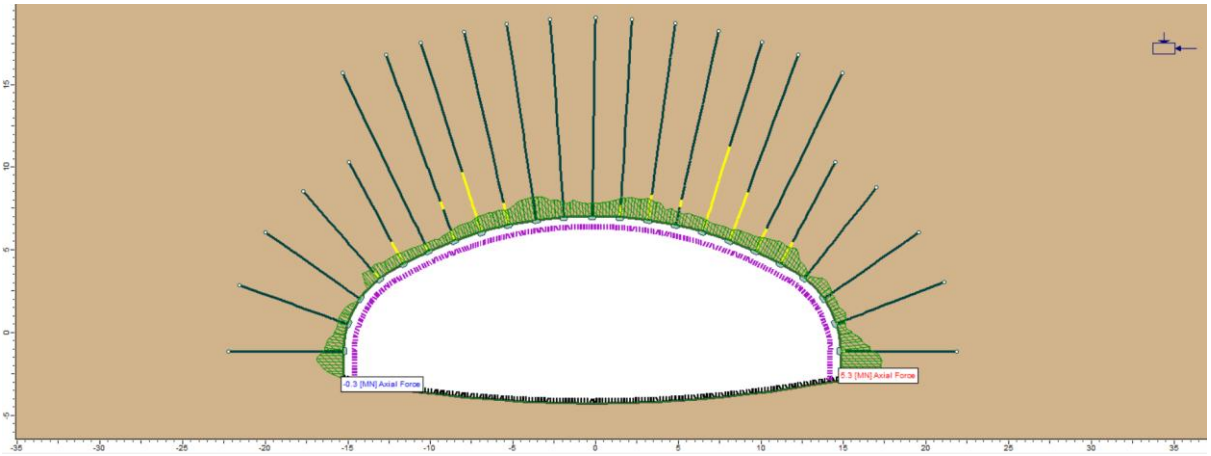

Figure 5-110. Axial Force on RRS - Model B, k=2

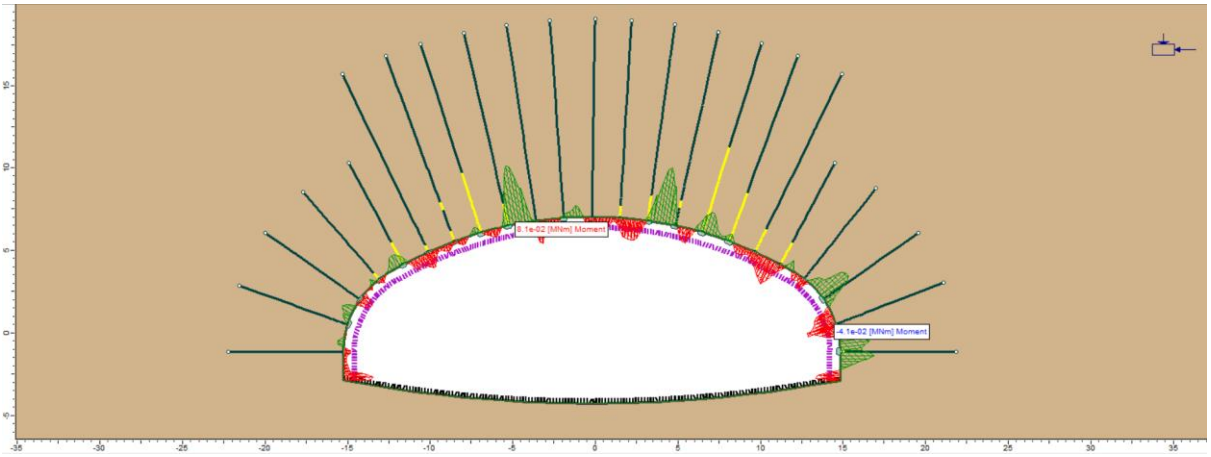

Figure 5-111.Bending moment on RRS - Model B, k=2

5.2.3.5. Support Capacity, Rock Bolts

12 bolts are yielded under tension forces near the excavation boundary.

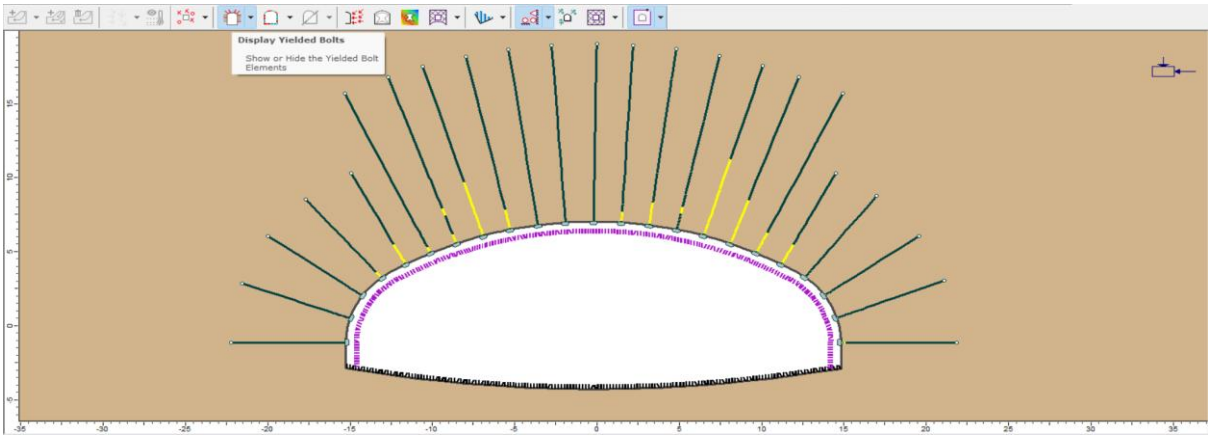

Figure 5-112. Displayed yielded bolts - Model B, k=2

5.2.3.6. Support Capacity, RRS

Following plots show the computation results of RRS capacity.

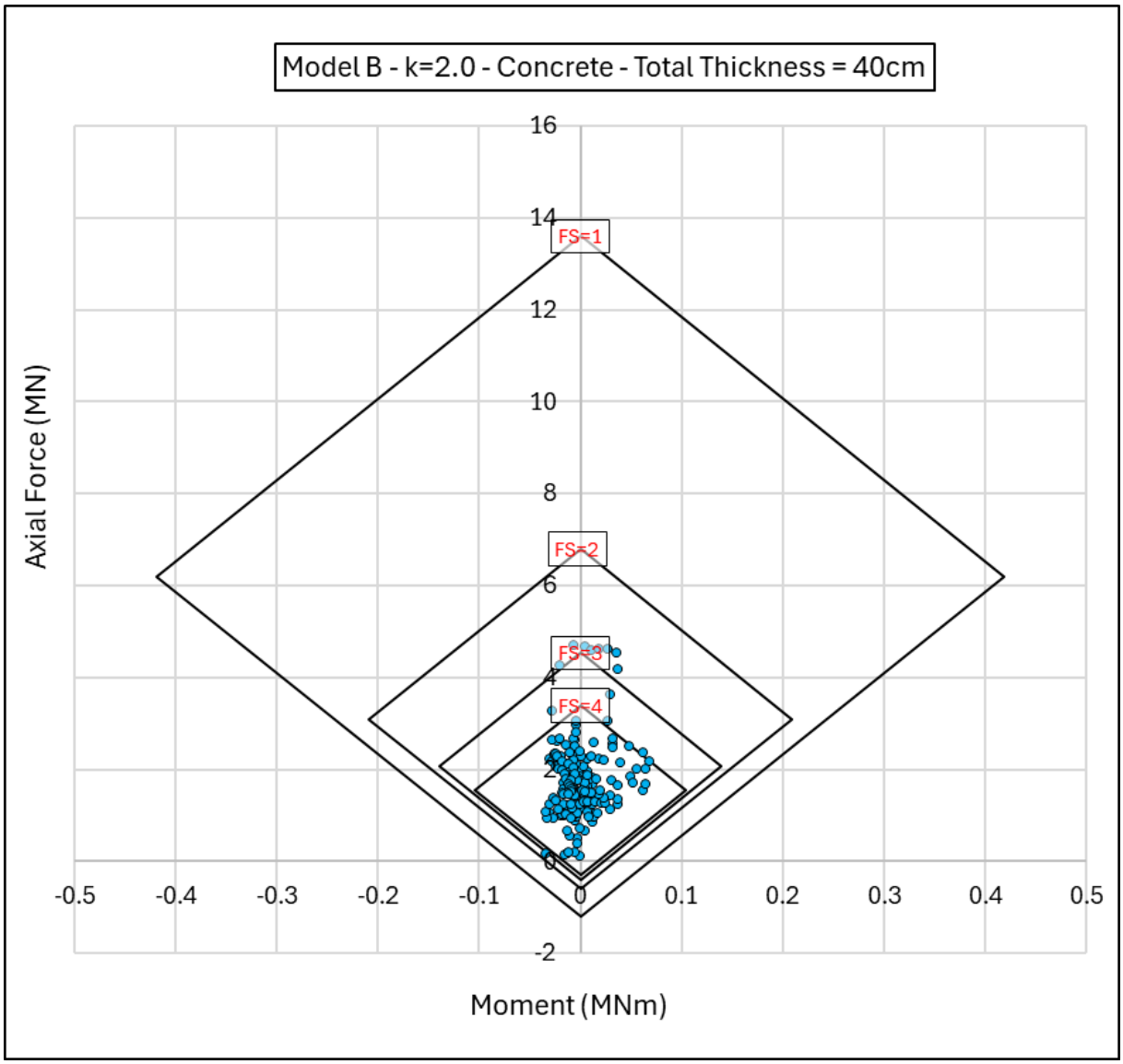

Figure 5-113. Axial Force-Moment plot of Concrete - Model B, k=2

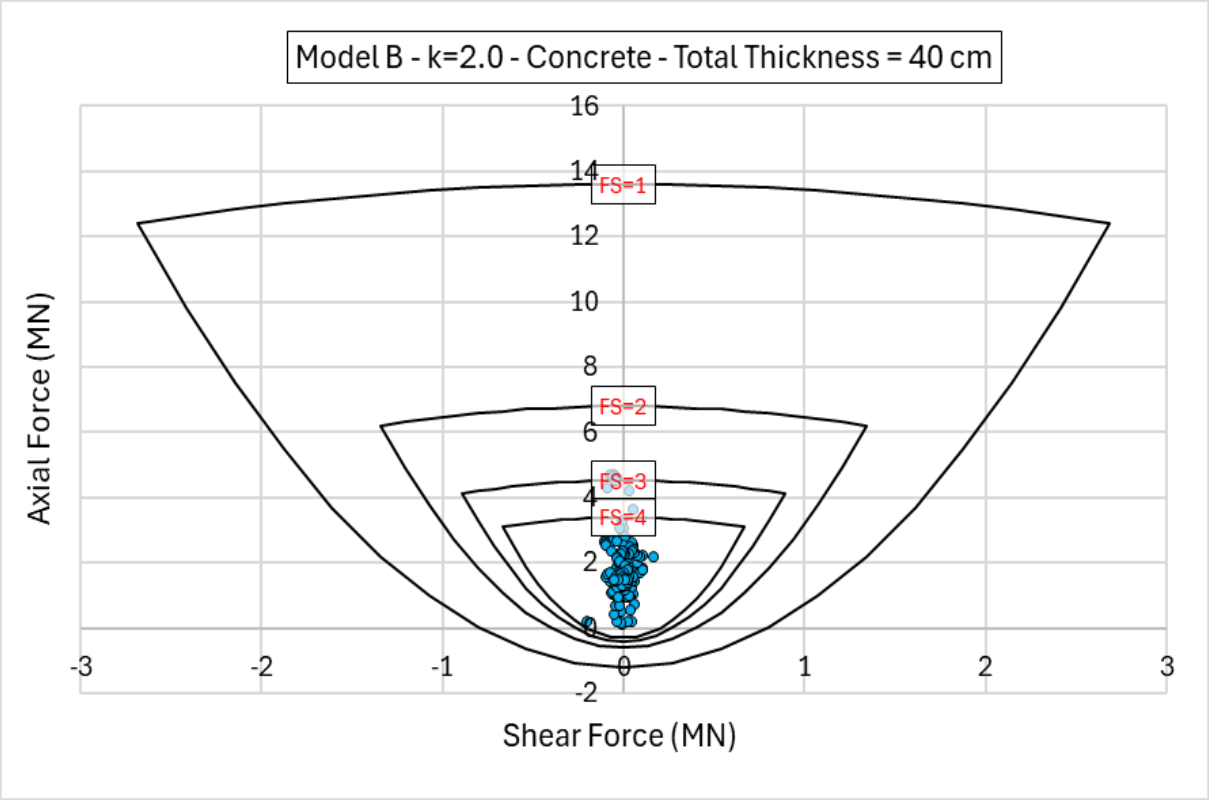

Figure 5-114. Axial Force-Shear Force plot of Concrete - Model B, k=2

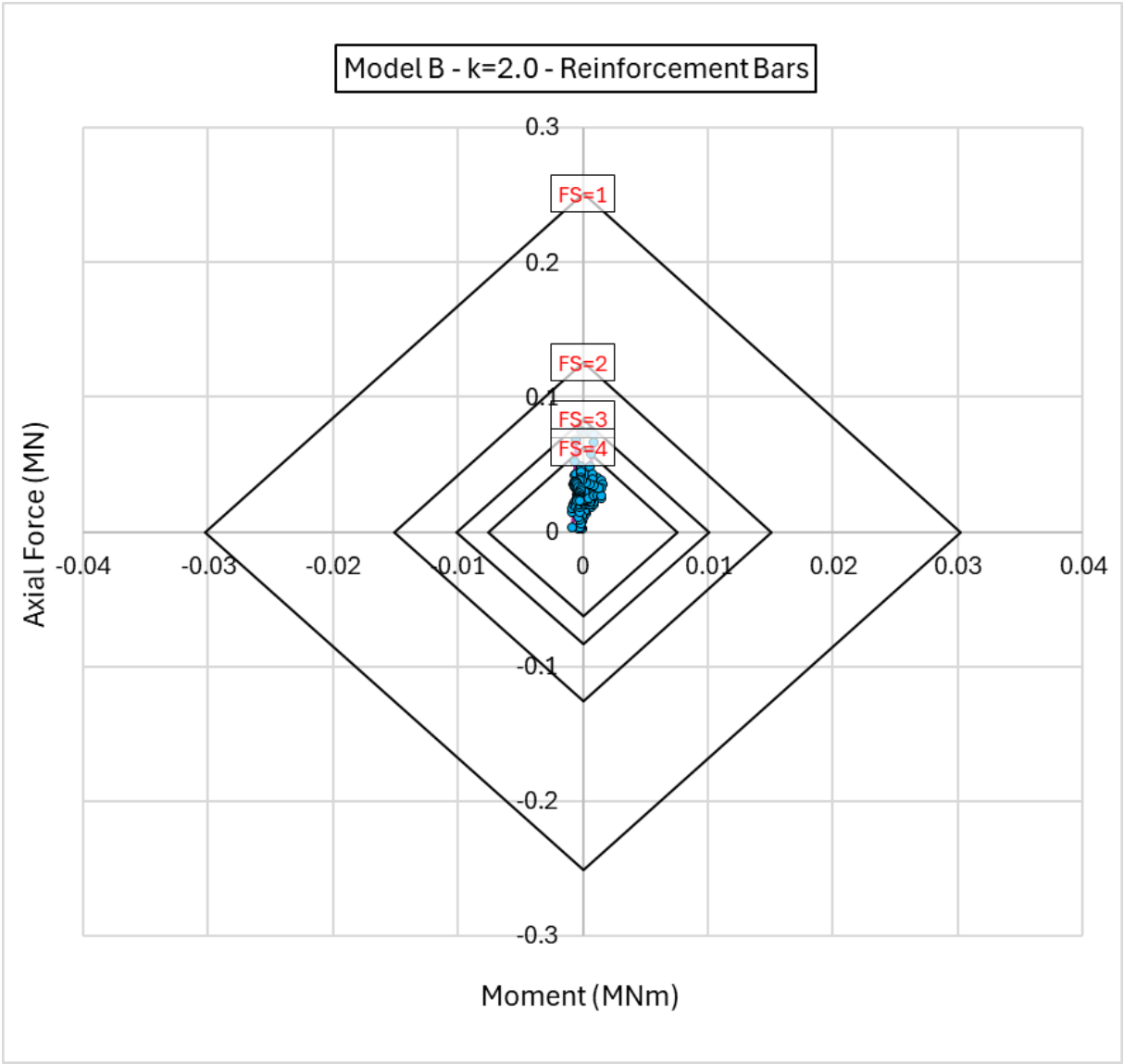

Figure 5-115. Axial Force-Moment plot of Steel Rebars - Model B, k=2

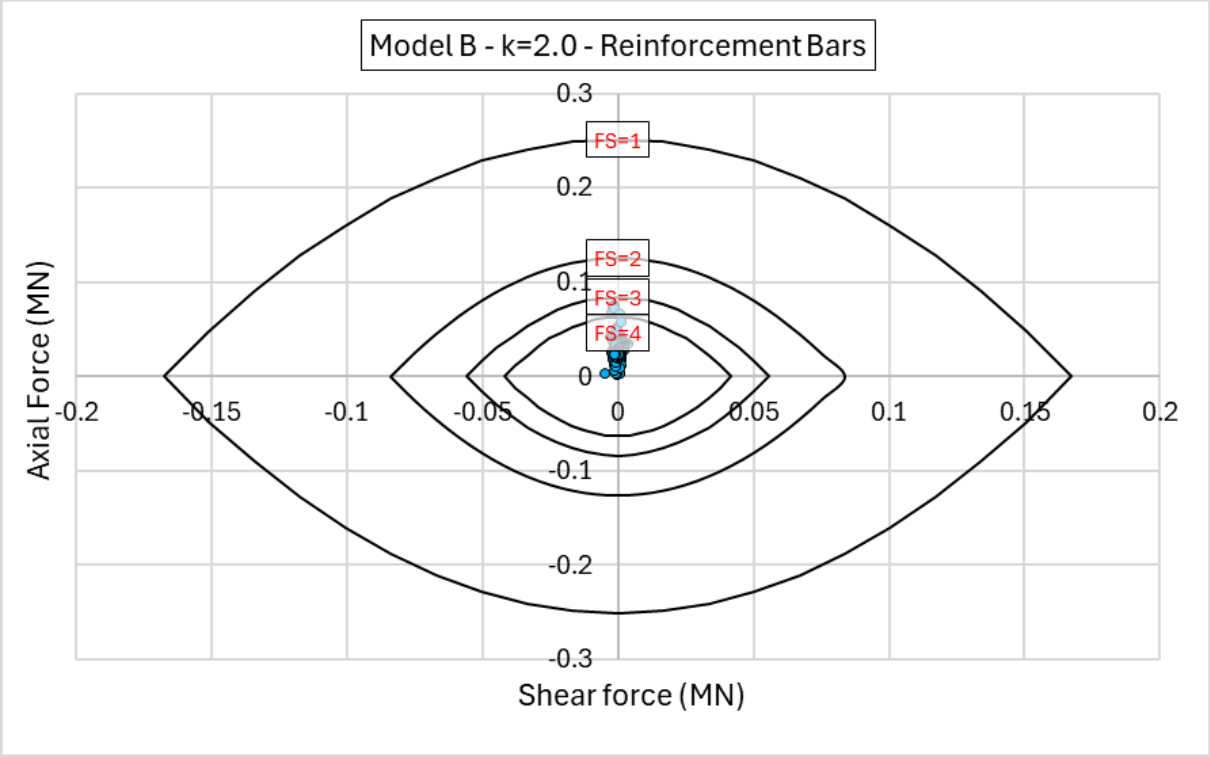

Figure 5-116. Axial Force-Shear Force on Steel Rebars - Model B, k=2

5.2.3.7. Summary of Results

Table 5-6 shows a summarized version of results.

Table 5-6. Summary of Results - Model B, k = 2

Model B – k = 2	
Maximum displacement at the walls [cm]	7.5
Maximum displacement at the roof [cm]	10
Maximum total displacement [cm]	11.2
Maximum radius measured for the plastic zone [m]	10.8
RRS properties	40 cm thickness c/c spacing 1.5 m
Maximum Compression on RRS [MN]	5.3
Maximum Tension on RRS [MN]	0
Min-Max Factor of Safety for RRS	Min: 2.7 Max: Higher than 4
Quantity of rock bolts and their lengths [m]	23 Rock Bolts 13 Rock Bolts 12 m 10 Rock Bolts 7 m
Rock bolt tributary area [mm^2]	207
Maximum axial force on rock bolts [MN]	0.2
Number of Yielded bolts and their location	12 rock bolts (Along the crown)
Rock Bolt Deformation [cm]	7.8

In summary, plastic zones progressively expand around each excavation step concentrated on the crown of the excavation boundaries until the last stage that reaches 10.8 m far from the cavern.

Rock bolts on the sidewalls are 7 m, and have 12 m of length in the roof; Their endpoint is in the elastic zone; twelve bolts are yielded with maximum deformation of 7.8 cm.

RRS liners are generally compressed with highest axial force of 5.3 MN; it can be declared that there is no tension acting on the RRS except very few points in the corner that are neglected.

Support capacity plots for concrete show best performance with lowest safety factor of 2.7 and mostly higher than 4.

5.3. Model C (TBH)

This section will present the results of computation of Model C with different stress ratios.

5.3.1. Model C – k = 0.5

Important parameters that were indicated in the previous models will be also presented for Model C.

5.3.1.1. Total Displacement

Displacement is almost equally concentrated on the center of roof and invert with highest amount of 8.5 cm. Deformation vectors are mostly vertically directed to the center of cavern except in the walls that follow an escaping way from center directed outside of the cavern.

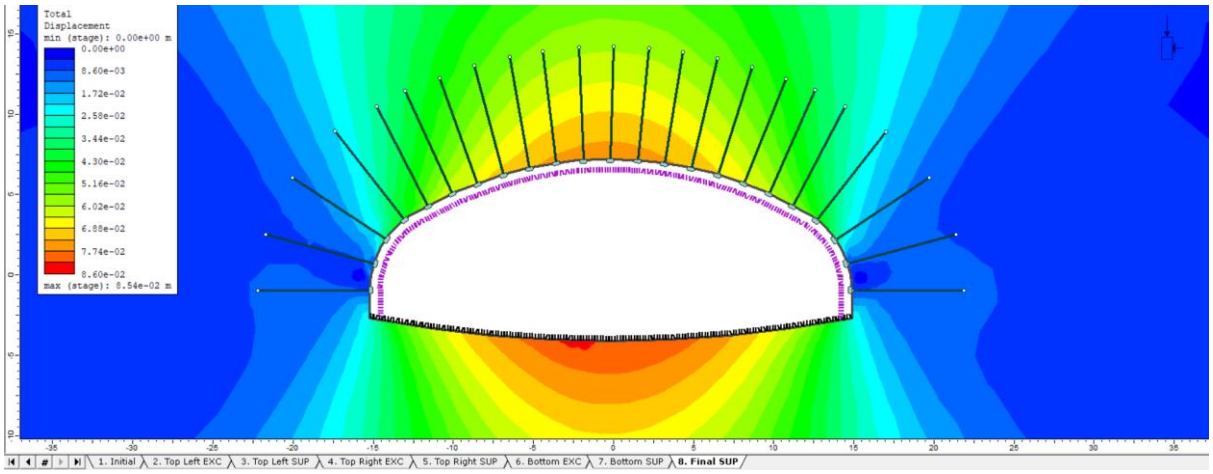

Figure 5-117. Total Displacement - Model C, k=0.5

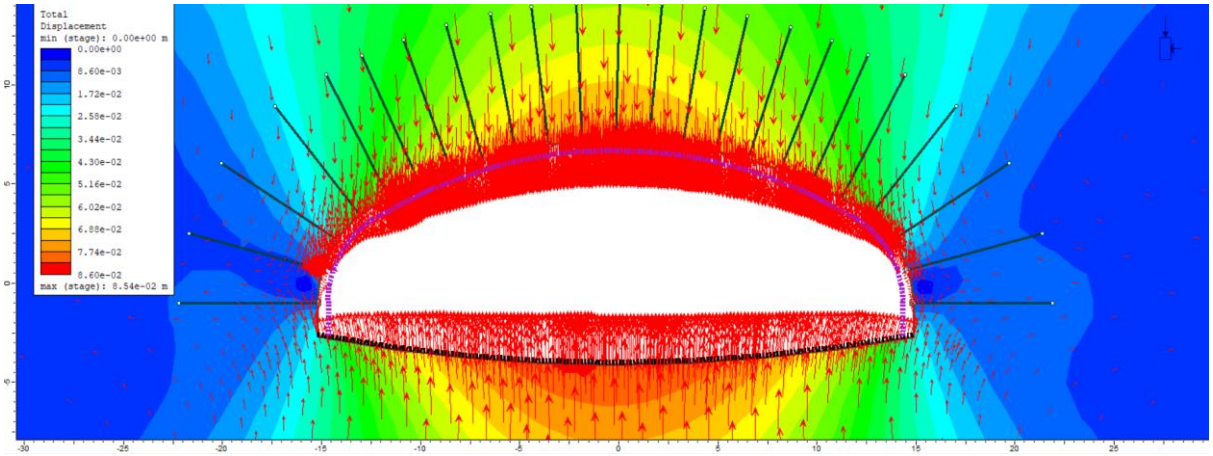

Figure 5-118. Deformation vectors and direction - Model C, k=0.5

5.3.1.2. Plastic Radius around the cavern

Maximum plastic radius reaches up to 5 m around the cavern; following pictures indicate progress of plastic radius around the cavern in each step.

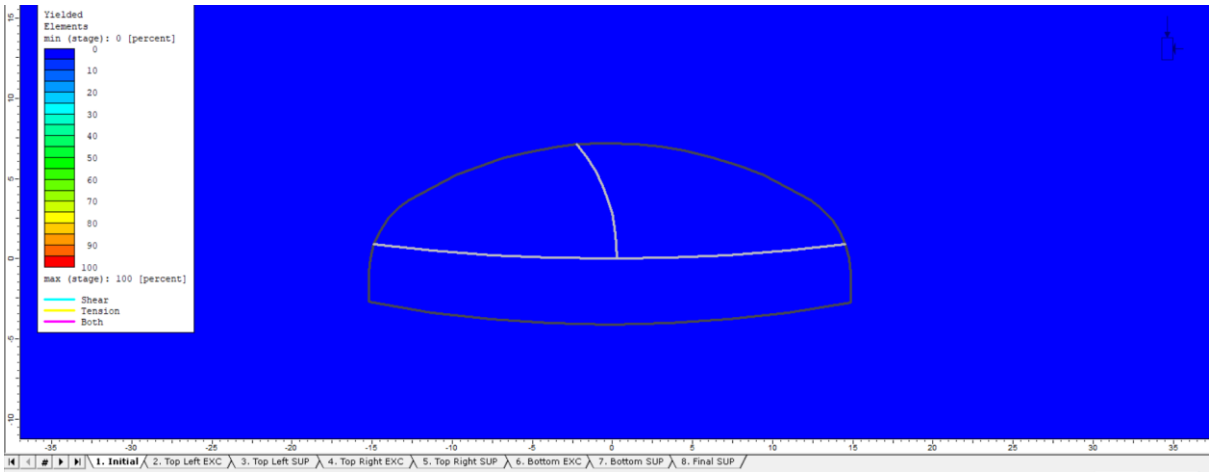

Figure 5-119. Yielded elements, Stage 1 - Model C, k=0.5

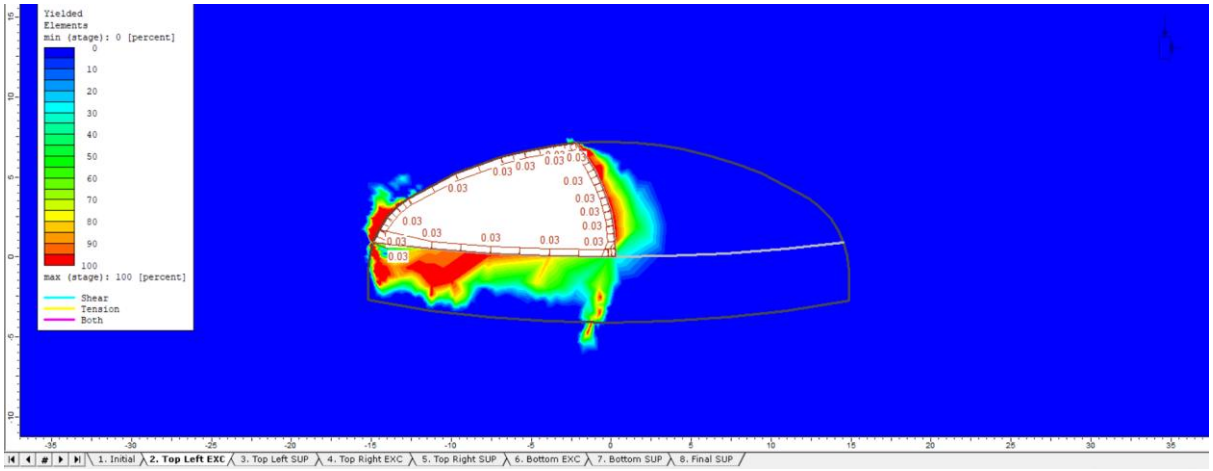

Figure 5-120. Yielded elements, Stage 2 - Model C, k=0.5

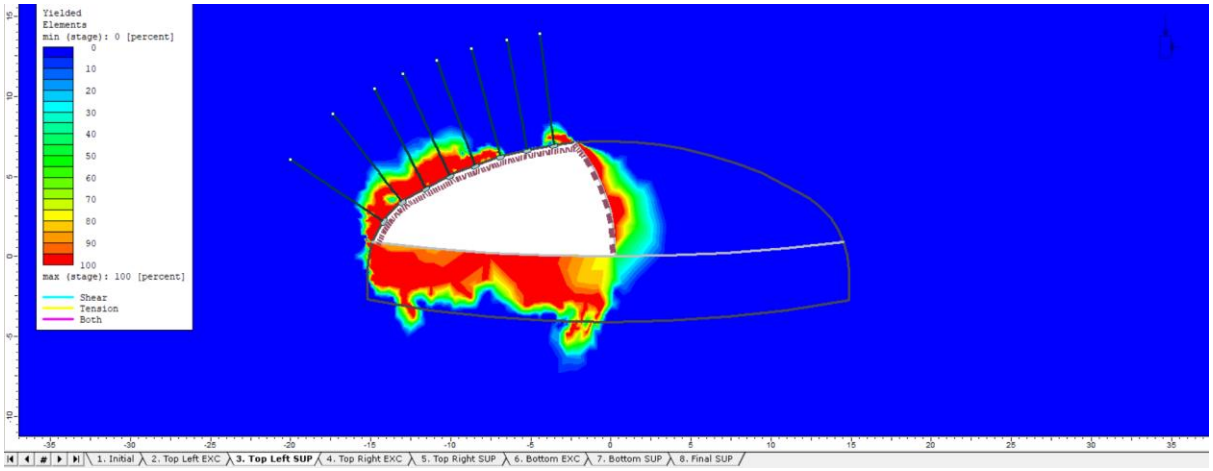

Figure 5-121. Yielded elements, Stage 3 - Model C, k=0.5

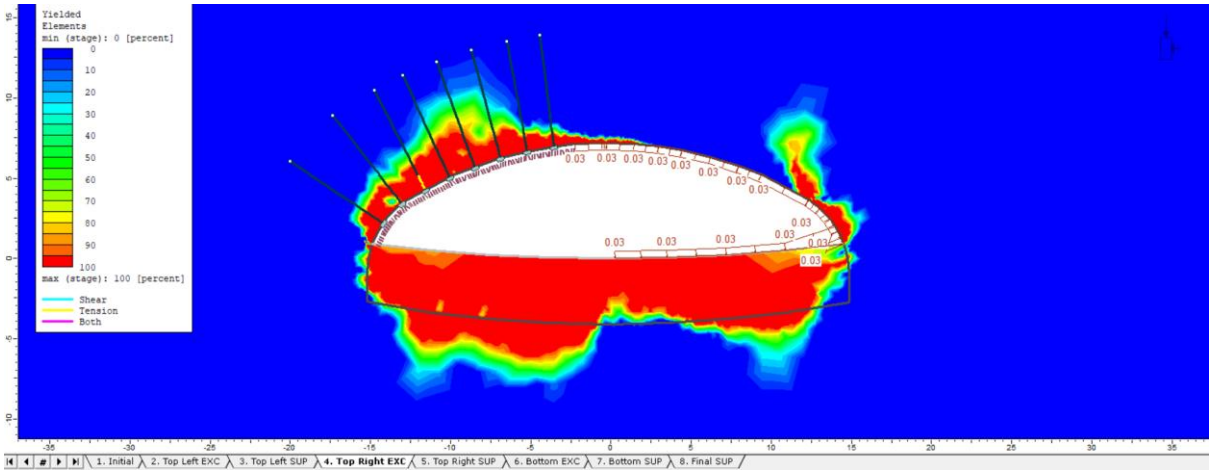

Figure 5-122. Yielded elements, Stage 4 - Model C, k=0.5

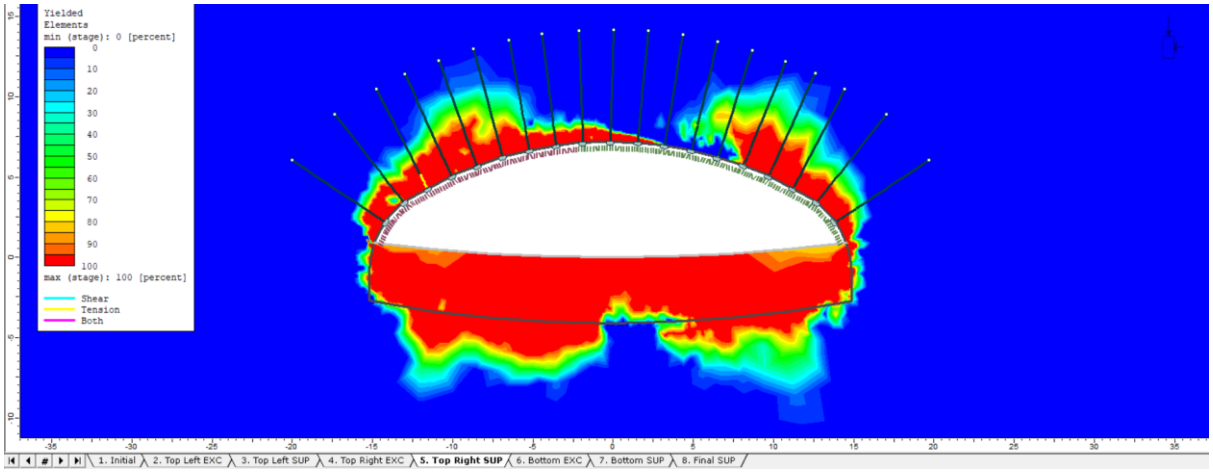

Figure 5-123. Yielded elements, Stage 5 - Model C, k=0.5

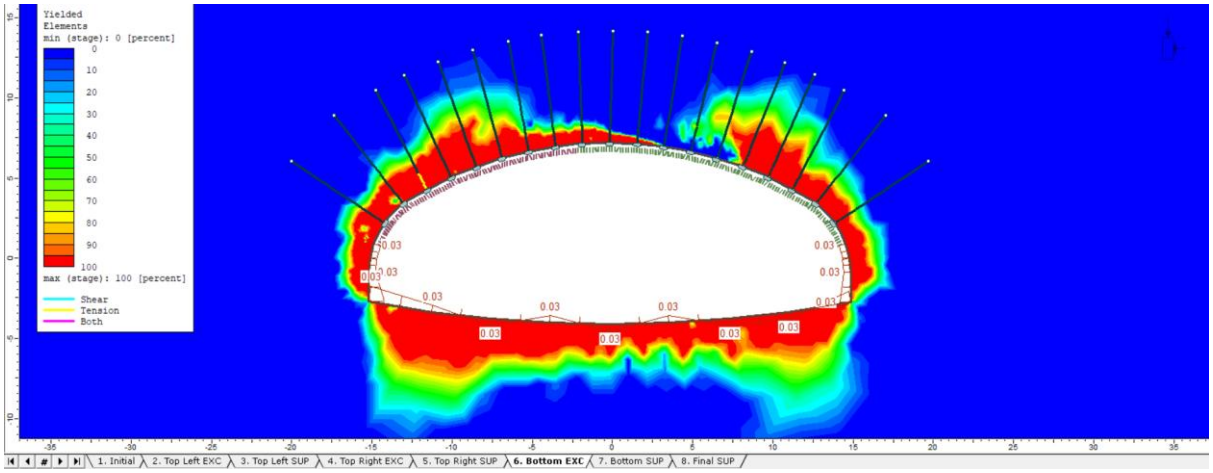

Figure 5-124. Yielded elements, Stage 6 - Model C, k=0.5

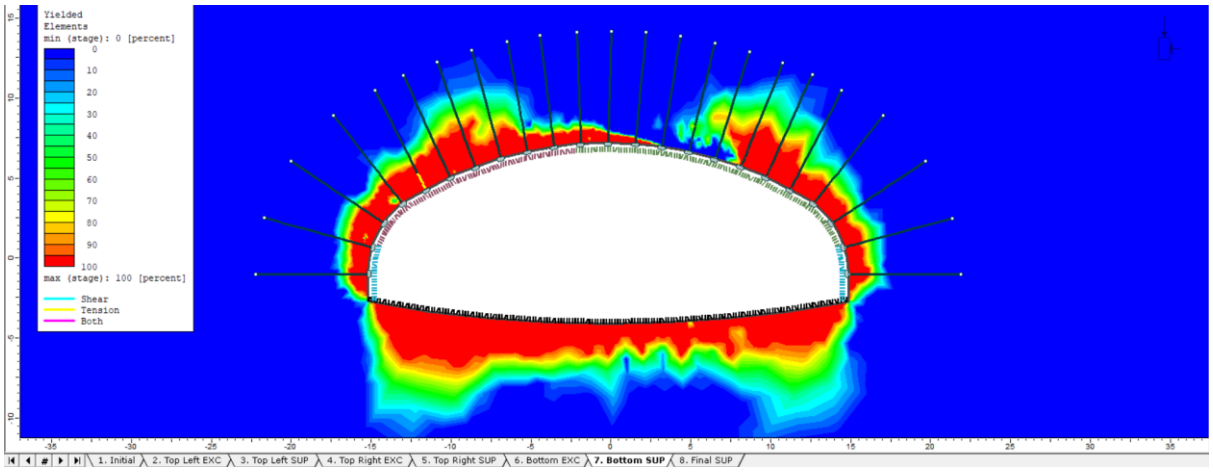

Figure 5-125. Yielded elements, Stage 7 - Model C, k=0.5

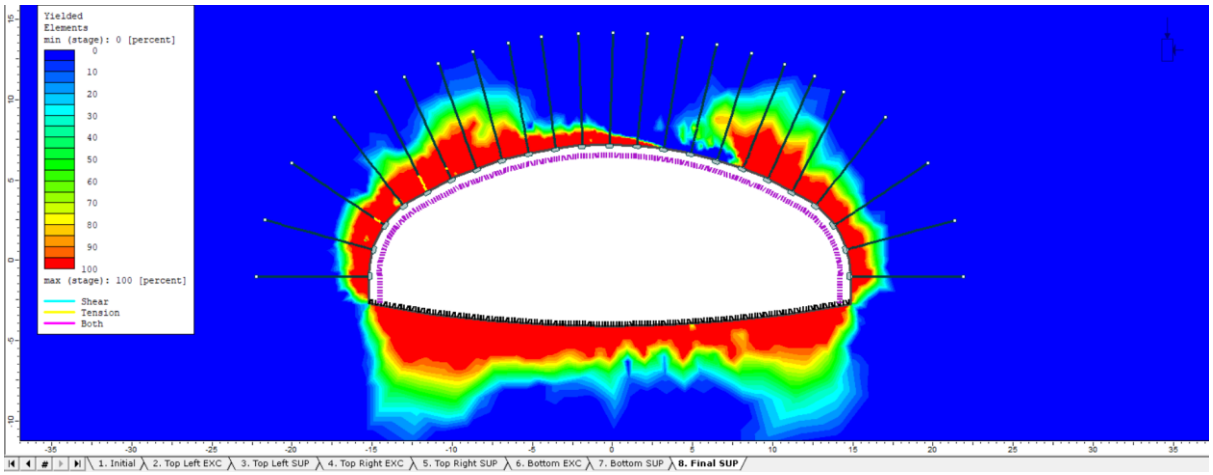

Figure 5-126. Yielded elements, Stage 8 - Model C, k=0.5

Plastic points around the cavern are illustrated in following figure; Most distant point is 4.5 m far from the cavern boundary.

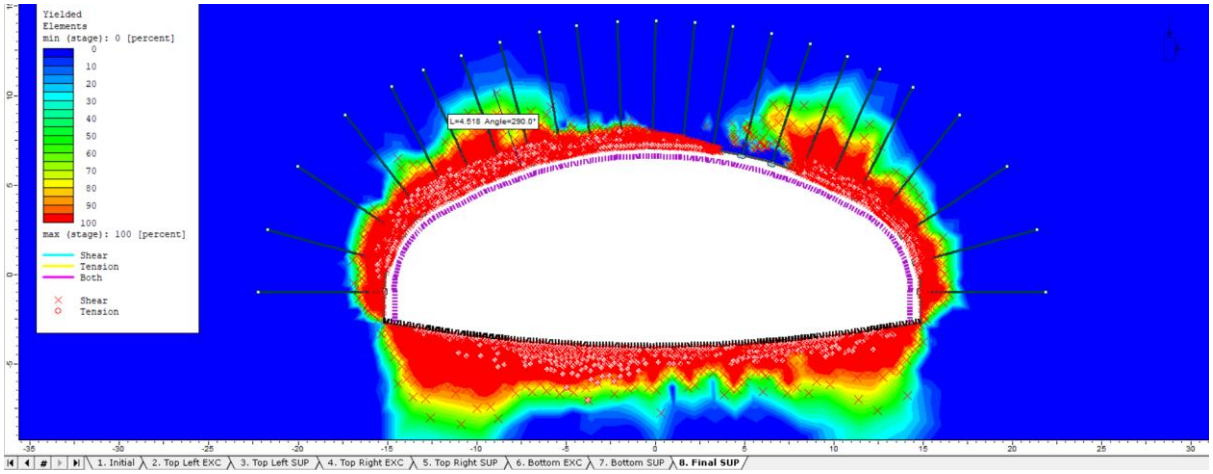

Figure 5-127. Plastic Points - Model C, k=0.5

5.3.1.3. Axial Force on Rockbolts

Highest axial force acting on the rock bolts is 0.2 MN (Figure 5-128).

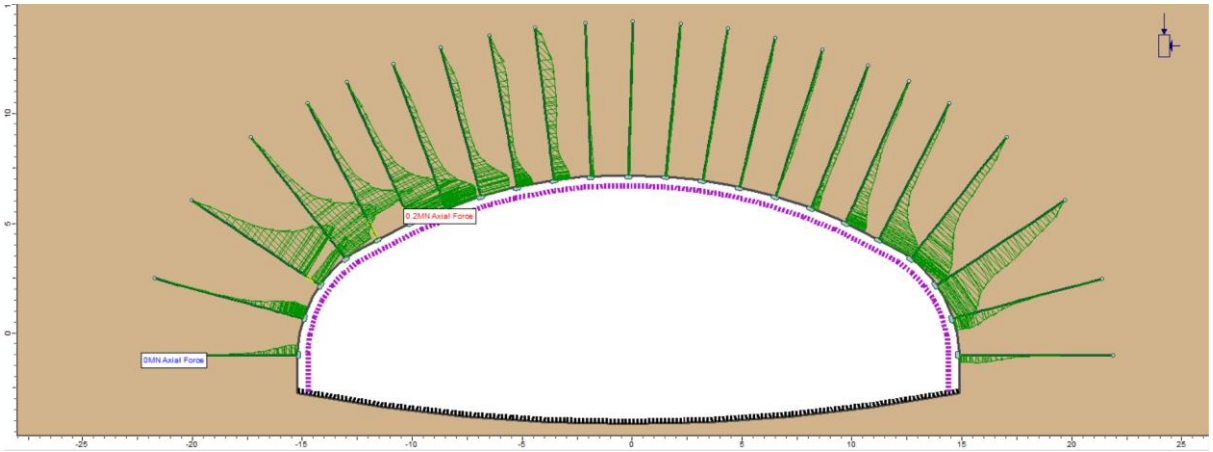

Figure 5-128. Axial Force on Rock Bolts - Model C, k=0.5

5.3.1.4. Axial Force and Bending Moment on RRS

Highest axial force acting on the RRS is concentrated in the walls and reaches up to 1.7 MN; Also, there are tension forces on the roof lower than 0.4 MN.

Bending Moment at its highest value reaches 0.04 MNm.

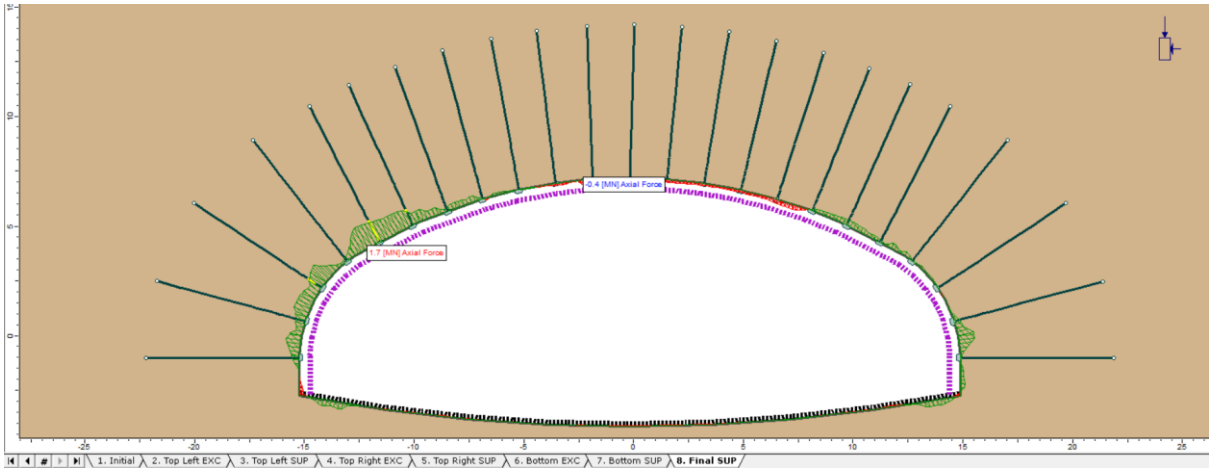

Figure 5-129. Axial Force on RRS - Model C, k=0.5

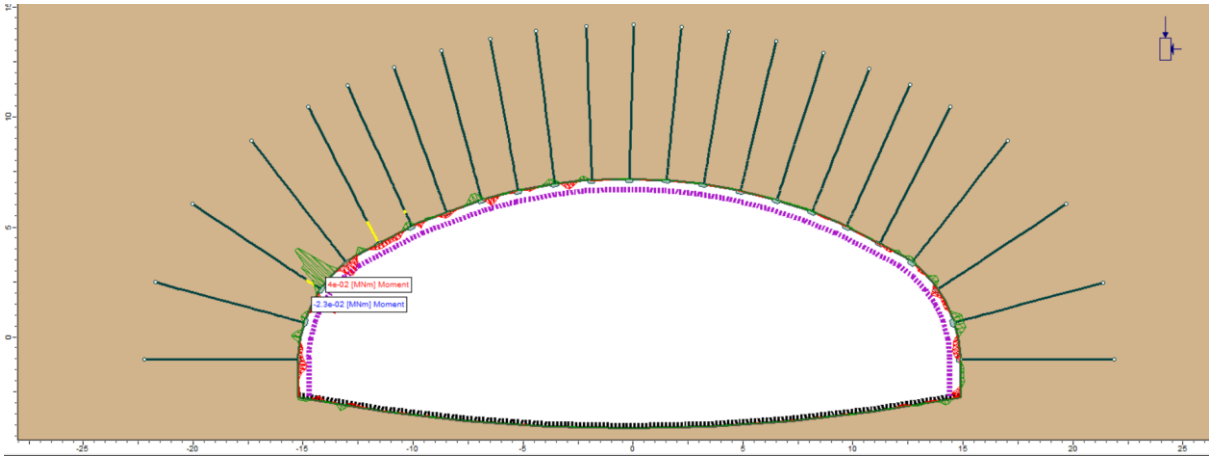

Figure 5-130. Bending Moment on RRS - Model C, k=0.5

5.3.1.5. Support Capacity, Rockbolts

Three rock bolts are yielded under tension on the left side of the crown.

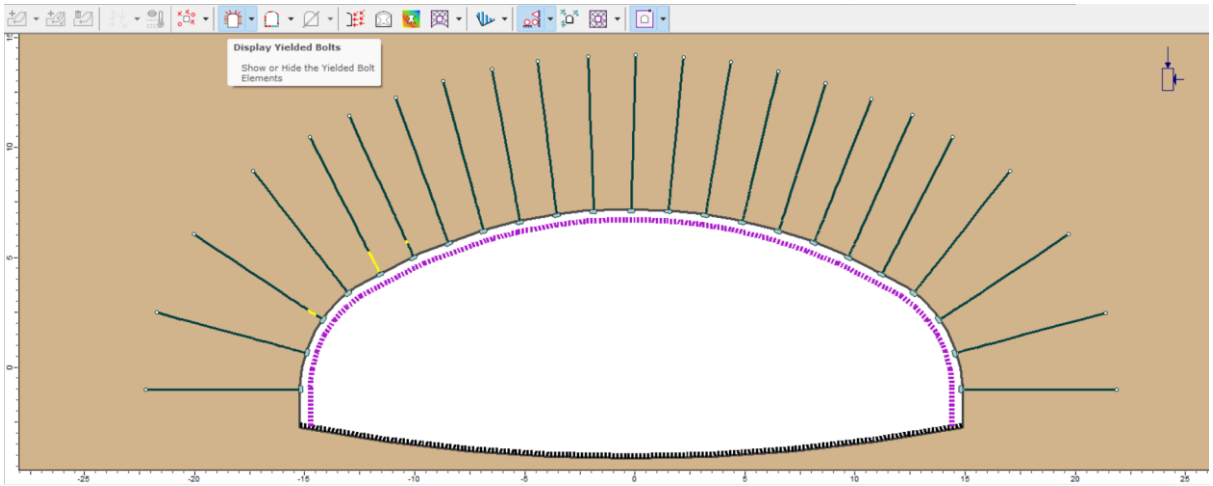

Figure 5-131. Displayed yielded bolts - Model C, k=0.5

5.3.1.6. Support Capacity, RRS

Following plots indicate the support capacity of Concrete and Rebars in the RRS.

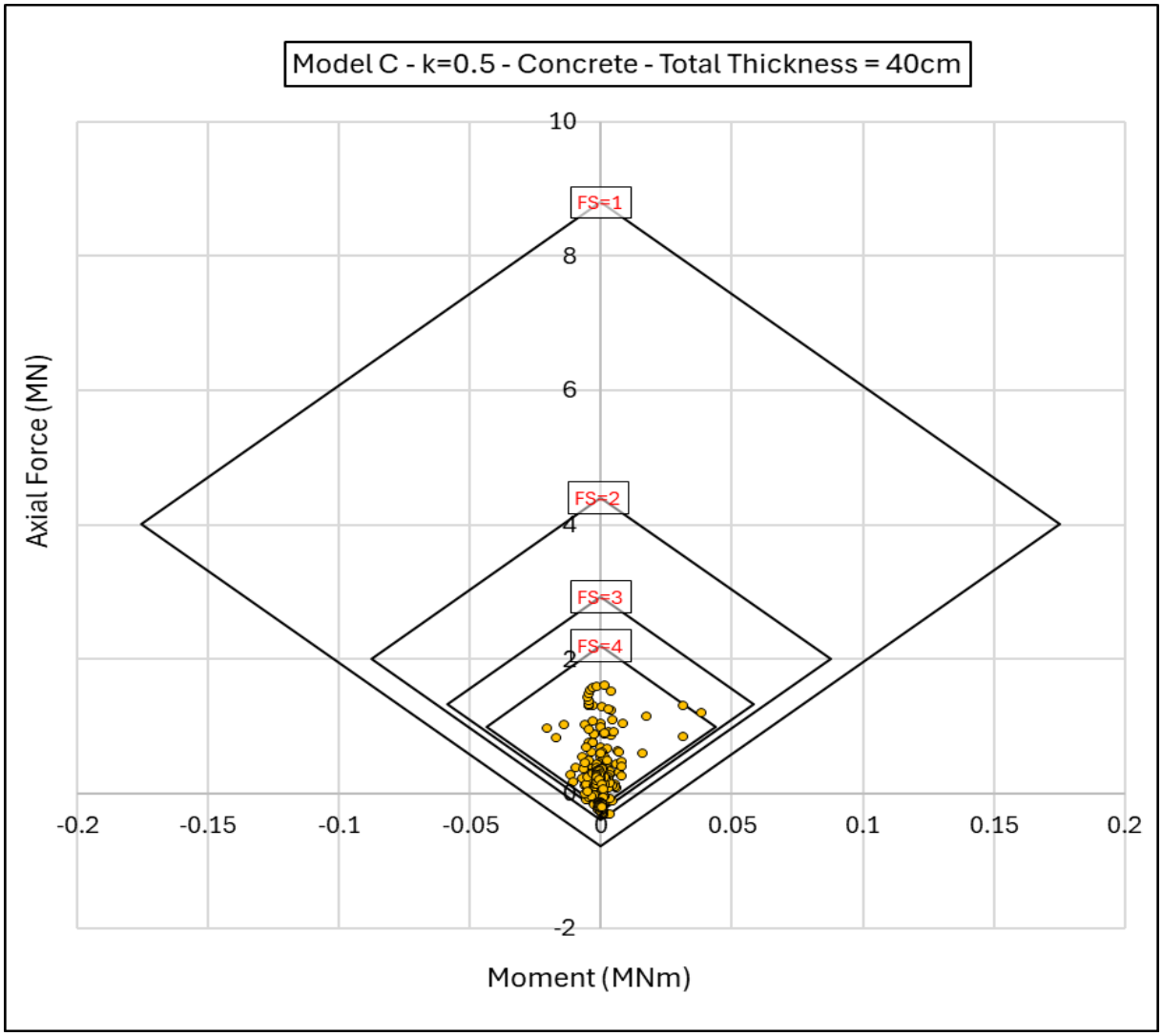

Figure 5-132. Axial Force-Moment plot of Concrete - Model C, k=0.5

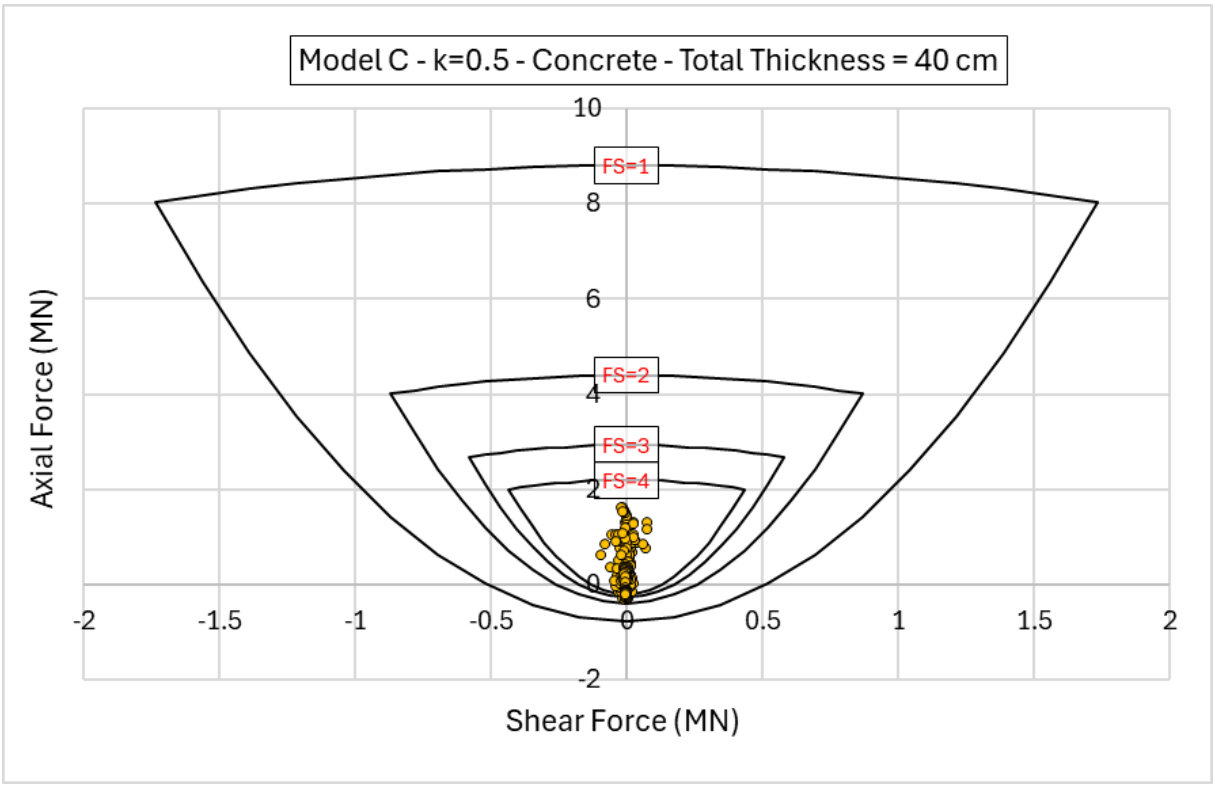

Figure 5-133. Axial Force-Shear Force plot of the Concrete - Model C, k=0.5

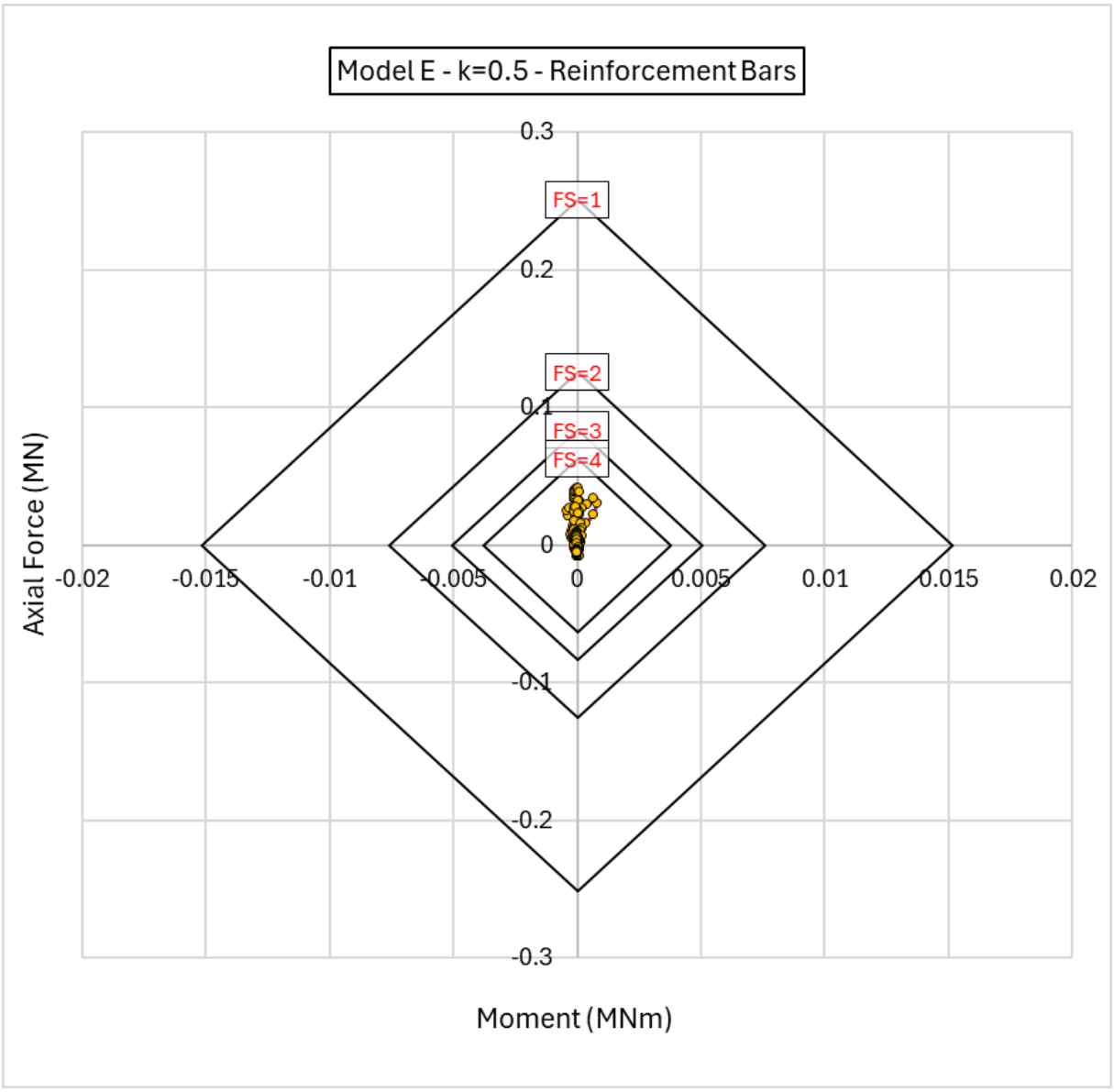

Figure 5-134. Axial Force-Moment plot of Steel rebars - Model C, k=0.5

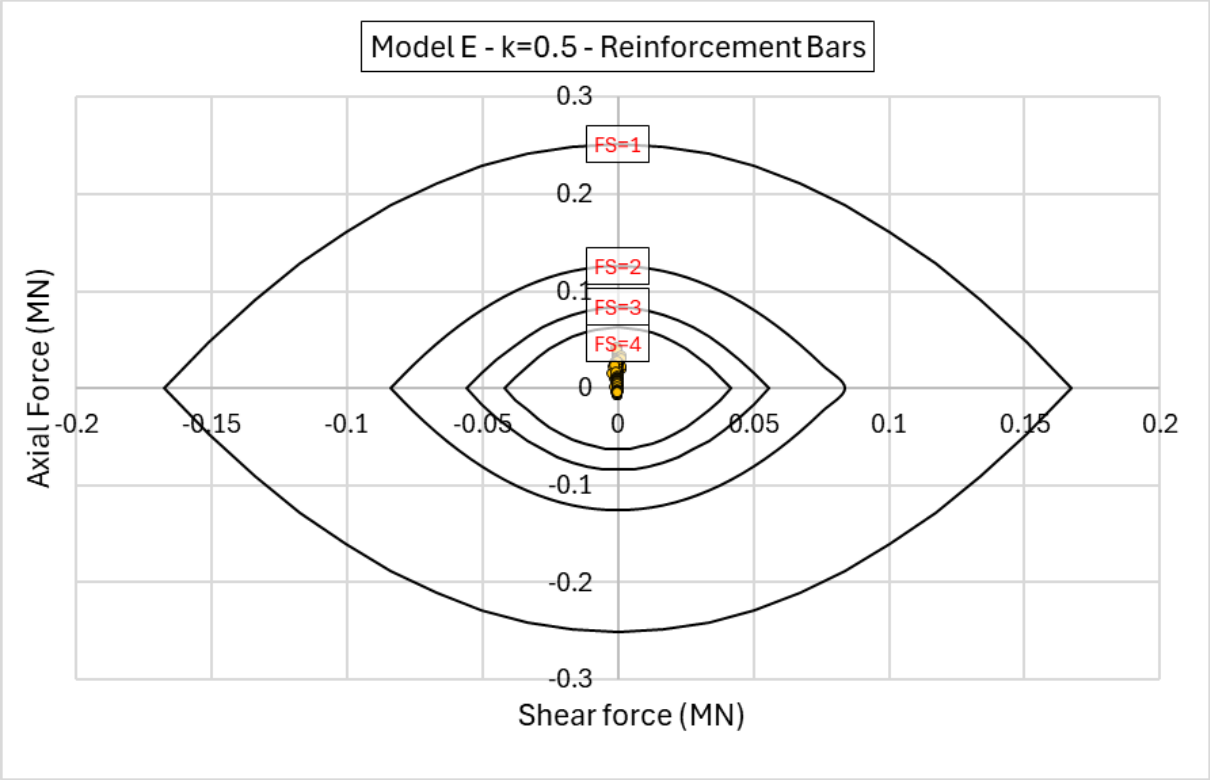

Figure 5-135. Axial Force-Shear Force plot of Steel rebars - Model C, k=0.5

5.3.1.7. Summary of Results

As we provided a summary for previous models, we provide summaries for Model C.

Table 5-7. Summary of Results - Model C, k = 0.5

Model C – k = 0.5	
Maximum displacement at the walls [cm]	5
Maximum displacement at the roof [cm]	7.5
Maximum total displacement [cm]	8.5
Maximum radius measured for the plastic zone [m]	5
RRS properties	40 cm thickness c/c spacing 4.5 m
Maximum Compression on RRS [MN]	1.7
Maximum Tension on RRS [MN]	0.4
Min-Max Factor of Safety for RRS	Min: 1.9 Max: Higher than 4
Quantity of rock bolts and their lengths [m]	23 Rock Bolts 7 m
Rock bolt tributary area [mm^2]	207
Maximum axial force on rock bolts [MN]	0.2
Number of Yielded bolts and their location	2 (left wall)
Rock Bolt Deformation [cm]	4.5

In summary, plastic zone is progressively increased around each excavation step in a balanced way until the last stage reaches 5.5 m far from the excavation borders.

Rock bolts are 7m and their endpoint in the elastic zone; Two of them are yielded and they have maximum deformation of 4.5 cm.

RRS liners are being compressed on the walls and partially on the roof with highest axial force of 1.7 MN. RRS in the roof is under a very limited amount of tension that reaches 0.4 MN of axial force.

Support capacity plots for concrete show a favorable performance with lowest safety factor of 1.9; Majority of the points have amount of safety factor significantly higher than 4.

5.3.2. Model C – k = 1

Achieved results of computation of Model C under hydrostatic pressure conditions are presented in this section.

5.3.2.1. Total Displacement

8.08 cm of displacement happens in the roof and the cavern; Deformations are almost vertically

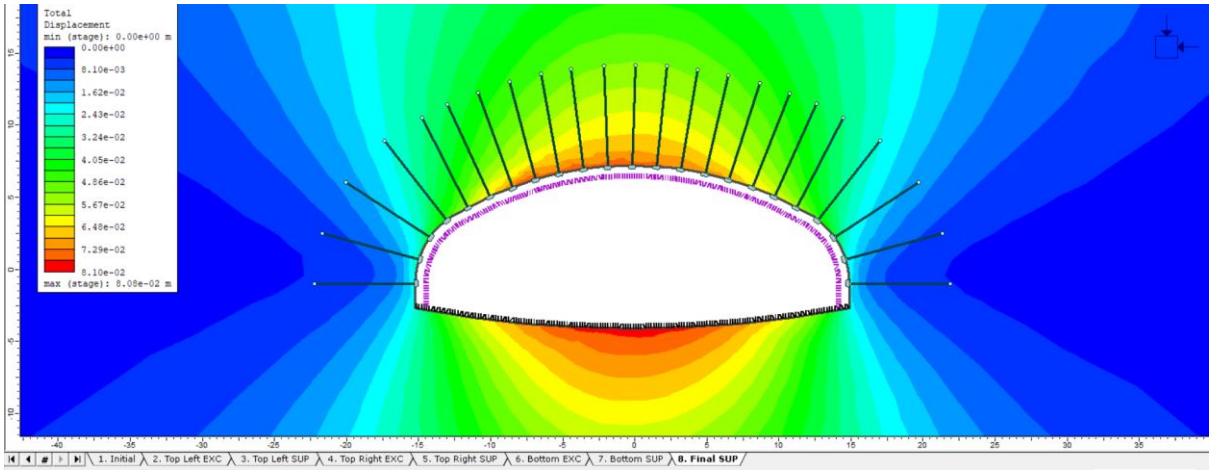

Figure 5-136. Total Displacement - Model C, k=1

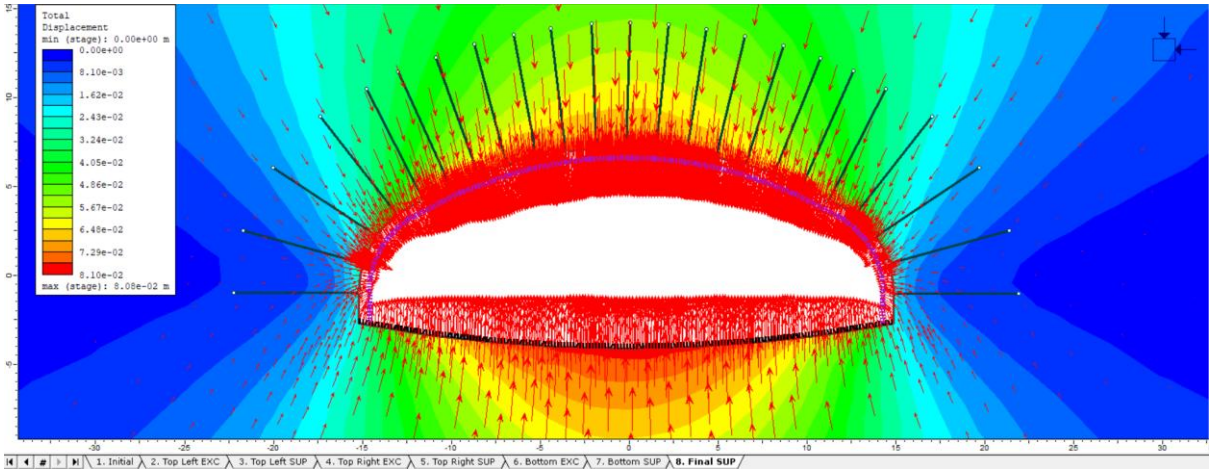

Figure 5-137. Deformation Vectors - Model C, k=1

5.3.2.2. Plastic Radius around the cavern

Plastic radius reaches up to 4.5 m up to the roof of the cavern in the final stage (Figure 5-138).

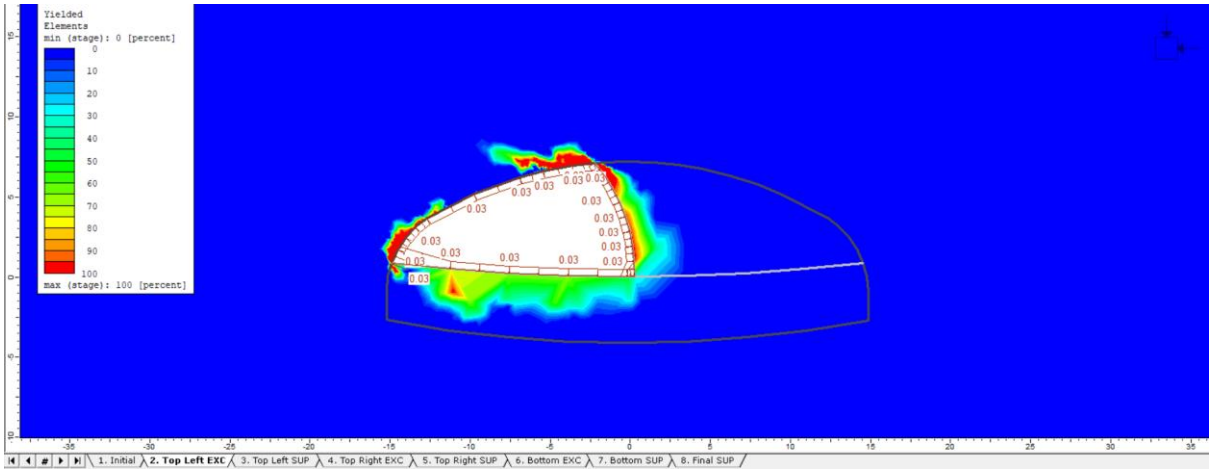

Figure 5-138.Yielded elements, Stage 2 - Model C, k=1

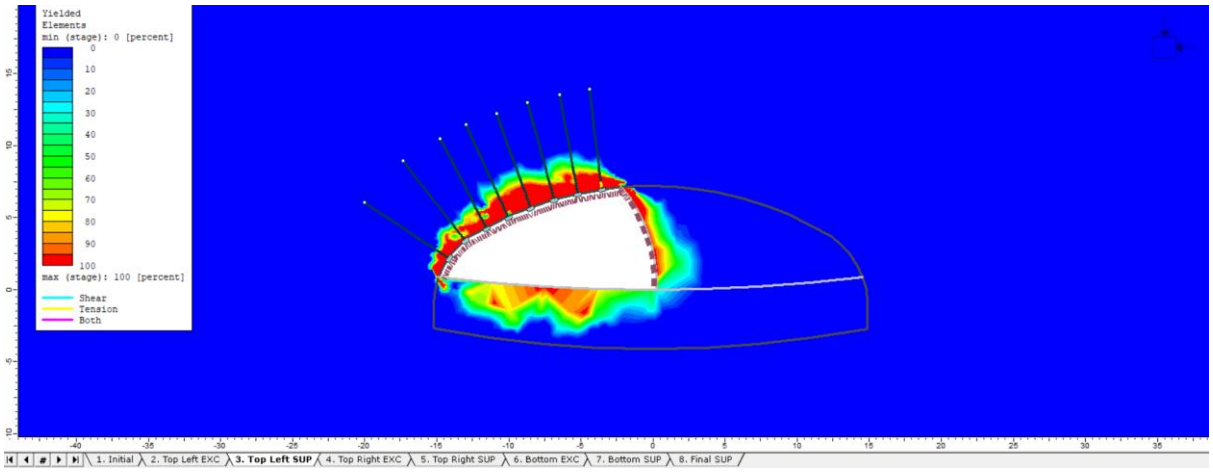

Figure 5-139. Yielded elements, Stage 3 - Model C, k=1

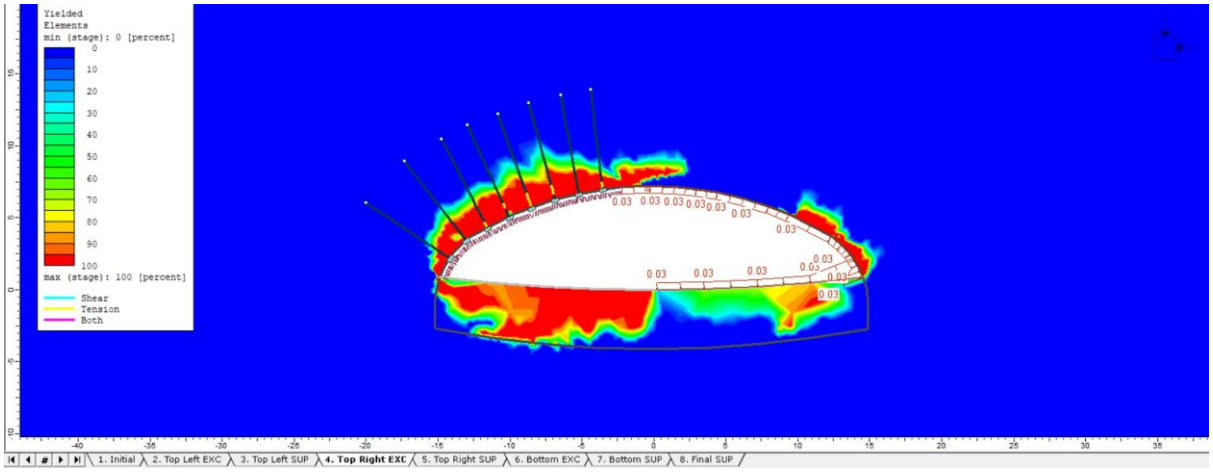

Figure 5-140. Yielded elements, Stage 4 - Model C, k=1

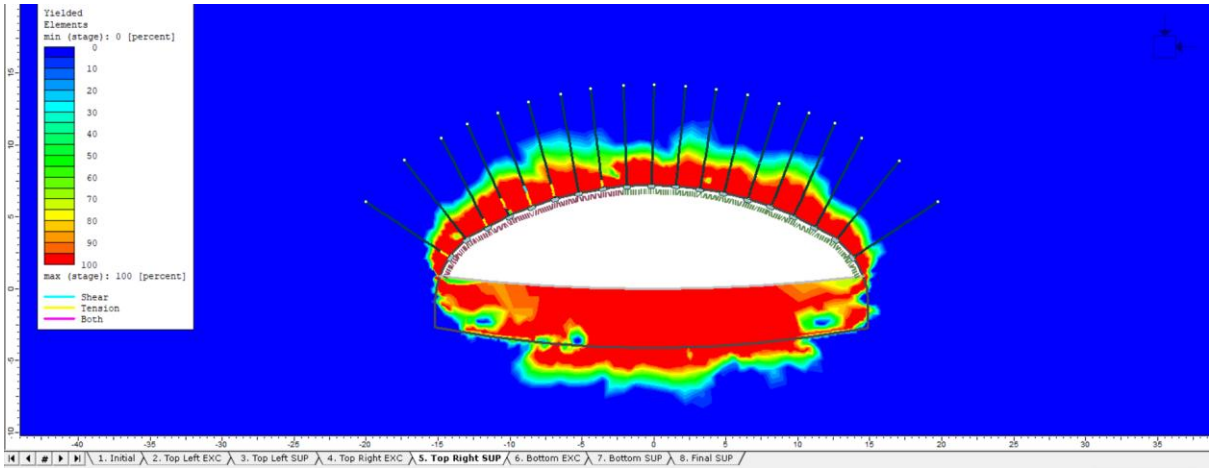

Figure 5-141. Yielded elements, Stage 5 - Model C, k=1

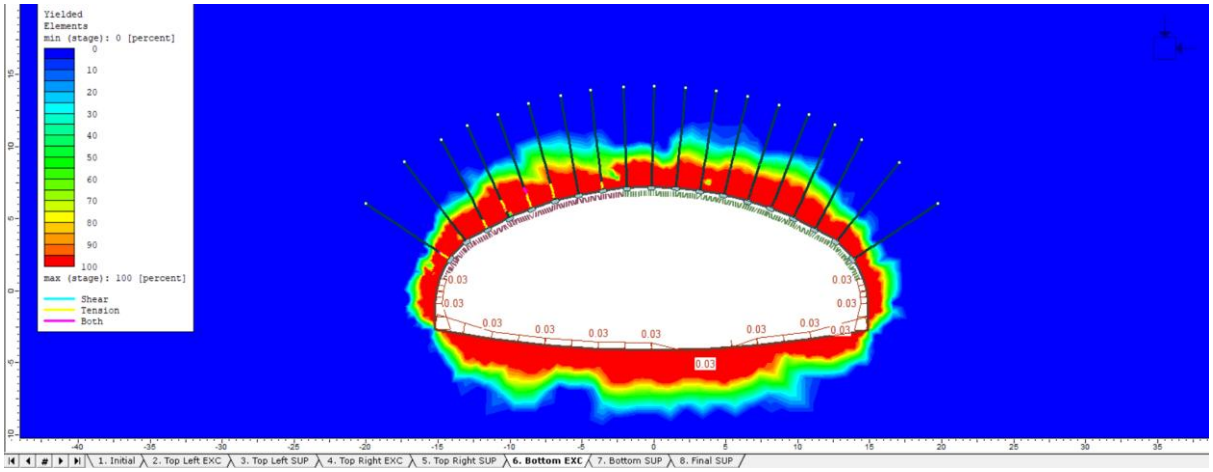

Figure 5-142. Yielded elements, Stage 6 - Model C, k=1

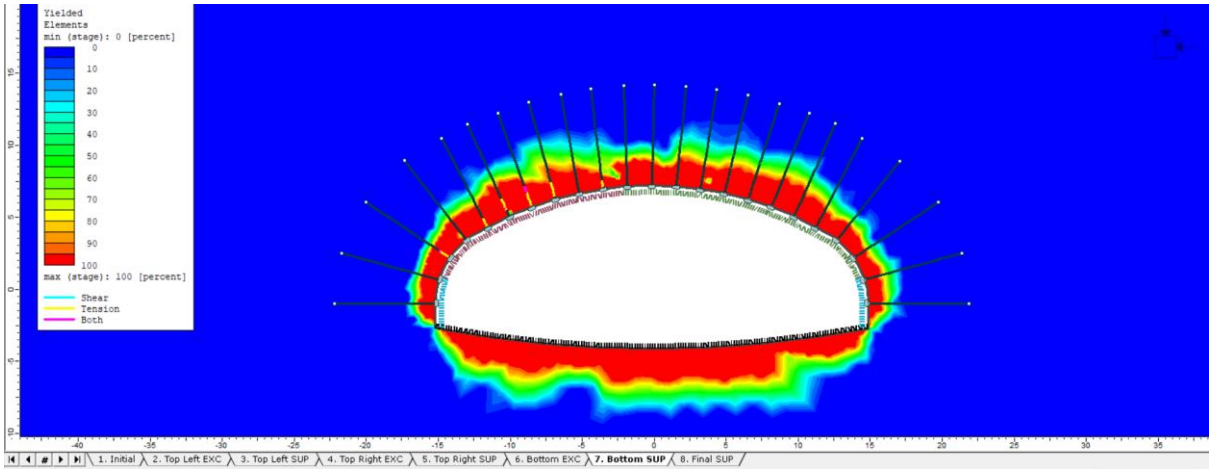

Figure 5-143. Yielded elements, Stage 7 - Model C, k=1

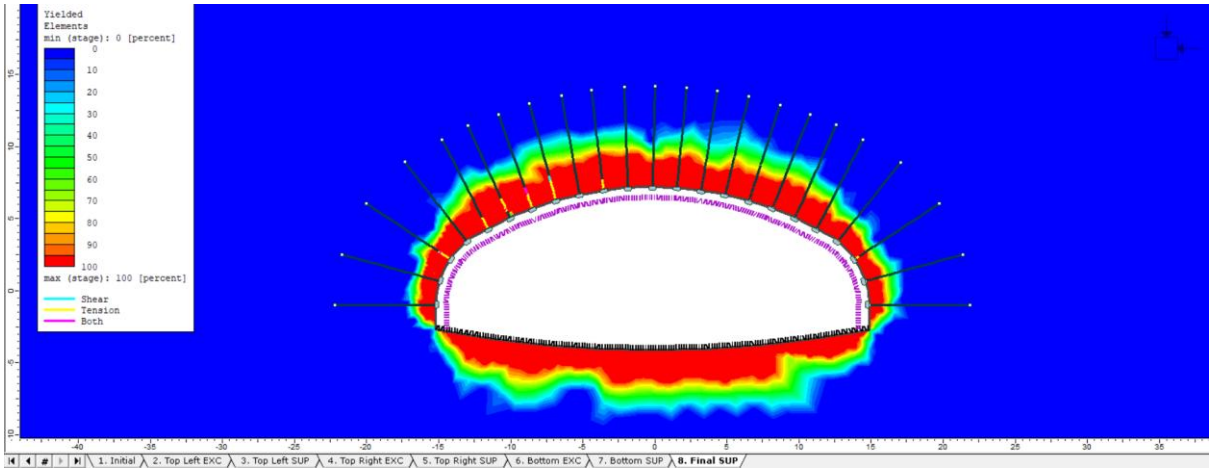

Figure 5-144. Yielded elements, Stage 8 - Model C, k=1

The Furthest plastic point is placed upside the cavern in distance of 3.5 m.

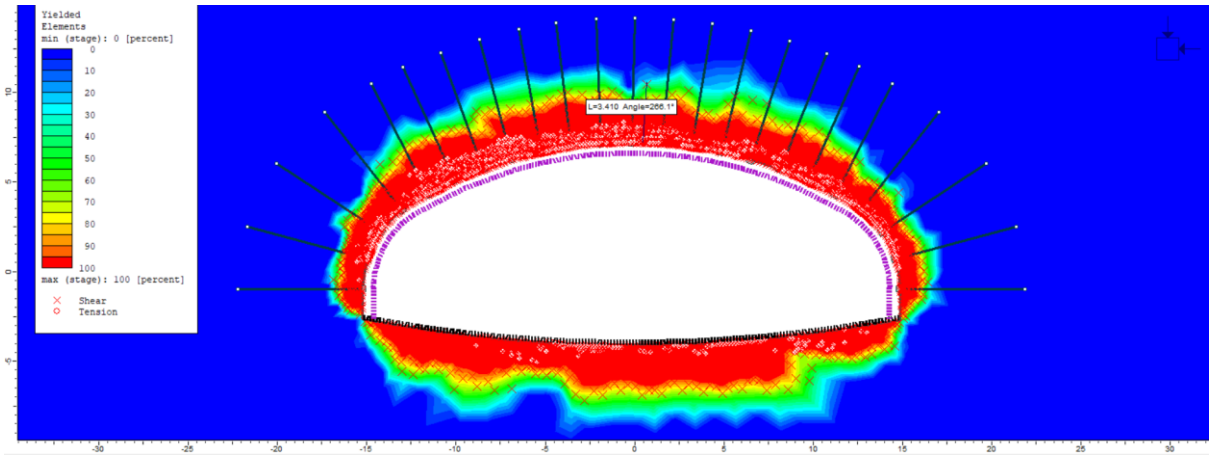

Figure 5-145. Plastic points - Model C, k=1

5.3.2.3. *Axial Force on Rockbolts*

Highest value of Axial Force acting on the Rock Bolts is 0.2 MN.

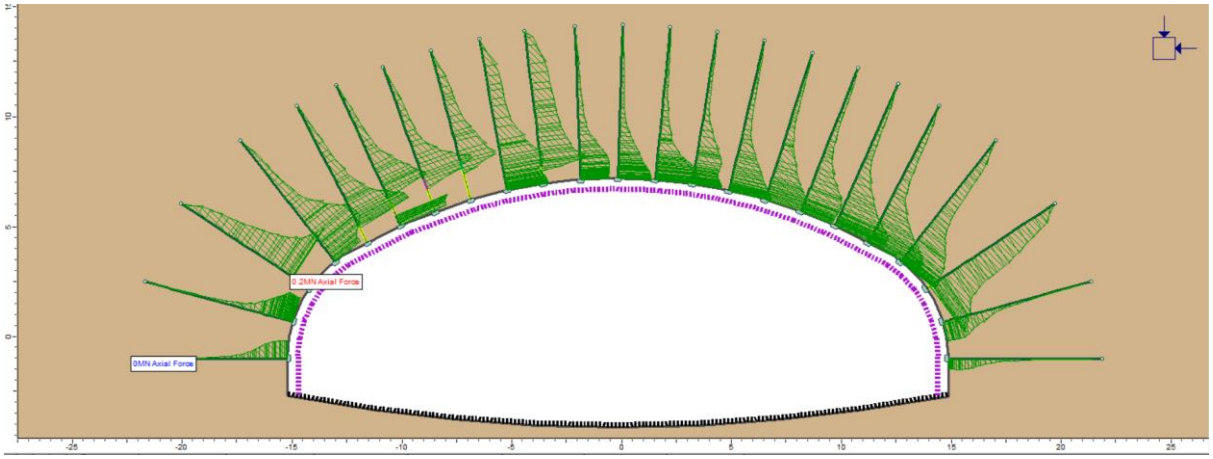

Figure 5-146. Axial force on Rockbolts - Model C, k=1

5.3.2.4. *Axial Force and Bending Moment on RRS*

Maximum Axial Force acting on RRS is 2.4 MN concentrating on the side walls; there are few negligible points under tension on the right side of the crown with low tension force maximumly 0.4 MN.

Bending Moment is presented positive and negative, maximum amount is 0.029 MNm

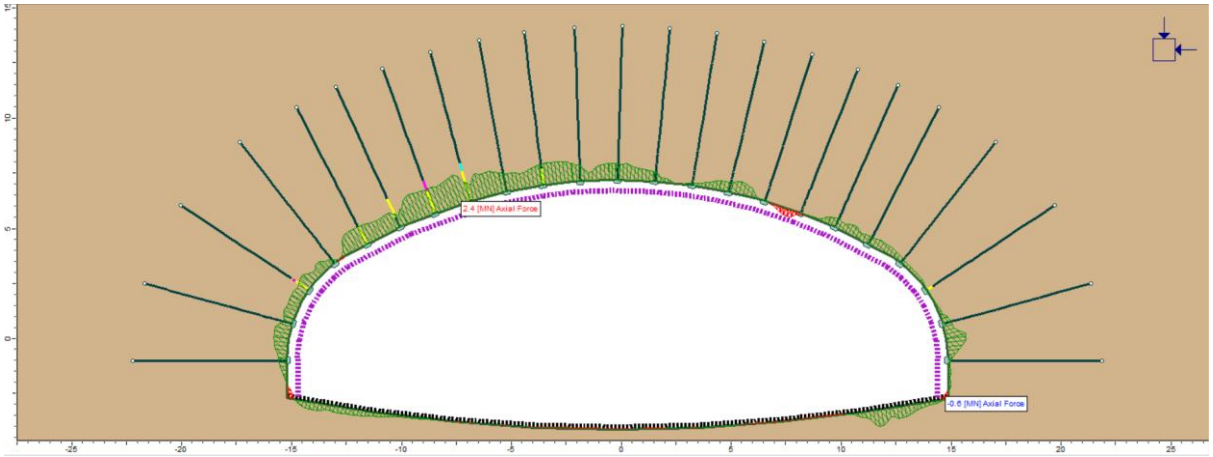

Figure 5-147. Axial Force on RRS - Model C, k=1

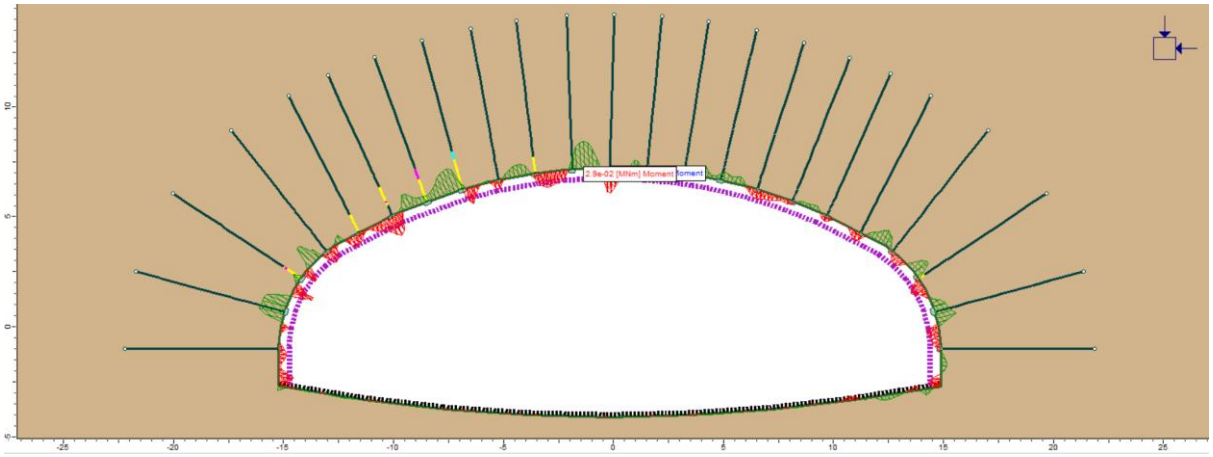

Figure 5-148. Bending Moment on RRS - Model C, k=1

5.3.2.5. Support Capacity, Rockbolts

Six rockbolts have been yielded under tension and shear forces.

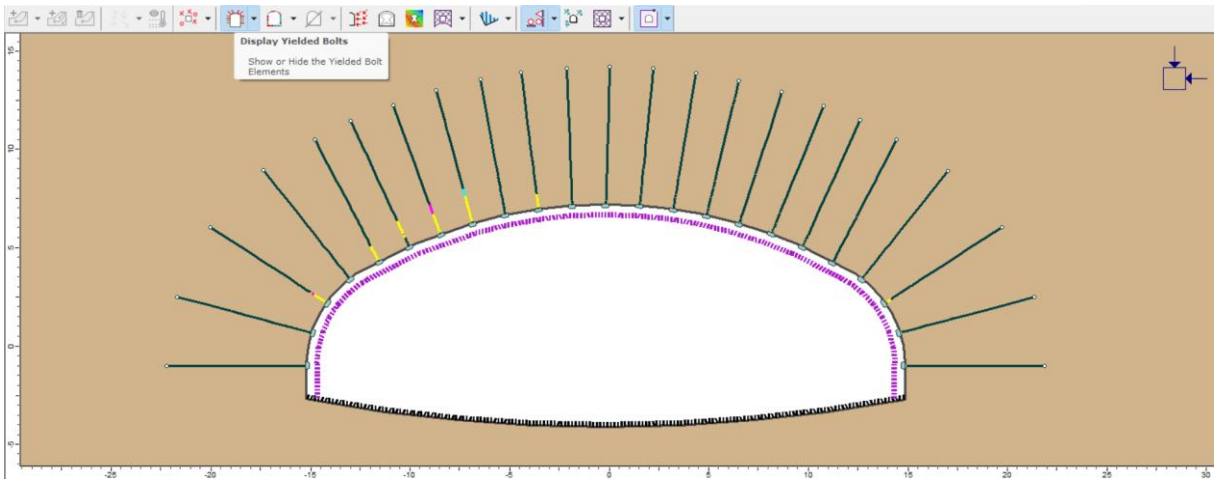

Figure 5-149. Displayed yielded bolts

5.3.2.6. Support Capacity, RRS

Plots indicating support capacity of RRs are presented in this section.

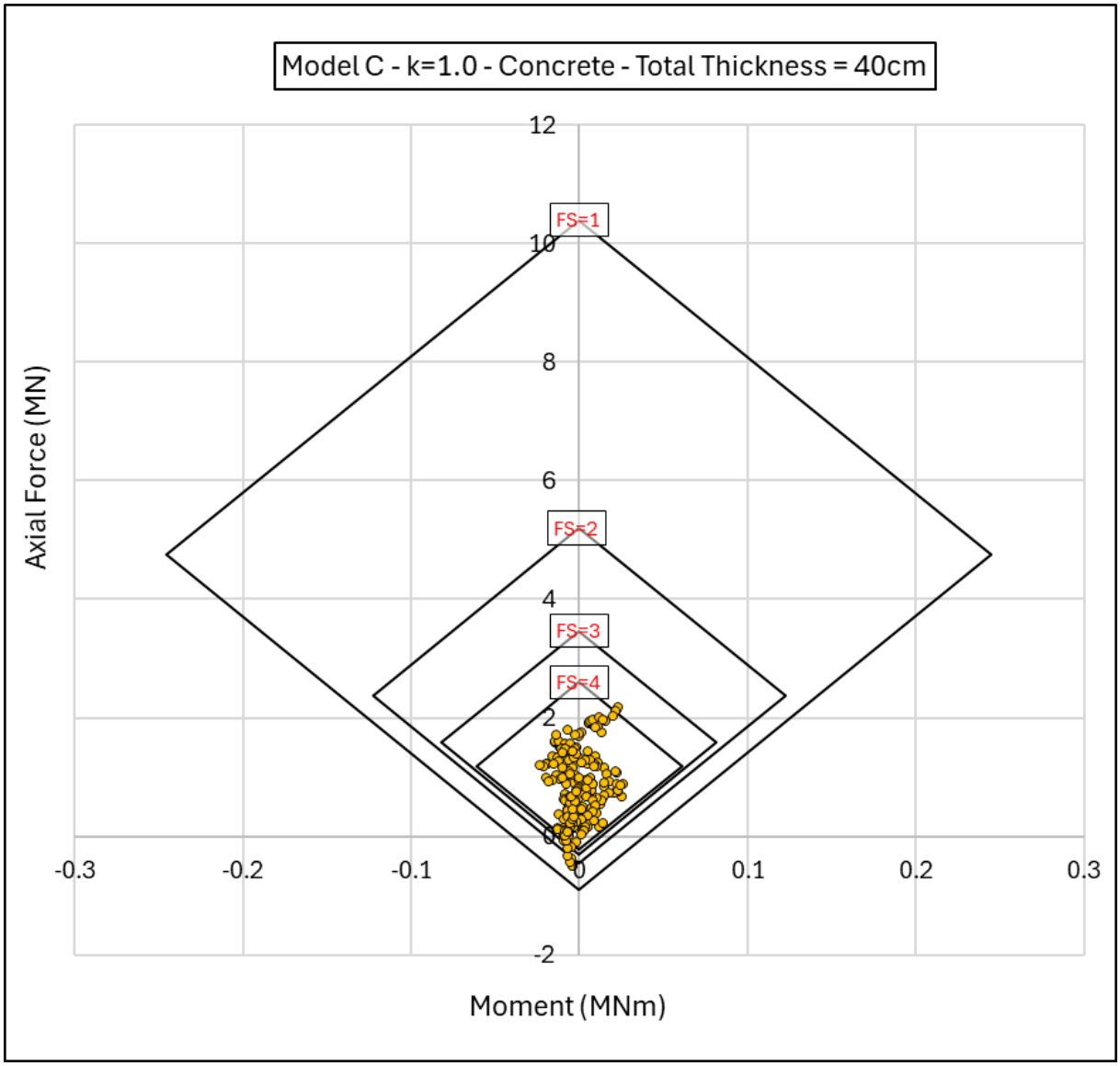

Figure 5-150. Axial Force-Moment Plot of Concrete - Model C, k=1

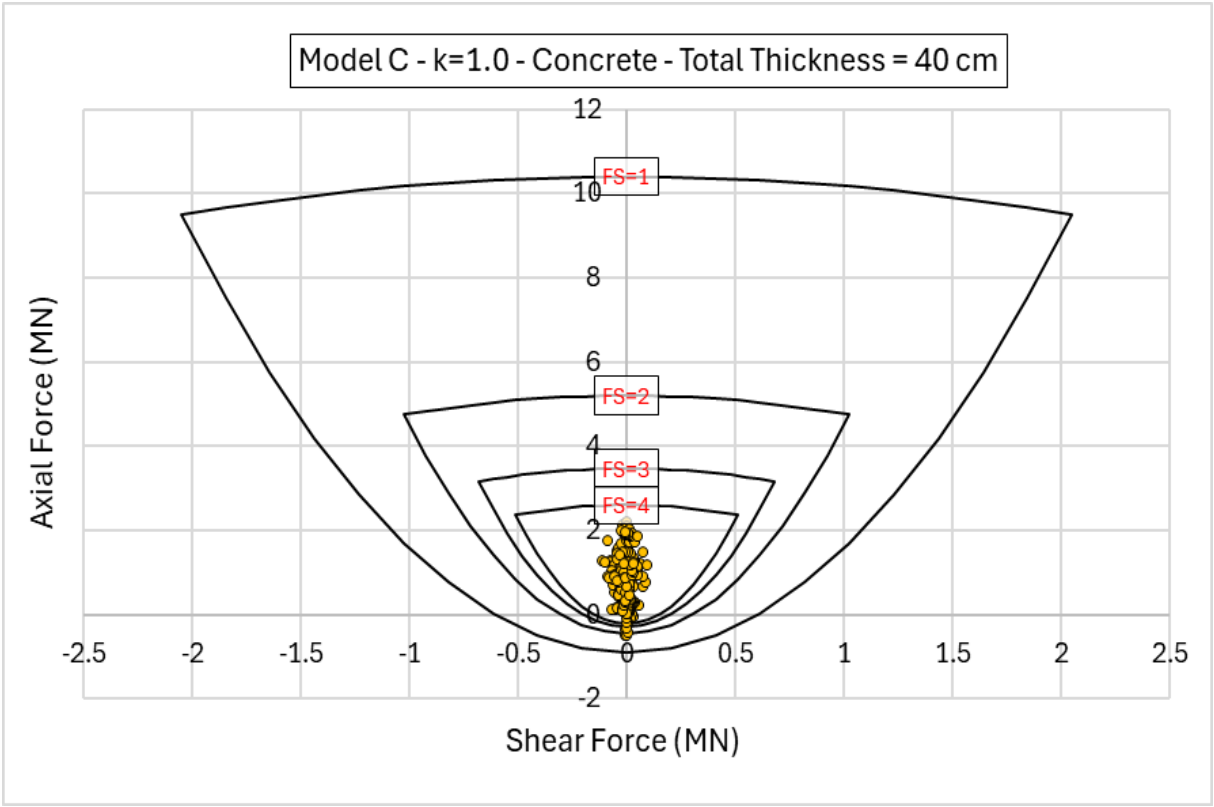

Figure 5-151. Axial Force-Shear Force of the Concrete - Model C, k=1

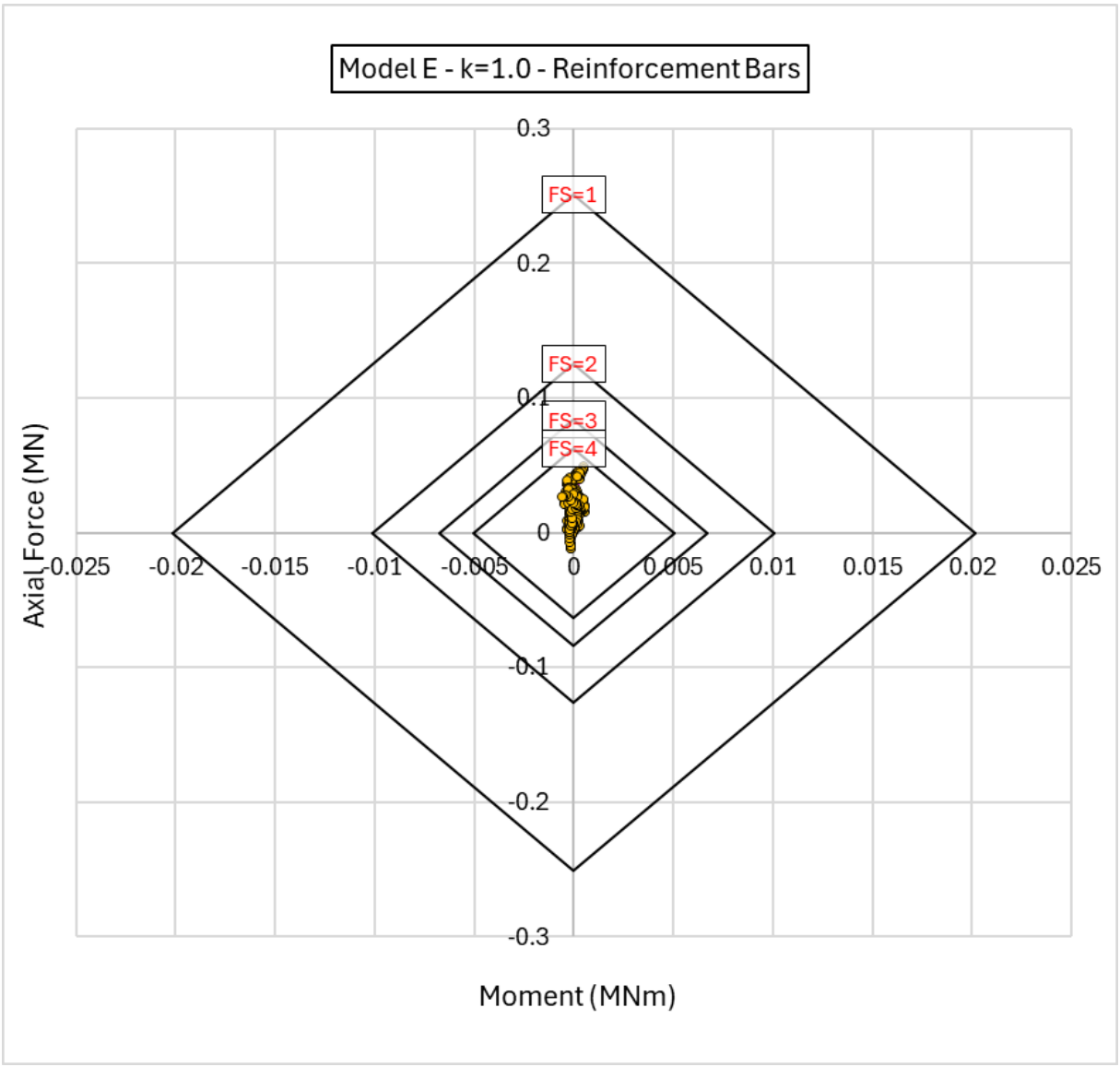

Figure 5-152. Axial Force-Moment plot of Steel Rebars - Model C, k=1

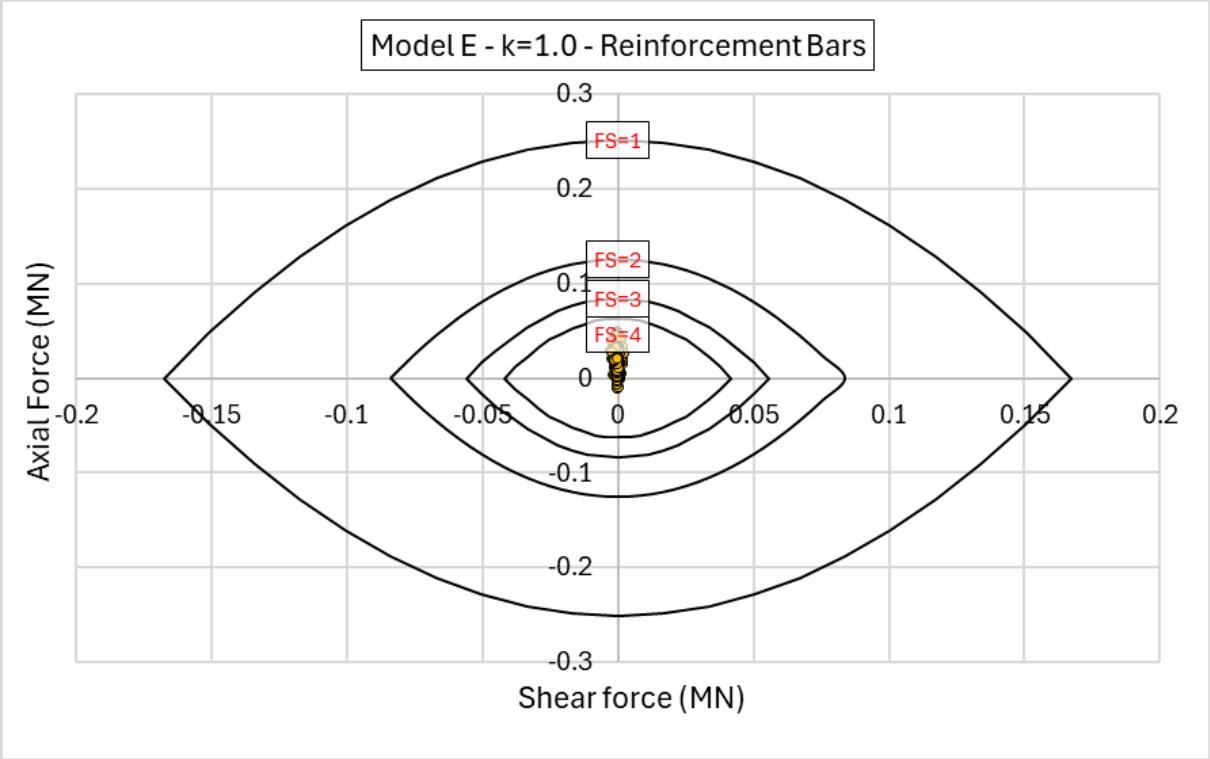

Figure 5-153. Axial Force-Shear Force plot of Steel Rebars - Model C, k=1

5.3.2.7. Summary of Results

Summarized outputs of Model C, under hydrostatic condition is presented below.

Table 5-8. Summarized results - Model C, k = 1

Model C – k = 1	
Maximum displacement at the walls [cm]	5
Maximum displacement at the roof [cm]	8
Maximum total displacement [cm]	8.1
Maximum radius measured for the plastic zone [m]	4.5
RRS properties	40 cm thickness c/c spacing 3 m
Maximum Compression on RRS [MN]	2.4
Maximum Tension on RRS [MN]	0.4
Min-Max Factor of Safety for RRS	Min: 1.4 Max: higher than 4
Quantity of rock bolts and their lengths [m]	23 Rock Bolts 7 m
Rock bolt tributary area [mm^2]	207
Maximum axial force on rock bolts [MN]	0.2
Number of Yielded bolts and their location	6 (left side of the Crown)
Rock Bolt Deformation [cm]	5

In summary, plastic zones progressively increased around each excavation step until the last stage that reaches 4.5 m far from the cavern on the roof.

Rock bolts are 7m and their endpoint is in the elastic zone; yielded bolts ae placed on the left side of the crown that was installed after first excavation stage under tension, and they have maximum deformation of 5 cm.

RRS liners are totally being compressed with highest axial force of 2.4 MN except for some few points between right wall and the crown under tension with maximum axial force of 0.4 MN.

Support capacity plots show acceptable performance in. The minimum safety factor is 1.4 although most of the points have higher safety factors than 3.

5.3.3. Model C – k =2

Highest value of stress ratio that was used in the modeling is applied to Model C and the results are presented below.

5.3.3.1. Total Displacement

Total displacement reaches up to 12.5 cm concentrating in the invert and roof in the final stage.

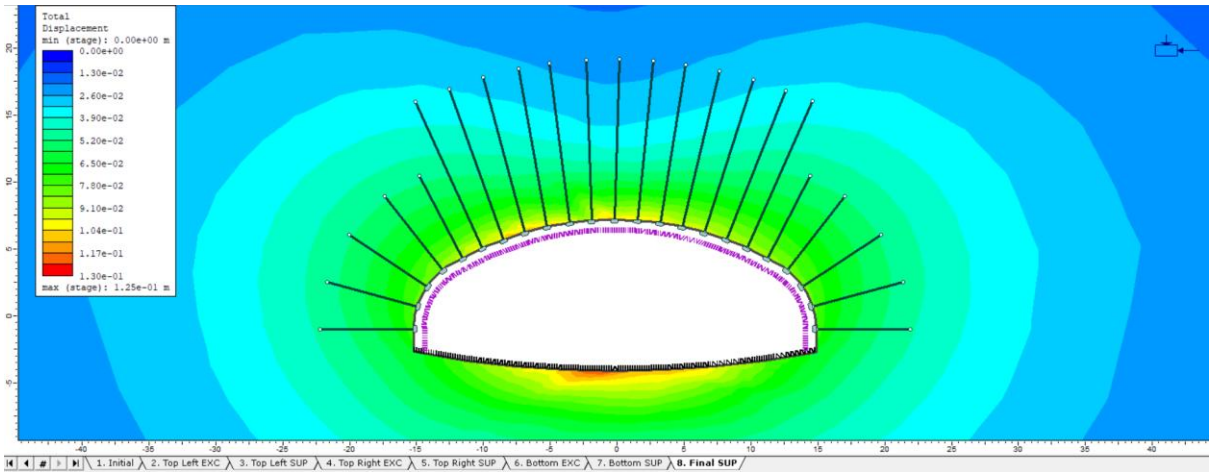

Figure 5-154. Total Displacement - Model C, k=2

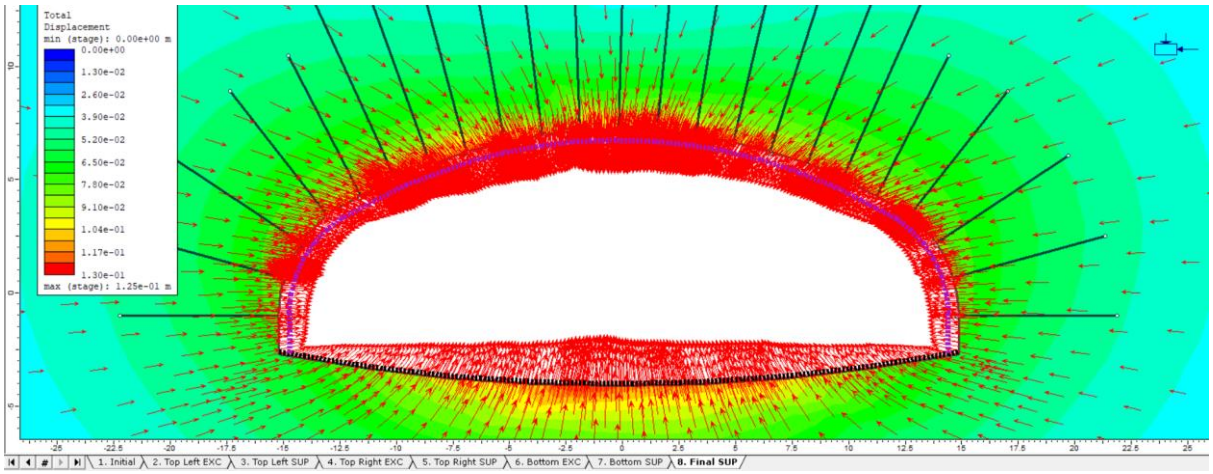

Figure 5-155. Deformation vectors - Model C, k=2

5.3.3.2. Plastic Radius around the cavern

Maximum Plastic radius reaches up to 10 m on the roof.

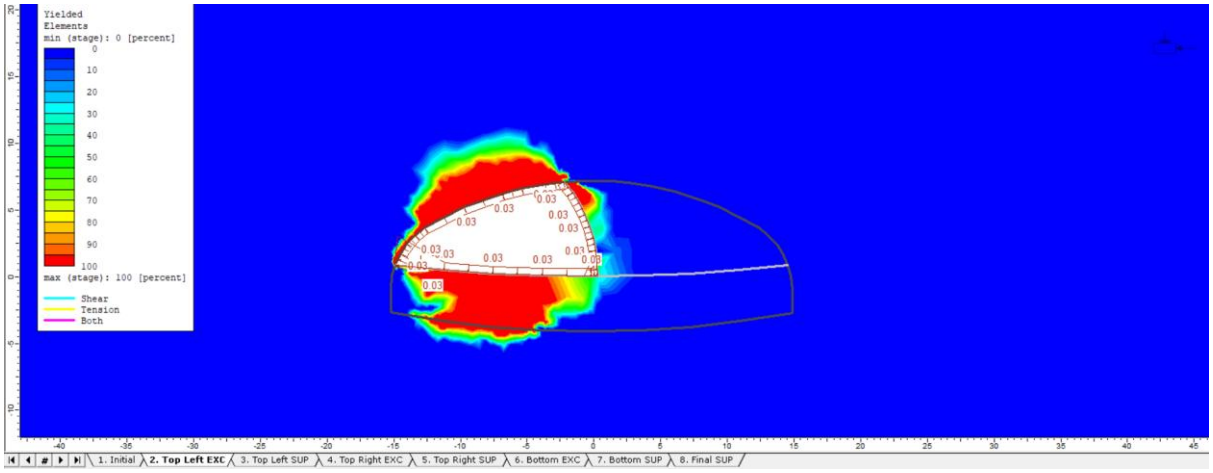

Figure 5-156. Yielded elements, Stage 2 - Model C, k=2

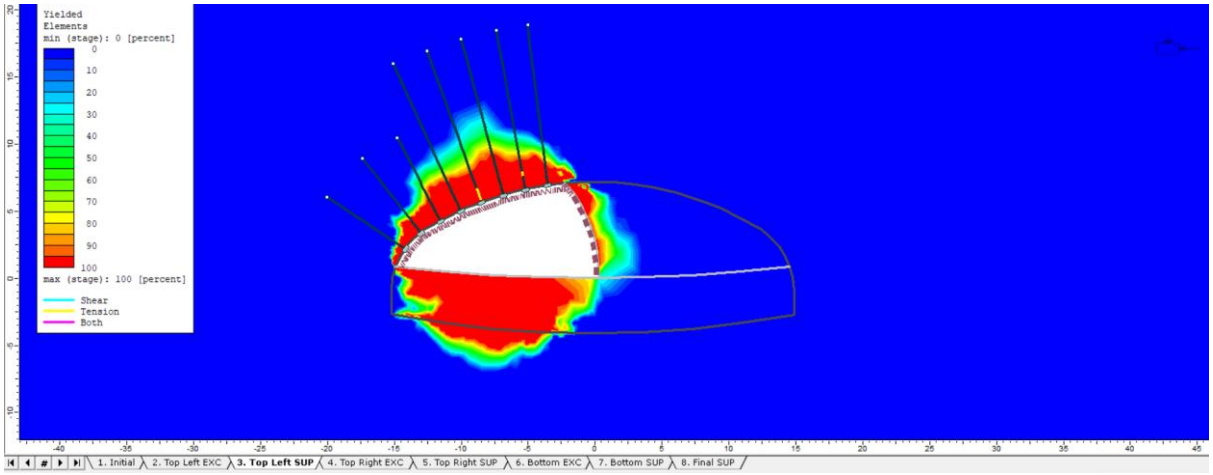

Figure 5-157. Yielded elements, Stage 3 - Model C, k=2

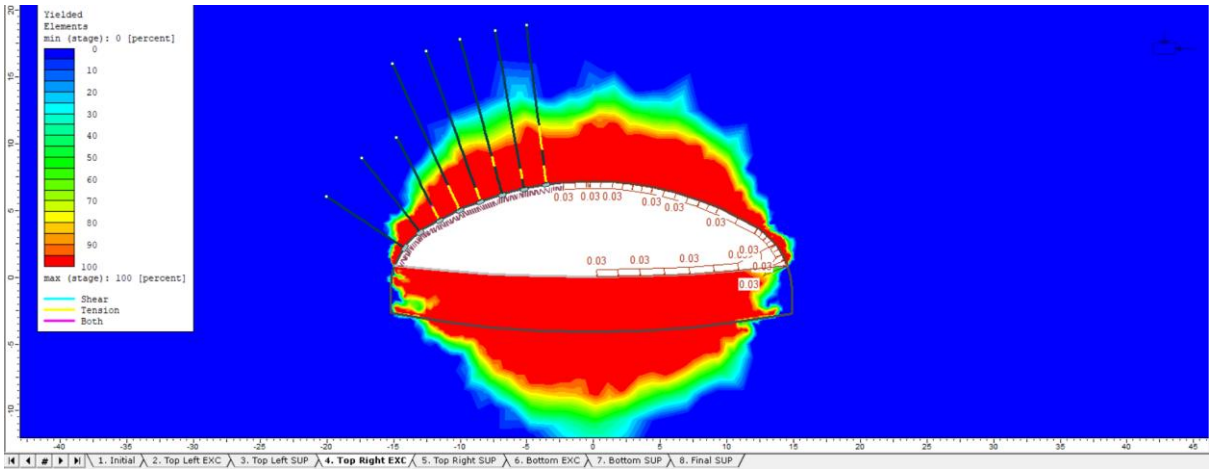

Figure 5-158. Yielded elements, Stage 4 - Model C, k=2

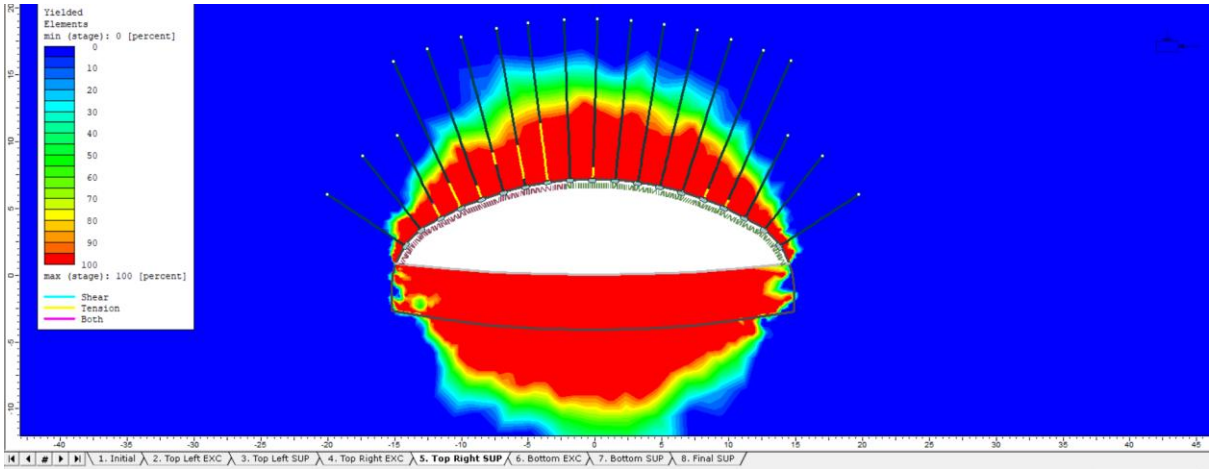

Figure 5-159. Yielded elements, Stage 5 - Model C, k=2

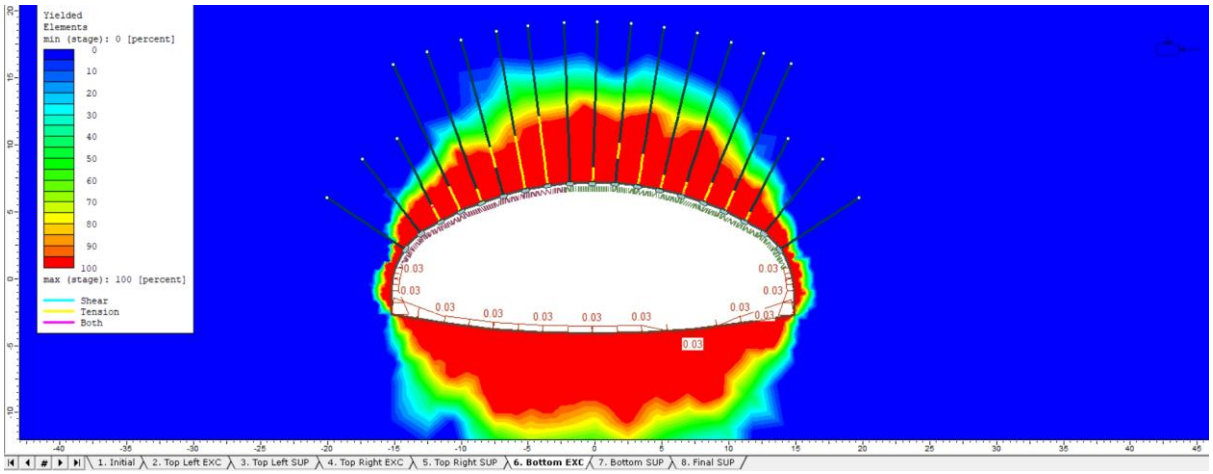

Figure 5-160. Yielded elements, Stage 6 - Model C, k=2

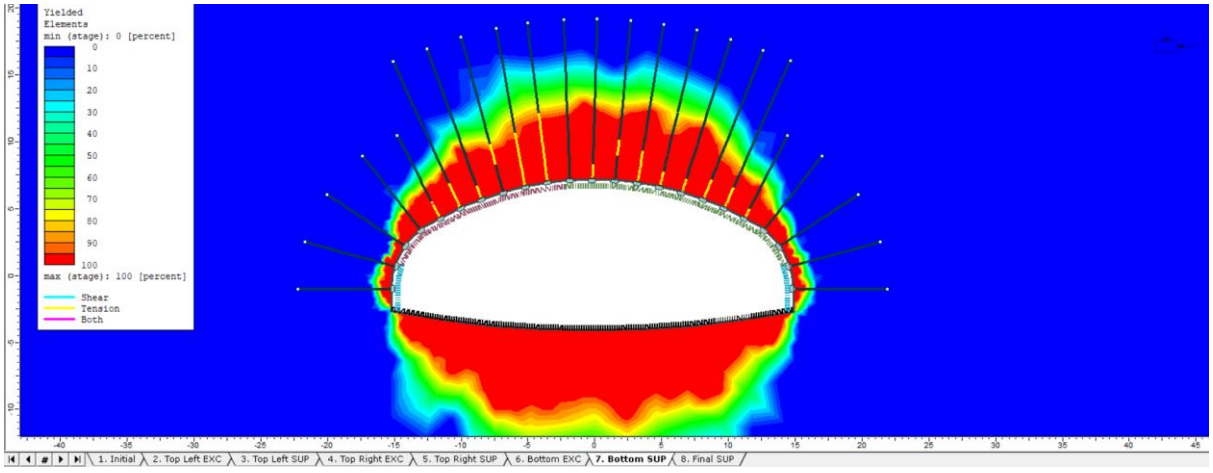

Figure 5-161. Yielded elements, Stage 7 - Model C, k=2

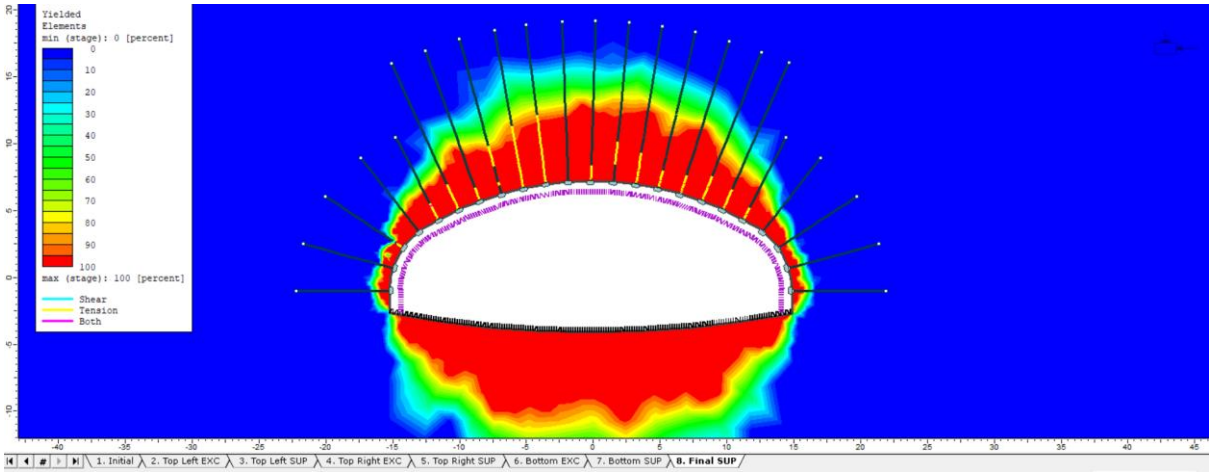

Figure 5-162. Yielded elements, Stage 8 - Model C, k=2

Furthest plastic point is 7.3 m far from the cavern boundary.

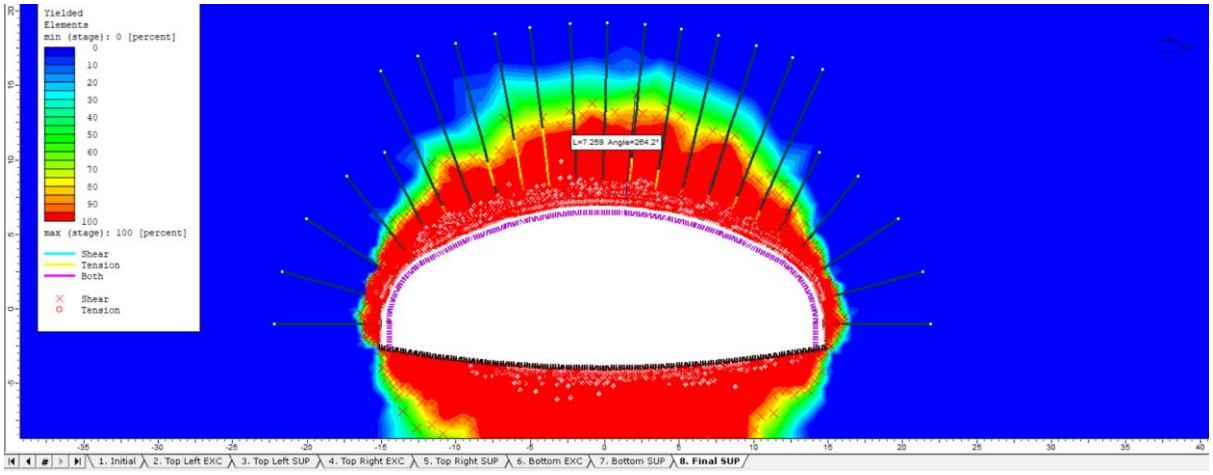

Figure 5-163. Plastic Points - Model C, k=2

5.3.3.3. Axial Force on Rockbolts

Axial force is affecting all rock bolts; Highest value is 0.2 MN.

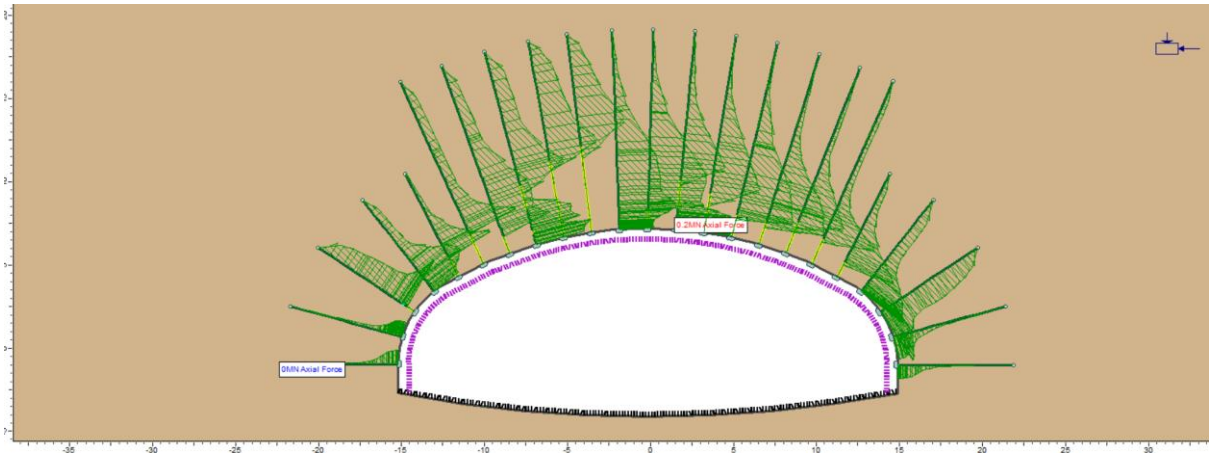

Figure 5-164. Axial force on rockbolts - Model C, k=2

5.3.3.4. *Axial Force and Bending Moment on RRS*

Maximum Axial Force acting on the RRs is compressing the roof with 3.4 MN. There are points under tension with very low value of axial force that can be neglected.

Bending Moment increases up to 0.08 MNm in the walls.

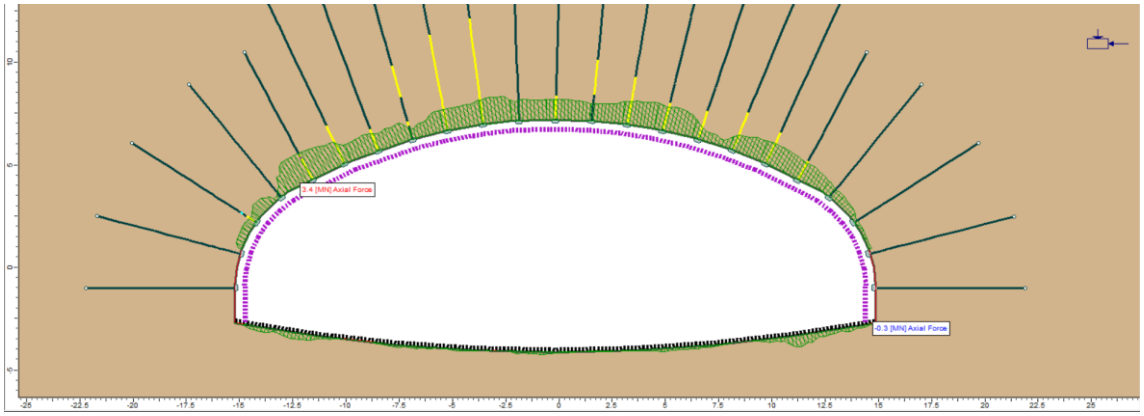

Figure 5-165. Axial Force acting on RRS - Model C, k=2

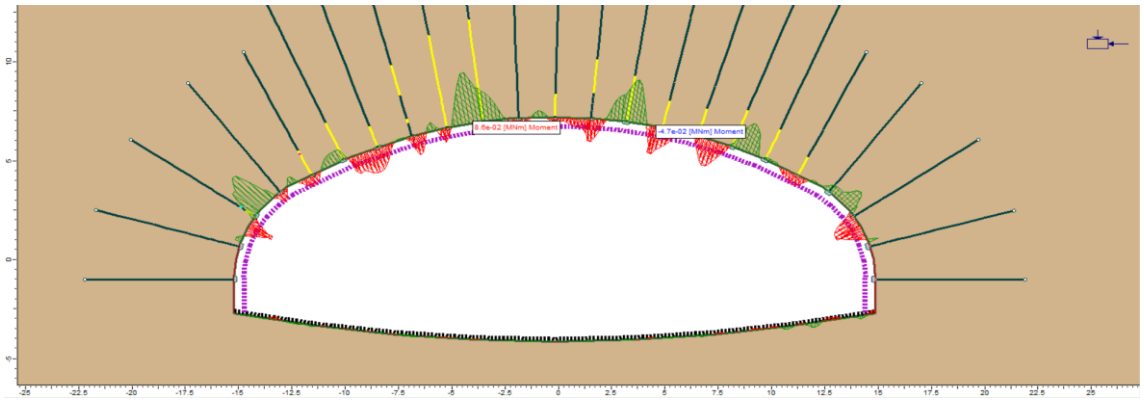

Figure 5-166. Bending Moment acting on RRS - Model C, k=2

5.3.3.5. *Support Capacity, Rockbolts*

Fifteen rockbolts in the center of the cavern are yielded under tension and shear forces.

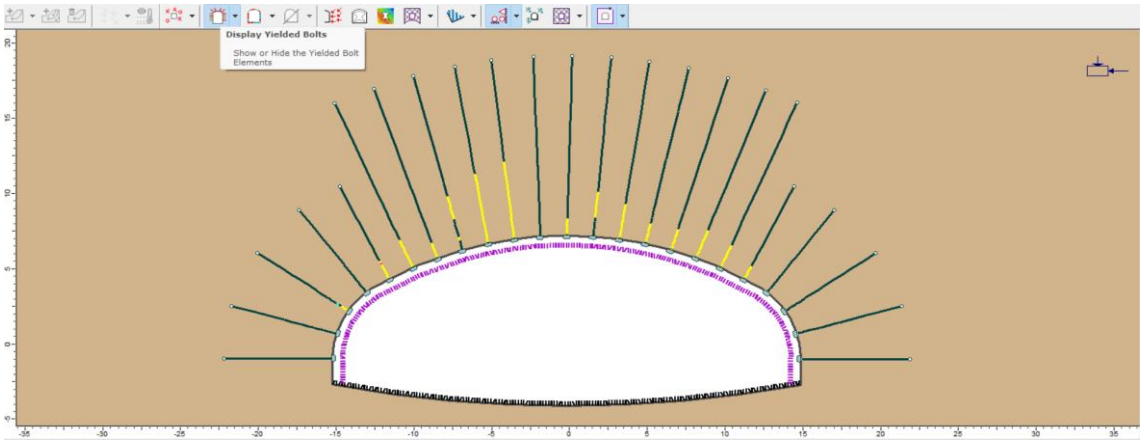

Figure 5-167. Displayed yielded bolts - Model C, k=2

5.3.3.6. Support Capacity, RRS

Capacity of Concrete and steel rebars in the RRS are presented in following plots.

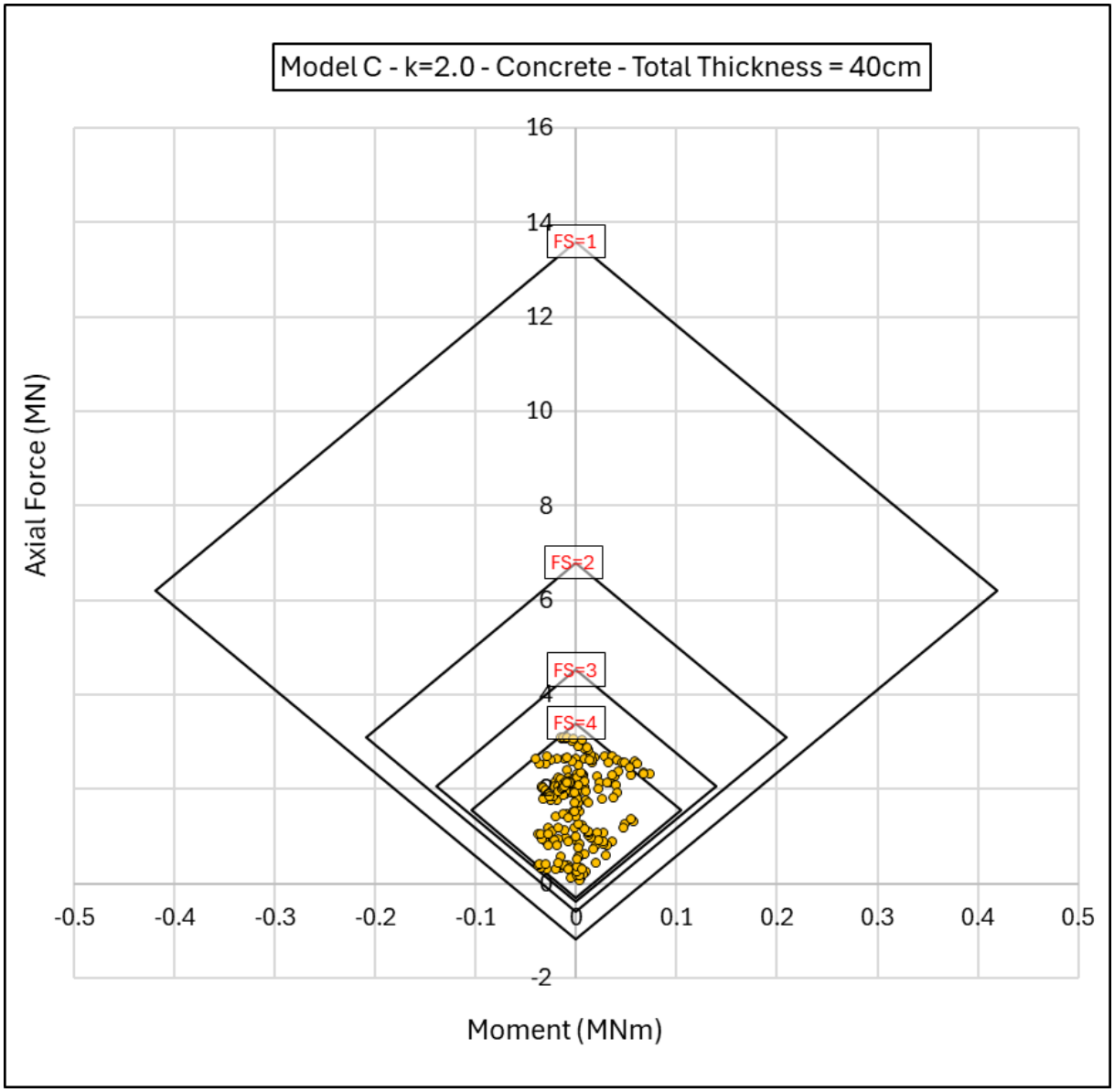

Figure 5-168. Axial Force-Moment plot of Concrete - Model C, k=2

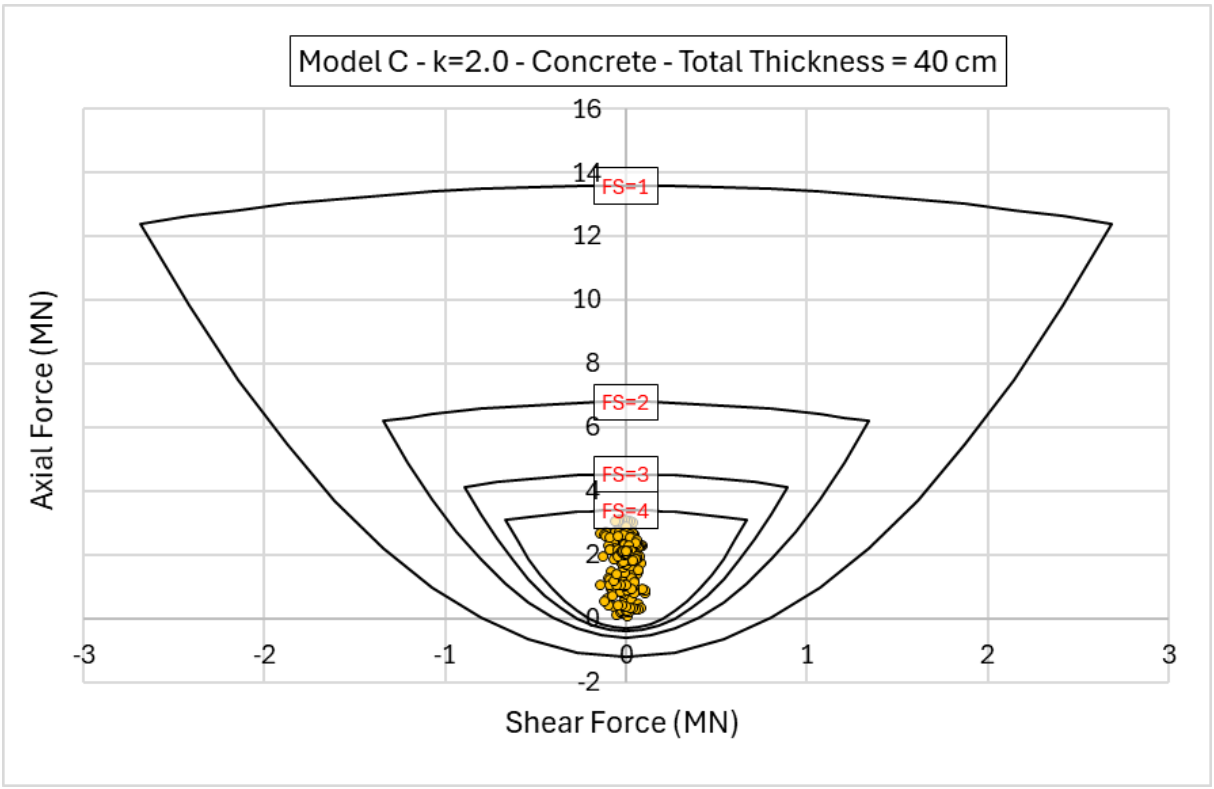

Figure 5-169. Axial Force-Shear Force plot of Concrete - Model C, k=2

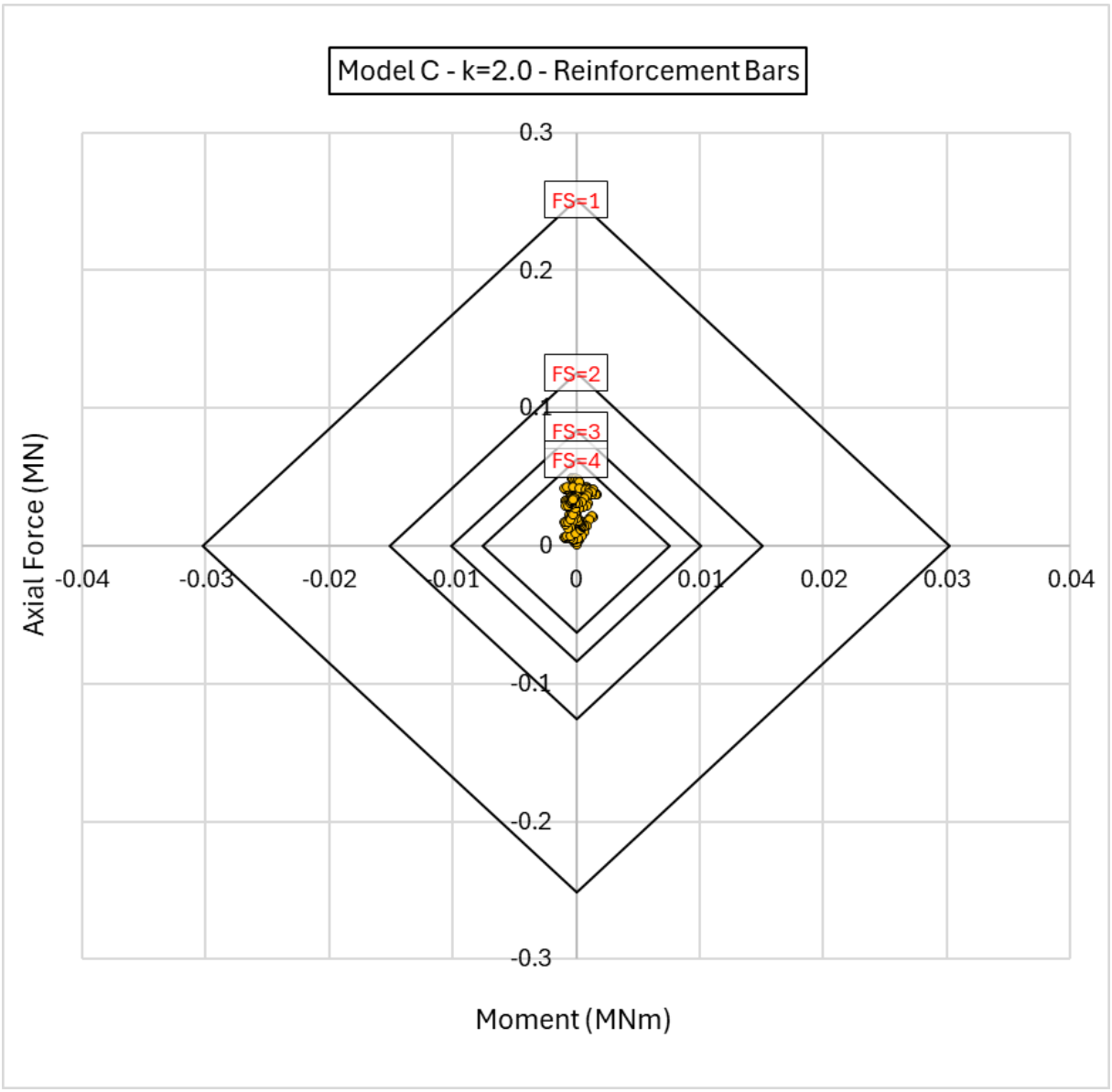

Figure 5-170. Axial Force-Moment plot of the Steel rebars - Model C, k=2

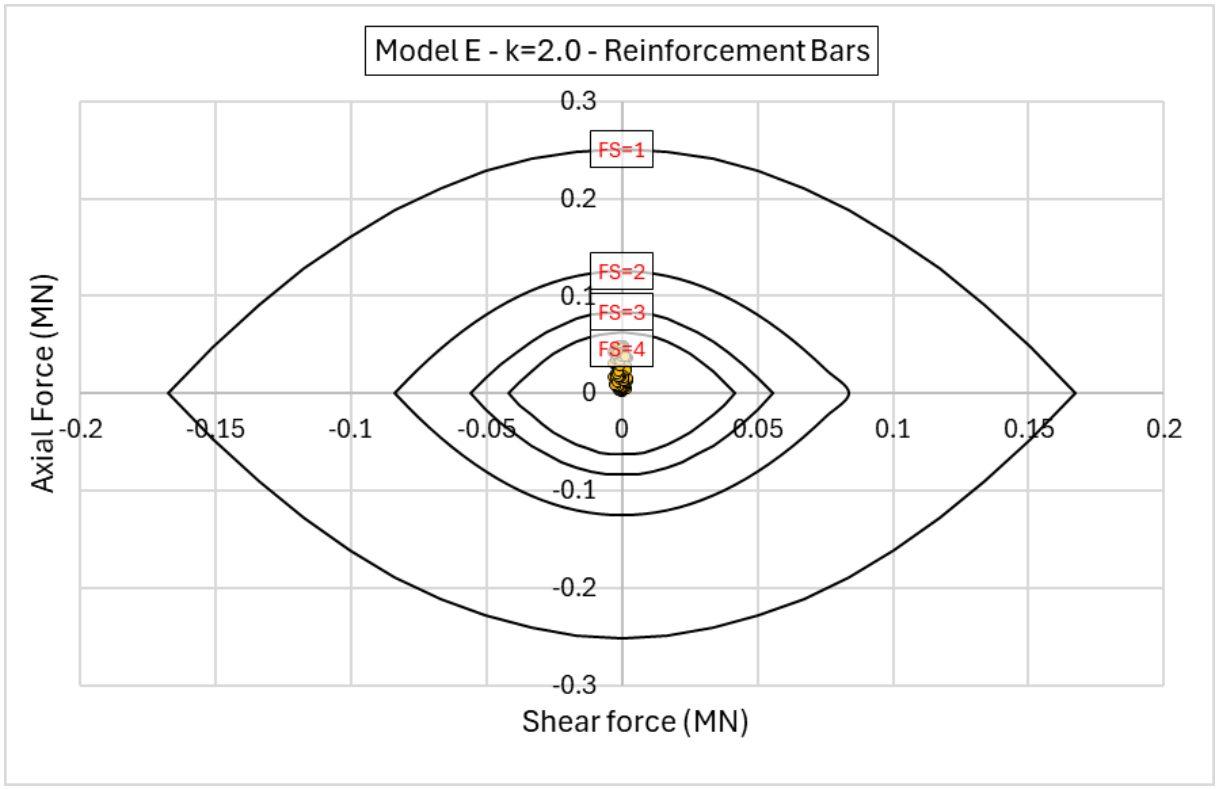

Figure 5-171. Axial Force-Shear Force plot of Steel Rebars - Model C, k=2

5.3.3.7. Summary of the results

Obtained outputs are presented in following table in summary.

Table 5-9. Summary of Results - Model C, k = 2

Model C – k = 2	
Maximum displacement at the walls [cm]	7.8
Maximum displacement at the roof [cm]	11
Maximum total displacement [cm]	12.5
Maximum radius measured for the plastic zone [m]	10
RRS properties	40 cm thickness c/c spacing 1.5 m
Maximum Compression on RRS [MN]	3.4
Maximum Tension on RRS [MN]	0
Min-Max Factor of Safety for RRS	Min: 3.7 Max: Higher than 4
Quantity of rock bolts and their lengths [m]	23 Rock Bolts 13 Rock Bolts 12 m 10 Rock Bolts 7 m
Rock bolt tributary area [mm^2]	207
Maximum axial force on rock bolts [MN]	0.2
Number of Yielded bolts and their location	15 rock bolts (Center of the roof)
Rock Bolt Deformation [cm]	9.3

In summary, plastic zones progressively expand around each excavation step concentrated on the crown of the excavation boundaries until the last stage that reaches 10 m far from the cavern.

Rock bolts on the sidewalls are 7 m and have 12 m of length in the roof; Their endpoint is in the elastic zone. Fifteen bolts are yielded with maximum deformation of 9.3 cm.

RRS liners are being compressed with highest axial force of 3.4 MN on the crown, but the walls are facing a very low amount of tension than can be considered as no tension environment,

Support capacity plots for concrete show good performance with highly favorable range of safety factors which is at least equal to 3.7.

5.4. Comparing results with analytical approach

As was mentioned before in the relevant chapter (3.2.4.), based on the convergence confinement method (Panet-Guénot), it is estimated to have 97% of relaxation pressure at 5 m distance from the excavation surface and 3% of induced total initial stress (17.6*0.03 = 0.52 MPa) has been applied to the boundaries of the excavation in our models.

The model that was made in GV4 software has the following properties.

- **Circular tunnel with 5m radius.** The radius was achieved by having the area of each excavation step in the models as an equivalent area of a circle that has approximately 5 m of radius.
- **Rock mass properties with Mohr-Coulomb parameters of the friction angle (ϕ) = 39° and cohesion = 1MPa.** These values were obtained by application of empirical formulas that contain Hoek-Brown mechanical parameters (m_b, a, s) and result the equivalent friction angle and cohesion of the rock mass (refer to 2.3.2.2.)
- **15 cm of shotcrete as the primary liner**
- **7 m of rockbolts with 1.7 m of radial spacing.**

However, it is known that Convergence-confinement method is based on consideration of circular shapes of a tunnel, it was decided to compare the outputs from this analytical approach with the results that were achieved in main models with RS2 software.

The most circular-shape is of the Model A at stage 3 that has a horseshoe shape with around 10 m of span and 6 m of height; in this stage, the total displacement around the excavation boundary after installation of the first layer of lining (15cm of shotcrete) is maximumly 2 cm at the crown (Figure 5-172).

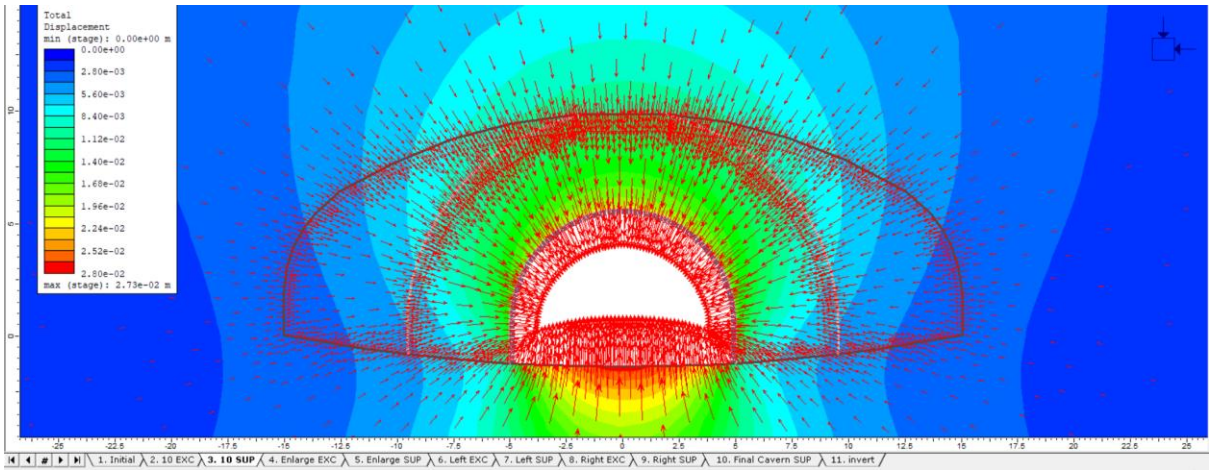

Figure 5-172. Displacement and convergence vectors, Model A-stage 3

It was also estimated to have approximately 3 cm of total displacement around the simulated circular tunnel analysis in GV4 software (Figure 5-173).

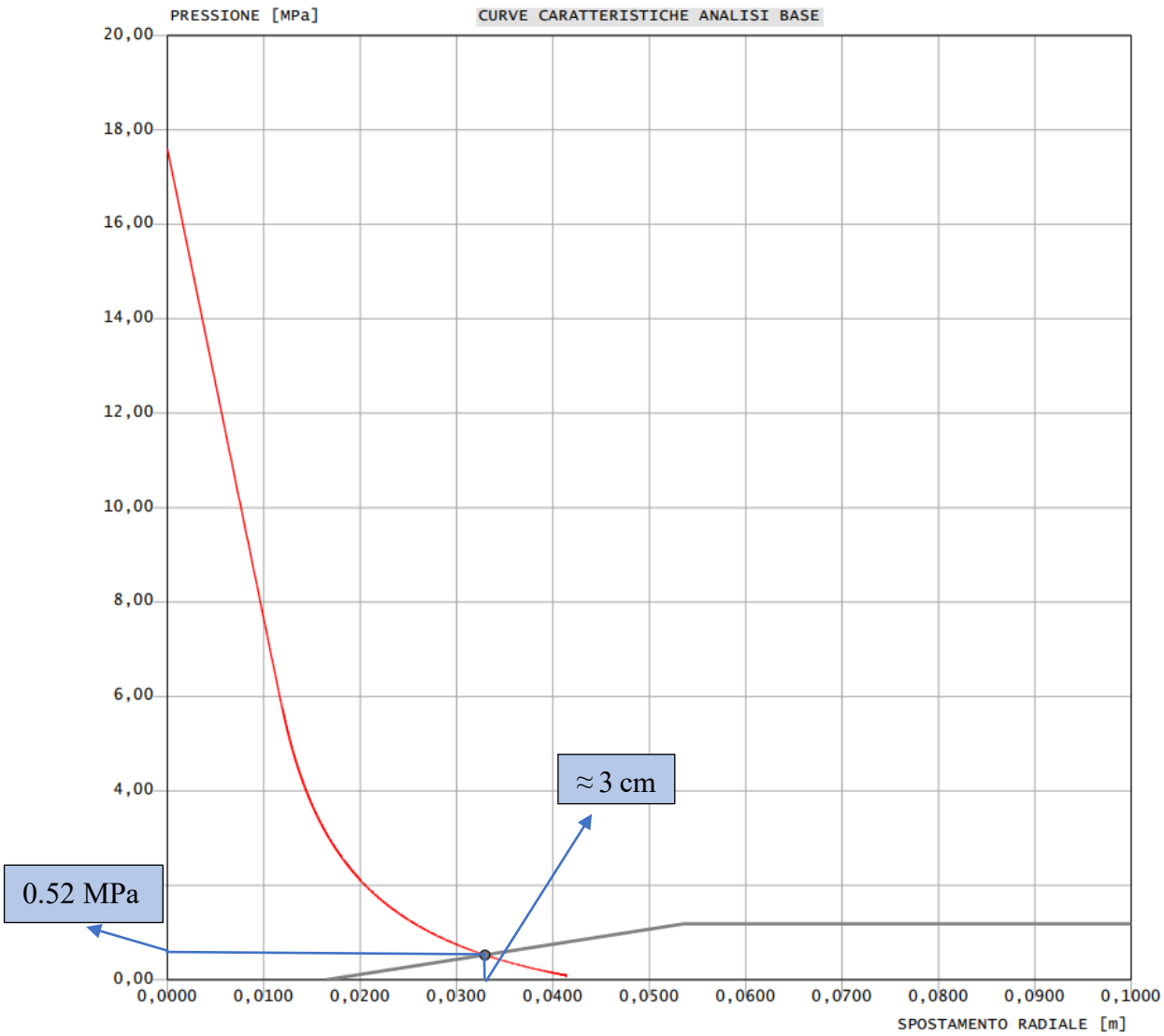

Figure 5-173. Ground reaction curve and support reaction curve intersection

Another factor to be verified is the plastic radius around the excavation boundary. In model A at stage 3, the plastic radius reaches maximumly around 7.2 m (from the center of horseshoe shape) around the excavation boundaries.

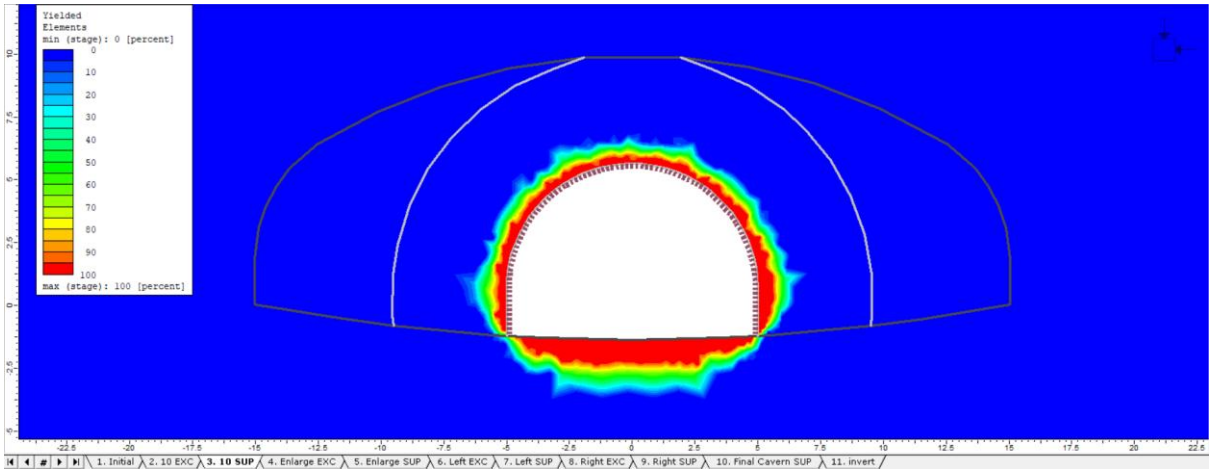

Figure 5-174. Model A- Stage 3, Plastic radius

This value in GV4 analysis reaches up to 7.6 m around the circular tunnel (Figure 5-175).

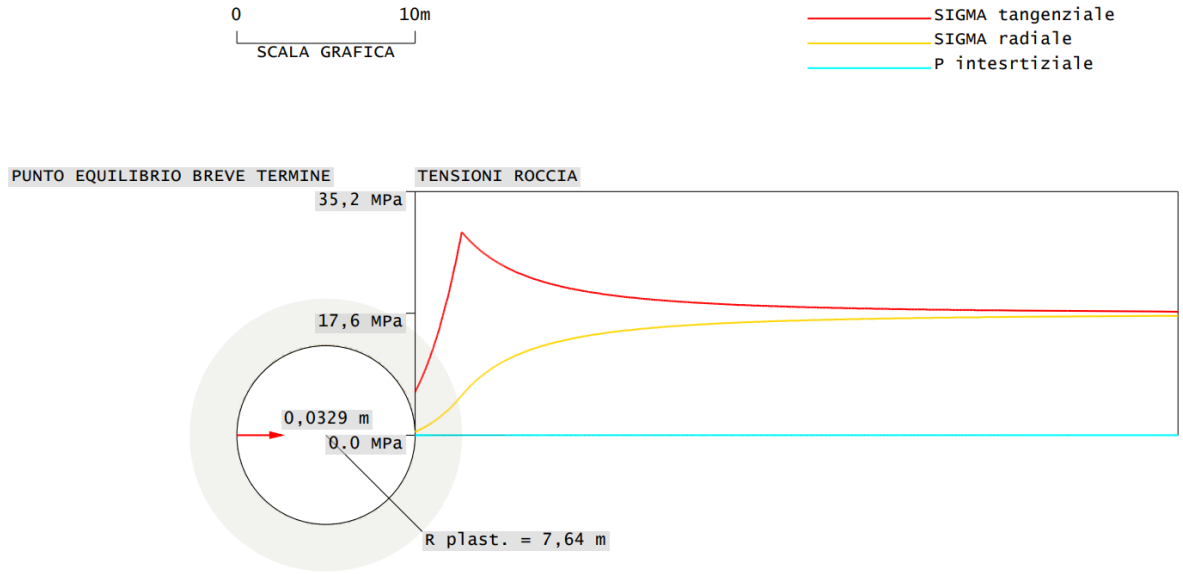

Figure 5-175. Plastic radius, GV4

The displacement values and the extent of the plastic zone obtained from both the analytical approach and the numerical modelling show very similar results. This consistency indicates that the RS2 numerical outputs are reliable and can be considered validated for the purposes of this analysis.

5.5. Summary of Results

This subchapter summarizes results of computation of all models based on horizontal-to-vertical stress ratios.

5.5.1. k = 0.5

5.5.1.1. Numerical results table

Table 5-10 shows results of computation of Model A, B and C with k=0.5.

Table 5-10. Summary of Results, k = 0.5

k = 0.5			
Excavation Style	**Model A (RPE)**	**Model B (SD)**	**Model C (TBH)**
Maximum displacement at the walls [cm]	2.5	4	5
Maximum displacement at the roof [cm]	7.4	7.3	7.5
Maximum total displacement [cm]	8.1	8.1	8.5
Maximum radius measured for the plastic zone [m]	4	5	5
Maximum Compression on RRS [MN]	1.7	5.4	1.7
Maximum Tension on RRS [MN]	0.6	0.6	0.4
Min-Max Factor of Safety for RRS	Min: 1.3 Max: Higher than 4	Min: 1.2 Max: Higher than 4	Min: 1.9 Max: Higher than 4
Maximum axial force on rock bolts [MN]	0.063	0.2	0.2
Rock Bolt Deformation [cm]	3	4.2	4.5

5.5.1.2. Support Capacity, RRS (Concrete)

Figure 5-176 shows comparison chart for all three models

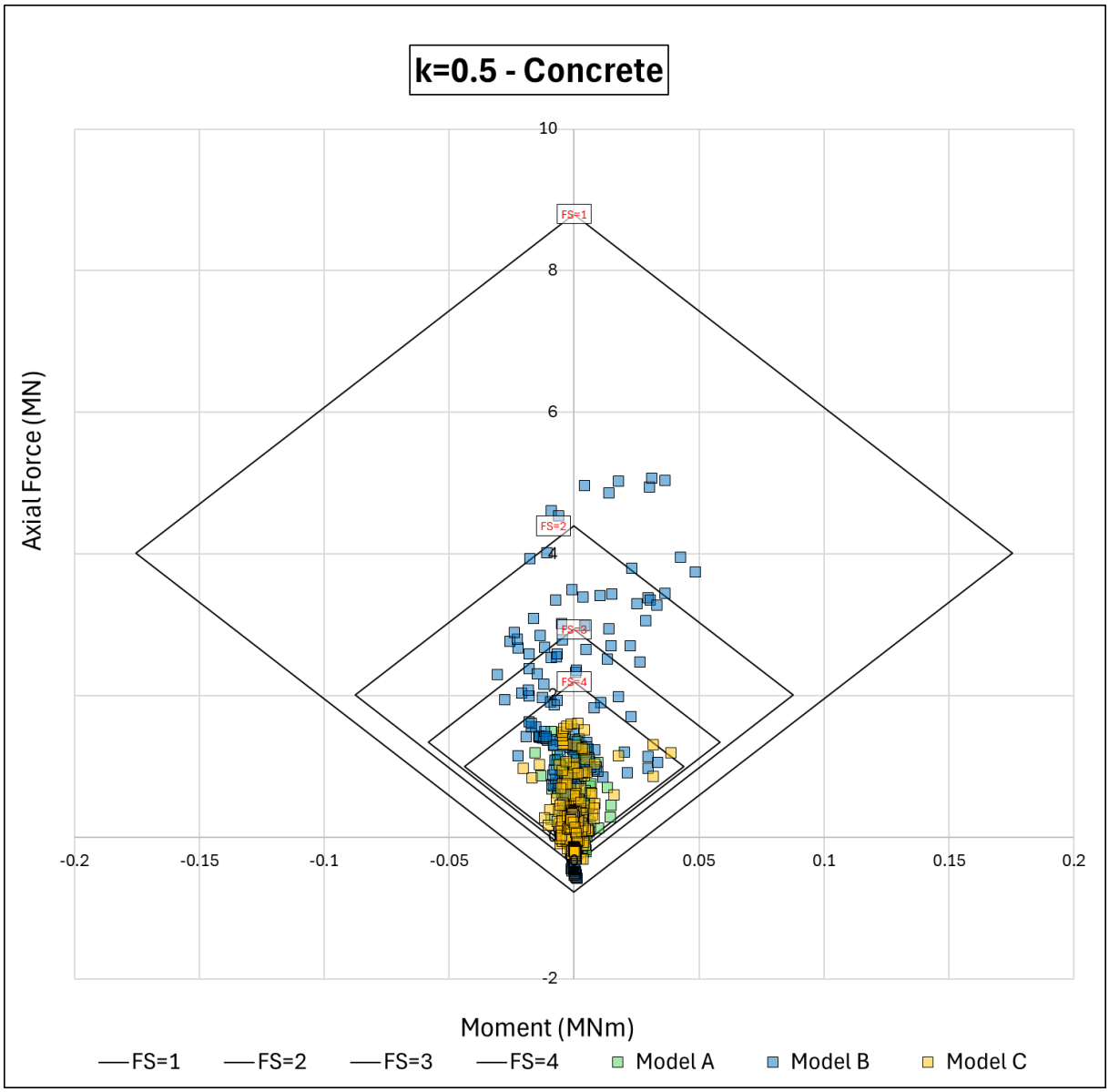

Figure 5-176. M-N support capacity diagrams of the RRS for all models, k=0.5

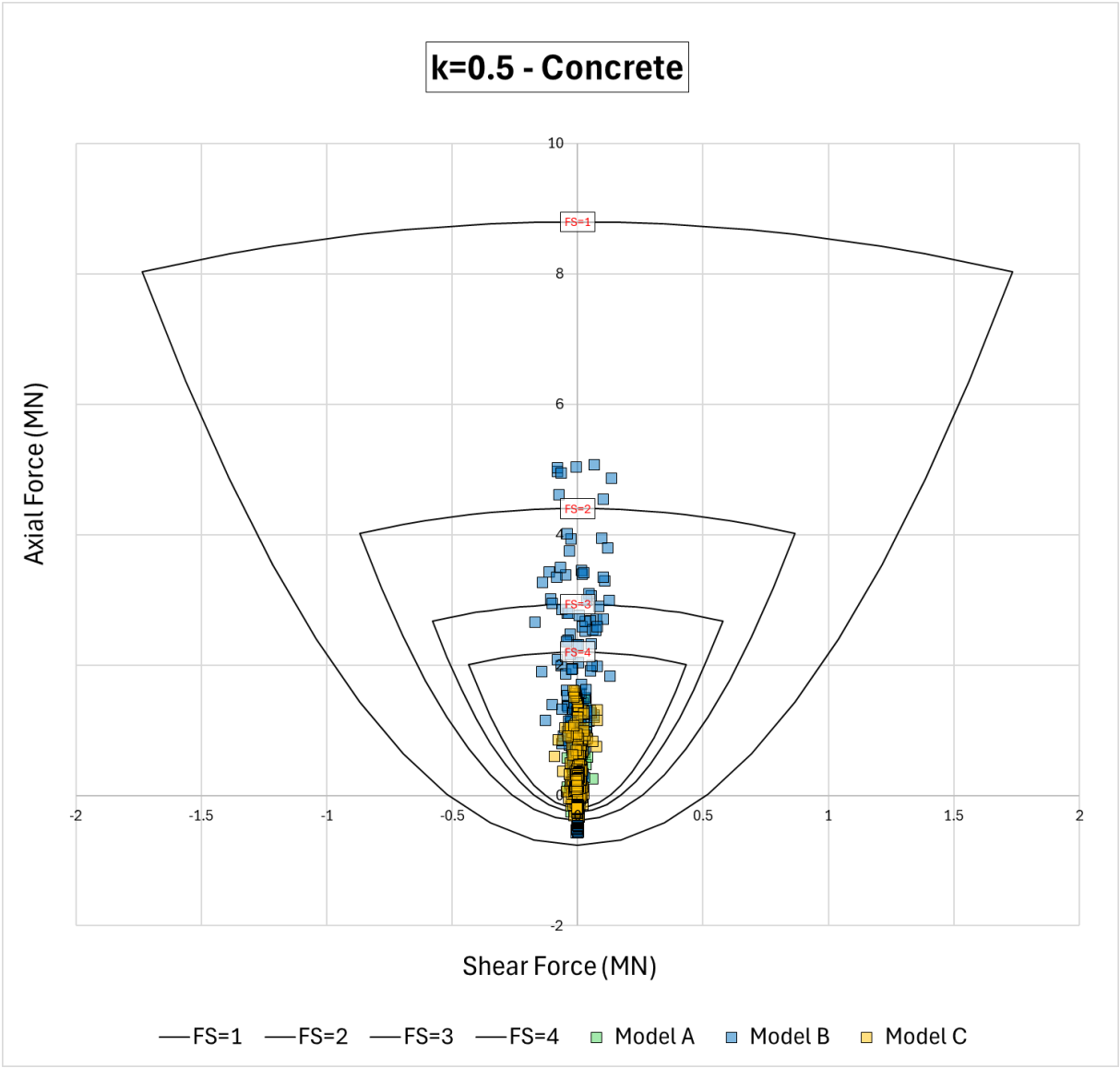

Figure 5-177. T-N support capacity diagrams of the RRS for all models, k=0.5

5.5.2. k = 1

5.5.2.1. Numerical results table

Table 5-11 shows results of computation of Model A, B and C with k=1.

Table 5-11. Summary of results, k = 1

k = 1			
Excavation Style	**Model A (RPE)**	**Model B (SD)**	**Model C (TBH)**
Maximum displacement at the walls [cm]	4	3.5	5
Maximum displacement at the roof [cm]	7.5	7.7	8
Maximum total displacement [cm]	7.9	8.1	8.1
Maximum radius measured for the plastic zone [m]	4	5	4.5
Maximum Compression on RRS [MN]	1.9	5.9	2.4
Maximum Tension on RRS [MN]	0.4	0.3	0.4
Min-Max Factor of Safety for RRS	Min: 1.7 Max: higher than 4	Min: 1.5 Max: higher than 4	Min: 1.4 Max: higher than 4
Maximum axial force on rock bolts [MN]	0.1	0.2	0.2
Rock Bolt Deformation [cm]	3.5	5	5.1

5.5.2.2. Support Capacity, RRS (Concrete)

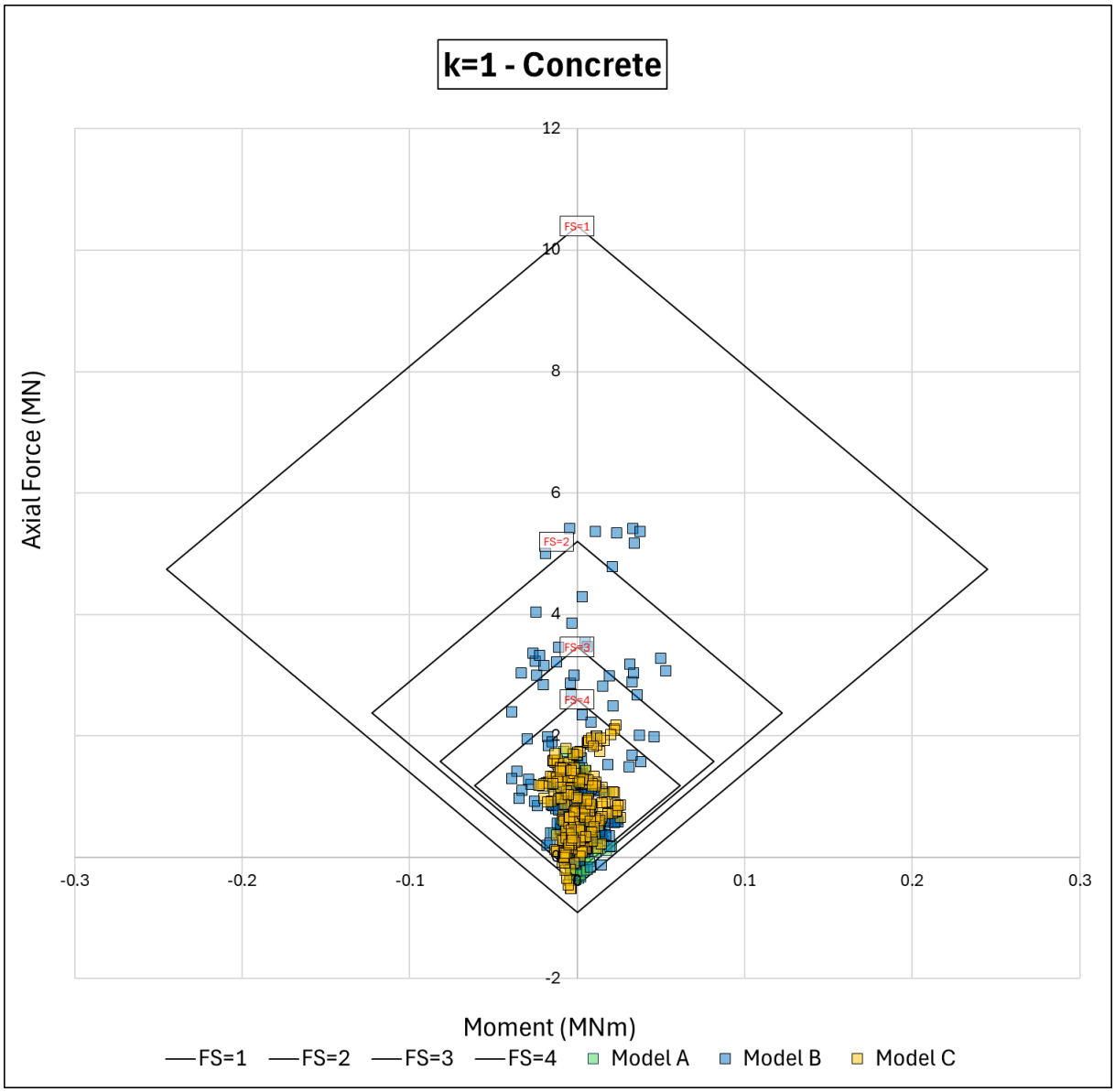

Figure 5-178. M-N support capacity diagrams of the RRS for all models, k=1

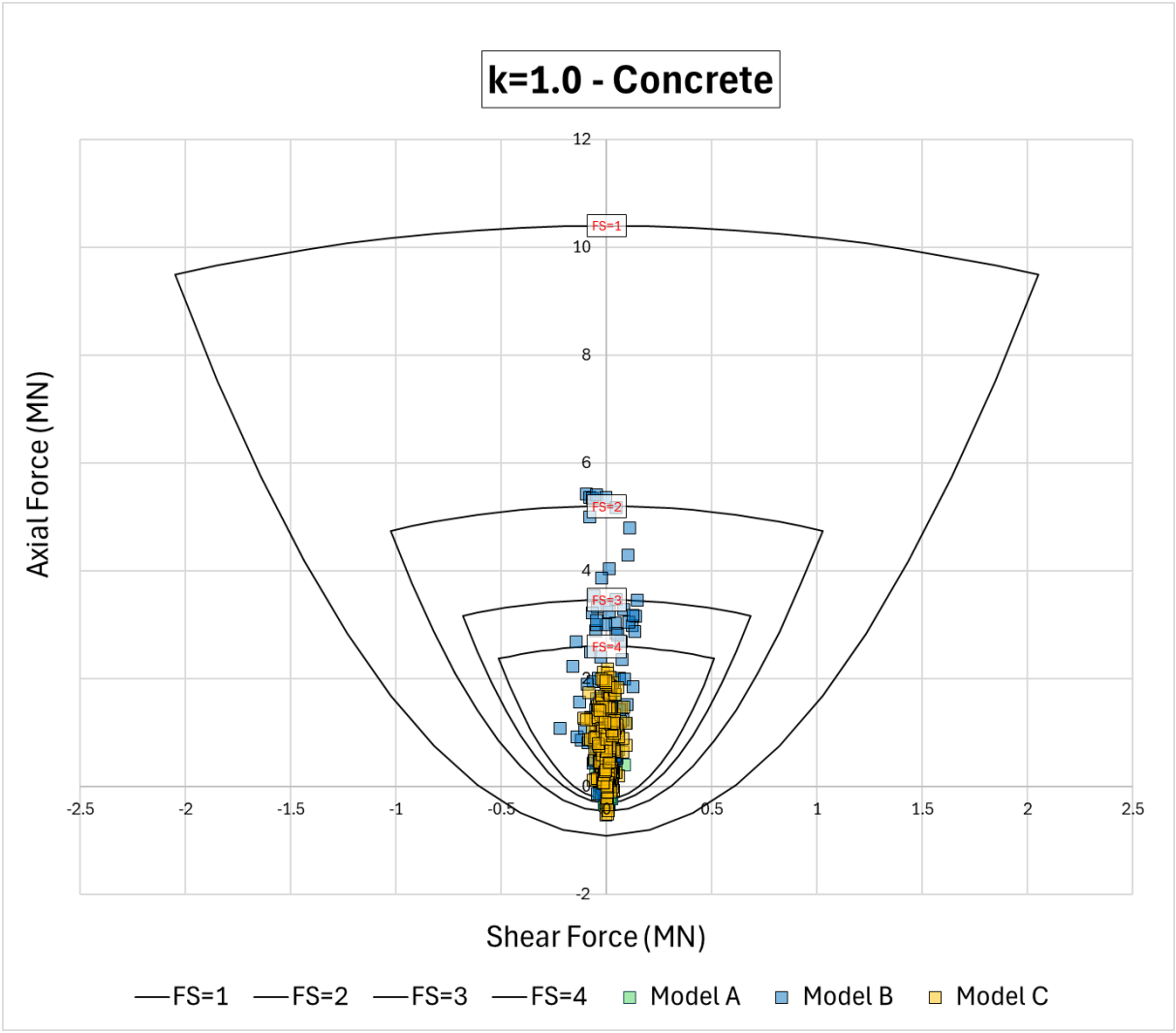

Figure 5-179. T-N support capacity diagrams of the RRS for all models, k=1

5.5.3. k = 2

5.5.3.1. Numerical Results table

Table 5-12 indicates results of computation of Model A, B and C with k=2.

Table 5-12. Summary of the results, k = 2

k = 2			
Excavation Style	**Model A (RPE)**	**Model B (SD)**	**Model C (TBH)**
Maximum displacement at the walls [cm]	6	7.5	7.8
Maximum displacement at the roof [cm]	10	10	11
Maximum total displacement [cm]	10.7	11.2	12.5
Maximum radius measured for the plastic zone [m]	10.5	10.8	10.5
Maximum Compression on RRS [MN]	1.9	5.3	3.4
Maximum Tension on RRS [MN]	0.3	0	0
Min-Max Factor of Safety for RRS	Min: 2.2 Max: Higher than 4	Min: 2.7 Max: Higher than 4	Min: 3.7 Max: Higher than 4
Maximum axial force on rock bolts [MN]	0.2	0.2	0.2
Rock Bolt Deformation [cm]	5.7	7.8	9.3

5.5.3.2. Support Capacity, RRS (Concrete)

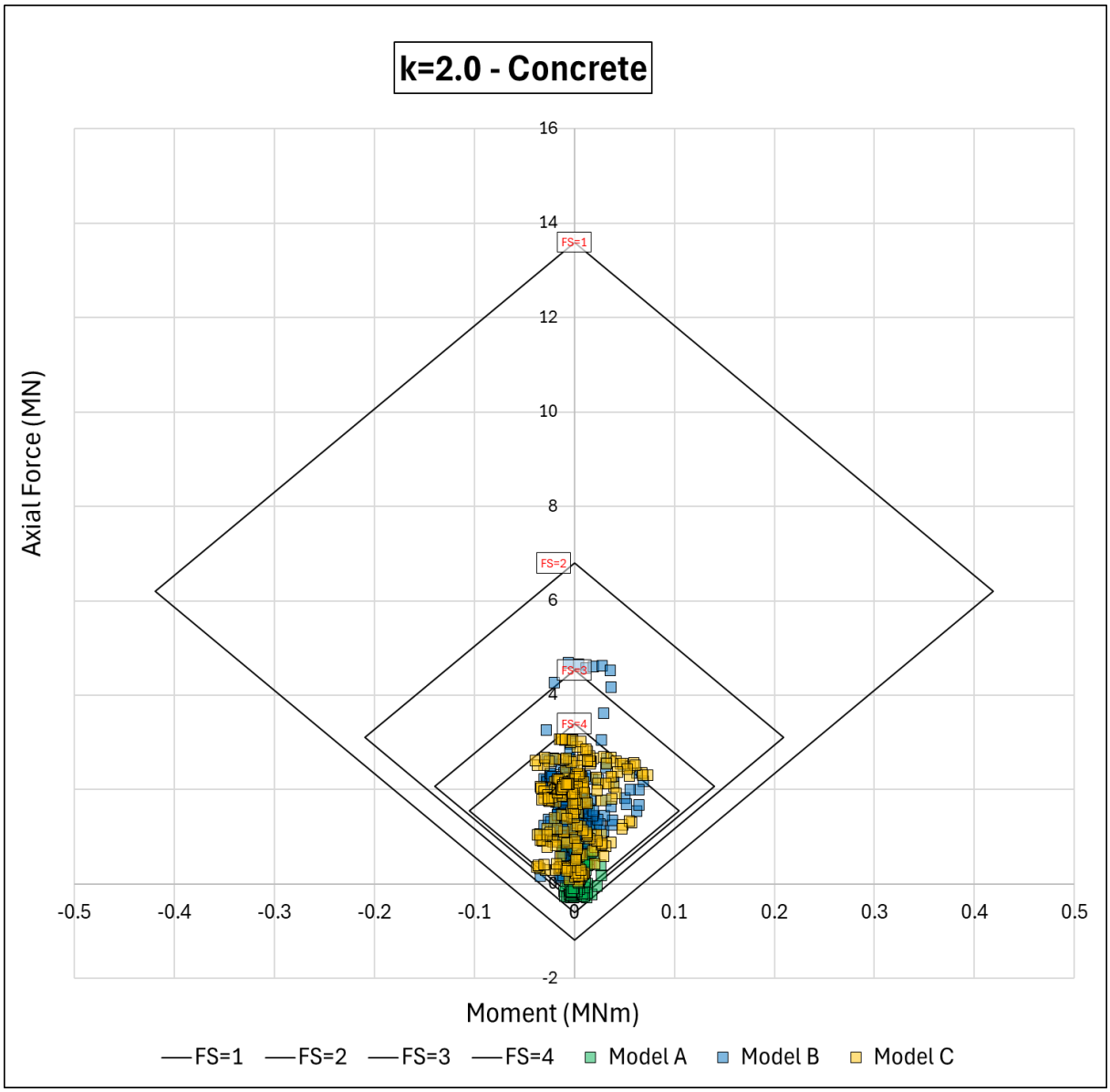

Figure 5-180. M-N support capacity diagrams of the RRS for all models, k=2

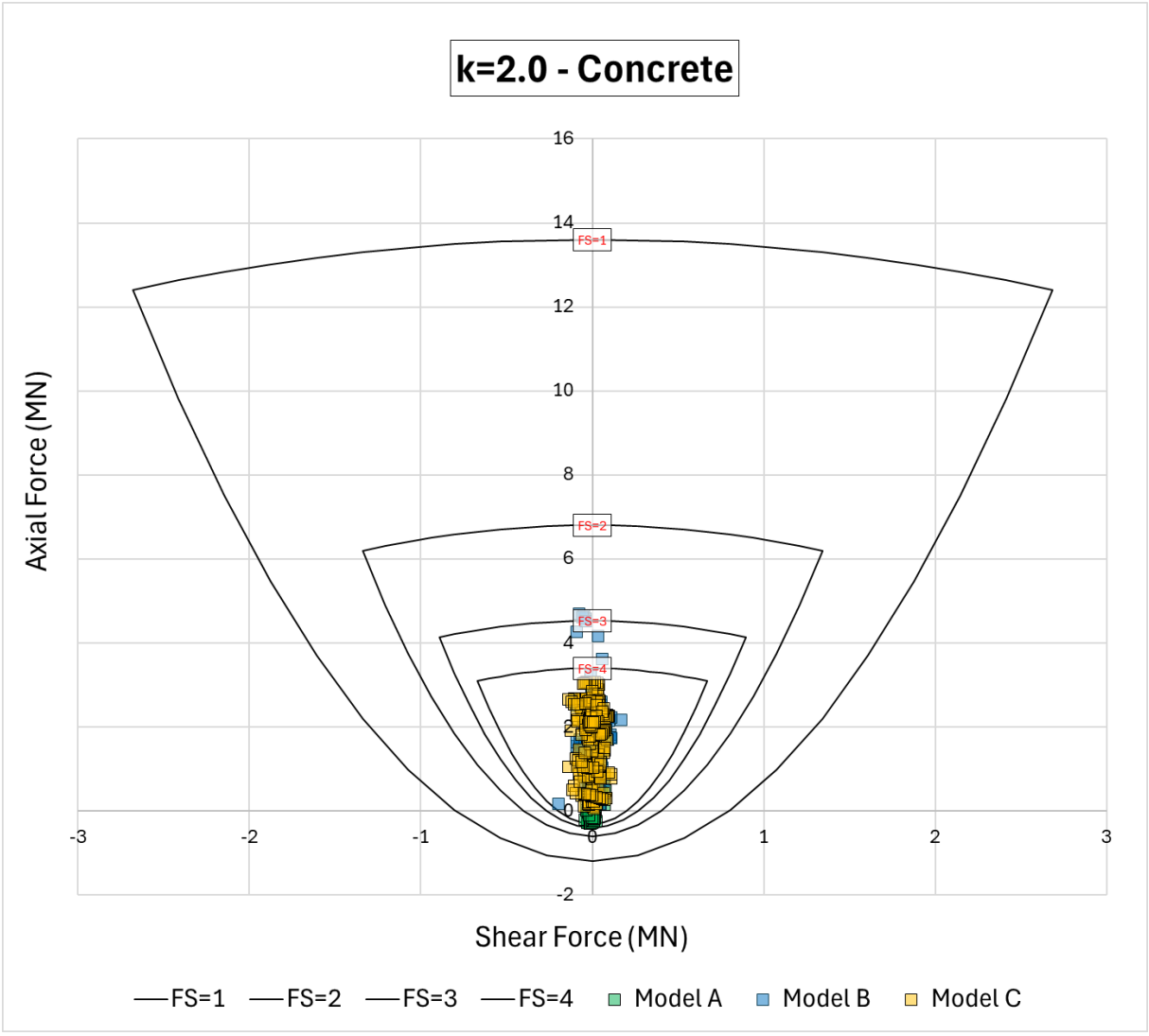

Figure 5-181. T-N support capacity diagrams of the RRS for all models, k=2

Chapter 6. Conclusions

The design and construction of deep, large-span caverns in rock demand a disciplined assessment of excavation methodology, compatibility of the selected support systems and the proper excavation sequences, based on the in-situ stress conditions. This study evaluated the performance of three distinct sequential excavation methods (SEM) for a 30 m span, 11 m high cavern in Norway, excavated within a gneissic rock mass at approximately 650 m depth. The geological setting, which is characterized by dry conditions and a relatively low Q-value of about 1.2, reflects a weak and potentially deformable rock mass, which requires reliable support throughout the excavation process. The excavation is assumed to be carried out with the application of Drill & Blast method which is highly adaptable and applicable across a wide range of rock Q-system values. This method is mostly applied in harder, higher-quality rock masses, but is also used in poor rock with the need of increased support.

The primary objective of the analysis was to identify a constructible, efficient and more suitable excavation strategy while ensuring that the support system (which has been preliminary selected in accordance with the Q-system, by the "well-known" Grimstad and Barton approach), performs effectively under varying stress regimes. In the same way also the stress-strained behavior of the rock mass, in terms of displacements and plastic zones, has been investigated.

As a matter of fact, three fundamentally different excavation sequences were examined, as below:

- **Radial Progressive Enlargement (RPE)** - Model A: Excavation initiated from the central core and gradually enlarged outward.
- **Side Drifts (SD)** - Model B: Excavation commenced with side drifts (left and right), followed by removal of the central core.
- **Top Heading and Bench (THB)** - Model C: Excavation executed in Top Heading (divided in two phases), and single bench.

Numerical models were developed to capture the deformation mechanisms, plastic zone evolution, and support residual capacity (in terms of Factor of Safety) associated with each excavation geometry and sequences. To assess the influence of the in-situ stress field, each model was analyzed under three horizontal-to-vertical stress ratios (k = 0.5, 1.0, and 2.0). The vertical stress remained constant at 17.6 MPa, derived from the 650 m overburden and a unit weight of 27 kN/m³, while horizontal stresses varied from 8.8 MPa to 35.2 MPa depending on the assigned k-value.

Across all scenarios, the support concept derived from Grimstad and Barton empirical approach consists of Reinforced Ribs of Sprayed Concrete (RRS), a heavy-duty system widely applied in weak or highly deformable rock masses where only systematic bolting associated to a layer of shotcrete is insufficient to provide enough support capacity. The system incorporates six or ten rebars arranged in one or two layers, fixed to rock bolts around the cavern perimeter and encapsulated in sprayed concrete. The installation sequence includes an initial layer of

fiber-reinforced shotcrete to stabilize the exposed rock surface (to ensure safety conditions), followed by placement of the reinforced ribs and a final layer of plain shotcrete to complete the support.

In accordance with Q-system recommendations, Support Category VI was adopted for all cases, corresponding to a total RRS thickness of 40 cm, including an initial 15 cm thick. fiber-reinforced shotcrete layer applied immediately after excavation. According to the same support category, 7m long rock bolts is suggested with a 1.7 m center-to-center spacing in both directions. Conservatively and to deal with bolt spacing compatible with the assumed spacing of RRS, 1.5m center-to-center spacing was finally considered for the longitudinal direction (direction of advance of excavation).

Therefore, based on the above and to account for the influence of the stress regime on support demand, the center-to-center spacing of the RRS elements varied: 4.5 m for k = 0.5, 3.0 m for k = 1.0, and 1.5 m for k = 2.0. In addition, to ensure that length of rock bolts is enough to reach elastic zone, thirteen rock bolts on the crown have been lengthened to 12 m for models computed with k = 2.0. Higher major horizontal principal stress was found to induce more extensive plastic zones and displacements, justifying the reduced spacing of the RRS in this case to achieve stable conditions for the excavation. It is important to highlight that support configuration with RRS with spacing of 1.5 m can be considered equivalent to a more "conventional" support system made by an initial 15 cm thick. fiber-reinforced shotcrete layer applied immediately after excavation plus a second layer of shotcrete reinforced with steel-reinforced concrete ribs and systematic bolting.

The numerical modelling was performed using the RS2 Finite-Element Analysis software, allowing comprehensive assessment of stress redistribution, deformation patterns, and support system performance.

Across the full range of stress conditions examined, the three excavation sequences exhibit fundamentally different behavior, each governed by how effectively the method maintains confinement, controls the stress re-distribution due to the excavation, and shapes the deformation field around the cavern.

Isotropic Stress Conditions (k = 1):

- **Model A (RPE)** demonstrates good performance because the radial expansion sequence removes the central core before the surrounding rock mass has fully mobilized its confinement. This sequencing causes early deconfinement of the central portion of the crown, which allows the roof to deform and results in a more effective redistribution of stresses due to the favorable shape (circular). However, the drawback is that this deconfinement also leads, after both sides' enlargement, to the development of tensile forces at the crown, and these tensile zones are undesirable because they make negative contributions to structural verifications for RRS. Total deformation around the cavern opening reaches 7.9 cm, and the plastic zone extends approximately 4 m into the rock mass. Yielding zone extension is almost constant all around the excavation profile, proving the redistribution of stresses. Even so, none of the bolts yield and all bolt

endpoints remain within the elastic zone, indicating that the existing bolt length remains adequate for this excavation approach.

- **Model B (SD)** advances the side drifts before removing the central core, creating an asymmetric but gradual stress release. This sequencing mobilizes the confinement on the sidewalls early and provides enough confinement to prevent the development of tensile forces in the lining. Although the structural reaction patterns on the RRS remain relatively uniform, it has been observed that shear forces, axial forces, and bending moments are all relatively higher compared with Model A. Importantly, almost no tension is found on the lining, which is a favorable outcome for structural verifications for the RRS. The maximum displacement reaches 8.17 cm around the cavern, which is slightly lower than in Model A, and relevant the plastic zone extends to a radius of about 4.5 m around the cavern. This extent remains within the anchorage capacity of the existing 7 m rock bolts, so no modification to bolt length is required.

- **Model C (THB)** advances by excavating and supporting the upper portion of the cavern which leads to concentration of compressive forces on the lining at the crown except minor tension points. This excavation sequence provides general confinement along the liner. Structural performance of RRS is mostly acceptable with at least safety factor of 1.4; additionally, it has structural reaction, i.e. low bending moment and shear force, which is similar to model A yet these values are lower than the ones on Model B. Maximum deformation around the cavern is 8cm which is nearly identical to Model A. plastic zone is balanced and has acceptable thickness of 5 m which shows that 7m bolts are sufficient to place them out of the plastic zone.

Low Horizontal Stress (k = 0.5):

- **Model A (RPE)** exhibits a uniform response under low horizontal stress by encouraging a symmetric deconfinement of the surrounding rock mass, thereby reducing the concentration of the localized stress that commonly arises during excavation. This symmetry allows the ground to adapt more gradually to the dominant vertical load, distributing deformation in a way that avoids abrupt overstressing of the lining. However, the temporary reduction in crown confinement inherent to this excavation sequence still leads to the formation of tensile forces at central portion of the roof, once the enlargements on both sides are completed. Additionally, the cavern opening has a maximum displacement of 8.1 cm which is quite like the deformations calculated on Model B and C. The plastic zone remains confined to a radius of approximately 4 m, which is compatible with the 7 m bolts, except at crown where rock mass remains predominantly in elastic condition. This is beneficial since yielding at crown may induce local opening of rock mass joints, with increasing risk of rock wedges instabilities. These results show that the overall stability of the excavation remains manageable, and the factor of safety calculated for RRS is sufficiently high.

- **Model B (Side Drifts)** exhibits the least favorable behavior under low horizontal stress conditions in terms of structural capacity of the RRS. Advancing the side drifts at an early stage removes the lateral confinement that would otherwise help stabilize the opening, while the roof remains the main part for carrying the dominant vertical load for the rest of the excavation sequence. This sequencing creates a structural imbalance that intensifies stress concentrations at the crown and haunches, leading to the development of tensile reactions in the crown and very high compression in the side walls. Bending moments remain high but the presence of both high tensile and compression forces along the RRS is the major concern for structural verifications. Around the cavern opening it is measured a maximum displacement of 8.1 cm, and the plastic zone expands to a radius of approximately 5.5 m, indicating a broader extent of yielded zones compared to Model A.

- **Model C (THB)** Low horizontal stress ratio naturally leads to have tension on the crown in all models; However Model C shows a better structural performance for the RRS by having lower amount of tension ensuring lowest safety factor equal to 2 and also a low value of compression and shear force that provide high safety factor range in M-N-T domain by stabilizing the upper portion of the cavern at initial stages. Maximum deformation around the cavern is 8.5 cm which is almost equal to the one in Model B and A. Plastic Zone on the crown is very tiny like other models and localized mostly between crown and sidewalls especially on the left side that indicates the effect of first step of excavation with highest thickness of 6 m showing that the rock bolt length is still sufficient to link their endpoint in the elastic zone.

<u>High Horizontal Stress (k = 2):</u>

- **Model A (RPE)** performs reasonably well under high horizontal stress, largely due to the symmetric release pattern, which helps moderate deformation and prevents sharp stress concentrations from developing around the opening but only at the first stage of the excavation. This balanced excavation sequence during the first two stages of excavation promotes a more uniform ground response and allows to partially compensate for the effect of the heterogenous state of field stress, minimizing tensile stresses at crown. In any case tensile forces are locally registered on the sidewalls only, during the enlargement of the excavation on both sides (coming from a circular shape to the final shape of the cavern). The real drawback is that the distribution of stresses in the lining is not symmetric, as it was in previous cases. This is because the enlargement on both sides is not carried out simultaneously and therefore, unbalanced conditions occur while dealing with a high horizontal principal stress. The plastic zone extends to roughly 10 m, and the maximum displacement reaches 10 cm—both values are almost at limits, even if still acceptable, for a rock mass subjected to a high-stress

environment. This is also proved by the fact that some bolts at crown are now yielded. Overall, RPE sequence seems to be applicable for k >1.0.

- **Model B (SD)** shows the most stable and favorable performance under high horizontal stress. Excavating and supporting the side drifts first allows the horizontal loads to be mobilized and redistributed before the central core is removed, creating a well-balanced stress environment around the opening. This staged progression significantly reduces abrupt deformation at the roof and sidewalls, keeping the lining predominantly in compression and limiting bending moment reactions to moderate levels, with no tensile reactions observed. The factor of safety in the combined M–N–T domain remains mostly above 3, reflecting a good structural response. The plastic zone extends to 10 m, and the maximum displacement around the cavern is 11.6 cm. Across all comparative performance indicators, SD method stands out as the preferred excavation sequence for high horizontal stress environments.

- **Model C (THB)** shows a favorable performance by initiating construction at the upper drift between the sidewalls and the crown, it adopts the stress-relief benefits of the Side Drift (SD) method and distinguishes itself by providing immediate support to the roof along the walls. it demonstrates a robust structural performance like Model B, by achieving a minimum Factor of Safety of 3 within the M–N–T domain while ensuring the entire lining remains out of tensile forces. Although the maximum displacement reaches 12.5 cm which is slightly higher than those observed in Models A and B, the plastic zone is 10 m equal to the one in other models showing sustainability of the current installed rock bolts with 12 m. This strategic sequence facilitates a favorable redistribution of vertical loads that maintains the crown in a state of compression.

These results show that each excavation method works best under certain stress conditions and choosing the method that matches the in-situ stress regime is key to achieving safe and reliable cavern excavation performance.

- **Radial Progressive Enlargement (RPE)** is the most effective under near-isotropic stress, where its symmetric stress release can be fully utilized, even if the side enlargement which is carried out not simultaneously may lead to partial tension areas, which are in any case manageable with adequate support.
- **Side Drifts (SD)** is most efficient under high horizontal stress, offering greater control of lateral loads.
- **Top Heading and Bench (THB)** method is a versatile and secure excavation strategy, proving resilient across various stress regimes, it shows most favorable performance in low horizontal-to-vertical stress ratio among all excavation models.

Across all stress ratios, the results confirm a key principle in deep cavern engineering: excavation sequence is not just a construction choice but a major factor controlling structural performance, and it must be selected to suit the prevailing stress conditions to ensure long-term stability and support efficiency. It is also true that the selection of the excavation sequences is also strictly related to the logistics (machineries, drilling rigs, etc.).

In a broader engineering context, this study demonstrates how advanced finite-element analysis can illuminate the complex interactions between excavation sequence, cavern geometry, support installation, and in-situ stress redistribution that govern the behavior of deep, large-span underground openings. By quantifying these mechanisms with far greater precision than empirical approaches alone (which are based on simplified and standardized cases), the work establishes a robust foundation for improving excavation planning, optimizing support design, and enhancing overall stability in challenging rock masses subjected to varying stress regimes. The findings are directly applicable to tunnelling projects worldwide, particularly as underground construction progresses into deeper, more heterogeneous, and more demanding geological environments.

Future research can build on this framework by incorporating time-dependent deformation processes, anisotropic or jointed rock mass (discontinued medium analyses), and real-time monitoring to further validate or calibrate and refine numerical predictions. There is also significant potential for developing adaptive excavation strategies, performance-based support systems, and probabilistic design methodologies that more effectively address geological uncertainty.

Overall, this study demonstrates the value of combining advanced numerical analysis with practical engineering judgement. It provides a solid technical basis for tunnelling engineers aiming to achieve safer, more efficient excavation, and offers researchers a foundation for further advancing modern underground engineering practice.

References

Administration, U. F. (2009). *Technical Manual for Design and Construction of Road Tunnels.* FHWA.

Amusing Planet. (2015). Retrieved from https://www.amusingplanet.com/2015/03/laerdal-tunnel-worlds-longest-road.html

Barton. (1974). Engineering classification of rock masses for the design of tunnel support.

Barton. (2002). Some new Q-value correlations to assist in site characterisation and tunnel design.

Barton, & Choubey. (1977). *The shear strength of rockfill materials.* Journal of soil mechanics and foundation Div.

Bieniawski, Z. (1989). *Engineering Rock Mass Classifications.*

Brady, & Brown. (2006). *Rock Mechanics For Underground Mining.*

Brown, & Hoek. (1980). *Underground Excavations in Rock.*

Bruland. (2012). *Classifications of properties influencing the drillability of rocks, based on the NTNU/SINTEF test method.* Retrieved from http://rockmass.net/files/strength_and_deform_values%20.pdf

Campervan Norway. (2023). Retrieved from https://www.campervannorway.com/blog/driving-norway/tunnels-in-norway

Carranza-Torres, & Diederichs. (2009). Mechanical analysis of circular liners with particular reference to composite supports. For example, liners consisting of shotcrete and steel sets.

Diedrichs, & Hoek. (2006). Empirical estimation of rockmass modulus.

Dyskin, & Germanovich. (1993). Model of crack growth in microcracked rock.

FHWA. (2009). *Technical Manual for Design and Construction of Road Tunnels.*

Gall, V. (2013). *Design guidlines for sequential excavation method (SEM).* Gall Zeidler Consultants.

Geotechnical Design. (2022, March 28). *Geotechnical Blogs*. Retrieved from https://geotechnicaldesigns.com.au/blogs/f/2d-finite-element-method---3d-simulation-of-tunnel-excavation

Hafeezur, R., & Wahid, A. (2018). Review of Rock-Mass Rating and Tunneling Quality Index Systems for Tunnel Design: Development, Refinement, Application and Limitation.

Havard, H., & Nilsen. (2018). Analysis of the stabilising effect of ribs of reinforced sprayed concrete.

Hoek. (1995). *Support of underground excavations in hard rock. A.A. Balkema.*

Hoek. (2000). *Big Tunnels in Bad Rock.*

Hoek. (2006). *Practical Rock Engineering.* PDH Center.

Hoek, & Marinos. (2000). *GSI- A Geologically friendly tool for rock mass strength estimation.* GeoEng 2000.

Hu, S. (2022). *Analysis of structural characteristics of underground caverns under high stress.* Journal of rock mechanics and geotechnical engineering.

Islands, V. F. (n.d.). *WORLD'S FIRST UNDER SEA ROUNDABOUT*. Retrieved from WORLD'S FIRST UNDER SEA ROUNDABOUT: https://visitfaroeislands.com/en/plan-your-stay/getting-around/world-first-under-sea-roundabout

Karlsrud. (2002). Water control when tunneling under urban areas in the Olso region.

Ketan, Gutierrez, & Hedayat. (2020). Tunnels in squeezing clay-rich rocks.

Kirsch. (1898). Die Theorie der Elastizität und die Bedürfnisse der Festigkeitslehre.

Li, B. (2022). *Damage and failure characteristics of surrounding rock in high-stress caverns.* Minerals.

Longitudinal Displacement Profiles for ConvergenceConfinement Analysis of Excavations: Applicability toTunnelling, Limitations and Current Advancement. (n.d.).

Mao, & Nilsen. (2011). Analysis of loading effects on reinforced shotcrete ribs caused by weakness zone containing swelling clay.

Mazaira, & Konicek. (2015). Intense rockburst impacts in deep underground construction and their prevention.

McQueen. (2004). *In Situ rock stress and its effect in tunnels and deep excavations.* Australian Geomechanics Journal.

N.Barton. (1994). Prediction and measured Performance of the 62m Span Norwegian Olympic Ice-Hockey Cavern at Gjovik.

NGI. (2025). *Using the Q system.*

NGU. (2025). *Bedrock Map*. Retrieved from https://www.ngu.no/en/geologiske-kart

Nie, & Zhang. (2018). *Performance-based support design for horseshoe-shaped tunnels using SEM.* Tunneling and underground space technology.

NTS. (2011). *Rock Mass Grouting by Norwegian Tunneling Society.*

NTS. (2016). *Norwegian Rock Caverns.*

Palmstrom, & Broch. (2006). Use and misuse of rock mass classification systems with particular reference to the Q-system.

Panet. (2001). Recomendations of Convergence Confinement Method.

Panet, & Guénot. (1982). Analysis of Convergence Behind The Face of A Tunnel.

Pei, Q. (2023). *Estimation method for an in-situ stress field along a super-deep tunnel.* building.

Rocscience. (2019). *In Situ and Induced stresses.* Practical rock engineering chapter.

Russo, G. (2014). An update of the "multiple graph" approach for the preliminary assessment of the excavation behaviour in rock tunnelling.

Sanyam, & Kirishna. (2025). Analysis of in-situ stress data in and around Norway.

Sharifzadeh, & Kiani. (2013). *Design of sequential excavation method for large span caverns.* Tunneling and underground space technology.

Smanioto, & Neuner. (2022). Experimental study of a wet mix shotcrete for primary tunnel lining-Part 1.

Sulem, J., & manh, H. t. (2014). Modelling of time-dependent anisotropic deformation.

Sun, N. (2023). *The deformation law of a soft-rock cavern by step-by-step excavation.* Applied science.

Sun, W. (2024). *Modeling of spalling failure of in situ rock mass for tunnels under high stress.* Engineering Geology.

Tunneling, T. a. (2013). *Invisible options - Tunnels*.

Vlachopoulos, N., & Su, Y. (2019). Longitudinal Displacement Profiles for ConvergenceConfinement Analysis of Excavations: Applicability toTunnelling, Limitations and Current Advancement.

Wang, M. (2024). *Deformation and failure mechanism of surronding rock in high stress tunnels.* Geomechanics and engineering .

Wei, Y., & Fu, W. (2019). Estimation of the equivalent Mohr–Coulomb parameters using the Hoek–Brown criterion and its application in slope analysis.

Wikipedia. (2008). *Svalbard Global Seed Vault*. Retrieved from Wikipedia: https://en.wikipedia.org/wiki/Svalbard_Global_Seed_Vault

Wikipedia. (2025). *New Austrian Tunneling Method*.

WSM. (2025). *World Stress Map.*

Yuan, C. (2024). *influence of tunnel excavation on the magnitude and distribution of in-situ stresses.* Journal of rock mechanincs and geotechnical engineering.

Zhang, & Wang. (2009). Elastic-plastic analysis for surrounding rock of pressure tunnel with lining based on material nonlinear softening.

Zheng, H. (2022). *Applying probabilistic approaches for reliable SEM Tunneling.* Transportation reaserch record.